UNIVERSIDAD AUTÓNOMA DE MADRID

FACULTAD DE MEDICINA

Instituto Teófilo Hernando de I+D del Medicamento
Departamento de Farmacología y Terapéutica

Novel multitarget chiral α7-nAChRs ligands with neuroprotective properties for Alzheimer's Disease treatment

Memoria de tesis para optar al grado de Doctor presentada por

Sheila Abril Comesaña

Madrid, 2019

D. RAFAEL LEON MARTINEZ, Investigador Contratado Miguel Servet II de la Fundación de Investigación Biomédica del Hospital de la Princesa,

y D. MERCEDES SALAICES SANCHEZ, Catedrática de Farmacología del Departamento de Farmacología de la Facultad de Medicina de la Universidad Autónoma de Madrid,

CERTIFICAN, que Dª. SHEILA ABRIL COMESAÑA ha realizado bajo su dirección el presente trabajo titulado "**Novel multitarget chiral α7-nAChRs ligands with neuroprotective properties for Alzheimer's Disease treatment**", como Tesis para alcanzar el grado de Doctor.

Para que conste a los efectos oportunos, expiden y firman la presente en Madrid a 2 de septiembre de 2019.

D. Rafael León Martínez	Dña. Mercedes Salaices Sánchez
Investigador Miguel Servet II	Catedrática de Farmacología

Abstract

Alzheimer's Disease (AD) is an age-related, chronic, progressive and continuous neurodegenerative disease and the most common form of dementia worldwide. Because of its high biological complexity, AD is considered a multifactorial disorder. Currently, there are only five Food and Drug Administration (FDA) marketed symptomatic drugs, which cannot stop disease progression. This has led to the development of the new therapeutic strategy of multitarget directed ligands (MTDLs).

In this context, we have obtained a two chiral MTDLs families based on important pathological routes involved in AD. Family A *de novo* synthesised compounds were simultaneously free radical scavengers, Nrf2 inducers, acetylcholinesterase (AChE) inhibitors, α7- neuronal nicotinic acetylcholine receptors (α7-nAChR)-selective ligands and neuroprotectant agents. The pharmacokinetic profile of selected hit compounds was assessed and systemic parameters were evaluated. The neuropharmacokinetic studies revealed they distribute within the brain and bind to brain parenchyma, accumulating intracellularly. However, free unbound drug was low, most probably due to the existence of an active efflux transport across the blood brain barrier. These results were valuable in order to re-design the second generation of MTDLs with advantageous physicochemical properties. Although Nrf2 induction activity was lost in Family B, the excellent free radical scavenger effect, as well as the selective activation of α7-nAChR, remained, leading to higher neuroprotectant activity.

These compounds were conceived to be directed to the aforementioned different therapeutic targets, and to act at complementary targets of the neurodegenerative process. Thus, activating the endogen survival cell routes, which could prevent or, at least, slow down the neurodegeneration process of AD

Resumen

La Enfermedad de Alzheimer (EA) es una enfermedad neurodegenerativa, crónica y progresiva, relacionada con el envejecimiento y es la forma más común de demencia en el mundo. Debido a su extraordinaria complejidad, la EA es considerada una enfermedad multifactorial. En la actualidad, solamente existen cinco fármacos aprobados por la FDA comercializados, los cuales son sintomáticos y no pueden parar la progresión de la enfermedad. Esto ha llevado a desarrollar la nueva estrategia terapéutica de ligandos multidiana.

En este contexto, hemos obtenido nos nuevas familias de compuestos multidiana basados en importantes rutas patológicas involucradas en la EA. Los compuestos *de novo* sintetizados de la Familia A resultaron ser simultáneamente captadores de radicales libres, inductores de Nrf2, inhibidores de AChE, ligandos selectivos de α7-nAChRy agentes neuroprotectores. Además, se realizaron estudios farmacocinéticos y de distribución cerebral con los compuestos seleccionados como cabeza de serie, donde se obtuvieron los parámetros sistémicos y los cuales revelaron que se distribuyen y se unen al parénquima cerebral, acumulándose intracelularmente. Sin embargo, la cantidad de compuesto libre fue muy baja, muy probablemente debido a la existencia de un transporte active de expulsión del cerebro a través de la barrera hematoencefálica. A pesar de ello, estos resultados fueron valiosos para rediseñar una segunda generación de compuestos multidiana con propiedades fisicoquímicas mejoradas. Aunque se perdió la actividad de inducción de Nrf2, los compuestos de la Familia B mostraron un potente efecto secuestrador de radicales libres, así como mantuvieron la activación selectiva de los α7-nAChR, dando lugar a una mayor capacidad neuroprotectora.

Estos compuestos fueron concebidos para ser dirigidos a diferentes dianas terapéuticas, con el fin de actuar sobre rutas complementarias del proceso neurodegenerativo. De este modo, mediante la activación de rutas de supervivencia endógenas, se podría evitar o, al menos, ralentizar el proceso neurodegenerativo de la EA.

Abbreviations and Acronyms

α4β2-nAChR:	α4β2 neuronal nicotinic acetylcholine receptor
α7-nAChR:	α7 neuronal nicotinic acetylcholine receptor
β-TrCP:	β–transducing repeat-containing protein
5-HT:	5-hydroxytryptamine, serotonin
A:	orthosteric site of α7-nAChR
AAPH:	2,2'-azobis(amidinopropane) dihydrochloride
Aβ:	amyloid-β
ACh:	acetylcholine
AChE:	acetylcholinesteraseAChEI: acetylcholinesterase inhibitor
ACN:	acetonitrile
AICD:	APP intracellular domain
AD:	Alzheimer's disease
ADMET:	adsorption, distribution, metabolism, excretion and toxicology
aECF:	artificial extracellular fluid
Akt:	protein kinase B
AMPc:	adenosine monophosphate cyclic
APOE4:	ε4 allele of apolipoprotein E
APP:	amyloid precursor protein
ARE:	antioxidante response element
AThCh:	acetylthiocholine
BACE1:	β-site amyloid cleaving enzyme 1
BBB:	blood brain barrier
BFCN:	basal forebrain cholinergic neurons
BFCS:	basal forebrain cholinergic system
BuChE:	butirylcholinesterase
BuThCh:	butirylthiocholine
bZIP:	basic–region leucine zipper
C:	closed resting state of α7-nAChR
ca.:	*circa*, approximately

CA: carnosic acid
CAP: cholinergic anti-inflammatory pathway
CAT: catalase
CDI: carbonyldiimidazole
Ch1: cholinergic neurons localized in medial septal cholinergic nucleus
Ch2: cholinergic neurons localized in vertical diagonal band of Broca
Ch3: cholinergic neurons localized in horizontal diagonal band of Broca
Ch4: cholinergic neurons localized in nucleus basalis of Meynert
ChAT: choline acetyl transferase
CICR: calcium induced calcium release
Cl: clearance
CMA: combinatory mapping approach
CNC: cap “n” collar
CNS: central nervous system
CSF: cerebrospinal fluid
CTF: C-terminal fragment of APP
Cul1/RBX: Cullin 1 and RING–box protein 1
Cul3/RBX: Cullin 3 and RING–box protein 1
CyPr: cyclopropyl
CyHx: cyclohexyl
D: direct allosteric activation site of α7-nAChR
D_i: PAM insensitive desensitized state of α7-nAChR
D_s: PAM sensitive desensitized state
DMEM: Dulbecco´s modified Eagle´s medium
DMSO: dimethyl sulfoxide
DMTs: disease modifying therapies
DNA: deoxyribonucleic acid
DTNB: 5,5’-dithiobis-(2-nitrobenzoic) acid
EA: Enfermedad de Alzheimer
ECD: extracellular domain
ECF: extracellular fluid

*Ee*AChE:	*Electrophorus electricus* acetylcholinesterase
*Eq*BuChE:	*Equine serum* butirylcholinesterase
EpRE:	electrophile response element
EMA:	European Medicines Agency
EOAD:	early onset of Alzheimer Disease
ETC:	electronic transport chain
F:	flip close state of α7-nAChR
FA:	formic acid
FBS:	fetal bovine serum
FDA:	United States Food and Drug Administration
FL:	fluorescein
FTDP-17:	frontotemporal dementia with parkinsonism linked to chromosome 17
$f_{u,brain}$:	unbound drug fraction in whole brain homogenate
$f_{u,plasma}$:	unbound drug fraction in plasma
GABA:	γ-aminobutiric acid
GPCRs:	G-protein coupled receptors
GSH:	glutathione
GSK3β:	glycogen synthase kinase 3 β
h:	hour
HC:	hippocampus
HEPES:	4-2(2-hydroxyethyl)-1-piperazineethane sulfonic acid
hERG:	Ether-go-go potassium channel
HO-1:	heme-oxygenase 1
HPLC:	high pressure liquid chromatography
IICR:	inositol induced calcium release
IC_{50}:	the concentration of the inhibitor required to reduce the rate of the enzymatic reaction by 50%
i.e.:	*id est* "in other words"
IL:	interleukin
IP_3:	inositol (1,4,5)-triphosphate

IP_3R:	inositol (1,4,5)-triphosphate receptors
JAK2:	Janus kinase 2
Keap1:	Kelch-like ECH-associated protein 1
$K_{p,brain}$:	brain-to-plasma partition coefficient
$K_{p,uu,brain}$:	unbound brain-to-unbound plasma partition coeeficient
$K_{p,uu,cell}$	unbound intracellular fluid-to-unbound extracellular fluid partition coefficient
LC_{50}:	concentration that reduces the 50% of cell viability
LC-MS/MS:	liquid chromatography tandem mass spectrometer
LOAD:	late onset of Alzheimer disease
LPS:	lipopolysaccharid
LY:	LY294002, PI3K inhibitor
LZ:	luzindole, MT1/MT2 inhibitor
mAChR:	muscarinic acetylcholine receptor
MAO:	monoamino oxidase
MAPK:	mitogen-activated protein kinase
MAPs:	microtubule associate proteins
MBD:	microtubules binding domain
MCM:	multi-compound medication
m-F-Ph:	*meta*-fluoro-phenyl
min:	minutes
MLA:	methyllycaconitine
MMT:	multi-medication therapy
MOA:	mechanism of action
MT1/MT2:	melatonin receptor 1 and melatonin receptor 2
MTDL:	multitarget-directed ligand
MTT:	3-(4,5-dimethylthizaol-2-yl)-2,5-diphenyltetrazoliumbromide
MnSOD:	manganese superoxide dismutase
nAChR:	nicotinic acetylcholine receptor
NADPH:	nicotinamide adenine dinucleotide phosphate
NAMs:	negative allosteric modulators

NeuroPK:	neuropharmacokinetics
Neh:	Nrf2-ECH homology domains
NGF:	neuronal growth factor
NF-κB:	nuclear factor κ–light–chain enhancer of activated B cells transcription factor
NFT:	neurofibrillary tangles
NLRs:	nucleotide-binding oligomerization-domain protein-like receptors
NMDARs:	N-methyl-D-aspartate receptor
Nrf2:	Nuclear Factor (Erythroid-Derived 2)-Like 2 transcription factor
NQO1:	NADPH:quinone oxidoreductase
O*:	open state of α7-nAChR
O':	PAM dependent open state
OA:	okadaic acid
OCB:	open channel blockers of α7-nAChR
P:	intra-subunit transmembrane cavity of α7-nAChR
PAM:	positive allosteric modulators
PAS:	peripheral anionic site of AChE
PBS:	phosphate-buffered solution
PD:	PD98059, MAPK inhibitor
PDPKs:	proline dependent directed kinases
PET:	positron emission tomography
Ph:	phenyl
PHF:	paired helical filaments
PI3K:	phosphatidyl inositol 3 phosphate kinase
PIP2:	phosphatidylinositol 4,5-bisphosphate
PK:	pharmacokinetic
PKA:	protein kinase A
PLC:	phospholipase C
Pol II:	RNA polymerase II
PP2A:	serine/threonine protein phosphatase 2A
Pr:	propyl

P/S:	penicillin/streptomycin
Psen1/2:	presenilin 1 and 2 genes
P-tau:	hyperphosphorylated tau
R/O:	rotenone and oligomycin A cocktail
RNA:	ribonucleic acid
RNS:	reactive nitrogen species
ROS:	reactive oxygen species
rt:	room temperature
s:	seconds
S:	alternative intra-subunit transmembrane cavity α7-nAChR
SAMs:	silent allosteric modulators
SFN:	sulforaphane
sMafs:	small masculoaponeurotic fibrosarcoma proteins
SnPP:	tin protoporphyrin, HO-1 inhibitor
TBHQ:	*tert*-butylhydroquinone
TCDI:	thiocarbonyldiimidazole
TH:	tyrosine hydroxylase
THF:	tetrahydrofuran
TLRs:	Toll-like receptors
TM:	transmembrane helices domain of α7-nAChR
TNFα:	tumor necrosis factor α
TR:	trigonelline, Nrf2 inhibitor
TREM2:	triggering receptor expressed on myeloid cells 2
Trolox:	(±)-6-hydroxy-2,5,7,8-tetramethylchromane-2-carboxylic acid, a vitamin E analogue
TXN:	thioredoxin
ULPC:	ultra-performance liquid chromatography
V_d:	volume of distribution
VDCCs:	voltage dependent calcium channels
$V_{u,brain}$:	volume of distribution of unbound fraction in whole brain

Index

1 Context and Purpose of the Thesis

The research for this Doctoral Thesis was conducted at *Instituto Fundación Teófilo Hernando (IFTH)*, an integral University Centre for Drug Discovery and Development, following one of its main research lines: pharmacological neuroprotection. Specifically, this Doctoral Thesis is focused on the development of new chemical entities with neuroprotective properties directed towards Alzheimer's Disease treatment.

After more than hundred years since being discovered, Alzheimer's Disease still has not efficacious treatment despite the utmost efforts of the scientific community. Therefore, the development of novel drugs able to stop the disease progression is an urgent socio-economic necessity. In this regard, this Doctoral Thesis is centred on the rational design, synthesis and pharmacological evaluation of new molecules belonging to the new class of MTDLs. The aim of this strategy is to combine, in a single scaffold, two or more pharmacophores which are able to act synergistically on different pathological events of Alzheimer's Disease in order to prevent its progression.

The results herein presented have been mainly performed and obtained at the Department of Pharmacology and Therapeutics at the Universidad Autónoma de Madrid (UAM), under the supervision of PhD Rafael León and Professor Mercedes Salaices. Additionally, there are compiled results obtained thanks to a short scientific stay in the Translational PKPD Group (Uppsala University, Sweden), under the supervision of PhD Irena Loryan and Professor Margareta Hammarlund-Udenaes, founded by Ministerio de Educación, Cultura y Deporte of the Government of Spain.

2 Introduction

2.1 Ageing

Ageing is attributed to a progressive accumulation of physiological changes due to genetic mutations, epigenetic and metabolic changes, molecular and cellular damage and environmental insults, leading to a gradual decline in the state of health and an increased susceptibility to age related diseases.

Over the last century, scientific and technological advances, improvements in quality of life and medical care access, have contributed to an increase in life expectancy. This tendency is expected to be maintained with a forecasted 25 % of the population aged 60 or over in high and middle-income countries, as reported by the World Health Organization in 2015.[1] As a prominent example, Spain, in the top three countries with the highest life expectancy, currently has 120 people aged over 64 for every 100 people under 16. Considering this numbers, by 2066 there will be 14 million elderly people, representing 35 % of the total population.[2]

A priori these demographic changes are good news, as they demonstrate an improvement in the quality of life. However, an ageing population has led to the appearance of a set of disorders associated with aging, such as cancer, cardiovascular diseases and neurodegenerative diseases. Thus, ageing has become a global concern with an important impact on health care systems, as well as having social and economic consequences that must be addressed urgently by implementing governmental policies.[1]

2.2 Alzheimer's Disease

Dr. Alois Alzheimer began to treat his patient Auguste Deter in 1901. She was admitted to a mental asylum because she experienced a progressive change in her personality, with impaired memory and hallucinations at the age of 51. Over time, she lost the ability to speak, displayed disorientation and confusion and became completely apathetic. After her death in 1906, Dr. Alzheimer examined her brain, describing the histological features found in the Handbook of Psychiatry, written by Emil Kraepelin, as a particularly serious form of senile dementia, introducing the term "AD" for the first time.[3]

As it is now recognized, AD is a chronic, progressive and continuous neurodegenerative process, which begins, years before the symptoms of Alzheimer's

dementia appear. It is the most common form of dementia, as it accounts for 60 to 80 % of cases.[4]

Despite significant advances made in different fields, such as genetics, molecular biology, or pharmacology, the uncertainty of the causes of sporadic AD are still unknown, 113 years since its first description.

Throughout the following sections, an overview of AD, including epidemiology, symptomatology, diagnosis, pathophysiological features, drug discovery hypothesis, therapies and current drug development, will be discussed.

2.3 Epidemiology, types and risk factors of Alzheimer's Disease

As stated above, the percentage of the population aged 65 and older, continues to rise, generating an increase in the number of patients with AD and other dementias. In 2016, these diseases were the fifth leading cause of global deaths, accounting for 2.1 million deaths (3.7 %).[5] In 2018, the number of people suffering from AD and other dementias was estimated to be 50 million, and it is projected to grow to 75 million by 2030, and 152 million by 2050.[5] In Spain, 15,202 people died of Alzheimer and other dementias in 2017. Currently, there are 800,000 patients with AD, and every year 40,000 new cases are diagnosed.[6] AD patients are classified as early onset of AD (EOAD) when they present symptoms before the age of 65, while after this age it is considered to be late onset of AD (LOAD). Only 10 % of cases are diagnosed as EOAD, most of them being genetically determined by mutations in three genes, the amyloid precursor protein (*App*), presenilin 1 and 2 (*Psen1, Psen2*), and/or Down's Syndrome or 21 trisomy.[7] Conversely, LOAD cases are sporadic, whose main risk factors are ageing and epigenetics, and to a lesser extent, a genetic predisposition to carrying ε4 allele of the apolipoprotein E (ApoE4) gene, or due to heterozygous mutations of the triggering receptor expressed on myeloid cells 2 (TREM2).[8]

2.4 Symptoms and diagnosis of Alzheimer's Disease

The severity of clinical symptoms is a reflection of the level of neuronal damage to different areas of the brain, leading to AD classification at several stages. Firstly, pre-dementia has no symptoms. Secondly, mild cognitive impairment presents as memory loss, especially forgetting recently learned information and the misplacement or loss of

things. Thirdly, early to moderate stage dementia displays as trouble with daily tasks, communication problems, reasoning difficulties, decreased or poor judgment and changes in mood or personality. Finally, late stage dementia signs are greater time and spatial disorientation, social isolation and complete dependency.[9] There is a correlation between clinical stages and the gradual development of changes in the brain, as established by Braak and Braak, and once the degeneration process begins, it inevitably continues.[10]

Current diagnosis is based on the medical and familiar history of the individual, and cognitive, physical and neurological tests. Even though the physician requires days or weeks to gather results and make the diagnose, 90 % of cases are accurately diagnosed.[4]

2.5 Treatments and drug development pipeline

Unfortunately, there is no effective treatment to slow down, stop or reverse AD progression. Since the first marketed therapy, tacrine **1** (Cognex®, Parke Davis division), in 1993, only five drugs have been approved by the FDA. They are currently prescribed due to tacrine being rapidly withdrawn because it was found to be hepatotoxic.[11]

Currently used treatments, donepezil **2** (Aricept®, 1993, Eisai), rivastigmine **3** (Exelon®, 2000, Novartis) and galantamine **4** (Raminyl®, 2001, Janssen Pharmaceutics) are AChE inhibitors (AChEIs), whose main mechanism of action (MOA) is to raise ACh levels in the synaptic cleft, preventing cholinergic system atrophy. In line with neurotransmission modulation, memantine **5** (Nameda®, Forest Labs) was, in 2003, the last drug to be approved as a N-methyl-D-aspartate receptors (NMDARs) antagonist. NMDARs are cationic channels gated by glutamate excitatory neurotransmitter, Aβ activates them, favouring an intracellular Ca^{2+} increase which exerts excitotoxicity. Finally, a combination of donepezil and memantine (Namzaric®, Forest Labs) was released in 2014 for moderate to severe AD stages.[12]

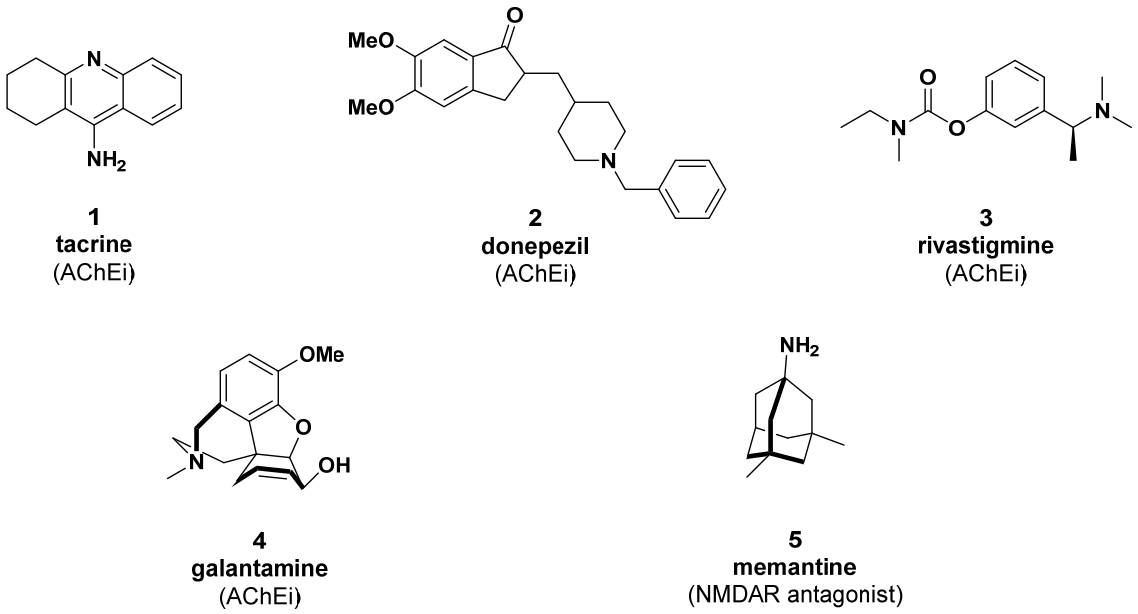

Figure 1. First (tacrine) and current symptomatic treatments for AD.

All of these are classified as symptomatic treatments as they subtly reduce cognitive decline and neuropsychiatric symptoms. Unfortunately, most patients do not respond. Therefore, significant efforts are still needed to find promising DMTs that prevent or delay the progression of AD. In fact, 17 out of 26 (65 %) candidate agents in Phase III clinical trials in 2018 are DMTs.[13]

Despite six new drugs being approved for central nervous system (CNS) disorders in 2017, none of them were for AD. The failure to find a DMT for AD treatment could be related to several causes, including anatomical and functional complexity, the inaccessibility of the areas of the brain required for taking samples in early stages of the disease, treatment of the biomarker potentially not treating the disease, CNS disease-triggering causes leading to problems in target identification and validation, inadequate knowledge of neuro-pharmacokinetics (neuro-PK) owing to the presence of the blood-brain barrier (BBB), an inability to reliably translate from animal models to humans and the relatively long time required to perform clinical trials to know whether a candidate agent affects the disease progression.[4,14]

2.6 Physiopathological hallmarks of Alzheimer's Disease

AD is mainly characterized by memory and cognitive function loss, due to drastic reduction in the number of cholinergic neurons in brain regions associated with attentional, spatial and functional memory.[15] AD classical histopathological features are amyloid-β (Aβ) aggregates which clump in extracellular senile plaques, interrupting the neuron-to-neuron communication, and intracellular neurofibrillary tangles (NFT), containing hyperphosphorylated tau protein(P-tau), hampering nutrient and other biomolecule transportation.[16] In addition to these two main characteristics first described by Alois Alzheimer, there are certainly some other brain changes involved, such as calcium homeostasis deregulation, mitochondrial dysfunction, oxidative stress and chronic neuroinflammation.[17] Therefore, researchers have been trying to explain the causes of the disease, focusing their efforts on one of these particular features. However, none of them have led to the development of an efficacious treatment able to stop the disease progression. Despite the ignorance of the causes of AD, several theories have been proposed over the years, and the main ones are below summarised.

2.6.1 Cholinergic hypothesis

This hypothesis is based on the observation of a significant loss of neurons in the cholinergic system in AD. Bartus and colleagues established the cholinergic hypothesis of age-related cognitive dysfunction and dementia in 1982,[18] based on studies describing significant changes in cholinergic markers in brains of elderly patients. These changes are related to a loss of cholinergic function at the neuronal level, leading to memory loss as the neuronal system disappears. The relationship between the cholinergic neurotransmission and memory was also demonstrated using cholinergic antagonists.[19]

The basal forebrain cholinergic system (BFCS) is mainly composed of cholinergic neurons which innervate the hippocampus (HC) (Ch1), limbic areas of the brain (Ch2 and Ch3) and the amygdala and brain cortex (Ch4). BFCS modulates attention, learning, memory, motivation, sleep and plasticity.[20]

As we age, a gradual loss of cholinergic function occurs due to gene expression alteration, intracellular signaling disruption, axonal transport dysfunction, and a decrease in axonal, synaptic and dendritic degeneration and trophic support. Furthermore, ageing

elevates the metabolic activity of basal forebrain cholinergic neurons (BFCN) greater than other cholinergic neurons, demanding more energy production. Therefore, acetyl-CoA resources are diverted from acetylcholine (ACh) synthesis to energy production, contributing to lower choline acetyl transferase (ChAT) activity, reduced ACh release, and, eventually, synaptic loss.[21] Although this atrophy occurs, the levels of nerve growth factor (NGF) implicated in the maintenance, development and function of BFCN, remain unaltered. NGF plays a key role in learning, memory processes, modulating ACh release and ChAT activity. This suggests that the cognitive decline in normal ageing is related to cholinergic dysfunction, which, over time leads to cell loss.[15]

In mild cognitive impairment and in the first stages of AD, a reduction of NGF high affinity receptor, TrkA, is related to an imbalance of NGF in favor of its precursor pro-NGF, which acts as a cell death mediator in BFCN.[22] In addition, decreased levels of NGF drives reduced ACh release and ChAT activity. Also, it diminishes choline reuptake, and reduces expression of muscarinic acetylcholine receptors (mAChRs) and nicotinic acetylcholine receptors (nAChRs) and promotes axonal, synaptic and dendritic atrophy. All these BFC deficits positively correlate with the degree of dementia which led to the formulation of the cholinergic hypothesis of AD, **Figure 2**.[15]

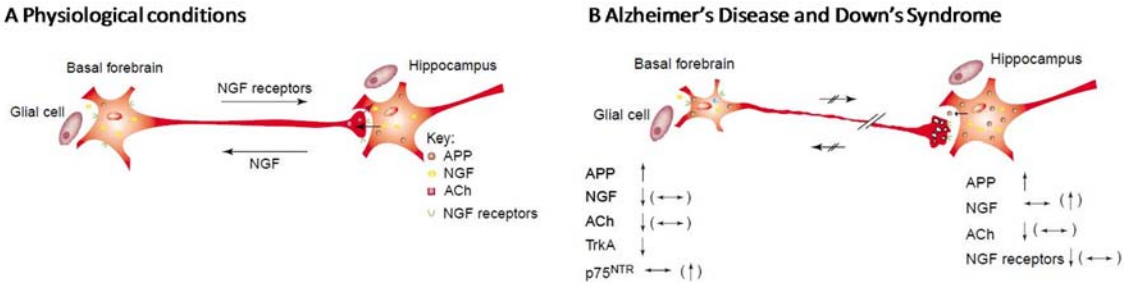

Figure 2. BCFN in **A)** normal conditions and **B)** pathological AD or DS. The signalling NGF-NGFr is mediated by sAPP. However, in AD or DS, the amyloidogenic processing of APP diminishes the sAPP form, leading to a reduction of NGF high affinity receptor, TrkA. This is related to reduced levels of NGF in BFCN, which in turn drives lower ACh release and ChAT activity. The decrease in trophic support due to axonal, synaptic and dendritic degeneration provokes gradual loss of cholinergic function and, eventually, neuron death. (Modified from Isacson *et al.*)[23]

Following this hypothesis, either by increasing the levels of ACh in the synaptic cleft, or selectively modulating the postsynaptic mAChRs or nAChRs, the cholinergic neurotransmission will be restored, preventing the cholinergic hypofunction, amd

therefore, cognitive impairment. Both ideas have already been exploited as therapeutic approaches that were commented on *Section 2.5.*

2.6.2 Amyloid beta hypothesis

Amyloid protein precursor (APP) is a type I transmembrane glycoprotein highly expressed in the brain. Although its precise biological function is still unknown, it seems to play a specific role in synaptogenesis and in neural maturation, differentiation and viability. Under physiological conditions, APP has a fast turn-over and is easily metabolized: α-secretase splits APP in an extracellular soluble sAPPα and a transmembrane C-terminal fragment (CTFα), which is further processed by γ-secretase leading to P3 and APP intracellular domain (AICD). None of these products are toxic. By contrast, under pathological conditions, APP is cleaved by β-secretase (also known as β-site amyloid cleaving enzyme 1, BACE1), releasing sAPPβ that is further processed by γ-secretase to produce mainly 40-aminoacid-long Aβ ($A\beta_{1-40}$) and AICD. However, the most expressed monomer in AD brains is $A\beta_{1-42}$, which is likely to form soluble oligomers, fibrils and finally, plaques **Figure 3**.[24]

Hardy and Higgins postulated the amyloid cascade hypothesis in 1992, based on the observation of accumulation of Aβ in the brain. The idea of Aβ accumulation as a critical event in the pathogenesis of AD was supported by the fAD patients characterization, in which it was discovered that mutations in *App*, and *Psen1* and *Psen2* enhanced the production of Aβ.[25] Conversely, clearance impairment, where APOE4 and higher BACE1 activity are involved, has been postulated as a driver for Aβ accumulation in AD.[26] This hypothesis postulates that the aggregation of soluble oligomers promotes P-tau which leads to the formation of NFT which promotes synaptic loss and, ultimately, cell death. This hypothesis is supported by the fact that cognitively healthy, elderly adults have high P-tau in HC, but no cell loss, suggesting that Aβ is triggering the development of AD.[27] However, no linear correlation between Aβ plaques and cognitive impairment has been detected. Aβ accumulation is an early event, starting 15-20 years before the onset of symptoms. Currently, it is increasingly accepted that it is a contributor to the advancement of the disease, although it is not the cause of AD.[28]

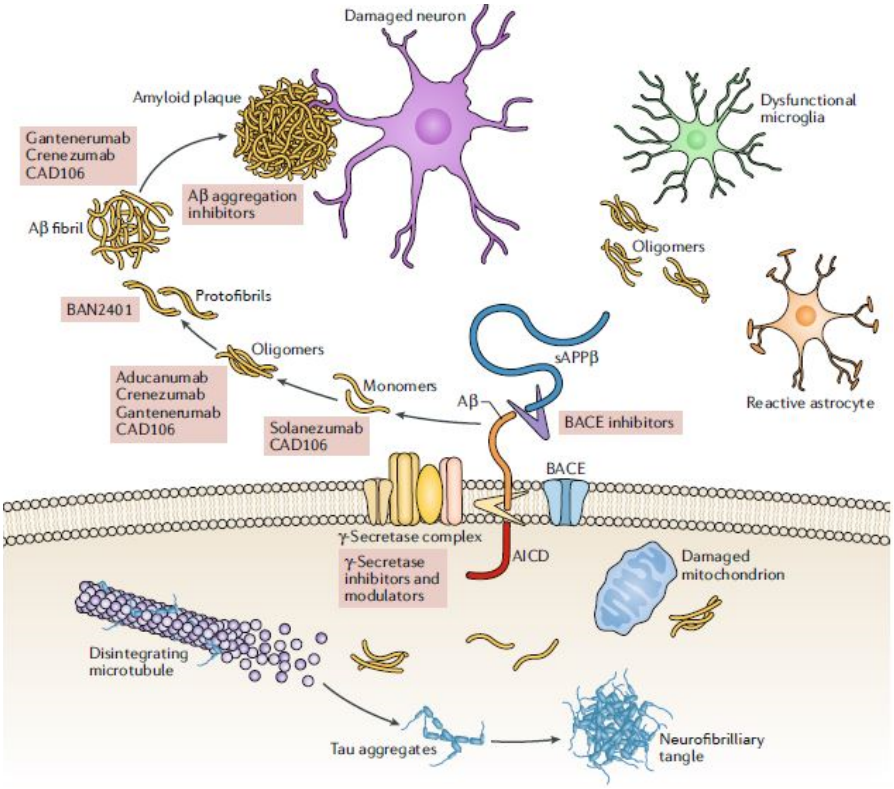

Figure 3. Amyloidogenic processing of APP under pathological conditions. APP is cleaved by BACE1, releasing sAPPβ that is further processed by γ-secretase to produce mainly $A\beta_{1-40}$ and AICD. However, the most expressed monomer in AD brains is $A\beta_{1-42}$, which forms soluble oligomers, fibrils and finally, plaques. Current anti-Aβ strategies in Phase III clinical trials for AD treatment are depicted.[26]

2.6.3 Tau hypothesis

This hypothesis is based on the appearance of P-tau. Tau's main function is to regulate the assembly and stability of microtubules, affecting axonal transport, synapses, protein trafficking and signalling.[29]

Tau has three domains: 1) the projection domain at the N-terminal half, 2) the proline rich domain and 3) the assembly domain at the C-terminal region. The proline rich domain is the target for serine/proline and threonine/proline directed kinases (PDPKs) to regulate the binding to tubulin by a phosphorylation/de-phosphorylation equilibrium. Finally, the assembly domain directly interacts with microtubules leading to their stabilization.[30]

Phosphorylation is required for optimal microtubule regulation. This action is executed by PDPKs, such as glycogen synthase kinase 3β (GSK-3β), or non-PDPKs, such

as protein kinase A (PKA) and CDK5, among others. The tau phosphorylation status is controlled by the serine/threonine protein phosphatase 2A (PP2A).[31] PP2A activity is compromised by 20 % to 30 % in AD. As a result, the amount of phosphorylated tau found is two to three fold higher when compared to physiological conditions. Finally, P-tau easily aggregates, generating paired helical filaments (PHF) and the subsequent NFTs formation.

P-tau disrupts microtubule assembly, which affects retrograde transportation, and eventually, leads to neuronal death. NFTs are one of the classic hallmarks of AD, and recently, it has been shown that the P-tau - free tau oligomers are toxic species that propagate trans-synaptically, as Braak described in 1997. Tauopathy spreading during ageing starts from the enthorinal region (stages I and II), continuing through limbic areas, such as the HC (stages III and IV), and on to the neocortex (stages V and VI), whereas Aβ exhibits the opposite progression, **Figure 4**.[32] Moreover, the asymptomatic stages I and II with P-tau already formed, do not present Aβ aggregates. In addition, recent PET studies have demonstrated that P-tau co-localises with neuronal atrophy and it is also directly proportional to the severity of cognitive impairment.[33]

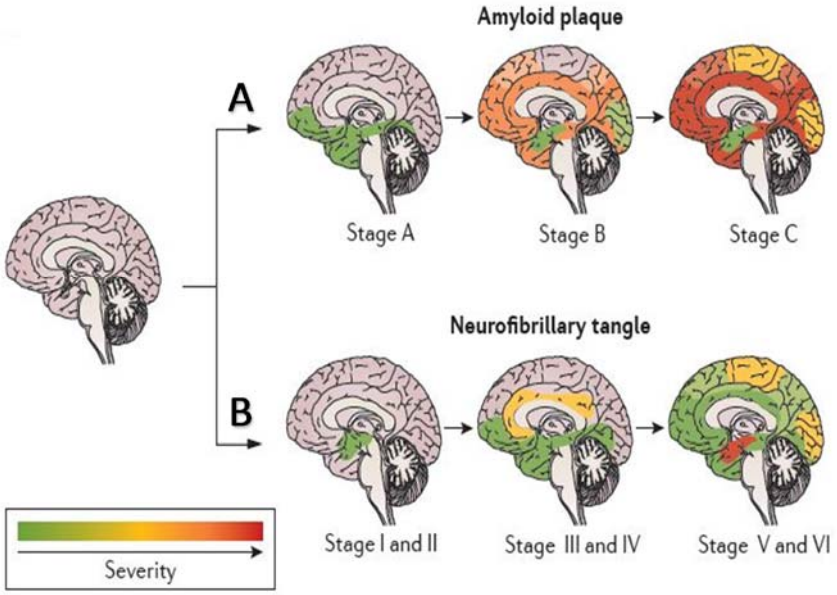

Figure 4. Pattern and severity of AD pathology with increased age. **A)** The evolution of Aβ deposition classified in the following stages: A, basal neocortex; B, neocortical areas and hippocampus; C, neocortex **B)** Spreading of tauopathy: I and II, transenthorinal region; III and IV, limbic area; V and VI, neocortex. (Modified from Masters *et al.*)[16]

This evidence suggests that tau pathology precedes Aβ accumulation and, although disease advancement is accompanied by Aβ plaque formation, Aβ fibrils do not induce NFTs formation. Recently, it has been shown that risk factors APOE4 and TREM2, as well as type II diabetes, are strongly connected with tau pathology.[34] In addition, the failures of anti-Aβ drug candidates, and the promising results of tau production suppression, indicate that tau is a key factor in AD progression, not Aβ.[34]

2.6.4 Oxidative stress hypothesis

From a chemical point of view, free radicals are species which contain one or more unpaired electrons in an atomic or molecular orbital. As electrophilic compounds, radicals are highly reactive, taking electrons from nucleophilic molecules, and thus, oxidizing them.[35] From a biological point of view, free radicals from O_2, known as reactive oxygen species (ROS) or N_2, reactive nitrogen species (RNS), are products of physiological metabolism.[36] For instance, NO is a signalling molecule involved in vasodilatation and immune response, being therefore ROS/RNS essential for life.[37]

The main source of ROS is the electronic transport chain (ETC) for ATP generation in mitochondria. For this purpose, electrons from energy rich molecules are needed, and it has been estimated that up to 2 % of them are leakage from Complex III in healthy conditions, reacting with O_2 to form superoxide anion radical, ($O_2^{\cdot -}$). This radical is readily eliminated by mitochondrial manganese superoxide dismutase (MnSOD) generating hydrogen peroxide (H_2O_2), **Figure 5**. In turn, H_2O_2 is transformed by glutathione (GSH) peroxidase and catalase (CAT)[22] into O_2 and H_2O molecules.[38] Another way of $O_2^{\cdot -}$ elimination is by metal (usually iron and copper couple) redox-cycling mechanism which involves two steps: firstly, $O_2^{\cdot -}$ reduces Fe^{3+} to Fe^{2+} obtaining O_2 and subsequently, Fenton reaction takes place where Fe^{2+} reduces H_2O_2, recovering Fe^{3+} and releasing hydroxyl anion, HO^- and hydroxyl radical, $HO^{\cdot}$, highly reactive radical with very short half-life.[39] Therefore, a tightly balance of these free radicals is accounted by two main mechanisms which maintain a tight control of free radical homeostasis.

However, during ageing, mitochondrial ROS balance is deregulated inducing an exacerbated oxidative damage. This observation led to the proposal of the *free radical theory of ageing* by Harman in 1956.[40] This theory try to explain ageing process as a free

radical accumulation, generating an imbalance between pro-oxidant and antioxidant defences, currently known, as the oxidative stress hypothesis. Further understanding on this field points to self-caused damage in mitochondria. ROS/RNS generated, damage mitochondrial deoxyribonucleic acid [41] causing accumulated mutations in ETC genes which results in an overproduction of ROS, driving a vicious cycle, **Figure 5**.[36]

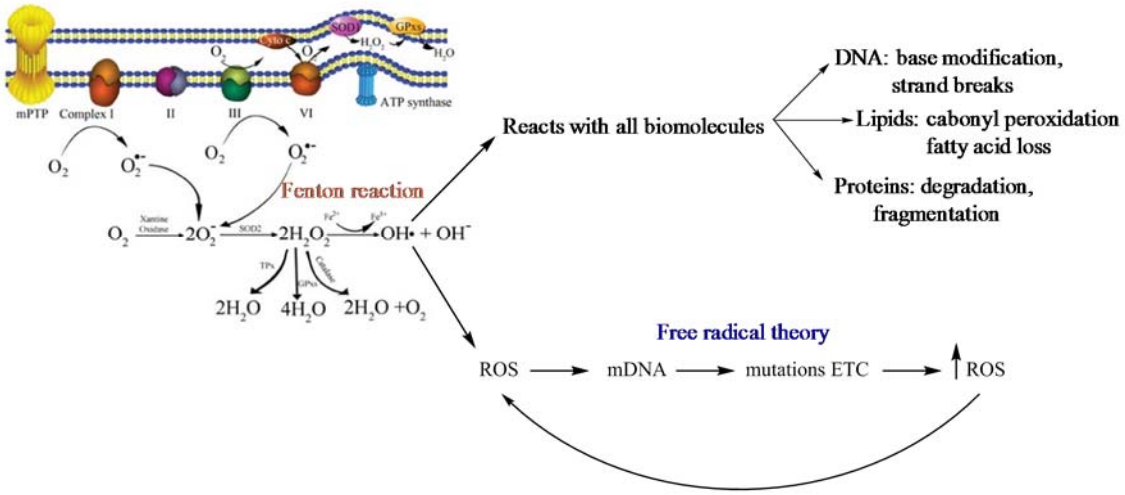

Figure 5. Scheme of oxidative damage derived from mitochondrial ROS generation. (Modified from Zhang *et al.*)[42]

Neurotransmission requires huge amounts of energy, thus brain consumes a large quantity of oxygen. This fact, along with low effectiveness of antioxidant system as well as high concentration of lipids in neurons, makes the brain even more susceptible to oxidative damage.[38] As ageing is a main risk factor of AD, oxidative stress and mitochondrial dysfunction are considered early contributors of the disease. Indeed, there are evidence of oxidative markers such as oxidized nucleosides derived from ribonucleic acid (RNA) or lipid peroxidation, that appear before neurofibrillary tangles formation or Aβ deposition.[43] Furthermore, a significant increase of oxidized proteins content in neurons has also been reported in presence of $A\beta_{1-42}$.[37] Thus, this hypothesis supports the idea that oxidative stress is a key player, not only as consequence, but also as causative of AD.[37]

2.7 Multifactorial hypothesis for Alzheimer's Disease

This hypothesis has been highly influential and many studies were carried out to demonstrate its validity. As AD knowledge advanced, new pathological insults were

found prompting the formulation of countless hypothesis to explain them, such as the cholinergic hypothesis, brain insulin resistance hypothesis, brain metabolic hypothesis, calcium hypothesis, innate immunity hypothesis, mitochondrial hypothesis, neuroinflammation hypothesis, oxidative stress hypothesis and excitotoxicity hypothesis.

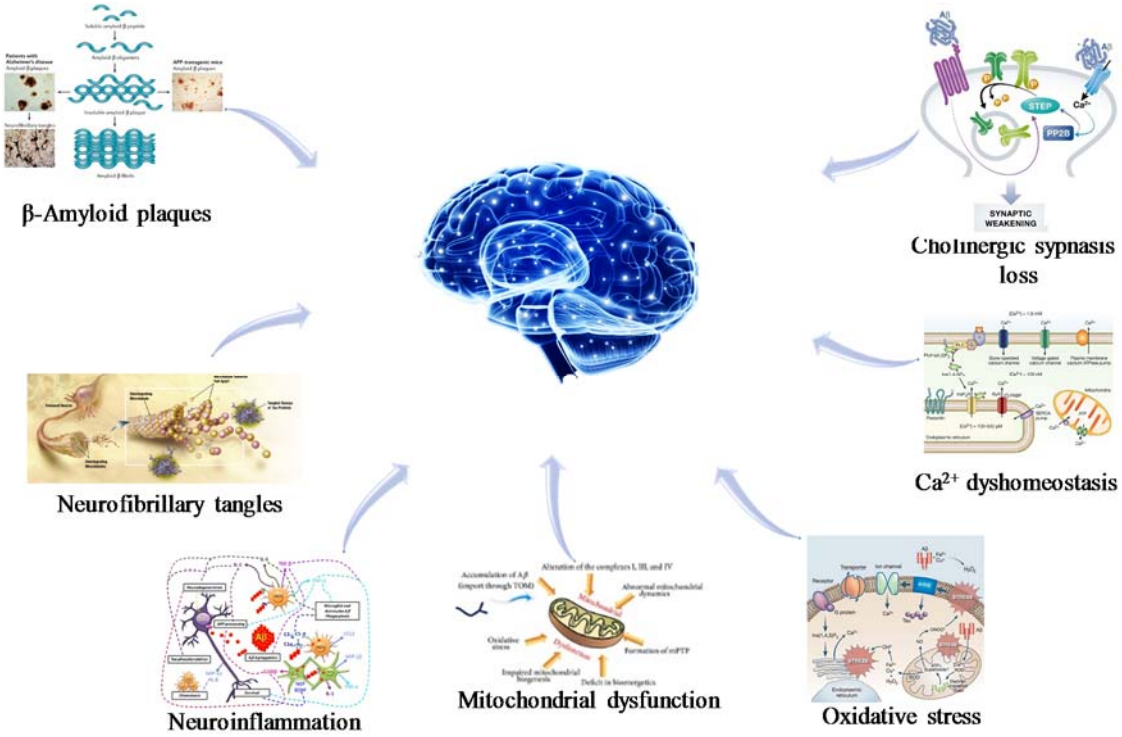

Figure 6. The multifactorial hypothesis of AD states that several etiopathological factors and mechanisms are involved in the pathogenesis of AD.

Nevertheless, Karl Herrup revisited and criticized the amyloid hypothesis in 2015. He elegantly explained that Aβ is neither necessary nor sufficient for AD. He suggested moving on from simplicity to complexity, and taking into account all the disease-causing options at the same time.[28] In this line, Gong *et al*[44] have recently proposed that the onset and development of LOAD arises from the imbalance between normal ageing and pathological risks, where insults are collectively provoked by the effects of multiple factors which are different for each individual. Therefore, an integrative multifactorial hypothesis is currently embraced. This new vision of AD invites to both targeting more than one pathological pathway to develop an effective therapy and recognizing the diversity among individuals, justifying the use of personalized medicine. Among the pathological pathways implicated in AD onset and development, we consider oxidative stress and neuroinflammation as key events contributing to AD prodromal phases.

2.8 Multitarget directed ligands as new approach of Alzheimer's Disease treatment

Current therapies are directed towards one target, based on the classical hypothesis of development "one target, one ligand", however it clearly failed to find a DMT. Thus, taking into account the multifactorial character of the disease, current AD drug discovery research is moving towards a new strategy which considers that acting on several targets simultaneously, would be a better strategy to stop the neurodegenerative process.[44] This can be achieved by multi-medication therapy (MMT), where a cocktail of two or more drugs with different MOAs are combined[45] and more recently proposed MTDLs, which are the objective of this Thesis.

In the MTDL strategy each pharmacophore may retain the ability of interaction with its target to produce the desired pharmacological response. Being only one molecule, it might show some of the advantages against MMT therapies like avoidance of drug-drug interactions which decreases off-target effects; improved bioavailability, pharmacokinetics, metabolism and therapeutic regimen as well as better patient compliance.[46] By contrast, despite the pathway for a single candidate focused on one target entails a tedious, costly and long term process, MTDLs added extra challenges. They should be carefully designed to obtain suitable binding affinity for multiple targets simultaneously, optimal adsorption, distribution, metabolism, excretion and toxicology (ADMET) properties, low off-target effects and the ability of permeate through BBB to effectively exert its required CNS action.

Focusing on the MTDL strategy, two main approaches can be performed to design this kind of molecules. Ligand-based design, implies known ligands for one target that either are screened against other targets or are tied to two pharmacophores together by a linker fragment, obtaining a single molecule. For instance, examples derived from this methodology are memoquin (**8, Figure 7**), that incorporates a benzoquinone fragment **6** into the scaffold of caproctamine **7**, being able to inhibit AChE, Aβ aggregation and showed free radical scavenger capacity; and, ladostigil (**10, Figure 7**), that combines rasagiline **9** and rivastigmine **3** to exert AChE, monoamino oxidase A (MAO-A) and

monoamino oxidase B (MAO-B) inhibition activity, anti-amyloidogenic properties and neuroprotective activity against oxidative stress toxicity.

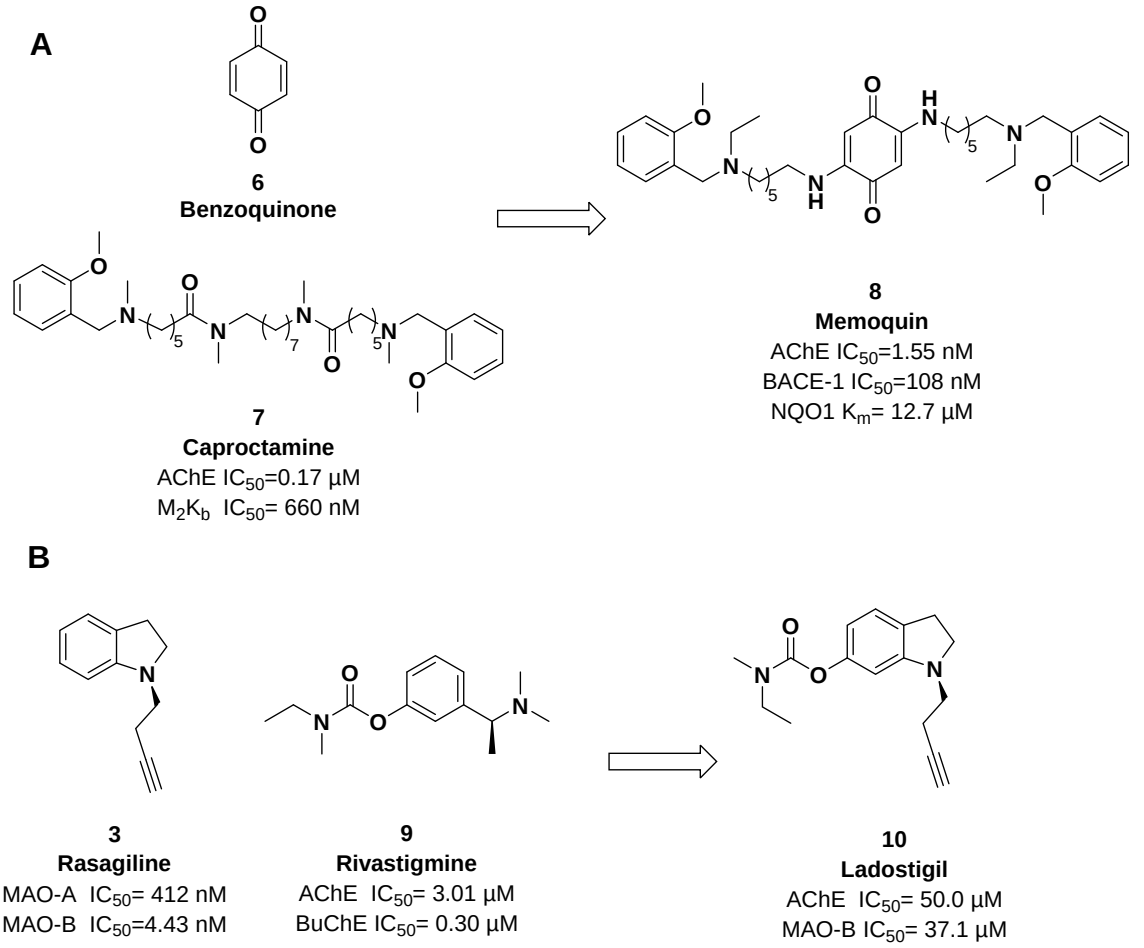

Figure 7. A) Memoquin and **B)** ladostigil, two examples of ligand.based design of MTDLs.

On the contrary, structure-based design focuses on structural requirements of the binding site of the selected target. In this case, *in silico* methods such as virtual screening, quantitative structure-activity relationships, molecular modelling and molecular simulations are helpful to optimize and accelerate the drug discovery process to find effective DMTs to treat AD.[47]

2.9 α7-nAChRs as therapeutic target in Alzheimer's Disease

The α7-nAChR participate in cholinergic neurotransmission, being mediators of cholinergic signalling involved in the modulation of memory and cognitive functions. Nevertheless, in AD their expression and function is altered, leading to the activation of pro- and anti-survival pathways depending on the stage of the disease, the cell type

implicated or the ligand used. For that reason, the α7-nAChR is a promising but complex target for the cholinergic-based treatment of AD.[48]

2.9.1 Structure, distribution and function

nAChRs are ligand-gated cation selective channels belonging to the Cys-loop superfamily, that includes a subset of receptors for γ-aminobutiric acid ($GABA_A$, $GABA_C$), 5-hydroxytryptamine (5-HT3, 5-HT-gated chloride channels) and glycine receptors.[49] The ionic pore is formed by the assembly of five subunits composed of a large amino-terminal and a short carboxy-terminal extracellular domains (ECD), four transmembrane helices (TM1-TM4) and a variable cytoplasmic loop, yielding homo- or hetero- pentameric receptors. Sixteen different human subunits have been identified at the moment: α1, β1, γ, δ (fetal) and ε (adult), expressed in muscle, and α2- α7, α9, α10, β2-β4, expressed more widely in the nervous system.[50] The endogenous neurotransmitter of nAChRs, ACh, binds to the orthosteric site (A). This site is located at the interface between two subunits, the principal, always an α-type subunit, and complementary subunit at the ECD.

The α7-nAChRs are homopentameric receptors with five orthosteric sites which are lined with aromatic residues highly conserved placed on the loops A, B, C on the principal face, and D, E, F loops on the complementary face.[51]. Although only one is needed for its activation, two non-consecutive sites are required for a stable open-state, as endogen ACh, causing the entry of Na^+, Ca^{2+}; the latter with high permeability. The third non-consecutive site occupied is more efficacious, as it enhances the stability, allowing positive modulation. However, if four or five orthosteric sites are occupied leads to its desensitization, a crucial state which controls the open-channel lifetime.[52] This positive allosteric modulator (PAM) insensitive desensitization state (D_i) was proposed to be the main mechanism to close the channel, and it cannot be immediately open. This could be interpreted as a mechanism to protect α7-nAChR expressing cells from cytotoxicity caused by Ca^{2+} overload.[53]

The α7-nAChR is one of the most predominant nAChR expressed in the brain, together with α4β2, especially within BFCS, a region intimately linked to cognition as described before. α7-nAChRs are located on neurons, outside of the synaptic cleft at pre-

and post-synaptic locations where they promote neuronal excitability and neurotransmitter release, as well as extrasynaptically, participating in non-excitable communication.[54] They are also expressed in non-neuronal cells, including astrocytes and microglia, where they are involved in inflammation and neuroprotection.[55,56]

2.9.2 α7-nAChR pharmacology: ligands, conformational states and binding sites

As a ligand gated cation channel, it has different conformational states depending on the type of ligand attached to it. Namely, agonists and antagonists, bind to the A. The former has affinity for the open state (O*) leading to cation influx, although, if the occupancy is too high, the channel conformation switches towards D_i, **Figure 8**.[57] There are partial agonists, which also have affinity for O*, although do not elicit a full response like endogen ligand. Therefore, they have an intrinsic activity ranged between 0, no activity, and 1, full agonist response. In addition, increasing concentrations of a partial agonist can block the effect of a full agonist. Whereas, an inverse agonist is a full agonist but, it gives an opposite pharmacological response.[58]

On the other hand, antagonists have affinity for the closed resting state (C), impeding cation entrance and receptor activation, leading to a null intrinsic activity, **Figure 8**.[57] If they bind reversibly to the orthosteric site, they are competing with the agonist, inducing a shift of the concentration-response curve of the agonist towards higher concentrations without modifying the maximum response. On the contrary, non-competitive antagonists decrease the maximum response due to irreversible binding to the same site of the agonist.[58]

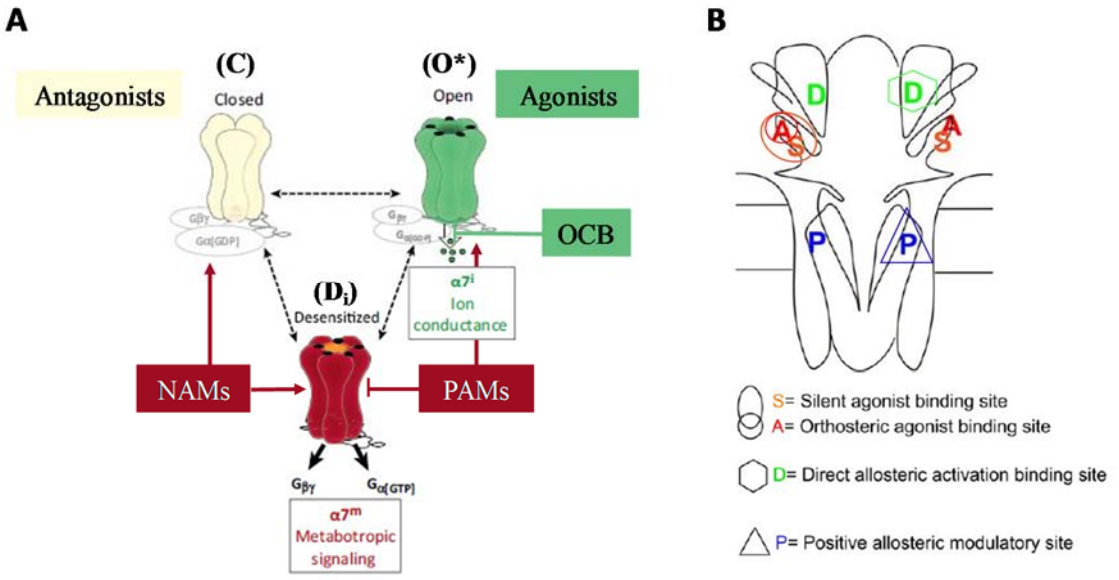

Figure 8. A) Representation of minimal conformational states, closed (C), open (O*) and desensitized (Di) driving ionotropic and metabotropic α7-nAChRs activities. Noticed that O* and D_i are ligand-bind states. Antagonists have affinity for C state, whereas agonists have affinity for O*. Open-channel blockers (OCB) bind to the channel, blocking cation entrance. Allosteric modulators can positively or negatively modulate D_i, and O* or C states, respectively. Scheme modified from Kabbani and Nichols.[59] **B)** Location of binding sites for most of the possible ligands in α7-nAChRs, modified from Papke *et al*.[57]

In addition, there are allosteric modulators which bind elsewhere apart from orthosteric site and they do not have activity themselves but positively or negatively modulate the receptor states.

Positive allosteric modulation (PAMs) enhance agonist effects being classified in two categories: 1) Type I PAMs stabilize O* without modifying desensitization, and 2) type II PAMs characterized to lengthen peak currents by increasing the energetic barrier between O* and D_i states, slowing down the onset of desensitization. Moreover, they are able to reactivate desensitized receptors by inducing three conformational changes, desensitized PAM sensitive, flip closed (F) and PAM-dependent open (O') states.[60]

Negative allosteric modulators (NAMs) inhibit agonist effects. Two types of NAMs are described, open channel blockers (OCB) which directly hinder the ion permeation not allowing rapid unblocking, and ligands which stabilize C or D_i states. It is noteworthy to mention that high concentration of some agonists can act as OCBs.[52]

Silent allosteric modulators[61] do not modulate orthosteric ligands but they do influence on allosteric modulators due to allosteric binding site competition.

Some molecular docking studies showed two main allosteric binding sites for PAMs, NAMs and SAMs. One located in the TM within four helices of a single subunits called intra-subunit transmembrane cavity (P), and the alternative (S), localized in the extracellular domain nearby A, consider them jointly as A/S.

Allosteric agonists, commonly known as ago-PAMs, are peculiar because they stabilize O* without an orthosteric ligand involving two binding sites simultaneously, the conventional PAM 'P' site and a new extracellular 'D' site, localized at the vestibule of the receptor.

Finally, silent agonists, produces little activation by itself stabilizing D_i, leading to a non-conducting state. However, in the presence of PAMs or allosteric agonist, the channel conformation changes towards D_s which connects with F and, consequently O', favouring a persistent channel activation.[57]

2.9.3 Intracellular signalling cascades and their implication in neuroprotection.

The α7-nAChR is unique within nAChR family because has a dual ionotropic and metabotropic nature. As a cationic transmembrane channel, property obtained predominantly because of α-helical M2 domain, α7-nAChRs initiates three types of calcium signals. First of all, direct influx due to its high permeability to Ca^{2+}; secondly, indirectly through the activation of voltage dependent calcium channels (VDCCs) due to the membranes depolarization induced by the activation of α7-nAChR; and finally, the first two sources can trigger the calcium induced calcium release (CICR) from the endoplasmic reticulum through the ryanodine and inositol (1,4,5)-triphosphate receptors (IP_3R). These three mechanisms promote different downstream intracellular signaling according to the duration and timing, such as regulation of cytoplasmatic Ca^{2+} (instantaneous effect), nAChR desensitization (short term effect) or involvement on synaptic plasticity or memory (long term effect).[62]

It is important to note that, although Ca^{2+} signal elicited by α7-nAChR activation induces neuroprotection cascade activation,[63] there are neuroprotection routes independent of ionotropic signalling property.[64] It is rather a result of metabotropic counterpart activation due to conformational changes of the receptor.

Thus, the metabotropic pathway has two main downstream signalling cascades. There are G proteins linked to M3-M4 intracellular loop of α7-nAChR.[48] When the receptor is stimulated, the $G\alpha_q$ subunit activates phospholipase C (PLC), to metabolize phosphatidylinositol 4,5-bisphosphate (PIP2) in IP3 fostering inositol induced calcium release (IICR). This cascade activates cytoskeletal remodelling including differentiation, migration and synaptogenesis.[59] In addition, PKC is activated by diacylglycerol formation, that, in turn, promotes the phase II antioxidant response.[48]

Moreover, it has been shown that Janus kinase 2 (JAK2) is physically associated to α7-nAChRs.[65] Kihara and colleagues demonstrated that when α7-nAChRs were stimulated with nicotine, the phosphorylation of JAK2 was observed, leading to the activation of the phosphatidyl inositol 3 phosphate kinase/protein kinase B (PI3K/Akt) pathway. As a consequence, the anti-apoptotic protein Bcl2 was upregulated, prevented cell death induced by Aβ-treated cortical neurons.[66] Significant increased levels of Bcl2 were also observed when galantamine, an allosteric modulator of nAChRs, was employed in Aβ-treated SH-SY5Y cells, and neuroprotection was reversed by the selective α7-nAChR antagonist, α-bungarotoxin.[67] Besides, another study in SH-SY5Y undergoing apoptosis, showed how α7-nAChRs stimulation with PNU282987, activated Nrf2-EpRE pathway (the main cell antioxidant defence mechanism, below detailed), since the expression of the antioxidant and anti-inflammatory enzyme heme-oxygenase 1 (HO-1) was observed.[63]. Those evidences indicate the main role of α7-nAChRs activation in the pro-survival and neuroprotective pathways.

2.9.4 α7-nAChRs and AD

Significant α7-nAChRs alterations have been reported in postmortem AD brains depending on the stage of the disease at transcription, translation and posttranscriptional modifications levels, as well as receptor reposition and function.[68] For instance, decreased protein levels of α7-nAChR in HC, but higher levels of α7 mRNA have been described in brain samples of AD patients.[69,70] There is, also, decreased radioligand binding sites indicating α7-nAChR loss of function. This lack of functionality has been related to the high binding affinity of $A\beta_{1\text{-}40}$ / $A\beta_{1\text{-}42}$ to α7-nAChRs.[71] In support of this observation, there are some evidences of increased levels of these receptors in neurons, astrocytes and

microglia after chronic Aβ exposure.[72] This effect might be a compensatory mechanism consequence of Aβ binding to α7-nAChRs inhibition by Aβ, triggering an upregulations of their expression that may play a toxic role. In fact, Dineley and colleagues showed a dual behaviour of this interaction. Aβ has a stimulatory role when there are a few monomers of Aβ interacting with α7-nAChRs, promoting a signalization pathway of neuroprotection. Nevertheless, as AD pathology advances and the number of oligomers increase, the effect is the opposite. Aβ oligomers antagonize α7-nAChRs, silencing them, promoting the loss of the cholinergic phenotype and synaptic plasticity deficits, which lead to learning and cognitive impairment, neuroinflammation and finally neurodegeneration.[54] Additionally, some experimental data indicates that this interaction promotes Aβ oligomers internalization and its accumulation inside the cell.[73] Its internalization may lead to the plaque formation when the host cell eventually dies and spreads its intracellular content in the brain parenchyma.[74] Connecting to the cholinergic hypothesis, the fact that the Aβ exerts high binding affinity to α7-nAChRs, might explain the cholinergic neuronal loss at BCFN, as these receptors are widely expressed in those regions.

2.9.5 α7-nAChR modulation as therapeutic target

The aforementioned facts, position α7-nAChRs as a promising but complex drug target for AD treatment. In fact, numerous preclinical studies showed the positive effects of α7-nAChR activation for AD treatment, as recently reviewed.[75] Selected examples are summarizing in this section.

PNU282989 (**11**, **Figure 9**), a potent full agonist α7-nAChR, protected against subchronic oxidative stress triggered by a cocktail of lipopolyssacharid (LPS) and antimycin A in rat hippocampal organotypic cultures via HO-1 induction.[76] Moreover, it regulates mitochondrial biogenesis in microglia through Nrf2/HO-1/PCG-α cascade mechanism.[77] Nevertheless, it was not safe as therapeutic target, as it presented activity on the human Ether-go-go potassium channel (hERG).[78]

GTS21 (**12**, **Figure 9**), a α7-nAChR partial agonist, showed *in vitro* a reduction in the depressed α7-nAChR response induced by $A\beta_{25-35,}$ as well as a reduction in tumor necrosis factor α (TNFα) formation induced by LPS. Also showed an improvement in

cognitive deficits in rodents and primates. It entered in phase I clinical trials after promising preclinical results, however, GTS21 did not show efficacy in cognitive improvement of schizophrenic patients who experimented a worsening negative symptoms. Of note, GTS-21 has higher binding affinity for α4β2 nAChR and also binds to α3β4. Thus, the lack of selectivity does not enable to ensure its pharmacological effects are result of just α7-nAChR activation.

Encenicline (EVP-6124) (**12**, **Figure 9**), a α7-nAChR partial agonist, has demonstrated promising results in phase I and II trials involving mild to moderate AD patients, being well tolerated and showing better cognitive function in comparison to placebo. Unfortunately, EVP-6124 was rejected after failure to improve endpoints compared to placebo group in a phase III trial for schizophrenia ended in 2016, and for that reason, an AD trial was withdrawn in 2017.

PNU120596 (**13**, **Figure 9**), is the most potent type II PAM. It extended the α7-nAChR activation in hippocampal neurons and glia and thus, enhancing the cognitive improvements of an AChEi in both rodents and primates. Nevertheless, it was not suitable for entering in clinical trials as it showed neurotoxicity by intracellular Ca^{2+} overload.

GAT107 (BP-TQS) (**14**, **Figure 9**), is an ago-PAM, and it was first described as anti-inflammatory and antinociceptive agent in a mouse model of chronic inflammation and neuropathic pain.[79]

Methyllycaconitine (MLA**)** (**15**, **Figure 9**), is a highly potent and selective natural toxin, which antagonizes α7-nAChR. Although it impedes the ion influx to cytoplasm, it reduced LPS-induced TNFα release of microglia.[80]

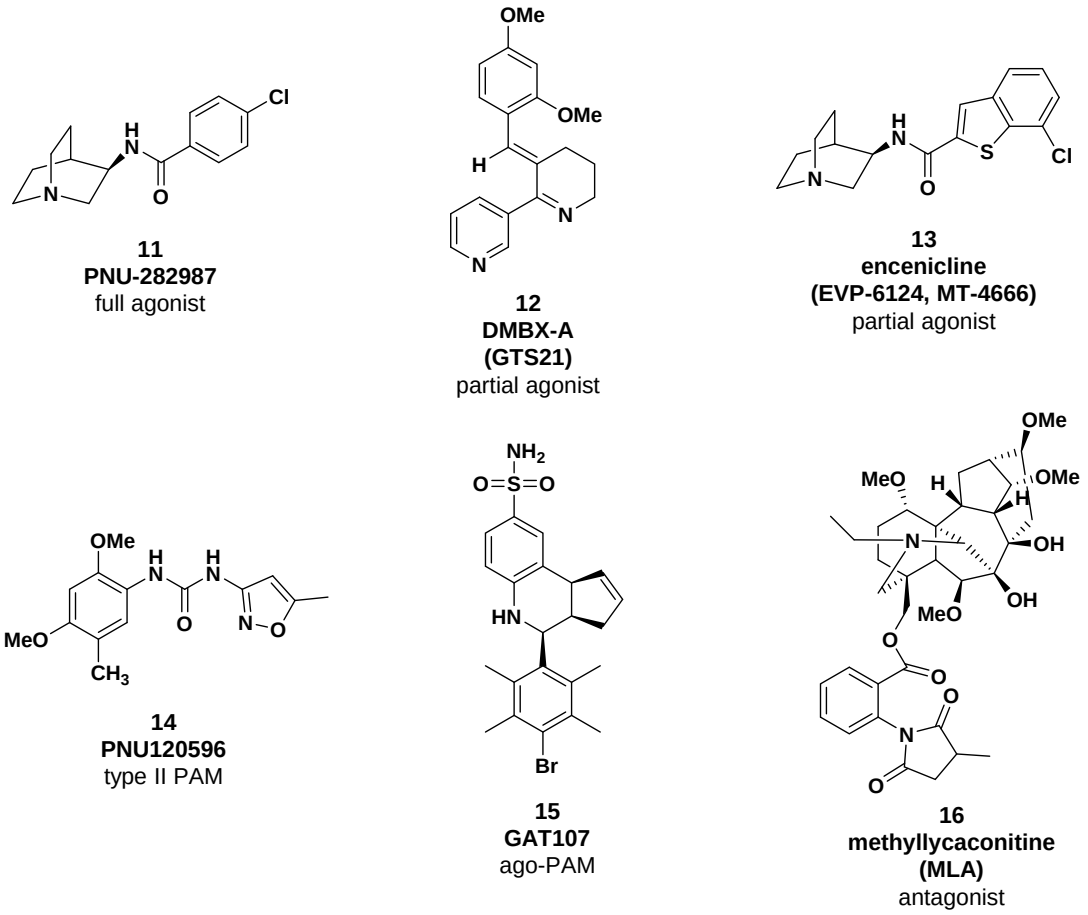

Figure 9. Structures of known α7-nAChR ligands.

In spite of exerting very different effects on channel activation, ligands can display similar pharmacological profiles, for instance GTS21 and MLA showed anti-inflammatory activities as cholinergic anti-inflammatory pathway inducers. The apparent contradiction of α7-nAChR activation or inactivation have both positive and negative effects relies on the α7-nAChR conformational changes and the ionotropic and metabotropic nature. Therefore, this field is highly interesting since understanding the behaviour of α7-nAChRs will allow the rational design of new molecules and the development of new drugs.

2.10 Nrf2 transcription factor as a key antioxidant therapeutic target

The Nuclear factor erythroid 2 – related factor 2 – electrophile response element (Nrf2-EpRE) pathway is the master regulator of the antioxidant phase II response.

Surprisingly, although oxidative stress is exacerbated in AD, this defence pathway is downregulated, which further contributes to oxidative damage and subsequent neuronal death.[81] Therefore, activation of the endogenous antioxidant machinery has been pointed as a key target to reduce characteristic AD increased oxidative stress.[82]

2.10.1 Nrf2 structure and activity regulation

Nrf2 is a key cell redox maintenance transcription factor which regulates over 250 genes. Consequently, its activity and abundance is tightly regulated at transcriptional and post-transcriptional level. It belongs to the cap "n" collar (CNC) subset of basic–region leucine zipper (bZIP) transcription factors family and it counts with seven Nrf2-ECH homology domains (Neh1-7). From amino–terminal to carboxyterminal, the domains host different functions. Neh2 domain presents two amino acid motifs (DLG and ETGE) which are recognized by the Nrf2 cytosolic repressor Kelch-like ECH-associated protein 1 (Keap1). Neh4 and Neh5 are transactivation domains as well as last positioned Neh3 domain, and together, they activate Nrf2 target genes transcription. Neh7 interacts with retinoid X receptor α leading to Nrf2 transcription activity repression. Neh6 contains two amino acid motifs (DSGIS and DSAPGS) which mediate the interaction with β-transducing repeat-containing protein (β-TrCP), a Nrf2 negative regulator. Neh1 domain is made up of CNC-bZIP region indispensable for DNA binding and small musculoaponeurotic fibrosarcoma (sMaf) proteins dimerization partners.[83]

Although there are different pathways for Nrf2 protein levels regulation, the following two proteasomal degradation processes are approachable for pharmacological targeting. In basal homeostatic conditions Nrf2 is bounded to the Keap1 dimer. This adaptor protein links Nrf2 with the E3 ligase complex comprised by Cullin 3 and RING-box protein 1 (Cul3/RBX1), promoting its ubiquitination and subsequent 26S proteasomal degradation. Another mechanism for Nrf2 proteasomal degradation is mediated by glycogen synthase kinase-3β (GSK-3β). This kinase phosphorylates DSGIS motif of Neh6 domain, favouring the association of β-TrCP, a protein adaptor of Cullin1 (Cul1) /RBX1 E3 ubiquitin ligase complex. Therefore, Nrf2 is constantly renewed, showing a very short half-life (*ca*. 20 minutes), maintaining its protein levels low in normal state.[84]

Under oxidative conditions or in the presence of xenobiotics, the main way of Nrf2 release is the "hinge and latch" mechanism where Keap1 is inactivated by oxidation of its several key cysteine residues. Then, non-repressed Nrf2 rapidly translocates into the nucleus where it associates with sMafs. This heterodimer binds to the EpRE in the promoter region of target genes. Once there, Nrf2 recruits co-activators such as CREB binding protein, components of the transcription machinery and chromatin remodelers, favouring the attachment of RNA polymerase II (Pol II).[83] Then, after phosphorylation of Ser2 and Ser5 of Pol II, gene expression is initiated. EpRE sequences encode genes involved in GSH production, γ-glutamyl cysteine ligase modulator subunit (*Gclc*) and γ-glutamyl cysteine ligase catalytic subunit *(Gclm)* and regeneration, ROS and xenobiotics detoxification NADPH:quinone oxidoreductase (*Nqo1*), glutathione peroxidase (*Gpx2*), glutathioneS-transferase pi 1 (*Gstp1*), thioredoxin (TXN)-based antioxidant system (*Txn*), nicotinamide adenine dinucleotide phosphate (NADPH) regeneration (*Pgd*), heme and iron metabolism (*Hmox1*), inflammatory response (*Il17d*), proteostasis (*Sqstm*), lipid (*Acc1*), pentoses (*G6pdh*) and purines (*Ppat*) metabolisms.[82]

Hence, Nrf2 induction promotes both constitutive and inducible expression of antioxidant and anti-inflammatory enzymes such as HO-1. HO-1 deserves special attention since catalyses heme group into biliverdin which is rapidly reduced by biliverdin reductase, in bilirubin, CO and Fe^{2+}. Both biliverdin and bilirubin are potent antioxidants, CO activates p38 mitogen-activated protein kinase (MAPK), therefore, inhibiting NF-κB nucleus translocation.[85]

2.10.2 Nrf2 and Alzheimer's Disease

Nrf2 expression is naturally decreased during ageing due to increase of its repressors. Therefore, the downstream processes dependent of this transcription factor are attenuated.[86] During ageing, GSK-3β is overexpressed, diminishing Nrf2 activation. As ageing is the main risk factor of AD, it is reasonable to think that Nrf2 levels are also downregulated. Additionally, due to exacerbated oxidative stress, high nuclear Nrf2 translocation would be expected, however, low levels of nuclear Nrf2 were found in HC neurons of AD human brains.[81] Thus, reduced expression of HO-1 has been detected in choroid plexus epitellium, cerebrospinal fluid (CSF), plasma, as well as a 25 % to 35 %

less expression in neurons. Conversely, high levels of HO-1 were reported in astroglia of HC and cortex[85] and Nrf2 upregulation in microglia.[87]

2.10.3 Nrf2 induction as therapeutic target

Clearly, the Nrf2-EpRE pathway is deregulated in AD. Hence, the reestablishment of its well-functioning is a good target candidate to develop disease modifying therapies. In fact preclinical and also, clinical studies demonstrate that the use of Nrf2 inducers promote antioxidant, anti-inflammatory effects.

As previously mentioned, since Nrf2 is finely regulated, there are different strategies to induce its release and stability. Some natural antioxidant dietary products such as sulforaphane (SFN) (**17**, **Figure 10**), from broccoli sprouts, resveratrol, from red grapes, or curcumin, from turmeric spice, share, chemically talking, the same electronic property. They are electrophilic molecules which can react and bind covalently to sulfhydryl groups of cysteines contained in Keap1 (**18**, **Figure 10**), impairing its substrate adaptor function leading to Nrf2 release.[88] For instance, SFN showed protection against $A\beta_{1\text{-}42}$ in mice neuroblastoma cells by the activation of proteasome.[89] Also, despite of having a short half-life, repeated supply of SFN led to long term HO-1 and NQO1 expression in astrocytes.[90] Furthermore, SFN improved memory impairment and attenuated Aβ aggregates in HC and cortex of mice treated with D-galactose and aluminium.[91] Noteworthy, similar to SFN as alkylating agent, dimethyl fumarate is actually the only Nrf2 inducer in clinic for the treatment of relapsing-remitting multiple sclerosis.[92] However, this kind of compounds can easily react with nucleophiles present in cells, showing off-target effects.[93]

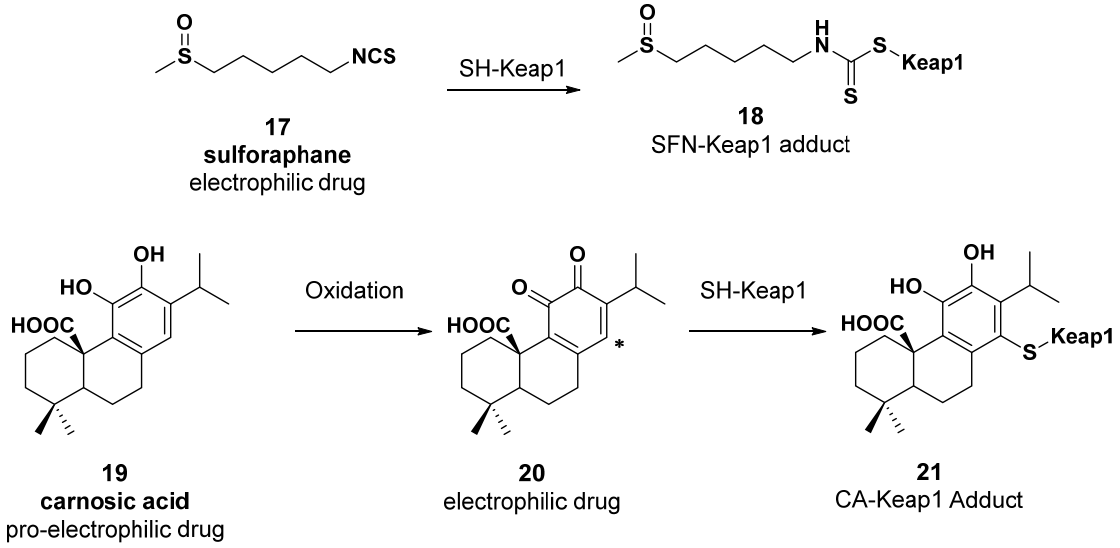

Figure 10. Examples of electrophilic and pro-electrophilic drugs and their mechanism of action.

To overcome secondary effects, pro-electrophilic drugs (PEDs) became a more attractive strategy. *p*-hydroquinone and *o*-hydroquinone structures act as pro-drugs as they are not active electrophiles until they are in the presence of oxidative conditions where they are converted into quinones, (**20**, **Figure 10**). Carnosic acid (CA) (**19**, **Figure 10**) was able to increase GSH by direct S-alkylation with Keap1 cysteines, protecting cortical neurons from NMDA damage.[94]

Additionally to PEDs, recently, non-covalent modifiers are gaining much attention. Several small molecules have been identified as Nrf2-Keap1 protein-protein interaction (PPI) inhibitors such as tetrahydroisoquinolines, thiopyrimidines or ureas, or Nrf2-β-Trcp PPI inhibitors, which are able to more specifically disrupt the interaction between Nrf2 and the repressor at a reversible manner, preventing the undesirable off-target effects.[95,96]

2.11 Melatonin as scaffold for drug development

N-acetyl-5methoxytryptamine (melatonin) was first isolated in cow pineal glands by Lerner and colleagues in 1958.[97] It is an evolutionary conserved molecule as it is present not only in vertebrates but also in alga, bacteria, fungi and plants. This wide distribution makes melatonin, to mediate diversity functions for instance, pigmentation, cell proliferation, differentiation, and the most recognized, circadian rhythm regulation.[98]

In mammalians, melatonin is a neuro-hormone synthetized mainly, but not exclusively, by the pineal gland, since there are some other extra-pineal sources like brain, bone marrow, immune cells, gut, retina or skin. It possesses a light-dependent circadian release pattern, achieving the maximum level at nighttime. Melatonin secretion starts six months after birth and reaches the highest peak between third and sixth years, followed by a constant decline during ageing, where after seventy years is almost absent.[99]

2.11.1 Functions and intracellular signal transduction

Precisely, because of easily oxidation, one of well-known functions of melatonin is its great ROS/RNS scavenger capacity. By donation of a single electron, melatonin can reduce $HO^{\cdot}$, $O_2^{\cdot -}$, H_2O_2 and $ONOO^{-}$, causing a series of radical chain reactions of which metabolites, AMFK and AMK among others, propagate the scavenger effect. Thus, for a single molecule of melatonin up until ten ROS can be reduced.[100]

Due to its amphiphilic character, melatonin is able to cross all cell membranes, thus it is widely distributed throughout the body. Melatonin can exert its brain functions by multiple manners. The most studied and characterized receptors are MT1 and MT2. They are G-protein coupled receptors (GPCRs), expressed by neurons and glial cells in HC, suprachiasmatic nucleus, retina, cerebral and cerebellar cortex, thalamus and pineal gland. Melatonin binding to MT1 produces adenylate cyclase inhibition, and hence, downregulates PKA.[101] Moreover, activates MAPK and PI3K/Akt signaling cascades promoting both neuroprotective and anti-inflammatory effects.[102] Also, MT1 plays a role in glutamatergic synaptic transmission.[103] In line with this, MT2 stimulation, is involved in synaptic plasticity and memory formation through the G_q protein. The MT2 signal transduction promotes a dual function of PKC activation and Ca^{2+} release that fundamentally regulates circadian rhythm.[103]

Another receptors related to melatonin are MT3, or human homolog NQO2, which promotes detoxifying effects; GPR50, although melatonin is not a ligand, it dimerizes with MT1 avoiding its activation and retinoid-related orphan nuclear hormone receptors (RORs) which mediates some of the melatonin circadian effects and also immunomodulatory effects.[101] Finally, melatonin can link to intracellular proteins like calmoduline, impeding its binding with Ca^{2+}. This rises brain derived neurotrophic factor

(BDNF) levels in HC with consequences in synaptic plasticity and transmission leading to cognitive function improvements.[103]

2.11.2 Melatonin in ageing and Alzheimer's Disease

Sleep-wake rhythm disruption due to melatonin decline is well-known during ageing. Pineal gland is progressively calcified with age, and it is thought that has an effect on disturbing circadian rhythmicity. However, there is no correlation of pineal metabolism decrease with calcification rising. Instead, some studies point out reduced environmental light exposure and less capacity of light transmission by lens as main reasons.[104]

In AD patients, melatonin decline is even more obvious. A study comparing subjects with no symptoms (Braak stage 0) with patients in preclinical Braak stages I/II (NFT in transentorhinal region with no symptoms) or AD patients Braak VI (NFT in neocortical area with AD dementia) showed alterations in the synthesis of melatonin as well as noradrenergic innervation of pineal gland. Regarding preclinical AD patients, the main differences found were disappearance of β_1-adrenergic receptor mRNA circadian rhythm which is responsible for lack of melatonin diurnal rhythmicity, and an upregulation of MAO-A which implies an increasing 5-HT oxidation, leading to a nocturnal melatonin drop. In AD patients, even less amount of melatonin is synthetized because of lower TPH mRNA levels impedes enough conversion of Trp into 5-HT. Furthermore, the day/night difference of β_1-adrenergic receptor mRNA levels presented in Braak stage 0, disappeared and MAO-A upregulation, reduced noradrenalin concentration. As consequence, noradrenergic system dysregulation was produced. Interestingly, melatonin decline was correlated with AD progression and due to the fact that a correlation between CSF and plasma levels was found, melatonin concentration is an indicative of AD progression. Thus, it could be considered as early marker.[105]

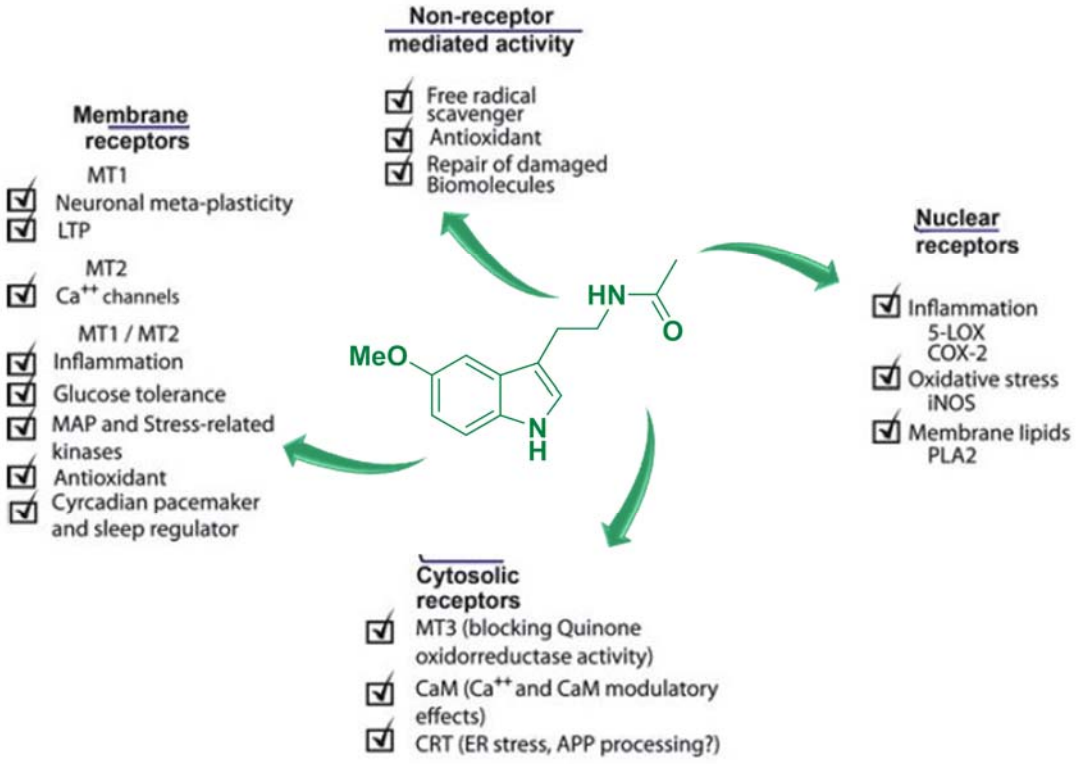

Figure 11. Pleiotropic effects of melatonin to decrease neurodegenerative process. This neurohormone can act in a receptor dependent or independent manner, leading to antioxidant and anti-inflammatory properties. (Figure modified from Rosales-Corral *et al*)[106]

Aforementioned facts make melatonin supplement a good clinical practice to avoid its deficiency. Certainly, a wide variety of actions were reported after its administration. Apart from its potent action against Aβ-induced oxidative stress by acting directly as scavenger,[107] or indirectly by upregulation antioxidant enzymes,[108] melatonin has anti-amyloidogenic,[109] anti-tau hyperphosphorylation,[110] anti-inflammatory,[111] anti-apoptotic[112] and immunomodulatory[113] effects as well as memory formation regulation.[103]

3 Hypothesis and Objectives

3.1 Hypothesis

AD is considered a multifactorial disease characterized by cholinergic synaptic loss and exacerbated oxidative stress among other factors. Brain has two main mechanisms to balance redox status. The antioxidant enzyme system regulated mainly by the Nrf2-EpRE pathway and the low molecular weight antioxidants such as melatonin. Nevertheless, despite increasing oxidative stress in AD, this defence pathway is downregulated, which further contributes to oxidative damage and subsequent neuronal death. On the other hand, melatonin is not only a great free radical scavenger but also increases the expression of antioxidant enzymes, regulates the mitochondria homeostasis, and has anti-inflammatory, anti-Aβ aggregation and anti-apoptotic among other effects.

The association of cholinergic hypofunction with cognitive deficits led to the formulation of the cholinergic hypothesis of memory dysfunction in senescence and in AD. In this regard, α7-nAChRs have emerged as a promising target because of their implication in pro-survival pathways, by its metabotropic activation.

The strategy of multitarget directed ligands seems to be the smartest way to find an efficacious treatment.

Following these observations, we postulated that the development of new multitarget ligands able to reduce both cholinergic dysfunction and oxidative stress, would promote neuroprotection, and therefore, could slow down or stop, disease progression.

3.2 Main objective:

Our main objective consists in the development of novel chiral MTDLs able to reduced cholinergic atrophy and oxidative stress, based on the hybridation methodology combining the following activities:

a) α7-nAChRs modulator
b) Nrf2-EpRE pathway inducer
c) Free radical scavenger

3.3 Specific objectives:

Thus, to achieve the main objective, in this Thesis we set out the following partial objectives:

I. Development of novel molecular chiral entities based on the hybridization methodology.

a) Design and synthesis of **Family A**: 2-iodo-7-(((2-(5-methoxy-1*H*-indol-3-yl)ethyl)amino)methyl)-1-phenyl-6,7,7a,8-tetrahydro-3*H*-pyrrolo[2,1-j]quinoline-3,9(5*H*)-diones .

b) *In vitro* pharmacological evaluation. This objective includes the study of their Nrf2 induction capacity, free radical scavenger activity, AChE inhibition and the activity over nAChRs, particularly α7-nAChRs. As consequence of the mentioned properties, their potential neuroprotectant effect.

c) *In vivo* pharmacokinetic and brain distribution studies of hit compounds.

II. Development of a second generation of MTDLs with improved physicochemical properties.

a) Re-design and synthesis of 1-(2-(5-substituted-1H-indol-3-yl)ethyl)-3-(quinuclidin-3-yl)-derivatives

b) *In vitro* pharmacological evaluation, including Nrf2 induction and free radical scavenger capacities, α7-nAChRs modulation and neuroprotection studies.

4 Experimental section, Materials and Methods

4.1 Objective I. Development of novel molecular chiral entities based on the hybridization methodology: 2-iodo-7-(((2-(5-methoxy-1*H*-indol-3-yl)ethyl)amino)methyl)-1-alkyl/aryl-6,7,7a,8-tetrahydro-3*H*-pyrrolo[2,1-j]quinoline-3,9(5*H*)-dione

4.1.1 Chemistry

All reagents were commercial compounds of the highest purity available. All reactions were carried out under an argon atmosphere, and those not involving aqueous reagents were carried out in oven-dried glassware. All solvents and anhydrous solutions were transferred through syringes and cannulae previously dried in the oven for at least 12 h and kept in a desiccator with KOH.

CH_2Cl_2, Et_3N, Et_2O and THF were dried by distillation over CaH_2, NaOH and last two, benzophenone and Na wire, respectively. DMF and DMSO were purchased in anhydrous form.

For reactions at low temperature, icewater or CO_2/acetone systems were used. For different cold temperatures, a CRYOCOOL CC-100 II Immersion Cooler (-100ºC - 15ºC) Neslab was used.

Analytical thin layer chromatography (TLC) was performed on aluminium plates with Merck Silicagel 60 F254 and visualized by UV irradiation (254 nm). Flash column chromatography was performed using Merck Kieselgel 60 (230-400 mesh) under positive pressure.

Proton nuclear magnetic resonance (^{1}H NMR) spectra were recorded in $CDCl_3$ or C_6D_6 at room temperature using a Bruker Advance AV 250 MHz with automatic injector BACS-60 spectrometer or a Bruker AV 500 MHz spectrometer at 400 MHz with residual protic solvent as the internal reference [$CDCl_3$, δ_H = 7.26 ppm; C_6D_6, δ_H = 7.16 ppm]; chemical shifts (δ) are given in parts per million (ppm), and coupling constant (*J*) are given in Hertz (Hz). The proton spectra is reported as follows: δ (multiplicity, coupling constant *J*, number of protons, assignment). Carbon nuclear magnetic resonance (^{13}C NMR) were recorded in $CDCl_3$ or C_6D_6 at room temperature using the same spectrometers at 63 MHz or 126 MHz, respectively, with residual central peak of [$CDCl_3$, δ_C = 77.16

ppm; C_6D_6, δ_C = 128.06 ppm] as the internal reference. Fluor nuclear magnetic resonance (^{19}F NMR) were recorded in $CDCl_3$ at room temperature using the same spectrometers at 235MHz. The DEPT135 pulse sequence, and sometimes also COSY and HSQC were used to aid in the assignment of signals in the ^{13}C NMR spectra.

HRMS were measured on a QSTAR pulsar i Q-TOF Applied Biosystems spectrometer using electrospray ionisation with positive ion detection mode (ESI+). The infrared spectra (IR) were obtained using a Agilent Technologies Cary 630 FTIR spectrophotometer from a thin film. Specific rotations were measured on a Perkin Elmer 241 Polarimeter with a Na lamp (glass cell 20x100mm) in MeOH. The enantiomeric excess were measured on an Agilent Technologies 1220 Infinity liquid chromatography (LC) VL G4288C ultraviolet-visible (UV-Vis) wavelength detector with an OVM Chiral Column. Melting points (m.p.) were recorded using STUART Scientific Melting Point Apparatus SMP3. Compound purities were estimated analyzing the total ion current (TIC) of chromatograms obtained using a high pressure liquid chromatography (HPLC) 1100 Agilent Technologies with a MAXIS II QTOF hybrid analyzer detector system and a diode array detector [6] in line with the spectrophotometer from 200 to 450 nm from Bruker (Bruker ESPAÑOLA, S.A., Madrid, Spain), employing ESI+ as ionization technique. Chromatographic separation was performed using a Zorbax Extend C18 15 cm x 4.6 mm i.d. and 5 µm particle size reverse phase column, with mobile phase H_2O 0.1 % formic acid (FA)/acetonitrile (ACN) 0.1 % FA gradient t = 0 min B = 10 %, t = 2 min B = 10 %, t = 35 min B = 95 %, flow 0.5 mL/min.

4.1.1.1 General procedure for carboxylation

To a solution of alkyne (1 eq) in Et_2O (4.32 mL/mmol) at -78 ºC, was added a solution of n-BuLi 1.6M in hexane (1.1 eq) dropwise. After stirring for 1 h at -78 ºC, excess solid carbon dioxide (dry ice) was added and reaction mixture was allowed to warm to room temperature. The reaction was quenched with a 10 % solution of H_2SO_4 until pH = 1. The aqueous layer was extracted with Et_2O three times, washed with H_2O and brine, dried over Na_2SO_4 and concentrated *in vacuo* to obtain the desired carboxylic acid.

4.1.1.2 General procedure for amine coupling with 3-substituted-prop-2-ynoic acid

A solution of (*N*-4,4-diethoxyalkyl)-4-methoxyaniline (1 eq), Et_3N (1.5 eq) in CH_2Cl_2 (5 mL/mmol) was added to a solution of 3-substituted-prop-2-ynoic acid (1.2 eq) and HATU (1.5 eq) in CH_2Cl_2 (5 mL/mmol) at 0 ºC. The resulting solution was stirred and warmed up to room temperature until completion, concentrated *in vacuo* and purified by flash chromatography on silica gel to afford the desired compounds.

4.1.1.3 General procedure for acetal removal

2N HCl (1.2 mL/mmol) was added dropwise to a solution of acetal (1 eq) in THF (6 mL/mmol) at room temperature, and the resulting solution was stirred until completion. The reaction was quenched with aqueous $NaHCO_3$ solution and extracted with CH_2Cl_2. The organic layer was dried over Na_2SO_4, concentrated in vacuo. Purification was not required.

4.1.1.4 General procedure for ECED transformation

a) ICl (2 eq) in CH_2Cl_2 (1 M) was added to a solution of the aldehyde (1 eq) in CH_2Cl_2 (50 mL/mmol) at -78 ºC over a period of 30 minutes using a mechanical syringe. The resulting solution was stirred for 10-30 minutes and quenched with saturated aqueous $Na_2S_2O_3$ solution. It was allowed to warm up to room temperature and extracted three times with CH_2Cl_2. The combined organic layers were dried over Na_2SO_4 and the solvent was evaporated. The residue was purified by column chromatography to afford the corresponding 4-(4-alkyl/aryl-3-iodo-2,8-dioxo-1-azaspiro[4.5]deca-3,6,9-trien-1-yl)butanal.

b) Catalyst [(*R*)-, (*S*)- or (±)-2-(diphenyl((trimethylsilyl)oxy)methyl)pyrrolidine] (0.2 eq) and benzoic acid (0.2 eq) were added to the solution of 4-(4-alkyl/aryl-3-iodo-2,8-dioxo-1-azaspiro[4.5]deca-3,6,9-trien-1-yl)butanal (1 eq) in CH_2Cl_2 (40 mL/mmol) at -20 ºC. The resulting mixture was stirred for 2 to 5 days, quenched by water and extracted with CH_2Cl_2 (3x). The combined organic layers were dried over Na_2SO_4, concentrated *in vacuo* and purified by flash chromatography on silica gel.

4.1.1.5 General procedure for reductive amination

To a solution of aldehyde (1eq) in CH_2Cl_2 (43 mL/mmol) was added 5-methoxy-tryptamine (1 eq). The mixture was stirred at room temperature for an hour to overnight depending on the derivative. Then was added carefully $Na(AcO)_3BH$ (1.3 eq) at 0 ºC. The solution was stirred and warm up overnight, quenched by saturated solution of $NaHCO_3$ and extracted with CH_2Cl_2 (3x). The combined organic layers were dried over Na_2SO_4, concentrated *in vacuo* and purified by flash chromatography on silica gel.

(*N*-4,4-diethoxybutyl)-4-methoxyaniline 24

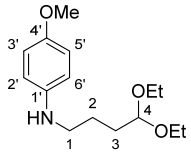

DMSO (40 mL) was added to a mixture of 4-iodoanisole **22** (5.00 g, 21.36 mmol), CuI (0.41 g, 2.1 mmol), L-proline (0.49 g, 4.3 mmol) and K_2CO_3 (powdered) (5.90 g, 42.7 mmol) in a round bottom flask, and it was flushed with Ar (3 times), followed by addition of 4,4-diethoxybutan-1-amine **23** (5.16 g, 32.04 mmol). The reaction mixture was degassed and stirred under Ar atmosphere at 80 ºC for 26 h, diluted with water and extracted with diethyl ether (3 x 25 mL). The combined organic layers were washed with water and brine, dried over Na_2SO_4, concentrated in vacuum and purified by flash chromatography on silica gel (Hex/EtOAc, 0-30 %) to afford 4.83 g (85 %) of the desired product **24** as a yellowish oil. The spectroscopic data matched with previously reported.[114] ^{1}H NMR (250 MHz, $CDCl_3$) δ 6.78 (dd, *J* = 9.0, 2.3 Hz, 2H, H6'), 6.57 (dd, *J* = 9.0, 2.3 Hz, 2H, H5'), 4.52 (t, *J* = 5.1 Hz, 1H, H4), 3.74 (s, 3H, OC*H*$_3$), 3.65 (dq, *J* = 9.3, 7.1 Hz, 2H, H1), 3.49 (dq, *J* = 9.3, 7.0 Hz, 2H, OC*H*$_2$CH$_3$), 3.09 (t, *J* = 6.4 Hz, 2H, OC*H*$_2$CH$_3$), 1.70 (h, *J* = 5.6, 5.2 Hz, 4H, H2, H3), 1.21 (t, *J* = 7.1 Hz, 6H, OCH$_2$C*H*$_3$) ppm.

3-(3-fluorophenyl)propiolic acid 29

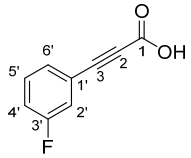

Following the *general procedure 4.1.1.1*, the reaction of 1-ethynyl-3-fluorobenzene **25** (1.0 g, 8.3 mmol), n-BuLi (3.7 mL, 9.2 mmol) in Et_2O (36 mL) and excess of CO_2 at -78 ºC for 15 min afforded quantitatively, without purification, 1.34 g of the desired compound **29** as a yellow solid. The spectroscopic data matched with previously reported.[115] ^{1}H NMR (300 MHz, $CDCl_3$) δ 9.61 (s, 1H, H1), 7.44 - 7.33 (m, 2H, H5', H6'), 7.30 (dt, *J* = 9.0, 1.8 Hz, 1H, H4'), 7.19 (dt, *J* = 15.3, 2.4 Hz, 1H, H2') ppm.

3-cyclopropylpropiolic acid 31

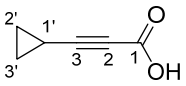

Following the *general procedure 4.1.1.1*, the reaction of ethynylcyclopropane **27** (700 mg, 10.6 mmol), n-BuLi (4.7 mL, 11.7 mmol) in Et_2O (4 mL) and excess of CO_2 at -78 ºC for 30 min afforded, without purification, 1.097 g (94 %) of the desired compound **31** as an off-white solid. The spectroscopic data matched with previously reported.[114] ^1H NMR (300 MHz, $CDCl_3$) δ 10.91 (s, 1H, H1), 1.39 (dq, *J* = 8.5, 5.2, 4.1 Hz, 1H, H1'), 0.94 (q, *J* = 6.6, 4.1 Hz, 4H, H2',H3') ppm.

3-cyclohexylpropiolic acid 32

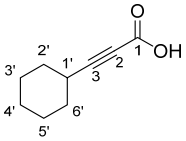

Following the *general procedure 4.1.1.1*, the reaction of ethynylcyclohexane **28** (1.00 g, 9.2 mmol), n-BuLi (6.4 mL, 10.2 mmol) in Et_2O (40 mL) and excess of CO_2 at -78 ºC for 15 min afforded, without purification, 1.39 g (99 %) of the desired compound **32** as an yellow solid. The spectroscopic data matched with previously reported.[116] ^1H NMR (300 MHz, $CDCl_3$) δ 10.48 (d, *J* = 34.3 Hz, 1H, H1), 2.49 (tt, *J* = 8.1, 3.9 Hz, 1H, H4), 1.78 (dt, *J* = 13.2, 3.8 Hz, 2H, H6', H2'), 1.65 (qd, *J* = 8.7, 5.4, 4.2 Hz, 2H, H6', H2'), 1.47 (dh, *J* = 8.8, 4.4 Hz, 3H, H3', H4', H5'), 1.29 (d, *J* = 7.9 Hz, 3H, H3', H4', H5') ppm.

***N*-(4,4-diethoxybutyl)-*N*-(4-methoxyphenyl)-3-phenylpropiolamide 33**

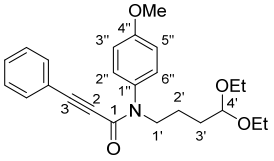

Following the *general procedure 4.1.1.2*, the reaction of **24** (1.00 g, 3.7 mmol), Et_3N (0.78 mL, 5.6 mmol) CH_2Cl_2 (18 mL) and 3-phenylprop-2-ynoic acid **28** (0.66 g, 4.5 mmol), HATU (2.13 g, 5.6 mmol) in CH_2Cl_2 (18 mL), for 1 h 40 min afforded, after purification by flash chromatography on silica gel (Hex/EtOAc, 10-30 %), 1.43 g (96 %) of the desired compound **33** as a yellowish solid. The spectroscopic data matched with previously reported.[114] ^1H NMR (250 MHz, C_6D_6) δ 7.11 - 7.03 (m, 2H, Ph), 6.96 (d, *J* = 8.8 Hz, 2H, H2'',H6''), 6.77 (tdd, *J* = 8.7, 7.0, 4.7 Hz, 2H, H3'',H5''), 6.64 (d, *J* = 8.8 Hz, 3H, Ph), 4.46 (q, *J* = 4.6, 3.4 Hz, 1H, H4'), 3.82 (dq, *J* = 7.4, 4.1 Hz, 2H, H1'), 3.52 (dq, *J* = 9.2, 7.1 Hz, 2H, OC*H*$_2$CH$_3$), 3.34 (dq, *J* = 9.3, 7.0 Hz, 2H, OC*H*$_2$CH$_3$), 3.21 (s, 3H, OC*H*$_3$), 1.72 (p, *J* = 3.0 Hz, 4H, H2'H3'), 1.11 (t, *J* = 7.0 Hz, 6H, OCH$_2$C*H*$_3$) ppm.

***N*-(4,4-diethoxybutyl)-3-(3-fluorophenyl)-*N*-(4-methoxyphenyl)propiolamide 34**

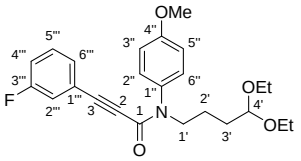

Following the *general procedure 4.1.1.2*, the reaction of **24** (789 mg, 3.0 mmol), Et_3N (0.62 mL, 4.4 mmol) CH_2Cl_2 (15 mL) and 3-(3-fluorophenyl)propiolic acid **29** (581 mg, 3.5 mmol), HATU (1.68 g, 4.4 mmol) in CH_2Cl_2 (15 mL), for 4 h afforded, after purification by flash chromatography on silica gel (Hex/EtOAc, 20-50 %), 1.18 g (97 %) of the desired compound **34** as a yellowish oil. Rf 0.39 (Hex/EtOAc 70:30) m.p. 91 – 93 ºC ^{1}H NMR (250 MHz, $CDCl_3$) δ 7.22 (td, *J* = 5.9, 5.3, 2.2 Hz, 3H, H2'', H6'', H5'''), 7.07 – 7.01 (m, 1H, H6'''), 7.00 - 6.91 (m, 3H, H3'',H5'', H4'''), 6.85 - 6.76 (m, 1H, H2'''), 4.48 (dt, *J* =5.0, 2.7 Hz, 1H, H4'), 3.86 (s, 3H, OC*H*$_3$), 3.80 (d, *J* = 7.4 Hz, 2H, H1'), 3.62 (dq, *J* = 9.1, 7.0 Hz, 2H, OC*H*$_2$CH$_3$), 3.47 (dq, *J* = 9.4, 7.1 Hz, 2H, OC*H*$_2$CH$_3$), 1.74 - 1.59 (m, 4H, H2', H3'), 1.18 (t, *J* = 7.1 Hz, 3H, OCH$_2$C*H*$_3$) ppm ^{13}C NMR (63 MHz, $CDCl_3$) δ 162.1 (d, *J* = 247.2 Hz), 159.4, 154.3, 134.4, 130.1 (d, *J* = 8.5 Hz), 129.8, 128.4 (d, *J* = 3.3 Hz), 122.5 (d, *J* = 9.5 Hz), 119.2 (d, *J* = 23.2 Hz), 117.4 (d, *J* = 21.3 Hz), 114.4, 102.6, 89.5 (d, *J* = 3.5 Hz), 83.4, 61.4, 55.7, 48.4, 30.9, 22.9, 15.4 ppm. ^{19}F NMR (235 MHz, $CDCl_3$) δ -112.64 - -112.84 (m) ppm. HRMS (ES^+) Theoretical mass calc. for $C_{24}H_{28}FNO_4$ 413.2002; found [$(M+Na)^+$], 436.1933; [$(2M+Na)^+$], 849.4019. IR (film) υ/cm^{-1} 2977, 2931, 2905, 2870, 2220, 1630, 1577, 1510, 1490, 1476, 1456, 1396, 1377, 1366, 1309, 1248, 1195, 1170, 1150, 1086, 1020, 1015, 1013, 941, 911, 875, 837, 801, 730, 683.

***N*-(4,4-diethoxybutyl)-*N*-(4-methoxyphenyl)hex-2-ynamide 35**

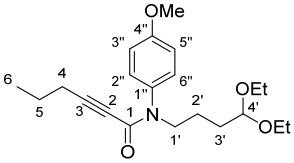

Following the *general procedure 4.1.1.2*, the reaction of **24** (525 mg, 2.0 mmol), Et_3N (0.41 mL, 2.9 mmol) CH_2Cl_2 (4.5 mL) and 2-hexynoic acid **30** (0.27 mL, 2.4 mmol), HATU (1.11 g, 2.9 mmol) in CH_2Cl_2 (6.5 mL), for 80 min afforded, after purification by flash chromatography on silica gel (Hex/EtOAc, 15-25 %), 687 mg (97 %) of the desired compound **35** as a yellowish oil. Rf 0.41 (Hex/EtOAc 70:30). ^{1}H NMR (250 MHz, C_6D_6) δ 6.94 (d, *J* = 8.8 Hz, 2H, H2'', H6''), 6.64 (d, *J* = 8.8 Hz, 2H, H3'', H5''), 4.44 (dd, *J* = 9.1, 4.8 Hz, 1H, H4'), 3.78 (p, *J* = 3.7 Hz, 2H, H1'), 3.51 (dq, *J* = 9.1, 7.0 Hz, 2H, OC*H*$_2$CH$_3$), 3.33 (dq, *J* = 9.3, 7.1 Hz, 2H, OC*H*$_2$CH$_3$), 3.22 (s, 3H, OC*H*$_3$), 1.74 – 1.69 (m, 4H, H4, H3'), 1.65 (t, *J* = 6.8 Hz, 2H, H2'), 1.10 (t, *J* = 7.0 Hz, 6H, OCH$_2$C*H*$_3$), 0.99

(q, *J* = 7.1 Hz, 2H, H5), 0.51 (t, *J* = 7.3 Hz, 3H, H6) ppm. ^{13}C NMR (75 MHz, C_6D_6) δ 159.4, 154.3, 135.57, 130.10, 114.4, 102.8, 92.7, 76.7, 61.1, 55.1, 48.4, 31.3, 23.4, 21.4, 20.7, 15.6, 13.2 ppm. HRMS (ES^+) Theoretical mass calc. for $C_{21}H_{31}NO_4$: 361.2253; found [$(M+Na)^+$], 384.2245. IR (film) υ/ cm^{-1} 2968, 2877, 1631, 1510, 1458, 1441, 1392, 1291, 1123, 1032, 998, 835, 733.

3-cyclopropyl-*N*-(4,4-diethoxybutyl)-*N*-(4-methoxyphenyl)propiolamide 36

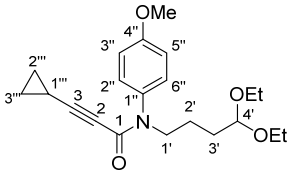

Following the *general procedure 4.1.1.2*, the reaction of **24** (911 mg, 3.4 mmol), Et_3N (0.71 mL, 5.1 mmol) CH_2Cl_2 (17 mL) and 3-cyclopropylpropiolic acid **31** (45 mg, 4.1 mmol), HATU (1.95 g, 5.1 mmol) in CH_2Cl_2 (17 mL), for 2 h afforded, after purification by flash chromatography on silica gel (Hex/EtOAc, 10-30 %), 1.10 g (90 %) of the desired compound **36** as a yellowish solid. The spectroscopic data matched with previously reported.[114] ^{1}H NMR (250 MHz, C_6D_6) δ 6.95 - 6.86 (m, 2H, H2'',H6''), 6.66 - 6.56 (m, 2H, H3'',H5''), 4.44 (s, 1H, H4'), 3.78 (t, *J* = 4.2 Hz, 2H, H1'), 3.50 (dq, *J* = 9.4, 7.0 Hz, 2H, OC*H*$_2$CH$_3$), 3.33 (dq, *J* = 9.4, 7.0 Hz, 2H, OC*H*$_2$CH$_3$), 3.21 (s, 3H, OC*H*$_3$), 1.76 – 1.61 (m, 4H, H2'H3'), 1.09 (t, *J* = 7.0 Hz, 6H, OCH$_2$C*H*$_3$), 0.64 (tt, *J* = 8.0, 5.0 Hz, 1H, C*H*$_2$, H1'''), 0.26 (ddt, *J* = 8.4, 5.8, 2.7 Hz, 2H, C*H*$_2$, H2'') 0.12 (dt, *J* = 8.5, 3.3 Hz, 2H, C*H*$_2$, H3''') ppm.

3-cyclohexyl-*N*-(4,4-diethoxybutyl)-*N*-(4-methoxyphenyl)propiolamide 37

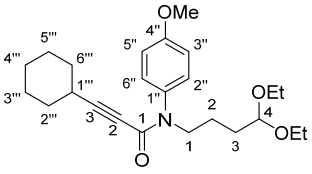

Following the *general procedure 4.1.1.2*, the reaction of **24** (960 mg, 3.6 mmol), Et_3N (0.75 mL, 5.4 mmol) CH_2Cl_2 (18 mL) and 3-cyclohexylpropiolic acid **32** (656 mg, 4.3 mmol), HATU (2.05 g, 5.4 mmol) in CH_2Cl_2 (18 mL), for 2 h afforded, after purification by flash chromatography on silica gel (Hex/EtOAc, 10-20 %), 1.39 g (97 %) of the desired compound **37** as a yellowish oil. Rf 0.39 (Hex/EtOAc 70:30) ^{1}H NMR (300 MHz, C_6D_6) δ 6.95 (d, *J* = 8.7 Hz, 2H, H2'', H6''), 6.65 (dd, *J* = 8.7, 2.0 Hz, 2H, H3'', H5''), 4.44 (q, *J* = 3.3 Hz, 1H, H4'), 3.79 (q, *J* = 5.7 Hz, 2H, H1'), 3.51 (dq, *J* = 9.2, 7.0 Hz, 2H, OC*H*$_2$CH$_3$), 3.43 – 3.26 (m, 2H, OC*H*$_2$CH$_3$), 3.24 (s, 3H, OC*H*$_3$), 2.07 (dt, *J* = 8.1, 4.2 Hz, 1H, H1'''), 1.70 (dq, *J* = 5.4, 3.1, 2.4 Hz, 4H, H2', H3'), 1.25 (dtd, *J* = 22.0, 12.2, 11.5, 4.9 Hz, 6H, 2xH2''', 2xH6''', H3''', H5'''), 1.09 (td, *J* = 7.0, 1.3 Hz, 6H, OCH$_2$C*H*$_3$), 0.93 (dd, *J* = 7.3, 3.7 Hz, 4H, H3''', H5''', 2xH4''') ppm. ^{13}C

NMR (75 MHz, C_6D_6) δ 159.3, 154.4, 135.7, 130.2, 114.4, 102.8, 96.1, 76.9, 61.0, 55.0, 48.4, 31.5, 31.2, 28.8, 25.9, 24.2, 23.5, 15.7 ppm. HRMS (ES^+) Theoretical mass calc. for $C_{24}H_{35}NO_4$ 401.2566; found [$(M+Na)^+$], 424.2503; found [$(2M+Na)^+$], 825.5126. IR (film) υ/ cm^{-1} 2971, 2928, 2854, 2223, 1633, 1510, 1444, 1392, 1292, 1126, 1060, 835, 734.

_N_-(4-methoxyphenyl)-_N_-(4-oxobutyl)-3-phenylpropiolamide 38

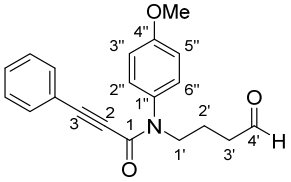

Following the *general procedure 4.1.1.3*, **33** (220 mg, 0.6 mmol) for 2 h afforded 179 mg (99 %) of the desired compound **38** as a yellowish oil. The spectroscopic data matched with previously reported.[114] ^1H NMR (250 MHz, C_6D_6) δ 9.26 (d, *J* = 1.2 Hz, 1H, H4'), 7.06 (dt, *J* = 6.5, 1.7 Hz, 2H, Ph), 6.95 - 6.86 (m, 2H, H2'', H6''), 6.83 - 6.70 (m, 3H, Ph), 6.69 - 6.62 (m, 2H, H3''. H5''), 3.60 (t, *J* = 7.1 Hz, 2H, H1'), 3.22 (s, 3H, OCH_3), 1.86 (t, *J* = 7.2 Hz, 2H, H3'), 1.63 (q, *J* = 7.2 Hz, 2H, H2') ppm.

3-(3-fluorophenyl)-_N_-(4-methoxyphenyl)-_N_-(4-oxobutyl)propiolamide 39

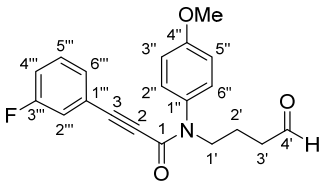

Following the *general procedure 4.1.1.3*, **34** (313 mg, 0.76 mmol) for 4 h quantitatively afforded 257 mg of the desired compound **39** as a yellowish oil. Rf 0.22 (Hex/EtOAc, 70:30) ^1H NMR (250 MHz, $CDCl_3$) δ 9.78 (s, 1H, H4'), 7.26 - 7.13 (m, 3H, H2'', H6'', H5'''), 7.04 (tdd, *J* = 8.5, 2.6, 1.1 Hz, 1H, H6'''), 6.99 - 6.92 (m, 3H, H3'', H5'', H4'''), 6.81 (ddd, *J* = 9.1, 2.7, 1.5 Hz, 1H, H2'''), 3.86 (s, 3H, OC*H*$_3$), 3.85 - 3.78 (m, 2H, H1'), 2.55 (td, *J* = 7.3, 1.2 Hz, 2H, H3'), 1.89 (p, *J* = 7.3 Hz, 2H, H2') ppm. ^{13}C NMR (63 MHz, $CDCl_3$) δ 201.3, 162.1 (d, *J* = 247.5 Hz), 159.5, 154.4, 134.1, 130.1 (d, *J* = 8.5 Hz), 129.6, 128.4 (d, *J* = 3.2 Hz), 128.2, 122.3 (d, *J* = 9.4 Hz), 119.2 (d, *J* = 23.1 Hz), 117.4 (d, *J* = 21.2 Hz), 114.5, 89.7 (d, *J* = 3.6 Hz), 83.1, 55.7, 47.9, 41.1, 20.2 ppm. ^{19}F NMR (235 MHz, $CDCl_3$) δ -112.63 (td, *J* = 8.9, 5.8 Hz) ppm. HRMS (ES^+) Theoretical mass calc. for $C_{20}H_{18}FNO_3$ 339.1271; found [$(M+H)^+$], 340.1323; [$(2M+Na)^+$], 679.2672. IR (film) υ/cm^{-1} 2933, 2836, 1719, 1628, 1579, 1509, 1483, 1429, 1392, 1297, 1246, 1182, 1106, 1028, 872, 788, 680.

_N_-(4-methoxyphenyl)-_N_-(4-oxobutyl)hex-2-ynamide 40

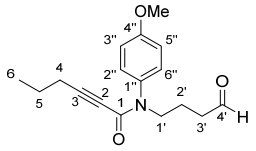

Following the *general procedure 4.1.1.3*, **35** (830 mg, 2.30 mmol) for 1 h afforded 658 mg (99 %) of the desired compound **40** as a yellowish oil. Rf 0.24 (Hex./EtOAc, 70:30) ^{1}H NMR (250 MHz, C_6D_6) δ 9.25 (t, *J* = 1.2 Hz, 1H, H4'), 6.97 - 6.82 (m, 2H, H2'', H6''), 6.76 – 6.52 (m, 2H, H3'', H5''), 3.56 (t, *J* = 7.1 Hz, 2H, H1'), 3.24 (d, *J* = 1.8 Hz, 3H, OC*H*$_3$), 1.94 - 1.76 (m, 2H, H3'), 1.62 (dt, *J* = 14.4, 7.1 Hz, 4H, H2', H4), 0.99 (h, *J* = 7.2 Hz, 2H, H5), 0.52 (t, *J* = 7.3 Hz, 3H, H6) ppm. ^{13}C NMR (63 MHz, C_6D_6) δ 200.0, 159.4, 135.4, 130.0, 114.5, 93.1, 76.6, 55.0, 47.8, 41.0, 21.4, 20.7, 20.5, 13.15 ppm. HRMS (ES$^+$) Theoretical mass calc. for $C_{17}H_{21}NO_3$: 287.1521; found [(M+H)$^+$], 288.1567. IR (film) υ/ cm^{-1} 3443, 2959, 2932, 2872, 2836, 2226, 1719, 1626, 1509, 1458, 1441, 1392, 1291, 1245, 1181, 1105, 1029, 835, 733.

3-cyclopropyl-_N_-(4-methoxyphenyl)-_N_-(4-oxobutyl)propiolamide 41

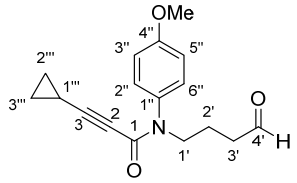

Following the *general procedure 4.1.1.3*, **36** (470 mg, 1.3 mmol) for 1 h quantitatively afforded 374 mg of the desired compound **41** as a yellowish oil. The spectroscopic data matched with previously reported.[114] ^{1}H NMR (250 MHz, C_6D_6) δ 9.24 (d, *J* = 1.3 Hz, 1H, H4'), 6.90 - 6.79 (m, 2H, H2'', H6''), 6.69 - 6.54 (m, 2H, H3'', H5''), 3.55 (t, *J* = 7.1 Hz, 2H, H1'), 3.21 (d, *J* = 4.7 Hz, 3H, OC*H*$_3$)), 1.83 (t, *J* = 7.2 Hz, 2H, H3'), 1.57 (p, *J* = 7.2 Hz, 2H, H2'), 1.47 - 1.27 (m, 1H), 0.64 (tt, *J* = 8.2, 5.0 Hz, 1H, H1'''), 0.26 (ddd, *J* = 6.4, 5.1, 3.3 Hz, 2H, H2'''), 0.11 (ddd, *J* = 7.6, 5.4, 3.5 Hz, 2H, H3''') ppm.

3-cyclohexyl-_N_-(4-methoxyphenyl)-_N_-(4-oxobutyl)propiolamide 42

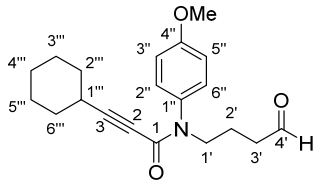

Following the *general procedure 4.1.1.3*, **37** (300 mg, 0.8 mmol) for 80 min, quantitatively afforded 245 mg of the desired compound **42** as a yellowish oil. Rf 0.24 (Hex/EtOAc 70:30). ^{1}H NMR (250 MHz, C_6D_6) δ 9.25 (t, *J* = 1.1 Hz, 1H, H4'), 6.89 (dd, *J* = 8.9, 2.1 Hz, 2H, H2'', H6''), 6.64 (dd, *J* = 8.9, 2.2 Hz, 2H, H3'', H5''), 3.57 (t, *J* = 7.1 Hz, 2H, H1'), 3.25 (s, 3H, OCH_3), 2.07 (dt, *J* = 8.0, 4.2 Hz, 1H, H1'''), 1.91 - 1.79 (m, 2H, H3'), 1.72 - 1.51 (m, 2H, H2'), 1.34 – 1.14 (m, 6H, 2xH2''', 2xH6''', H3''', H5'''), 1.08 (dd, *J* = 9.8, 3.9 Hz, 2H, H3''', H5'''), 0.92 (dt, *J* = 7.2, 3.4 Hz, 2H,

H4’’’) ppm. ^{13}C NMR (63 MHz, C_6D_6) δ 200.0, 159.4, 154.6, 135.5, 130.1, 114.4, 96.5, 76.7, 55.0, 47.8, 41.0, 31.5, 28.8, 25.9, 24.2, 20.5 ppm. HRMS (ES^+) Theoretical mass calc. for $C_{20}H_{25}NO_3$ 327.1834; found [$(M+H)^+$], 328.1897; found [$(M+Na)^+$], 350.1708; found [$(2M+H)^+$], 655.3825; found [$(2M+Na)^+$], 677.3619 IR (film) υ/ cm^{-1} 3425, 2928, 2852, 1720, 1633, 1509, 1443, 1391, 1291, 1180, 1105, 1029, 935, 834, 733.

4-(3-iodo-2,8-dioxo-4-phenyl-1-azaspiro[4.5]deca-3,6,9-trien-1-yl)butanal 43

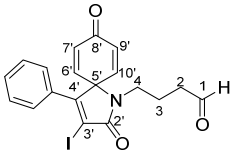

Following the *general procedure 4.1.1.4a*, the reaction of **38** (200 mg, 0.6 mmol) and ICl (1.26 mL, 1.3 mmol) in CH_2Cl_2 (32 mL) afforded after purification by flash chromatography on silica gel (CH_2Cl_2/Acetone, 2-5 %), 200 mg (73 %) of the desired product **43** as a white solid. The spectroscopic data matched with previously reported.[114] ^{1}H NMR (250 MHz, C_6D_6) δ 9.24 (s, 1H, H1), 6.99 (ddd, *J* = 9.9, 4.7, 3.2 Hz, 5H, Ph), 5.93 (d, *J* = 10.0 Hz, 2H, H6’, H10’), 5.39 (d, *J* = 10.0 Hz, 2H, H7’, H9’), 2.89 (t, *J* = 7.1 Hz, 2H, H4), 1.76 (t, *J* = 7.1 Hz, 2H, H2), 1.51 (q, *J* = 6.8 Hz, 2H, H3) ppm.

4-(4-(3-fluorophenyl)-3-iodo-2,8-dioxo-1-azaspiro[4.5]deca-3,6,9-trien-1-yl) 44

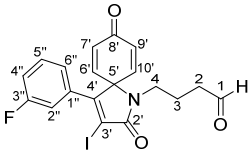

Following the *general procedure 4.1.1.4a*, the reaction of **39** (174 mg, 0.51 mmol) and ICl (1.0 mL, 1.0 mmol) in CH_2Cl_2 (25 mL) for 4 h 40 min, afforded after purification by flash chromatography on silica gel (CH_2Cl_2/Acetone, 1-5 %), 106 mg (46 %) of the desired product **44** as an off-white solid. Rf 0.34 (CH_2Cl_2/Acetone 95:5) m.p. 110 - 112 ºC ^{1}H NMR (250 MHz, $CDCl_3$) δ 9.77 (d, *J* = 0.9 Hz, 1H, H1), 7.36 (td, *J* = 8.0, 5.8 Hz, 1H, H5’’), 7.21 - 7.06 (m, 1H, H6’’), 7.06 - 7.01 (m, 1H, H2’’), 6.98 (dt, *J* = 9.3, 2.2 Hz, 1H, H4’’), 6.56 (d, *J* = 10.3 Hz, 2H, H7’, H9’), 6.46 (d, *J* = 10.2 Hz, 2H, H6’, H10’), 3.38 (dd, *J* = 7.9, 6.6 Hz, 2H, H4), 2.59 (t, *J* = 6.8 Hz, 1H, H2), 1.91 (p, *J* = 7.1 Hz, 2H, H3) ppm. ^{13}C NMR (63 MHz, $CDCl_3$) δ 201.2, 184.0, 168.0, 162.8 (d, *J* = 248.6 Hz), 157.4, 144.1, 134.1 (d, *J* = 8.0 Hz), 133.7, 131.0 (d, *J* = 8.4 Hz), 124.0 (d, *J* = 3.2 Hz), 117.6 (d, *J* = 20.9 Hz), 115.5 (d, *J* = 23.3 Hz), 99.7, 71.1, 41.9, 41.6, 22.7 ppm. ^{19}F NMR (235 MHz, $CDCl_3$) δ -111.23 (td, *J* = 9.0, 5.9 Hz) ppm. HRMS (ES^+) Theoretical mass calc. for $C_{19}H_{15}FINO_3$ 451.2302; found [$(M+H)^+$], 452.0127; [$(M+Na)^+$], 473.9955. IR (film) υ/ cm^{-1} 3050, 2932, 2821, 1689, 1665, 1629, 1480, 1390, 1269, 1179, 857, 797, 745, 687.

4-(3-iodo-2,8-dioxo-4-propyl-1-azaspiro[4.5]deca-3,6,9-trien-1-yl)butanal 45

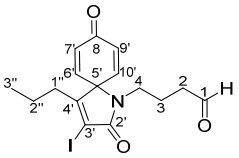

Following the *general procedure 4.1.1.4a*, the reaction of **40** (130 mg, 0.5 mmol) and ICl (0.9 mL, 0.9 mmol) in CH_2Cl_2 (23 mL) afforded after purification by flash chromatography on silica gel (CH_2Cl_2/Acetone, 1-5 %), 140 mg (72 %) of the desired product **45** as a yellowish oil. Rf 0.36 (CH_2Cl_2/Acetone 95:5) ^{1}H NMR (250 MHz, $CDCl_3$) δ 9.74 (t, *J* = 1.0 Hz, 1H, H1), 6.54 (d, *J* = 10.3 Hz, 2H, H7', H9'), 6.40 (d, *J* = 10.2 Hz, 2H, H6', H10'), 3.32 (dd, *J* = 7.8, 6.7 Hz, 2H, H4), 2.54 (td, *J* = 7.1, 1.0 Hz, 2H, H2), 2.19 – 2.03 (m, 2H, H1''), 1.85 (p, *J* = 7.1 Hz, 2H, H3), 1.60 - 1.42 (m, 2H, H2''), 0.94 (t, *J* = 7.3 Hz, 3H, H3'') ppm. ^{13}C NMR (63 MHz, $CDCl_3$) δ 201.0, 184.2, 168.2, 160.0, 144.7, 133.0, 96.7, 71.1, 41.5, 41.3, 31.5, 22.5, 22.0, 14.5 ppm. HRMS (ES^+) Theoretical mass calc. for $C_{16}H_{18}INO_3$: 399.0331; found [$(M+H)^+$], 400.0410. IR (film) υ/ cm^{-1} 3383, 2960, 2872, 1689, 1662, 1624, 1437, 1387, 1058, 1018, 853, 749, 666.

4-(4-cyclopropyl-3-iodo-2,8-dioxo-1-azaspiro[4.5]deca-3,6,9-trien-1-yl)butanal 46

Following the *general procedure 4.1.1.4a*, the reaction of **41** (239 mg, 0.8 mmol) and ICl (1.7 mL, 1.7 mmol) in CH_2Cl_2 (42 mL) afforded after purification by flash chromatography on silica gel (CH_2Cl_2/Acetone, 1.5-4 %), 230 mg (69 %) of the desired product **46** as an off-white solid. Rf 0.31 (CH_2Cl_2/Acetone 95:5) m.p. 102 - 105 ºC ^{1}H NMR (250 MHz, C_6D_6) δ 9.22 (t, *J* = 1.6 Hz, 1H, H1), 6.19 - 5.92 (m, 2H, H7', H9'), 5.28 (dq, *J* = 10.2, 2.4 Hz, 2H, H6', H10'), 2.89 - 2.74 (m, 2H, H4), 1.74 (t, *J* = 7.1 Hz, 2H, H2), 1.51 - 1.37 (m, 2H, H3), 1.06 - 0.90 (m, 2H, H2''), 0.87 - 0.66 (m, 1H, H1''), 0.33 (dtd, *J* = 9.5, 4.2, 3.7, 2.2 Hz, 2H, H3'') ppm. ^{13}C NMR (63 MHz, C_6D_6) δ 199.6, 183.6, 167.6, 158.3, 144.9, 132.5, 90.5, 70.9, 41.0, 40.9, 22.6, 11.6, 7.5 ppm. HRMS (ES^+) Theoretical mass calc. for $C_{16}H_{16}INO_3$ 397.0175; found [$(M+H)^+$], 398.0253; found [$(M+Na)^+$], 420.0049; found [$(2M+Na)^+$], 817.0220 IR (film) υ/ cm^{-1}: 3008, 2925, 2809, 1668, 1630, 1602, 1392, 1363, 1329, 942, 837, 801, 748.

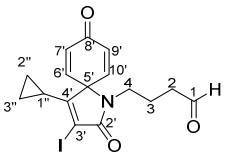

4-(4-cyclohexyl-3-iodo-2,8-dioxospiro[4.5]deca-3,6,9-trien-1-yl)butanal 47

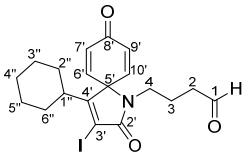

Following the *general procedure 4.1.1.4a*, the reaction of **42** (238 mg, 0.73 mmol) and ICl (1.5 mL, 1.5 mmol) in CH_2Cl_2 (37 mL) for 40 min, afforded after purification by flash chromatography on

silica gel (CH_2Cl_2/Acetone, 1.5-2 %), 230 mg (72 %) of the desired product **47** as an off-white solid. Rf 0.37 (CH_2Cl_2/Acetone 95:5) m.p. 146 - 148 ºC ^{1}H NMR (250 MHz, C_6D_6) δ 9.27 (s, 1H, H1), 6.11 (dq, *J* = 10.3, 2.6, 2.0 Hz, 2H, H7', H9'), 5.47 - 5.33 (m, 2H, H6', H10'), 2.90 (t, *J* = 7.2 Hz, 2H, H4), 2.00 - 1.69 (m, 5H, H2, 2xH2'', H3''), 1.62 - 1.36 (m, 5H, H3, 2xH6'', H4''), 1.24 (d, *J* = 11.2 Hz, 2H, H3'', H5''), 1.12 - 0.75 (m, 3H, H3'', H4'', H5'') ppm. ^{13}C NMR (63 MHz, C_6D_6) δ 199.8, 183.6, 167.9, 161.1, 144.2, 132.9, 94.3, 71.7, 41.3, 41.0, 38.9, 29.2, 26.3, 25.6, 22.5 ppm. HRMS (ES^+) Theoretical mass calc. for $C_{19}H_{22}INO_3$ 439.0644; found [$(M+H)^+$], 440.0690; found [$(M+Na)^+$], 462.0522. IR (film) υ/ cm^{-1}: 3378, 2929, 2846, 2725, 1694, 1666, 1625, 1391, 1301, 1280, 1065, 1026, 995, 864, 840, 750.

2-iodo-3,9-dioxo-1-phenyl-5,6,7,7a,8,9-hexahydro-3*H*-pyrrolo[2,1-j]quinoline-7-carbaldehyde (±)-48

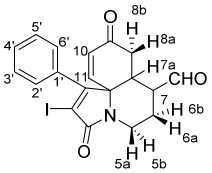

Following the *general procedure 4.1.1.4b*, the reaction of **43** (100 mg, 0.2 mmol), (±)-catalyst (11 mg, 0.04 mmol) and benzoic acid (5 mg, 0.04 mmol) in CH_2Cl_2 for 3 days 21 h at -20 ºC afforded, after purification by flash chromatography on silica gel (CH_2Cl_2/Acetone, 1-5 %), 49 mg (57 %) the desired product **(±)-48** as an off-white solid. The spectroscopic data matched with previously reported.[114] ^{1}H NMR (250 MHz, $CDCl_3$) δ 9.62 (s, 1H, CHO), 7.44 (d, *J* = 7.2 Hz, 3H, Ph), 7.23 - 7.09 (m, 2H, Ph), 6.52 (dd, *J* = 10.1, 1.8 Hz, 1H, H11), 6.37 (d, *J* = 10.1 Hz, 1H, H10), 4.46 (d, *J* = 12.9 Hz, 1H, H5b), 3.24 - 3.02 (m, 1H, H5a), 2.71 (d, *J* = 8.7 Hz, 2H, H8a, H7a), 2.54 (d, *J* = 18.8 Hz, 1H, H7), 2.31 (d, *J* = 13.8 Hz, 1H, H8b), 2.13 (dd, *J* = 18.7, 6.6 Hz, 1H, H6b), 1.58 (t, *J* = 12.8 Hz, 1H, H6a) ppm.

(7*S*,7a*R*,11a*R*)-2-iodo-3,9-dioxo-1-phenyl-5,6,7,7a,8,9-hexahydro-3*H*-pyrrolo[2,1-j]quinoline-7-carbaldehyde (-)-48

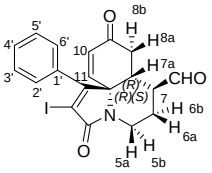

Following the *general procedure 4.1.1.4b*, the reaction of **43** (150 mg, 0.4 mmol), (*R*)-catalyst (23 mg, 0.07 mmol) and benzoic acid (9 mg, 0.07 mmol) in CH_2Cl_2 (12 mL) for 3 days 21 h at -20 ºC afforded, after purification by flash chromatography on silica gel (CH_2Cl_2/Acetone, 1-5 %), 134 mg (89 %) the desired product **(-)-48** as an off-white solid.

The spectroscopic data matched with previously reported.[114] $[\alpha]_D^{25}$ = - 80.00 º (*c*. 0.80 mg/mL, MeOH).

(7*S*,7a*S*,11a*R*)-2-iodo-3,9-dioxo-1-phenyl-5,6,7,7a,8,9-hexahydro-3*H*-pyrrolo[2,1-j]quinoline-7-carbaldehyde (+)-48

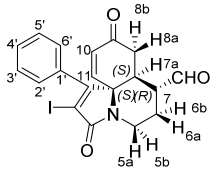

Following the *general procedure 4b*, the reaction of **43** (110 mg, 0.25 mmol), (*S*)-catalyst (16 mg, 0.05 mmol) and benzoic acid (6 mg, 0.05 mmol) in CH_2Cl_2 (9 mL) for 2 days 16 h at -20 ºC afforded, after purification by flash chromatography on silica gel (CH_2Cl_2/Acetone, 2-5 %), 87.6 mg (79 %) the desired product **(+)-48** as an off-white solid. The spectroscopic data matched with previously reported.[114] $[\alpha]_D^{27}$= + 92.50 º (*c*.1.20 mg/mL, MeOH).

1**-(3-fluorophenyl)-2-iodo-3,9-dioxo-5,6,7,7a,8,9-hexahydro-3*H*-pyrrolo[2,1-j]quinoline-7-carbaldehyde (±)-49**

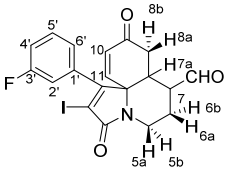

Following the *general procedure 4.1.1.4b*, the reaction of **44** (50 mg, 0.11 mmol), (±)-catalyst (7.2 mg, 0.022 mmol) and benzoic acid (2.7 mg, 0.022 mmol) in CH_2Cl_2 (7 mL) for 5 days 15 h at -20 ºC afforded, after purification by flash chromatography on silica gel (CH_2Cl_2/Acetone, 1-5 %), 45 mg (90 %) the desired product **(±)-49** as an off-white solid. Rf 0.14 (CH_2Cl_2/Acetone 95:5) m.p. 112 - 114 ºC ^{1}H NMR (250 MHz, $CDCl_3$) δ 9.59 (d, *J* = 1.6 Hz, 1H, CHO), 7.44 (td, *J* = 8.0, 5.7 Hz, 1H, H5'), 7.18 (tdd, *J* = 8.4, 2.6, 1.0 Hz, 1H, H4'), 7.01 (ddd, *J* = 7.6, 1.6, 1.0 Hz, 1H, H2'), 6.94 (dt, *J* = 9.0, 2.2 Hz, 1H, H6'), 6.40 (d, *J* = 1.0 Hz, 2H, H10, H11), 4.58 (ddd, *J* = 13.6, 4.7, 2.0 Hz, 1H, H5b), 3.01 (td, *J* = 13.0, 2.7 Hz, 1H, H5a), 2.77 - 2.63 (m, 1H, H8b), 2.54 (dd, *J* = 11.6, 5.0 Hz, 1H, H7a), 2.25 - 2.15 (m, 1H, H8a), 2.11 – 2.02 (m, 1H, H7), 1.90 (dd, *J* = 17.8, 5.1 Hz, 1H, H6b), 1.37 (qd, *J* = 12.7, 4.5 Hz, 1H, H, H6a) ppm.^{13}C NMR (63 MHz, $CDCl_3$) δ 199.6, 195.1, 164.8, 162.7 (d, *J* = 249.9 Hz), 161.0, 144.3, 136.1 (d, *J* = 8.1 Hz), 134.3, 131.3 (d, *J* = 8.5 Hz), 123.7 (d, *J* = 3.2 Hz), 117.2 (d, *J* = 20.9 Hz), 115.2 (d, *J* = 22.8 Hz), 100.2, 68.8, 49.6, 39.1, 38.5, 37.5, 25.9 ppm. ^{19}F NMR (235 MHz, $CDCl_3$) δ -110.33 (td, *J* = 8.8, 5.8 Hz) ppm. HRMS (ES^+) Theoretical mass calc. for $C_{19}H_{15}FINO_3$: 451.0081; found [$(M+H)^+$], 452.0193; [$(M+Na)^+$], 473.9978; [$(2M+Na)^+$], 925,0191, IR: (film) υ/ cm^{-1}: 3062, 2920, 2865, 1674, 1578, 1481, 1296, 1243, 1000, 969, 946, 793, 767, 679

(7*S*,7a*R*,11a*R*)-1-(3-fluorophenyl)-2-iodo-3,9-dioxo-5,6,7,7a,8,9-hexahydro-3*H*-pyrrolo[2,1-j]quinoline-7-carbaldehyde (-)-49

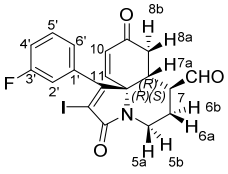

Following the *general procedure 4.1.1.4b*, the reaction of **44** (100 mg, 0.22 mmol), (*R*)-catalyst (14 mg, 0.04 mmol) and benzoic acid (5.4 mg, 0.04 mmol) in CH_2Cl_2 (13 mL) for 1 day 15 h at -20 ºC afforded, after purification by flash chromatography on silica gel (Hex/EtOAc, 30-70 %), 85 mg (85 %) the desired product **(-)-49** as an off-white solid. $[\alpha]_D^{20}$= - 93.75 º (C = 0.8 mg/ml, MeOH).

(7*R*,7a*S*,11a*S*)-1-(3-fluorophenyl)-2-iodo-3,9-dioxo-5,6,7,7a,8,9-hexahydro-3*H*-pyrrolo[2,1-j]quinoline-7-carbaldehyde (+)-49

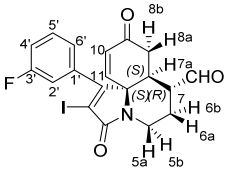

Following the *general procedure 4.1.1.4b*, the reaction of **44** (140 mg, 0.31 mmol), (*S*)-catalyst (20 mg, 0.06 mmol) and benzoic acid (7.6 mg, 0.06 mmol) in CH_2Cl_2 (19 mL) for 2 days 20 h at -20 ºC afforded, after purification by flash chromatography on silica gel (Hex/EtOAc. 30-60 %), 130 mg (93 %) the desired product **(+)-49** as an off-white solid. $[\alpha]_D^{21}$ = + 52.22 º (C = 0.90 mg/mL, MeOH).

2-iodo-3,9-dioxo-1-propyl-5,6,7,7a,8,9-hexahydro-3*H*-pyrrolo[2,1-j]quinoline-7-carbaldehyde (±)-50

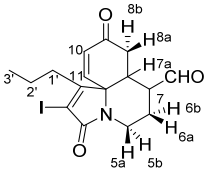

Following the *general procedure 4.1.1.4b*, the reaction of **45** (40 mg, 0.10 mmol), (±)-catalyst (6.5 mg, 0.02 mmol) and benzoic acid (2.4 mg, 0.02 mmol) in CH_2Cl_2 (4 mL) for 2 days 19 h at -20 ºC afforded, after purification by flash chromatography on silica gel (CH_2Cl_2/Acetone, 1-5 %), 28.9 mg (72 %) the desired product **(±)-50** as an off-white solid. Rf 0.29 (CH_2Cl_2/Acetone 95:5) m.p. 132 - 134 ºC ^{1}H NMR (300 MHz,C_6D_6) δ 8.72 (d, *J* = 1.7 Hz, 1H, CHO), 5.80 (d, *J* = 10.2 Hz, 1H, H10), 4.92 (dd, *J* = 10.2, 2.1 Hz, 1H, H11), 4.08 (ddd, *J* = 13.3, 4.7, 2.0 Hz, 1H, H5b), 2.40 (d, *J* = 3.6 Hz, 2H, H1'), 2.07 - 1.94 (m, 2H, H8b, H8a), 1.94 - 1.85 (m, 1H, H5a), 1.84 - 1.78 (m, 1H, H2'), 1.76 - 1.60 (m, 1H, H2'), 1.43 (dddd, *J* = 13.3, 11.2, 7.7, 6.1 Hz, 1H, H7a), 1.13 (tdd, *J* = 12.7, 7.4, 5.4 Hz, 1H, H7), 0.85 (ddt, *J* = 10.7, 6.3, 2.9 Hz, 1H, H6b), 0.65 (t, *J* = 7.3 Hz, 3H, H3'), 0.45 (qd, *J* = 12.7, 4.7 Hz, 1H, H6a) ppm. ^{13}C NMR (75 MHz, C_6D_6) δ 199.1, 194.0, 164.4, 162.8, 146.2, 132.7, 98.8, 67.7, 49.7, 39.2, 38.3, 36.6, 32.9, 25.4, 21.7, 14.3 ppm.

HRMS (ES$^+$): Theoretical mass calc. for $C_{16}H_{18}INO_3Na$ 422.0229; found [$(M+Na)^+$], 422.0223; found[$(2M+Na)^+$], 821.0499. IR (film) υ/cm^{-1} 3435, 3031, 2960, 2930, 2873, 2849, 2822, 2722, 1728, 1706, 1680, 1452, 1403, 1297, 1178, 1033, 957, 755

(7*S*,7a*R*,11a*R*)-2-iodo-3,9-dioxo-1-propyl-5,6,7,7a,8,9-hexahydro-3*H*-pyrrolo[2,1-j]quinoline-7-carbaldehyde (-)-50

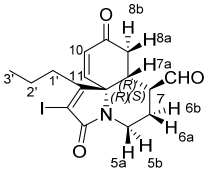

Following the *general procedure 4.1.1.4b*, the reaction of **45** (109 mg, 0.27 mmol), (*R*)-catalyst (17.6 mg, 0.05 mmol) and benzoic acid (6.6 mg, 0.05 mmol) in CH_2Cl_2 (11 mL) for 5 days 14 h at -20 ºC afforded, after purification by flash chromatography on silica gel (CH_2Cl_2/Acetone; 1-5 %), 86.7 mg (80 %) the desired product **(-)-50** as an off-white solid. $[\alpha]_D^{29}$= - 109.09 º (c. 0.99 mg/mL, MeOH).

(7*R*,7a*S*,11a*S*)-2-iodo-3,9-dioxo-1-propyl-5,6,7,7a,8,9-hexahydro-3*H*-pyrrolo[2,1-j]quinoline-7-carbaldehyde (+)-50

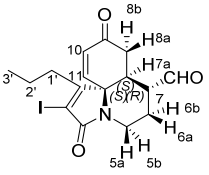

Following the *general procedure 4.1.1.4b*, the reaction of **45** (90.5mg, 0.23 mmol), (*S*)-catalyst (16.3 mg, 0.05 mmol) and benzoic acid (6.1 mg, 0.05 mmol) in CH_2Cl_2 (8 mL) for 4 days 19 h at -20 ºC afforded, after purification by flash chromatography on silica gel (CH_2Cl_2/Acetone, 1-5 %), 73.5 mg (81 %) the desired product **(+)-50** as an off-white solid. $[\alpha]_D^{30}$= + 72.03 º (C = 1.18 mg/mL, MeOH).

(1-cyclopropyl-2-iodo-3,9-dioxo-5,6,7,7a,8,9-hexahydro-3*H*-pyrrolo[2,1-j]quinoline-7-carbaldehyde (±)-51

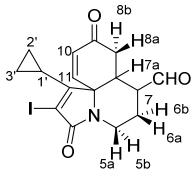

Following the *general 4.1.1.4b*, the reaction of **46** (100 mg, 0.25 mmol), (±)-catalyst (16.3 mg, 0.05 mmol) and benzoic acid (6.1 mg, 0.05 mmol) in CH_2Cl_2 (10 mL) for 1 day 15 h at -20 ºC afforded, after purification by flash chromatography on silica gel (CH_2Cl_2/Acetone, 2-5 %), 60 mg (60 %) the desired product **(±)-51** as an off-white solid. The spectroscopic data matched with previously reported.[114] ^{1}H NMR (300 MHz, C_6D_6) δ 8.78 (d, *J* = 1.7 Hz, 1H, C*H*O), 5.84 (d, *J* = 10.2 Hz, 1H, H11), 5.00 (dd, *J* = 10.1, 1.9 Hz, 1H, H10), 4.10 (ddd, *J* = 13.4, 4.7, 2.0 Hz, 1H, H5b), 2.85 (dd, *J* = 17.9, 5.0 Hz, 1H, H8b), 2.43 (d, *J* = 17.9 Hz, 1H, H8a), 2.03 (td, *J* = 13.1, 3.0 Hz, 1H, H5a), 1.92 - 1.62 (m, 2H, H7a, H7),

1.32 (dt, *J* = 9.8, 5.1 Hz, 1H, H1'), 0.89 (dq, *J* = 13.0, 2.8 Hz, 1H, H6b), 0.79 - 0.63 (m, 2H, H2', H3'), 0.63 - 0.40 (m, 1H, H6a), 0.36 - 0.20 (m, 2H, H2', H3') ppm.

(7*S*,7a*R*,11a*R*)-1-cyclopropyl-2-iodo-3,9-dioxo-5,6,7,7a,8,9-hexahydro-3*H*-pyrrolo[2,1-j]quinoline-7-carbaldehyde (-)-51

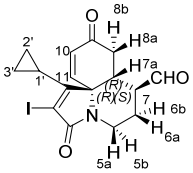

Following the *general procedure 4.1.1.4b*, the reaction of **46** (177 mg, 0.45 mmol), (*R*)-catalyst (29.3 mg, 0.09 mmol) and benzoic acid (11.0 mg, 0.09 mmol) in CH_2Cl_2 (35 mL) for 3 days 18 h at -20 ºC afforded, after purification by flash chromatography on silica gel (CH_2Cl_2/Acetone, 2-4 %), 150 mg (85 %) the desired product **(-)-51** as an off-white solid. $[\alpha]_D^{24}$= -101.48 º (*c*. 1.35 mg/mL, MeOH).

(7*R*,7a*S*,11a*S*)-1-cyclopropyl-2-iodo-3,9-dioxo-5,6,7,7a,8,9-hexahydro-3*H*-pyrrolo[2,1-j]quinoline-7-carbaldehyde (+)-51

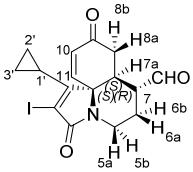

Following the *general procedure 4.1.1.4b*, the reaction of **46** (144 mg, 0.36 mmol), (*S*)-catalyst (23.4 mg, 0.07 mmol) and benzoic acid (8.8 mg, 0.07 mmol) in CH_2Cl_2 (13 mL) for 3 days 18 h at -20 ºC afforded, after purification by flash chromatography on silica gel (CH_2Cl_2/Acetone, 2-5 %), 123 mg (86 %) the desired product **(+)-51** as an off-white solid. $[\alpha]_D^{24}$= + 140.00 º (*c*. 0.70 mg/mL, MeOH).

1-cyclohexyl-2-iodo-3,9-dioxo-5,6,7,7a,8,9-hexahydro-3*H*-pyrrolo[2,1-j]quinoline-7-carbaldehyde (±)-52

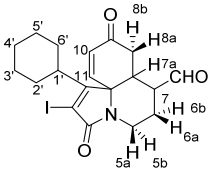

Following the *general procedure 4.1.1.4b*, the reaction of **47** (90 mg, 0.20 mmol), (±)-catalyst (13 mg, 0.04 mmol) and benzoic acid (4.9 mg, 0.04 mmol) in CH_2Cl_2 (16 mL) for 4 days 20.5 h at -20 ºC afforded, after purification by flash chromatography on silica gel (CH_2Cl_2/Acetone, 1-3 %), 66.7 mg (74 %) the desired product **(±)-52** as an off-white solid. Rf 0.38 (CH_2Cl_2/Acetone 95:5) m.p. 146 - 148 ºC ^{1}H NMR (300 MHz, C_6D_6) δ 8.68 (d, *J* = 1.9 Hz, 1H, C*H*O), 5.86 (d, *J* = 10.2 Hz, 1H, H10), 4.98 (dd, *J* = 10.2, 1.9 Hz, 1H, H11), 4.09 (ddd, *J* = 13.3, 4.9, 2.0 Hz, 1H, H5b), 2.57 - 2.41 (m, 2H, H8aH8b), 2.39 - 2.16 (m, 1H, H1'), 2.11 (dd, *J* = 12.2, 3.3 Hz, 1H, H2'), 2.04 (dd, *J* = 8.7, 3.0 Hz, 1H, H6'), 1.95 (dd, *J* = 13.0, 3.0 Hz, 1H, H5a), 1.87 - 1.76 (m, 1H, H7a), 1.69 (ddd, *J* = 12.8, 3.8, 1.7 Hz, 1H, H7), 1.58 (d, *J* = 13.1 Hz, 2H, H4', H6'), 1.37 (t, *J* = 16.5 Hz, 2H, H3', H5'), 1.10

(dt, *J* = 12.6, 3.5 Hz, 2H, H2', H4'), 0.92 - 0.70 (m, 3H, H6b, H3', H5'), 0.59 - 0.34 (m, 1H, H6a) ppm. ^{13}C NMR (75 MHz, C_6D_6) δ 199.2, 194.1, 165.1, 145.3, 133.3, 94.0, 68.9, 50.3, 39.2, 39.1, 36.9, 28.8, 28.4, 26.5, 25.6, 25.3 ppm. HRMS (ES^+) Theoretical mass calc. for $C_{19}H_{22}INO_3$, 439.0644; found [$(M+H)^+$], 440.0718; found[$(M+Na)^+$], 462.0536; found [$(2M+Na)^+$], 901.1207. IR (film) υ/cm^{-1} 2921, 2851, 1675, 1446, 1400, 1298, 1214, 1029, 951, 891, 864, 813, 790, 745.

(7*S*,7a*R*,11a*R*)-1-cyclohexyl-2-iodo-3,9-dioxo-5,6,7,7a,8,9-hexahydro-3*H*-pyrrolo[2,1-j]quinoline-7-carbaldehyde (-)-52

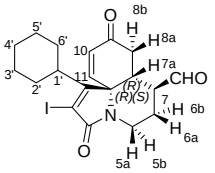

Following the *general procedure 4.1.1.4b*, the reaction of **47** (90 mg, 0.20 mmol), (*R*)-catalyst (13 mg, 0.04 mmol) and benzoic acid (4.9 mg, 0.04 mmol) in CH_2Cl_2 (7 mL) for 3 days 21 h at -20 ºC afforded, after purification by flash chromatography on silica gel (CH_2Cl_2/Acetone, 2-4 %), 79.7 mg (89 %) the desired product **(-)-52** as an off-white solid. α_D^{20} = - 195.79 º (C = 0.95 mg/mL, MeOH).

(7*R*,7a*S*,11a*S*)-1-cyclohexyl-2-iodo-3,9-dioxo-5,6,7,7a,8,9-hexahydro-3*H*-pyrrolo[2,1-j]quinoline-7-carbaldehyde (+)-52

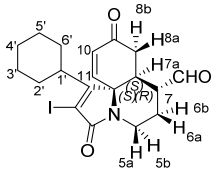

Following the *general procedure 4.1.1.4b*, the reaction of **47** (112 mg, 0.26 mmol), (*S*)-catalyst (17 mg, 0.052 mmol) and benzoic acid (6.3 mg, 0.052 mmol) in CH_2Cl_2 (9 mL) for 2 days 17 h at -20 ºC afforded, after purification by flash chromatography on silica gel (CH_2Cl_2/Acetone, 2-4 %), 78.4 mg (70 %) the desired product **(+)-52** as an off-white solid. α_D^{21} = + 118.27 º (C = 1.04 mg/mL, MeOH).

2-iodo-7-(((2-(5-methoxy-1*H*-indol-3-yl)ethyl)amino)methyl)-1-phenyl-6,7,7a,8-tetrahydro-3*H*-pyrrolo[2,1-j]quinoline-3,9(5*H*)-dione (±)-54

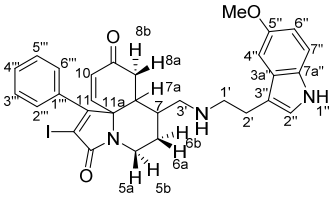

Following the *general procedure 4.1.1.5*, the reaction of **(±)-48** (100 mg, 0.2 mmol), 5-methoxy-tryptamine **53** (43.9 mg, 0.2 mmol) and $Na(AcO)_3BH$ (61.3 mg, 0.3 mmol) in CH_2Cl_2 (10 mL) for 20 h afforded, after purification by flash chromatography on silica gel (CH_2Cl_2/MeOH; 0-6 %), 98 mg (71 %) of the desired compound **(±)-54** as an off-white solid. Rf 0.22 (CH_2Cl_2/MeOH 95:5). m.p. 124 - 126 ºC. ^{1}H NMR (250 MHz, $CDCl_3$) δ 7.95 (s, 1H, H1''), 7.51 - 7.34 (m, 3H, H3''', H4''', H5'''),

7.25 (d, *J* = 8.3 Hz, 1H, H7''), 7.22 - 7.13 (m, 2H, H2''', H6'''), 7.00 (d, *J* = 3.0 Hz, 1H, H2''), 6.98 (d, *J* = 3.1 Hz, 1H, H4''), 6.85 (dd, *J* = 8.8, 2.4 Hz, 1H, H6''), 6.35 (dd, *J* = 10.1, 1.8 Hz, 1H, H11), 6.29 (d, *J* = 10.1 Hz, 1H, H10), 4.40 (dt, *J* = 13.7, 3.1, 1.3 Hz, 1H, H5b), 3.84 (d, *J* = 3.6 Hz, 3H, OC*H*$_3$), 2.84 (d, *J* = 4.2 Hz, 5H, H5a, 2xH1', 2xH2'), 2.69 (dd, *J* = 12.3, 3.1 Hz, 1H, H3'), 2.52 - 2.28 (m, 2H, H8b, H3'), 2.01 (d, *J* = 10.2 Hz, 1H, H7a), 1.81 (dd, *J* = 17.5, 5.0 Hz, 1H, H8a), 1.73 - 1.43 (m, 3H, H6b, H7, NH), 1.33 - 1.12 (m, 1H, H6a) ppm. ^{13}C NMR (63 MHz, $CDCl_3$) δ 196.5, 165.1, 162.7, 154.0, 145.1, 134.8, 133.8, 131.6, 129.8, 129.2, 127.8, 127.8, 123.0, 113.4, 112.4, 112.1, 100.7, 99.6, 70.2, 56.1, 51.7, 50.1, 43.5, 38.6, 37.6, 36.7, 30.0, 25.7 ppm. IR (film) υ/cm^{-1} 3330, 3312, 2908, 2359, 1673, 1581, 1483, 1439, 1398, 1296, 1212, 1171, 1028, 920, 792, 759, 702. Compound purity was estimated by reversed phase C18 HPLC, with a UV detector at 254 nm, from ACN/H_2O, 5:95 + 0.1 % FA to ACN/H_2O, 95:5 + 0.1 % FA, and the major peak area of the tested compound was 100 %.

(7*S*, 7a*R*, 11a*R*)-2-iodo-7-(((2-(5-methoxy-1*H*-indol-3-yl)ethyl)amino)methyl)-1-phenyl-6,7,7a,8-tetrahydro-3*H*-pyrrolo[2,1-j]quinoline-3,9(5*H*)-dione (-)-54

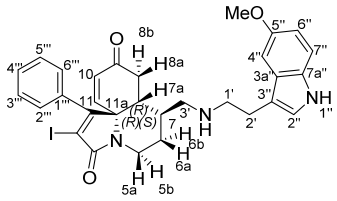

Following the *general procedure 4.1.1.5*, the reaction of **(-)-48** (100 mg, 0.2 mmol), 5-methoxy-tryptamine **53** (44 mg, 0.2 mmol) and Na(AcO)$_3$BH (64 mg, 0.3 mmol) in CH_2Cl_2 (10 mL) for 20 h afforded, after purification by flash chromatography on silica gel (CH_2Cl_2/MeOH, 0-5 %), 93 mg (66 %) of the desired compound **(-)-54** as an off-white solid. $[\alpha]_D^{24}$= - 90.53 º (*c*. 0.95 mg/mL, MeOH). e.e. 89 % The enantiomers were separated by HPLC (ULTRON ES OVM Chiral Analytical Reverse Phase, 5μm, 4.6 mm x 150 L, buffer $H_2PO_4^-$ pH 4.3/ MeOH 70:30, flow 1.0 mL/min, retention time 3.167 min (minor) and 3.787 min (major). Compound purity was estimated by reversed phase C18 HPLC, with a UV detector at 254 nm, from ACN/H_2O, 5:95 + 0.1 % FA to ACN/H_2O, 95:5 + 0.1 % FA, and the major peak area of the tested compound was 100 %.

(7*R*,7a*S*,11a*S*)-2-iodo-7-(((2-(5-methoxy-1*H*-indol-3-yl)ethyl)amino)methyl)-1-phenyl-6,7,7a,8-tetrahydro-3*H*-pyrrolo[2,1-j]quinoline-3,9(5*H*)-dione (+)-54

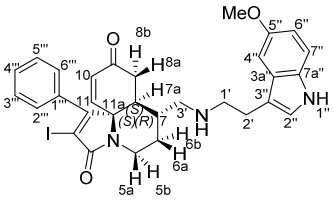

Following the *general procedure 4.1.1.5*, the reaction of **(+)-48** (83 mg, 0.2 mmol), 5-methoxy-tryptamine **53** (36 mg, 0.2 mmol) and $Na(AcO)_3BH$ (55 mg, 0.3 mmol) in CH_2Cl_2 (8 mL) for 20 h afforded, after purification by flash chromatography on silica gel (CH_2Cl_2/MeOH, 0-5 %), 83 mg (72 %) of the desired compound **(+)-54** as an off-white solid. $[\alpha]_D^{24}$= + 124.62 º (*c*.0.65 mg/mL, MeOH) e.e. 87 % The enantiomers were separated by HPLC (ULTRON ES OVM Chiral Analytical Reverse Phase, 5 μm, 4.6 mm x 150 L,buffer $H_2PO_4^-$ pH 4.3/MeOH 70:30, flow 1.0 mL/min, retention time 2.977 min (major) and 3.607 min (minor). Compound purities were estimated by reversed phase C18 HPLC, with a UV detector at 254 nm, from ACN/H_2O, 5:95 + 0.1 % FA to ACN/H_2O, 95:5 + 0.1 % FA, and the major peak area of the tested compound was 100 %.

1-(3-fluorophenyl)-2-iodo-7-(((2-(5-methoxy-1*H*-indol-3-yl)ethyl)amino)methyl)-6,7,7a,8-tetrahydro-3*H*-pyrrolo[2,1-j]quinoline-3,9(5*H*)-dione (±)-55

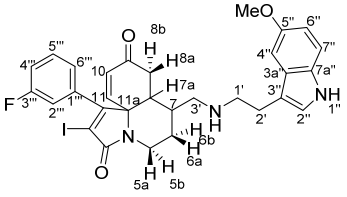

Following the *general procedure 4.1.1.5*, the reaction of **(±)-49** (45 mg, 0.1 mmol), 5-methoxy-tryptamine **53** (19 mg, 0.1 mmol) and $Na(AcO)_3BH$ (28 mg, 0.1 mmol) in CH_2Cl_2 (4 mL) for 20 h afforded, after purification by flash chromatography on silica gel (CH_2Cl_2/MeOH, 1-4 %), 33 mg (52 %) of the desired compound **(±)-55** as an off-white solid. Rf 0.17 (CH_2Cl_2/MeOH 95:5) m.p. 122 - 124 ºC ^{1}H NMR (500 MHz, $CDCl_3$) δ 7.99 (s, 1H, H1’’), 7.40 (td, *J* = 8.0, 5.7 Hz, 1H, H5’’’), 7.25 (d, *J* = 8.2 Hz, 1H, H7’’), 7.15 (td, *J* = 8.5, 2.4 Hz, 1H, H4’’’), 7.01 (d, *J* = 2.3 Hz, 2H, H2’’, H4’’), 6.96 (d, *J* = 7.7 Hz, 1H, H6’’’), 6.90 (d, *J* = 8.6 Hz, 1H, H2’’’), 6.86 (dd, *J* = 8.8, 2.4 Hz, 1H, H6’’), 6.32 (d, *J* = 1.4 Hz, 2H, H10, H11), 4.38 (dd, *J* = 13.4, 4.4 Hz, 1H, H5b), 3.85 (s, 3H, OC*H*3), 2.89 (dd, *J* = 10.5, 7.1 Hz, 4H, H1’, H2’), 2.81 (td, *J* = 13.3, 2.8 Hz, 1H, H5a), 2.71 (dd, *J* = 12.5, 3.1 Hz, 1H, H3’), 2.46 (dd, *J* = 12.5, 6.8 Hz, 1H, H3’), 2.40 (dd, *J* = 17.3, 2.1 Hz, 1H, H8b), 2.04 (d, *J* = 8.2 Hz, 1H, H7a), 1.84 (dd, *J* = 17.3, 4.9 Hz, 1H, H8a), 1.71 (t, *J* = 13.4 Hz, 2H, H6b, H7), 1.28 - 1.15 (m, 1H, H6a) ppm. ^{13}C NMR (126 MHz, $CDCl_3$) δ 196.1, 164.8, 162.8 (d, *J* = 249.5 Hz), 161.2 (d, *J* =

2.3 Hz), 154.1, 144.8, 136.7 (d, *J* = 8.1 Hz), 134.0, 131.7, 131.2 (d, *J* = 8.6 Hz), 127.8, 123.7 (d, *J* = 3.3 Hz), 123.1, 117.0 (d, *J* = 20.9 Hz), 115.3 (d, *J* = 22.6 Hz), 113.2, 112.5, 112.1, 100.8, 100.5, 70.2, 56.1, 51.5, 50.0, 43.4, 38.6, 37.7, 36.6, 29.9, 25.4 ppm. ^{19}F NMR (235 MHz, $CDCl_3$) δ -110.69 (td, *J* = 8.7, 5.8 Hz) ppm IR (film) υ/cm^{-1} 3314, 2916, 1673, 1579, 1481, 1437, 1399, 1284, 1211, 1171, 1065, 1027, 962, 827, 791, 766, 745, 712. Compound purity was estimated by reversed phase C18 HPLC, with a UV detector at 254 nm, from ACN/H_2O, 5:95 + 0.1 % FA to ACN/H_2O, 95:5 + 0.1 % FA, and the major peak area of the compound was 99 %.

(7*S*,7a*R*,11a*R*)-1-(3-fluorophenyl)-2-iodo-7-(((2-(5-methoxy-1*H*-indol-3-yl)ethyl)amino)methyl)-6,7,7a,8-tetrahydro-3*H*-pyrrolo[2,1-j]quinoline-3,9(5*H*)-dione (-)-55

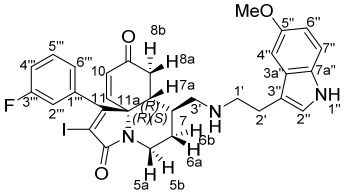

Following the *general procedure 4.1.1.5*, the reaction of **(-)-49** (70 mg, 0.2 mmol), 5-methoxy-tryptamine **53** (30 mg, 0.2 mmol) and $Na(AcO)_3BH$ (45.9 mg, 0.2 mmol) in CH_2Cl_2 (8 mL) for 21 h afforded, after purification by flash chromatography on silica gel (CH_2Cl_2/MeOH, 2-5 %), 71 mg (70 %) of the desired compound **(-)-55** as an off-white solid. $[\alpha]_D^{21}$= - 100.00 º (*c*. 1.30 mg/mL, MeOH) e.e. 91 % The enantiomers were separated by HPLC (ULTRON ES OVM Chiral Analytical Reverse Phase, 5 μm, 4.6 mm x 150 L,buffer $H_2PO_4^-$ pH 4.3/ MeOH 70:30, flow 1.0 mL/min, retention time.180 min (minor), 3.487 min (major). Compound purity was estimated by reversed phase C18 HPLC, with a UV detector at 254 nm, from ACN/H_2O, 5:95 + 0.1 % FA to ACN/H_2O, 95:5 + 0.1 % FA, and the major peak area of the compound was 100 %.

(7*R*,7a*S*,11a*S*)-1-(3-fluorophenyl)-2-iodo-7-(((2-(5-methoxy-1*H*-indol-3-yl)ethyl)amino)methyl)-6,7,7a,8-tetrahydro-3*H*-pyrrolo[2,1-j]quinoline-3,9(5*H*)-dione (+)-55

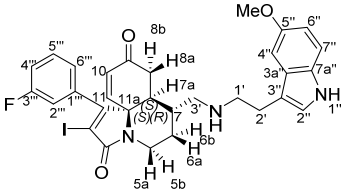

Following the *general procedure 4.1.1.5*, the reaction of **(+)-49** (40 mg, 0.1 mmol), 5-methoxy-tryptamine **53** (17 mg, 0.1 mmol) and $Na(AcO)_3BH$ (39 mg, 0.2 mmol) in CH_2Cl_2 (4 mL) for 23 h afforded, after purification by flash chromatography on silica gel (CH_2Cl_2/MeOH, 2-5 %), 29 mg (52 %)

of the desired compound **(+)-55** as an off-white solid. $[\alpha]_D^{24}$= + 50.00 º (*c*.0.75 mg/mL, MeOH) e.e. 89 % The enantiomers were separated by HPLC (ULTRON ES OVM Chiral Analytical Reverse Phase, 5 μm, 4.6 mm x 150 L,buffer $H_2PO_4^-$ pH 4.3/ MeOH 70:30, flow 1.0 mL/min, retention time 3.203 min (major), 3.637 min (minor). Compound purity was estimated by reversed phase C18 HPLC, with a UV detector at 254 nm, from ACN/H_2O, 5:95 + 0.1 % FA to ACN/H_2O, 95:5 + 0.1 % FA, and the major peak area of the compound was 95 %.

2-iodo-7-(((2-(5-methoxy-1*H*-indol-3-yl)ethyl)amino)methyl)-1-propyl-6,7,7a,8-tetrahydro-3*H*-pyrrolo[2,1-j]quinoline-3,9(5*H*)-dione (±)-56

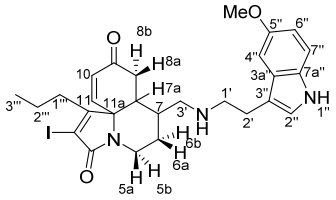

Following the *general 4.1.1.5*, the reaction of **(±)-50** (100 mg, 0.3 mmol), 5-methoxy-tryptamine **53** (48 mg, 0.3 mmol) and Na(AcO)$_3$BH (71 mg, 0.3 mmol) in CH_2Cl_2 (11 mL) for 24 h afforded, after purification by flash chromatography on silica gel (CH_2Cl_2/MeOH, 0-5 %), 108 mg (75 %) of the desired compound **(±)-56** as an off-white solid. Rf 0.17 (CH_2Cl_2/MeOH 95:5) m.p. 86 - 88 ºC ^{1}H NMR (250 MHz, $CDCl_3$) δ 7.92 (s, 1H, H1’’), 7.26 (d, *J* = 8.8 Hz, 1H, H7’’), 7.02 (s, 2H, H2’’, H4’’), 6.86 (dd, *J* = 8.8, 2.4 Hz, 1H, H6’’), 6.28 (d, *J* = 10.2 Hz, 1H, H10), 6.10 (dd, *J* = 10.0, 1.9 Hz, 1H, H11), 4.32 (dd, *J* = 13.3, 4.0 Hz, 1H, H5b), 3.86 (d, *J* = 0.6 Hz, 3H, OC*H*$_3$), 2.88 (d, *J* = 8.5 Hz, 5H, 2xH1’, 2xH2’, H8b), 2.81 - 2.68 (m, 3H, H5a, H8a, H3’), 2.50 (dd, *J* = 12.4, 6.5 Hz, 1H, H3’), 2.39 (dd, *J* = 11.1, 5.8 Hz, 1H, H1’’’), 2.35 - 2.23 (m, 1H, H1’’’), 2.07 - 1.91 (m, 1H, H7a), 1.87 - 1.58 (m, 4H, H6b, H7, NH, H2’’’), 1.47 (d, *J* = 6.6 Hz, 1H, H2’’’), 1.30 – 1.08 (m, 1H, H6a), 1.01 (t, *J* = 7.2 Hz, 3H, H3’’’) ppm. ^{13}C NMR (75 MHz, $CDCl_3$) δ 196.6, 165.4, 163.6, 154.1, 147.4, 132.9, 131.7, 127.9, 122.9, 113.7, 112.4, 112.0, 100.9, 98.2, 69.7, 56.1, 52.0, 50.3, 43.2, 38.4, 38.3, 37.3, 33.4, 30.16, 25.8, 21.8, 14.7 ppm. IR (film) υ/cm^{-1} 3313, 2923, 2871, 1728, 1706, 1670, 1483, 1451, 1401, 1379, 1294, 1211, 1170, 1100, 1066, 1028, 920, 792, 747, 684. Compound purity was estimated by reversed phase C18 HPLC, with a UV detector at 254 nm, from ACN/H_2O, 5:95 + 0.1 % FA to ACN/H_2O, 95:5 + 0.1 % FA, and the major peak area of the compound was 99 %.

(7*S*,7a*R*,11a*R*)-2-iodo-7-(((2-(5-methoxy-1*H*-indol-3-yl)ethyl)amino)methyl)-1-propyl-6,7,7a,8-tetrahydro-3*H*-pyrrolo[2,1-j]quinoline-3,9(5*H*)-dione (-)-56

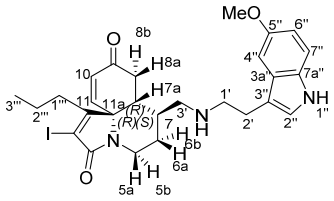

Following the *general procedure 5*, the reaction of **(-)-50** (80 mg, 0.2 mmol), 5-methoxy-tryptamine **53** (38 mg, 0.2 mmol) and $Na(AcO)_3BH$ (87 mg, 0.4 mmol) in CH_2Cl_2 (9 mL) for 22 h afforded, after purification by flash chromatography on silica gel (CH_2Cl_2/MeOH, 0-5 %), 90 mg (79 %) of the desired compound **(-)-56** as an off-white solid. $[\alpha]_D^{24}$= -113.75 º (*c*. 0.80 mg/mL, MeOH) e.e. 85 % The enantiomers were separated by HPLC (ULTRON ES OVM Chiral Analytical Reverse Phase, 5µm, 4.6 mm x 150 L, buffer $H_2PO_4^-$ pH 4.3/MeOH 70:30, flow 1.0 mL/min, retention time 3.040 min (minor), 4.300 min (major). Compound purity was estimated by reversed phase C18 HPLC, with a UV detector at 254 nm, from ACN/H_2O, 5:95 + 0.1 % FA to ACN/H_2O, 95:5 + 0.1 % FA, and the major peak area of the tested compound was 100 %.

(7*R*,7a*S*,11a*S*)-2-iodo-7-(((2-(5-methoxy-1*H*-indol-3-yl)ethyl)amino)methyl)-1-propyl-6,7,7ª,8-tetrahydro-3*H*-pyrrolo[2,1-j]quinoline-3,9(5*H*)-dione (+)-56

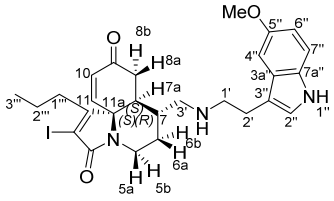

Following the *general procedure 4.1.1.5*, the reaction of **(+)-50** (72 mg, 0.2 mmol), 5-methoxy-tryptamine **53** (34 mg, 0.2 mmol) and $Na(AcO)_3BH$ (51 mg, 0.2 mmol) in CH_2Cl_2 (8 mL) for 18 h afforded, after purification by flash chromatography on silica gel (CH_2Cl_2/MeOH, 0-5 %), 72 mg (70 %) of the desired compound **(+)-56** as an off-white solid. $[\alpha]_D^{24}$= + 145.45 º (*c*.0.55 mg/mL, MeOH). e.e. 88 % The enantiomers were separated by HPLC (ULTRON ES OVM Chiral Analytical Reverse Phase, 5 µm, 4.6 mm x 150 L, buffer $H_2PO_4^-$ pH 4.3/MeOH 70:30, flow 1.0 mL/min, retention time 2.960 min (major), 4.613 min (minor). Compound purity was estimated by reversed phase C18 HPLC, with a UV detector at 254 nm, from ACN/H_2O, 5:95 + 0.1 % FA to ACN/H_2O, 95:5 + 0.1 % FA, and the major peak area of the compound was 95 %.

1-cyclopropyl-2-iodo-7-(((2-(5-methoxy-1*H*-indol-3-yl)ethyl)amino)methyl)-6,7,7a,8-tetrahydro-3*H*-pyrrolo[2,1-j]quinoline-3,9(5*H*)-dione (±)-57

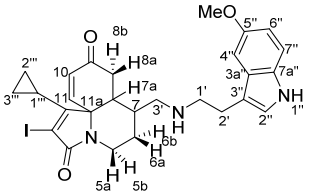

Following the *general procedure 4.1.1.5*, the reaction of **(±)-51** (60 mg, 0.2 mmol), 5-methoxy-tryptamine **53** (29 mg, 0.2 mmol) and $Na(AcO)_3BH$ (49 mg, 0.2 mmol) in CH_2Cl_2 (7 mL) for 16 h afforded, after purification by flash chromatography on silica gel (CH_2Cl_2/MeOH, 0-5 %), 88 mg (62 %) of the desired compound **(±)-57** as an off-white solid. Rf 0.16 (CH_2Cl_2/MeOH 95:5) m.p. 145 - 147 ºC ^{1}H NMR (250 MHz, $CDCl_3$) δ 7.96 (s, 1H, H1''), 7.26 (d, *J* = 8.0 Hz, 1H, H7''), 7.09 - 7.00 (m, 2H, H2'', H4''), 6.86 (dd, *J* = 8.8, 2.5 Hz, 1H, H6''), 6.29 (d, *J* = 10.2 Hz, 1H, H10), 6.24 - 6.13 (m, 1H, H11), 4.32 (dd, *J* = 13.7, 3.9 Hz, 1H, H5b), 3.87 (d, *J* = 1.8 Hz, 3H, OC*H*$_3$), 3.30 (dd, *J* = 17.8, 5.1 Hz, 1H, H8b), 2.89 (d, *J* = 2.4 Hz, 4H, 2xH1', 2xH2'), 2.77 (ddd, *J* = 10.3, 8.2, 5.3 Hz, 3H, H5a, H8a, H3'), 2.52 (dd, *J* = 12.3, 6.4 Hz, 1H, H3'), 2.03 (d, *J* = 6.2 Hz, 1H, H7a), 1.81 - 1.55 (m, 4H, H6b, H7, H2''', NH), 1.57 - 1.38 (m, 1H, H3'''), 1.30 - 1.16 (m, 1H, H2'''), 1.15 – 1.01 (m, 2H, H6a, H3'''), 0.92 (dt, *J* = 8.1, 5.5 Hz, 1H, H1''') ppm. ^{13}C NMR (63 MHz, $CDCl_3$) δ 197.1, 165.8, 161.6, 154.1, 147.7, 133.1, 131.6, 127.8, 123.0, 113.4, 112.4, 112.1, 100.7, 92.4, 70.5, 56.1, 51.8, 50.1, 43.7, 38.4, 38.2, 37.3, 30.0, 25.7, 12.7, 9.0, 7.7 ppm. HRMS (ES^+) Theoretical mass calc. for $C_{27}H_{30}IN_3O_3$ 571.1332; found [$(M+H)^+$], 572.1423 IR (film) υ/cm^{-1} 3313, 2902, 2827, 1670, 1597, 1483, 1441, 1406, 1298, 1211, 1171, 1106, 1065, 1027, 919, 794, 747. Compound purity was estimated by reversed phase C18 HPLC, with a UV detector at 254 nm, from ACN/H_2O, 5:95 + 0.1 % FA to ACN/H_2O, 95:5 + 0.1 % FA, and the major peak area of the compound was 99 %.

(7*S*,7a*R*,11a*R*)-1-cyclopropyl-2-iodo-7-(((2-(5-methoxy-1*H*-indol-3-yl)ethyl)amino)methyl)-6,7,7a,8-tetrahydro-3*H*-pyrrolo[2,1-j]quinoline-3,9(5*H*)-dione (-)-57

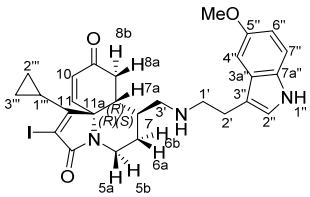

Following the *general procedure 4.1.1.5*, the reaction of **(-)-51** (147 mg, 0.4 mmol), 5-methoxy-tryptamine **53** (70 mg, 0.4 mmol) and $Na(AcO)_3BH$ (105 mg, 0.5 mmol) in CH_2Cl_2 (16 mL) for 21 h afforded, after purification by flash chromatography on silica gel (CH_2Cl_2/MeOH, 0-5 %), 134 mg (64 %) of the desired

compound **(-)-57** as an off-white solid. $[\alpha]_D^{24}$= - 106.67 º (*c*. 0.75 mg/mL, MeOH) e.e. 92 % The enantiomers were separated by HPLC (ULTRON ES OVM Chiral Analytical Reverse Phase, 5 µm, 4.6 mm x 150 L, buffer $H_2PO_4^-$ pH 4.3/MeOH 70:30, flow 1.0 mL/min, retention time 3.247 min (minor), 7.102 min (major). Compound purity was estimated by reversed phase C18 HPLC, with a UV detector at 254 nm, from ACN/H_2O, 5:95 + 0.1 % FA to ACN/H_2O, 95:5 + 0.1 % FA, and the major peak area of the compound was 99 %.

(7*R*,7a*S*,11a*S*)-1-cyclopropyl-2-iodo-7-(((2-(5-methoxy-1*H*-indol-3-yl)ethyl)amino)methyl)-6,7,7a,8-tetrahydro-3*H*-pyrrolo[2,1-j]quinoline-3,9(5*H*)-dione (+)-57

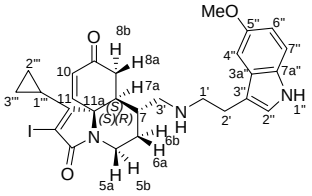

Following the *general procedure 4.1.1.5*, the reaction of **(+)-51** (110 mg, 0.3 mmol), 5-methoxy-tryptamine **53** (53 mg, 0.3 mmol) and $Na(AcO)_3BH$ (80 mg, 0.4 mmol) in CH_2Cl_2 (12 mL) for 21 h afforded, after purification by flash chromatography on silica gel (CH_2Cl_2/MeOH, 0-5 %), 115 mg (72 %) of the desired compound **(+)-57** as an off-white solid. $[\alpha]_D^{24}$= + 107.14 º (*c*.0.70 mg/mL, MeOH) e.e. 95 % The enantiomers were separated by HPLC (ULTRON ES OVM Chiral Analytical Reverse Phase, 5 µm, 4.6 mm x 150 L, buffer $H_2PO_4^-$ pH 4.3/MeOH 70:30, flow 1.0 mL/min, retention time 3.133 min (major), 7.157 min (minor). Compound purity was estimated by reversed phase C18 HPLC, with a UV detector at 254 nm, from ACN/H_2O, 5:95 + 0.1 % FA to ACN/H_2O, 95:5 + 0.1 % FA, and the major peak area of the compound was 99 %.

1-cyclohexyl-2-iodo-7-(((2-(5-methoxy-1*H*-indol-3-yl)ethyl)amino)methyl)-6,7,7a,8-tetrahydro-3*H*-pyrrolo[2,1-j]quinoline-3,9(5*H*)-dione (±)-58

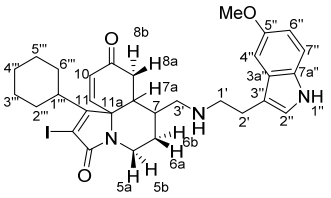

Following the *general 4.1.1.5*, the reaction of **(±)-52** (65.0 mg, 0.2 mmol), 5-methoxy-tryptamine **53** (28.5 mg, 0.2 mmol) and $Na(AcO)_3BH$ (98.3 mg, 0.5 mmol) in CH_2Cl_2 (6.5 mL) for 23 h afforded, after purification by flash chromatography on silica gel (CH_2Cl_2/MeOH, 2-5 %), 54.0 mg (59 %) of the desired compound **(±)-58** as an off-white solid. Rf: 0.20 (CH_2Cl_2/MeOH 95:5) m.p. 128 – 130 ºC. ^{1}H NMR (500 MHz, $CDCl_3$) δ 7.95 (s, 1H, H1''), 7.26 (d, *J* = 8.4 Hz, 1H, H7''), 7.02

(d, *J* = 2.8Hz 1H, H4''), 7.01 (d, *J* = 2.8Hz 1H, H2''),6.85 (dd, *J* = 8.8, 2.5 Hz, 1H, H6''), 6.33 (d, *J* = 10.1 Hz, 1H, H10), 6.19 (dd, *J* = 10.2, 2.0 Hz, 1H, H11), 4.31 (dd, *J* = 13.2, 4.2 Hz, 1H, H5b), 3.86 (s, 3H, OC*H*$_3$), 2.96 - 2.82 (m, 5H, 2xH1', 2xH2', H8b), 2.80 - 2.69 (m, 3H, H3', H5a, H8a), 2.49 (dd, *J* = 12.4, 6.6 Hz, 1H, H3'), 2.32 (dd, *J* = 18.8, 9.9 Hz, 2H, H1''', H6'''), 2.25 (q, *J* = 11.4, 10.7 Hz, 1H, H2'''), 1.96 (dd, *J* = 11.1, 5.3 Hz, 1H, H7a), 1.88 (d, *J* = 13.0 Hz, 1H, H5'''), 1.80 (d, *J* = 13.1 Hz, 1H, H3'''), 1.74 - 1.61 (m, 4H, H6b, H7, H4''', H6'''), 1.36 - 1.23 (m, 2H, H2''', H4'''), 1.23 - 1.10 (m, 3H, H6a, H3''', H5''') ppm. ^{13}C NMR (126 MHz, $CDCl_3$)δ 196.6, 166.1, 165.9, 154.1, 146.3, 133.4, 131.7, 127.9, 123.0, 113.5, 112.5, 112.1, 100.8, 93.1, 70.7, 56.1, 52.0, 50.1, 44.1, 39.1, 38.6, 38.2, 37.6, 30.1, 28.8, 28.6, 26.5, 26.4, 25.7, 25.5 ppm. IR (film) υ/cm^{-1} 3312, 2920, 2850, 1670, 1581, 1483, 1444, 1405, 1297, 1213, 1171, 1065, 1029, 968, 921, 792, 745, 705 Compound purity was estimated by reversed phase C18 HPLC, with a UV detector at 254 nm, from ACN/H_2O, 5:95 + 0.1 % FA to ACN/H_2O, 95:5 + 0.1 % FA, and the major peak area of the compound was 100 %.

(7*S*,7a*R*,11a*R*)-1-cyclohexyl-2-iodo-7-(((2-(5-methoxy-1*H*-indol-3-yl)ethyl)amino)methyl)-6,7,7a,8-tetrahydro-3*H*-pyrrolo[2,1-j]quinoline-3,9(5*H*)-dione (-)-58

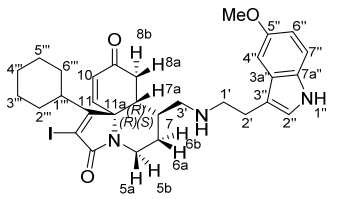

Following the *general 4.1.1.5*, the reaction of **(-)-52** (80 mg, 0.2 mmol), 5-methoxy-tryptamine **53** (34 mg, 0.2 mmol) and $Na(AcO)_3BH$ (79 mg, 0.4 mmol) in CH_2Cl_2 (8 mL) for 24 h afforded, after purification by flash chromatography on silica gel (CH_2Cl_2/MeOH, 2-5%), 47.9 mg (43 %) of the desired compound **(-)-58** as an off-white solid. α_D^{24} = - 103.33 º (C = 0.90 mg/mL, MeOH) e.e. 84 % The enantiomers were separated by HPLC (ULTRON ES OVM Chiral Analytical Reverse Phase, 5 μm, 4.6 mm x 150 L,buffer $H_2PO_4^-$ pH 4.3/MeOH 70:30, flow 1.0 mL/min, retention time 4.300 min (minor), 5.313 (major). Compound purity was estimated by reversed phase C18 HPLC, with a UV detector at 254 nm, from ACN/H_2O, 5:95 + 0.1 % FA to ACN/H_2O, 95:5 + 0.1 % FA, and the major peak area of the compound was 97 %.

(7*R*,7a*S*,11a*S*)-1-cyclohexyl-2-iodo-7-(((2-(5-methoxy-1*H*-indol-3-yl)ethyl)amino)methyl)-6,7,7a,8-tetrahydro-3*H*-pyrrolo[2,1-j]quinoline-3,9(5*H*)-dione (+)-58

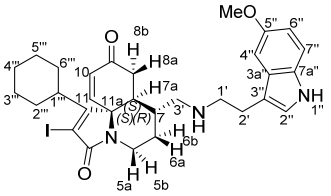

Following the *general procedure 4.1.1.5*, the reaction of **(+)-52** (62.0 mg, 0.1 mmol), 5-methoxy-tryptamine **53** (26.6 mg, 0.1 mmol) and $Na(AcO)_3BH$ (61.2 mg, 0.3 mmol) in CH_2Cl_2 (6 mL) for 20 h afforded, after purification by flash chromatography on silica gel (CH_2Cl_2/MeOH, 2-5 %), 46.3 mg (54 %) of the desired compound **(+)-58** as an off-white solid. α_D^{24} = + 65.45 º (C = 1.10 mg/mL, MeOH) e.e. 81 % The enantiomers were separated by HPLC (ULTRON ES OVM Chiral Analytical Reverse Phase, 5 μm, 4.6 mm x 150 L, buffer $H_2PO_4^-$ pH 4.3/MeOH 70:30, flow 1.0 mL/min, retention time 4.147 (major), 5.693 (minor). Compound purity was estimated by reversed phase C18 HPLC, with a UV detector at 254 nm, from ACN/H_2O, 5:95 + 0.1 % FA to ACN/H_2O, 95:5 + 0.1 % FA, and the major peak area of the compound was 100 %.

4.1.2 Pharmacological evaluation

4.1.2.1 Reagents

Dulbecco´s Modified Eagle´s Medium (DMEM), fetal bovine serum (FBS), GlutaMAX, geneticin (G418), Nutrient Mixture F-12, and non-essential aminoacids were purchased from GIBCO, Life Technologies (Madrid, Spain). 2,2'-azobis(amidinopropane) dihydrochloride (AAPH), acetonitrile (ACN), ascorbic acid , acethylthiocholine iodide (AThChI), AChE (*Electrophorus electricus*), butirylcholinesterase (BuChE) (*Equine serum*) butirylthiocoline iodide (BuThChI), $CaCl_2$, dimethylsulfoxide (DMSO), 5,5'-dithiobis-(2-nitrobenzoic) acid (DTNB), fluorescein (FL), formic acid (FA), glucose, *4*-(2-hydroxyethyl)-1-piperazineethanesulfonic acid (HEPES), hygromycin B, K_2HPO_4, KH_2PO_4, $MgCl_2$, $MgSO_4 \cdot 7H_2O$, $MnCl_2$, 3-(4,5-dimethylthizaol-2-yl)-2,5-diphenyltetrazoliumbromide (MTT), NaCl, $NaHCO_3$, Na_2HPO_4, NaOH, oligomycin A (O), okadaic acid ammonium salt (OA), penicillin/streptomycin (P/S), rotenone (R), sodium pyruvate, *tert*-butylhydroquinone (TBHQ), trigonelline (TR), tripsine-EDTA, triton X-100, (±)-6-hydroxy-2,5,7,8-tetramethylchromane-2-carboxylic acid (trolox), were acquired from

Sigma-Aldrich (Madrid, Spain). Sn(IV) protoporphyrin-IX dichloride (SnPP) was purchased from Frontier Scientific Europe (Lancashire, UK). Luzindole (LZ) was acquired from Enzo Life Science. 2-(2-amino-3-methoxyphenyl)-4*H*-1-benzopyran-4-one (PD98059), and LY294002 (LY) were purchased from Tocris (Biogen Científica, Madrid, Spain). Luciferase Assay System (Promega E1500) was obtained from Promega (Madison, WI, USA). Saline sodium chloride 0.9% (w/v) solution for intravenous infusion was obtained from Baxter Healthcare Ltd. (Norfolk, UK). The water was purified using a MilliQ Academic System (Millipore, Bedford, MA).

4.1.2.2 Solutions for assays

- ORAC assay, PBS 10 mM pH 7.4: 80.2 mL of K_2HPO_4 and 19.8 mL KH_2PO_4
- AChE inhibition assay, PBS 0.1 M pH 8.0: 94 mL of K_2HPO_4 and 6 mL KH_2PO_4
- Intracellular [Ca^{2+}] measurements, Krebs-Hepes (KH) pH 7.4: NaCl (145 mM), KCl (4.9 mM), $MgCl_2$ (1.2 mM), $CaCl_2$ (2 mM), HEPES (10 mM), Glucose (11 mM).

4.1.2.3 AREc32 cell line

4.1.2.3.1 AREc32 culture

AREc32 cell line was developed by Wang *et al*. from the human mammary MCF-7 breast cancer cells.[117] AREc32 cells are constitutively transfected with a plasmid which contains the pGL-8xARE luciferase gen reporter inserted after the EpRE sequences. Thus, the induction of Nrf2 results in luciferase expression. AREc32 were kindly provided by Prof. Roland Wolf (University of Dundee, U.K.).

AREc32 cells were cultured in DMEM with GlutaMAX and high glucose, supplemented with 1 % P/S (10,000 units), 1.6 % G418 (0.8 mg/ml), and 10 % FBS, incubated at 37 ºC in a 5 % CO_2-supplemented air atmosphere. Cells were harvested in a 75 cm^2 flask with 11 mL of specified medium and they were transferred in a new flask each 4-6 days when the confluence was around 80 %.

4.1.2.3.2 Determination of Nrf2 induction activity

Cells were seeded in 96-well white plate (COSTAR 3917) 60,000 cells/well density, using 100 μL/well. Twenty four hours after seeding, cells were treated with compounds at desired concentrations (1, 5, 10, 15 μM) for 24 h, incubated at 37 ºC and 5 % CO_2. Each well plate had a basal, a control with TBHQ (10 μM, positive control) variables and problem variables in a final volume of 100 μL. After 24 h incubation, the luciferase activity was measured through a bioluminescence assay, using "Luciferase assay system" (Promega E1500) proceeding as follows: treatments were removed and 20 μL of "lysis buffer" reagent were added to each well. After 10 minutes, the 96-well plate was introduced in a luminescence multi-well reader, Orion II microplate luminometer (Berthold, Germany). Measurements were done by duplicate and the values were normalized to basal luminescence considered as 1.

4.1.2.4 Oxygen Radical Absorbance Capacity (ORAC) assay

ORAC-FL test developed by Cao *et al.*,[118] and modified by Ou *et al.*,[119] was employed to evaluate the oxygen free radical scavenger capacity of the compounds. The different solutions of trolox (1, 2, 4, 6, 8 μM) as reference compound, melatonin, as positive control, and new compounds (0.03, 0.1, 0,3, 1, 3 and 5 or 10 μM) were freshly prepared using PBS (10 mM, pH 7.4) at 37 ºC. Black with clear flat bottom 96-well microplate (COSTAR 3904) was used to measure fluorescence in the plate reader FluoStar Optima (BMG Labtech, Offenburg, Germany) with 485 nm excitation and 520 nm emission filters. In each well 150 μL of FL (70 nM) was added as well as 25 μL of PBS buffer for blank, 25 μL of trolox solution for standard and 25 μL of melatonin or compound, for sample. Firstly, a fluorescence measurement was done to determine the basal signal. Then, 25 μl of AAPH (12 mM) was quickly added, since the reaction starts immediately after addition. All samples were carried out in duplicate at, at least, three different experiments. The fluorescence was measured during 90 min at 37 ºC to obtain the area under the fluorescence decay curve. After blank correction, plotting the AUC versus concentration, linear regressions were obtained for each compound. The final results were expressed in trolox equivalents (TEq), where the slope of the sample linear regression was divided by the slope of trolox.

4.1.2.5 Neuroblastoma cell lines

4.1.2.5.1 SH-SY5Y culture

Human neuroblastoma SH-SY5Y cell line,[120] possesses neurofilament proteins, neuron specific proteins, and neurotransmitter and hormone receptors such as tyrosine hydroxylase (TH) and dopamine-β-hydroxylase as well as, dopamine transporter and receptors 1 and 2 type, characteristic of catecholaminergic neurons; VDCCs and voltage-dependent K^+ channels, P2X7 purinergic receptors and opioid receptors, and α3, α5, α7, β2 and β4 subunits of nAChRs[121] and MT1 melatonin receptor,[122] of particularly interest for us.

SH-SY5Y cells [ECACC 94030304] from passages between 4 and 16 after defreezing, were maintained in MEM containing 15 % non-esential aminoacids and supplemented with 10 % of FBS, sodium pyruvate 1 M, $NaHCO_3$ 24 mM, 50 units/mL and 50 μg/mL of P/S, respectively. Cells were harvested in 75 cm^2 flask (CORNING 430641U) and incubated at 37 ºC with wet atmosphere and 5 % of CO_2 doing passages 1:4 twice a week. Once 80-85 % of confluence was reached, cells were transferred to a new culture flask and, seeded in the appropriate plate for its experimental use, employing trypsin/EDTA and centrifuging at 400 revolutions per minute (rpm) for 10 minutes (min).

4.1.2.5.2 SH-EP1$_{hα4β2}$ culture

Lukas and colleagues used the human epithelial cell line SH-EP1 to overexpress human α4β2-nAChRs.[123] To perform some experiments included in this Thesis, SH-EP1$_{hα4β2}$ were kindly provided by Dr. Dominik Feuerbach from Novartis Pharma AG (Switzerland).

Harvesting of SH-EP1$_{hα4β2}$ was done by the same token as previously described. SH-EP1$_{hα4β2}$, required 100 μg/mL of G418 and 100 μg/mL of hygromycin B in addition to DMEM 10 % FBS SH-SY5Y medium.

4.1.2.6 Calcium fluorimetry. Measurement of cellular response stimulating nicotinic receptors with ACh or α7-nAChR selective agonist PNU282987.

According to experimental requirements, SH-SY5Y were seeded in 96-well black plates at 100,000 cells/well density until reaching confluence. In brief, neuroblastoma cells were incubated with the Ca^{2+} sensitive fluorescent dye fluo-4 AM at 5 μM for 1 h at

37 ºC in KH, and 0.05 % pluronic acid. After that, cells were washed twice with KH solution and 175 µL of KH (as basal response) or treatments at 10 µM without (for ACh injection) or with PNU120596 at 10 µM (for PNU282989 injection) were added and incubated for 10 minutes. Prior to the stimulation of nicotinic receptors with ACh 100 µM or PNU282987 10 µM using an automatic injector, basal fluorescence (F_0) was recorded and then, fluorescence was measured for 13.5 s in a multi-well reader (FluoStar Optima, BMG, Germany), being the excitation and emission wavelengths 485 and 520 nm, respectively. To obtain normalized signals, the determination of maximum and minimum fluorescence values of each well were obtained adding 50 µL of Triton 5X (F_{max}) following 50 µL of $MnCl_2$ 1 M (F_{min}). The results were presented as normalized response to acetylcholine or PNU282987+ PNU120596 calculated as $(F_{measured} - F_0)/(F_{max} - F_{min})$.

4.1.2.7 AChE and BuChE enzymes inhibitory activity.

Ellman's method was employed to determine the inhibitory capacity of the AChE (*Electrophorus electricus*) and BuChE (*Equine serum*).[124] The compounds were studied at five (0.3, 1, 3, 10 y 30 µM) and six (1, 3, 10, 30, 60, 100 µM) concentrations for AChE and BuChE, respectively, to obtain inhibition curves which allow calculate the concentration of the inhibitor required to reduce the rate of the enzymatic reaction by 50% (IC_{50}) values. The assays were performed at room temperature, using PBS (0.1 M, pH 8) as solvent. Transparent 48-well microplates (COSTAR 3548) were used and in each one a blank was included. The compounds were incubated at decided concentrations with the enzyme (0.09 U/mL) and with DTNB (0.35 mM) during 10 min. Afterwards, the enzyme substrates AChThI (0.35 mM) or BuChThI (0.35 mM), were added with a final volume of 1 mL. The microplate was incubated at room temperature during 15 min. Then, the absorbance was measured at 420 nM using the microplate reader FluoStar Optima (BMG Labtech). The enzymatic activity was calculated subtracting the absorbance of the blank to the absorbance of the sample and divided by the absorbance of the maximum activity subtracted to blank absorbance, multiplied by hundred to obtain the percentage. Once obtained the enzymatic activities, subtracting from hundred, the inhibition activity was

calculated and plotted versus concentration to obtain IC_{50} for AChE and BuChE, through sigmoidal non lineal adjustment. All the experiments were performed at least in triplicate.

4.1.2.8 AChE kinetic characterization

Inhibitors were solubilized in DMSO at a stock concentration of 10^{-2} M and maintained at -20 ºC. AChE inhibition was assayed spectrophotometrically at 30 ºC according to the method of Ellman. Assay buffer was PBS 0.1 M, pH 8.0. A stock solution of AChE (270 U/mL) in assay buffer was kept at -80 ºC, and a 1:70 dilution was prepared immediately before starting the measurement. AThCh (10 mM) and DTNB (1 mM) were dissolved in assay buffer and kept at -80 ºC. Stock solutions of compounds **54-58** were prepared in DMSO, and seven concentrations (0.03, 0.05, 1, 3, 5, 10, 15 μM) were assayed.

Experiments were performed in a transparent 48-well plate (COSTAR 3548) containing each well 350 μL of the DTNB solution 1 mM, variable volumes of buffer solution between 546 and 626 μL, 10 μL DMSO or inhibitor solution to give desired final concentration, and five different concentrations of ACh (0.1, 0.2, 0.4, 0.6, and 0.8 mM. The mixture was thoroughly mixed. The reaction was initiated by adding 14 μL of an AChE solution (3.6 U/mL) at 30 ºC to give a final volume of 1 mL. Uninhibited enzyme activity was determined by adding DMSO instead of the inhibitor solution. The rates of AChE-catalyzed ACh hydrolysis were corrected by those of the non-enzymatic hydrolysis of ACh as determined by using 10 μL of assay buffer, instead of ACh. Progress curves were monitored at 412 nm over 2 min in an absorbance/fluorescence plate-reader Fluostar Optima (BMG-technologies, Germany). Progress curves were characterized by a linear steady-state turnover of the substrate and values of a linear regression were fitted according to Lineweaver–Burk replots using Origin software (version 7.0). Double reciprocal plots were generated using the same statistical package. The relative Ki's and types of inhibition were determined by plotting the slopes of the double reciprocal plots versus concentration of inhibitor.

Briefly, from the initial Michaelis–Menten equation for Lineweaver– Burk plot $1/V_0 = 1/V_{max} + (K_M/V_{max})/[S]$, $1/V_0 = (1+[I]/K_i)/V_{max} + [(K_M/V_{max}) \text{ x } (1+[I]/K_i)]/[S]$ where the slope for each inhibitor concentration is $\rho = K_M/V_{max} + K_M/(V_{max} K_i) \text{ x } [I]$.

Thus, representing slopes versus concentration inhibitor, we can calculate K_M/V_{max} from *y* axis intercept and the K_i. All rate measurements were performed in triplicate.

4.1.2.9 SH-SY5Y *Per se* toxicity studies

For the toxicity experiments, cells were seeded in 96-well plate (VWR 734-2327) at 80,000 cells/well density and treated with compounds before reach confluence, in DMEM with 1% of FBS. Cells were incubated with three different concentrations (1, 10 and 30 μM) for 24 h to obtain concentration-survival curves which allow calculate the concentration that reduces the 50% of cell viability (LC_{50}).

4.1.2.10 Cell viability assessment by MTT method

MTT method is a rapid colorimetric technique which measures cellular viability developed by Mosmann in 1983.[125] MTT is a yellow colour tetrazolium salt, reduced to a purple insoluble formazan salt by the action of mitochondrial.

After required time of incubation, to assess cell survival, 10% of well volume, (100 μL) of MTT dissolved in distillate water at 5 mg/mL was added for 2 h. Then, the medium was removed and the purple formazan crystals formed were dissolved using 100 μL of DMSO. FluoStar Optima spectrophotometer was used to measure the absorbance at 570 nm. Data was normalized compared to basal untreated cells considered as 100 % viability.

4.1.2.11 SH-SY5Y *in vitro* neuroprotection studies

For the neuroprotection experiments, SH-SY5Y cells were seeded in 96-well plates at 60,000 cells/well density.

To evaluate the potential neuroprotective effect in an oxidative stress model, the combination of rotenone (30 μM) and oligomycin A (10 μM) (R/O) were selected as they disturb the flow of electrons in the mitochondrial respiratory chain. Similarly to the one use in previous model, SH-SY5Y were pre-incubated with compounds at 1 μM for 24 h. Then, they were co-incubated in the presence of R/O 24 h more, evaluating cell viability by MTT reduction method. Melatonin at 1 μM was used as positive control.[102]

Neuroprotection studies against Tau hyperphosphorylation exerted by OA were evaluated as follows. Cells were preincubated with compounds at 1 μM for 24 h. After that period, the medium was removed and substituted by medium at 1% with FBS, the compounds at concentration of 1 μM and OA at 20 nM. After 18 h, cell viability was addressed by MTT reduction method. Each pharmacological assay had a positive control, melatonin at 1 μM, with comparative purposes and to evaluate the reliability of the method.[126]

4.1.3 Docking and molecular dynamic studies on α7-nAChR

4.1.3.1 Homology modelling of α7 ECD

In order to find a proper template for the construction of the homology model of α7 ECD, we performed a search alignment against the proteins with 3D structures deposited at the Protein Data Bank (PDB) using the Protein-Protein Basic Local Alignment Search Tool (BLASTp) available at the National Center for Biotechnology Information webpage.[127] The structure that shared the highest identity percentage with α7 ECD (68 % sequence identity on a 99 % query cover) was found to be the crystallographic structure of a humanized acetylcholine binding protein resolved at 2.57 Å resolution complexed with lobeline at the orthosteric site and an allosteric binder (PDB code: 5oug). Thus, after ensuring that most residues located close to the orthosteric sites were identical between this structure and the α7 ECD, we used it as template. Homology modelling was performed with MODELLER v9.21[128] considering the full pentamer. 100 models were generated and after visual inspection, the one with the lowest DOPE score was selected and assessed with Molprobity[129] and WHATCHECK,[130] finding that 95 % of residues were in the favored region of the Ramachandran plot which correlates with a Ramachandran Z-score of -2.1 which is within the allowed range for a comparative model. This structure was then prepared in MAESTRO version 11.8.012[131] by means of the Protein Preparation Wizard tool. Briefly, hydrogen atoms were added, disulfide bonds were created and residues protonation states at physiological pH were predicted with PROPKA. Histidines protonation state were manually assigned according to their chemical environment. Finally, a restrained minimization was performed with OLPS3e

as force field[132] with convergence of heavy atoms set to RMSD 0.3 Å. The resulting structure was employed for docking studies.

4.1.3.2 Ligands preparation

Ligands 3D coordinates were generated in MAESTRO and then prepared with the LigPrep tool included in the software package.[133] Ionization states were predicted with Epik[134] for a physiological pH and structures were minimized with OPLS3e force field.

4.1.3.3 Docking

Docking of compounds was performed by means of a consensus docking approach using a combination of Glide[135],[136] and AutoDock4.[137] Docking grids were centered at the orthosteric site between subunits A and B of the homology model. For docking with Glide, inner box size was set to 10 x 10 x 10 Å while outer box dimensions were 30 x 30 x 30 Å. The standard precision method was employed and the number of post docking minimizations was set to 15. The maximum number of poses to be written was set to 8. Regarding AutoDock4, a three dimensional grid of 40 x 40 x 40 points with a spacing of 0.375 Å was employed and the Lamarckian Genetic Algorithm was selected as the search algorithm. Initial coordinates, dihedrals and orientation of the ligands were randomized. A population size of 150 was selected while the maximum number of energy evaluations was set to 2500000. The maximum number of generations was 27000, a mutation rate of 0.02 was chosen and the crossover rate was established at 0.06. The number of runs was fixed at 10. Poses predicted for each ligand by both methods were compared and the root mean square deviation (RMSD) between them was calculated. Due to the high flexibility of the linker, notable differences were found regarding indole location which led to a high RMSD values even when the overall predicted binding mode by both methods was similar. Thus, we based RMSD calculations on the compounds core of the predicted poses setting a value of 2.0 Å as threshold. If one pose predicted by Glide differed in more than 2.0 Å to all poses predicted by AutoDock4 it was discarded and vice versa. Then, consensus poses were ranked according to their predicted binding energy, and those which were simultaneously the more energetically favorable in both AD4 and Glide were selected as the correct pose. If there was no agreement in the predicted binding energy ranking between both methods, two consensus poses were

selected, the one with the lowest in energy in Glide and the one more energetically favorable in AD4.

4.1.3.4 Molecular dynamics simulations

Molecular dynamics simulations of compounds **(-)-54** and **(+)-54** complexed to all five orthosteric sites of the α7 ECD model were performed with AMBER18[138] with GAFF[139] and ff14SB[140] employed as force fields. The pose predicted for each ligand by the docking study was used as the starting conformation for the ligand at every site. The complex was solvated in XLEaP[141] with a cubic TIP3P water box, leaving at least 12 Å between each protein or ligand atom and the edge of the box. Na+ and Cl- ions were added in order to reach a physiological ionic concentration of 0.15 M. Compounds **(-)-54** and **(+)-54** charges were derived using the AM1-BCC charge method and atom types and force field missing parameters for ligands atoms were obtained utilizing the antechamber package included in AMBER18.[142] Minimization of the system prior to molecular dynamics simulation was performed using the sander module of AMBER18. It was divided in five steps, starting from harmonic positional restraints of 100 kcal/mol·Å^2 applied to protein and ligand atoms to no restraints. Then the system was heated from 0 to 310 K for 50 ps at the NVT ensemble with soft harmonic positional restraints of 2.0 kcal/mol·Å^2 applied to the protein and ligand and then equilibrated with no restraints at 310 K in the NPT ensemble for 1 ns. Finally, the entire system was simulated with no restraints for 300 ns. During the entire procedure, periodic boundary conditions were applied and a cutoff of 9.0 Å was used for non-bonded interactions. Long range electrostatic interactions were computed with the Particle Mesh Ewald (PME) method. Temperature was controlled using the Langevin thermostat with a collision frequency of 2.0 ps^{-1}. The Berendsen barostat was employed for pressure control. For hydrogen-containing bonds the SHAKE algorithm was applied so a timestep of 2 fs was employed. Analysis of the trajectories was performed using the cpptraj module[143] of AMBER and they were visualized using VMD.[144]

4.1.4 Pharmacokinetic and intra brain distribution studies

4.1.4.1 Animals

Experiments were performed in accordance with guidelines from Swedish National Board for Laboratory Animals approved by the Animal Ethics Committee of Uppsala, Sweden (ethical approval C188/14 and C189/2). All drug-naïve male Sprague Dawley rats weighing 250-300 g (Taconic, Lille Skensved, Denmark) were housed in groups at 20 to 22°C under humidity controlled conditions in a 12-h light/dark cycle with *ad libitum* access to food and water.

4.1.4.2 Pharmacokinetic concepts of drug transport across the BBB

According to the free drug hypothesis, only the unbound fraction of drug (C_u) is able to distribute through membranes and to initiate pharmacological response.[145] Taking this into account, a general assumption of pharmacokinetics (PK) is that unbound drug concentrations on both sides of a membrane at steady state are equal. Nevertheless, regarding brain PK, the presence of high activity influx and efflux transporters as well as metabolising enzymes in the BBB together with tight junctions and drug distribution to CSF, makes previous statement, not always true.

Brain PK of a drug is driven by two main distributional features: rate and extent of transport. Rate describes how fast the drug can pass through BBB from blood to brain. It is associated with permeability. On the contrary, extent of transport is of higher relevance as it accounts of how much drug is transported from blood to brain.[146] Thus, the delivery of a drug to the brain is expressed as a ratio between total (bound and unbound) brain and blood concentrations at steady state ($C_{ss,brain}$ and $C_{ss,plasma}$, respectively), also known as brain-to-blood partition coefficient, $K_{p,brain}$ (Eq. 1), or for computational chemists and pharmacometricians BB, commonly used as its logarithmic form, logBB. $K_{p,brain}$ can be estimated as area under the total drug concentration *versus* time curves for brain ($AUC_{tot,brain}$) and plasma ($AUC_{tot,plasma}$).

$$K_{p,brain} = \frac{C_{ss,brain}}{C_{ss,plasma}} = \frac{AUC_{tot,brain}}{AUC_{tot,plasma}} \quad \text{[Eq.1]}$$

However, in light of free drug hypothesis, $K_{p,brain}$ have to be corrected. As a result, Hammarlund-Udeanes and colleagues[146] introduced $K_{p,uu,brain}$ concept. This new partition

coefficient represents the extent of unbound drug transport across the BBB, where only unbound brain interstitial fluid (ISF) and blood concentrations are compared, (Eq. 2).

$$K_{p,uu,brain} = \frac{AUC_{u,brainISF}}{AUC_{u,plasma}} = \frac{CL_{in}}{CL_{out}} \quad \text{[Eq.2]}$$

Hence, $K_{p,uu,brain}$ is a clinically relevant parameter as it provides information about which is the most important mode of transport of the drug. Whether $K_{p,uu,brain}$ is equal to one, means that passive transport dominates whereas if it is lower or higher, efflux or influx active transport dominates, respectively.

Following the same reasoning, the concept of $K_{p,uu,cell}$ has been first time proposed by Friden *et al.*[147] as the ratio between unbound intracellular ($C_{u,cell}$) and brain ISF ($C_{u,brainISF}$) drug concentrations, as expressed in Eq.3. Similarly to $K_{p,uu,brain}$, $K_{p,uu,cell}$ describes extent of transport across the cellular membrane of average brain parenchymal cells and gives a hint about whether the drug is accumulated inside or outside cells, which is important to know if it located in the desired site of action.

$$K_{p,uu,cell} = \frac{C_{u,cell}}{C_{u,brainISF}} \quad \text{[Eq.3]}$$

4.1.4.3 Combinatory Mapping Approach (CMA)

Ideally $K_{p,uu,brain}$ is assessed by unbound brain to unbound plasma steady state concentration ratio, using cerebral microdialysis, a gold standard method for evaluation of neuropharmacokinetics (neuroPK).[55] Nevertheless, the new recently proposed CMA for the estimation of $K_{p,uu,brain}$ in the preclinical conditions developed by Loryan *et al.*[148] is is a rational and time-efficient alternative to cerebral microdialysis, allowing reasonable assessment of unbound drug neuroPK, **Figure 12**.

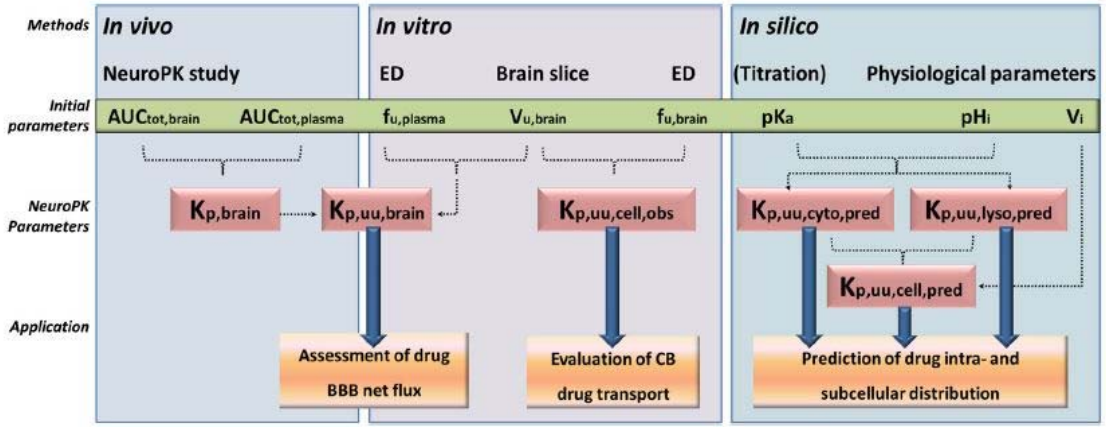

Figure 12. Scheme describing Combinatorial Mapping Approach (Image from Loryan *et al.*)[148]

The CMA provides quantitative knowledge about BBB and cellular barrier transport in the preclinical conditions using a set of *in vitro* and *in vivo* methods. Thanks to this methodological platform we could obtain information about:

a) *in vitro* lead compound tissue binding studies for determination of unbound drug in plasma ($f_{u,plasma}$), and in the whole brain homogenate ($f_{u,brain}$).
b) *in vitro* brain slice studies for evaluation of binding and intracellular distribution by measuring the volume of distribution of unbound fraction in whole brain ($V_{u,brain}$).
c) *in vivo* neuroPK studies performed in rodents followed by measurement of partition coefficient ($K_{p,brain}$).

Once done all of these studies, $K_{p,uu,brain}$ was thereafter assessed through a combination of the experimentally determined $K_{p,brain}$, $f_{u,\ brain}$, (or $V_{u,brain}$) and $f_{u,\ plasma}$ using the following equation:

$$K_{p,uu,brain} \approx K_{p,brain} \frac{f_{u,brain}}{f_{u,plasma}} = \frac{K_{p,brain}}{V_{u,brain} \cdot f_{u,plasma}} \quad \text{[Eq 4]}$$

Also, the $K_{p,uu,cell}$ could be estimated employing the following formula:

$$K_{p,uu,cell} = V_{u,brain} \cdot f_{u,brain} \quad \text{[Eq 5]}$$

4.1.4.4 Pharmacokinetic study

To study systemic pharmacokinetics of new melatonin derivatives **(±)-56** and **(±)-57**, the femoral vein and artery of three drug-naïve male Sprague Dawley rats were surgically catheterized 24 h before the experiment. The compounds were administered in 17.5 % DMSO, 0.9 % saline and 0.1 % of FA as a short intravenous infusion. Blood samples (200 μM) were taken from the arteria femoralis (on heparin) at 0, 2.5, 5, 9, 15, 30, 60, 120, 240, 420 min and 24 h after the start of the infusion. Plasma was obtained following the centrifugation at 4 ºC for 5 min at 1900 g and samples were placed on -20 ºC before storing them to -80 ºC prior to analysis. The PKSolver software, an add-in program for pharmacokinetic and pharmacodynamics data analysis in Microsoft Excel, was used to obtain primary pharmacokinetic parameters.

4.1.4.5 *In vivo* neuropharmacokinetic studies

Six drug-naïve male Sprague Dawley rats (Taconic, Lille Skensved, Denmark) were intravenously infused with **(±)-56** and **(±)-57**, (three rats per compound). The femoral vein and artery were surgically catheterized a day before the experiment. Due to low solubility compounds were administered in the following vehicles 5.9 % DMSO, 0.1 % of FA in 0.9 % saline (**(±)-56**) and 4.8 % DMSO, 0.1 % of FA in 0.9 % saline (**(±)-57**). Compounds were administered as a bolus injection for 5 min followed by a 4 h constant-rate intravenous infusion, using a flow rate of 1 mL/kg h^{-1} to reach steady state. Four blood samples were taken from the arteria femoralis (on heparin) at 0, 1 h, 2 h and 4 h. Plasma was obtained following the centrifugation at 4 ºC for 5 min at 1900 g and samples were placed on -20 ºC. At the end of the experiment, the rats were anaesthetized and were sacrificed through exsanguination by heart puncture. The brain were rapidly removed and stored at -20 ºC until analysis.

4.1.4.6 *In vitro* brain homogenate and plasma protein binding studies

The perfused brain was diluted with 9 parts of PBS pH 7.36 and it was sonicated to obtain the homogenate with the ultrasonic processing VibraCell VCX-130 (Sonics and Materials Inc, CT, USA). The 1:9 (w:v) brain homogenate in PBS was vortex and stored in cold pending the experiment. The plasma was not diluted. The semipermeable membranes (MWCO 14-16 kDa) were prepared according to the manufacture (HTDialysis LLC, CT, USA) the day before experiment. The brain homogenate and the plasma were spiked with 1 µM of the Pr **(±)-56** and CyPr **(±)-57** derivatives. Once the equilibrium chamber HTD96b (HTDialysis LLC, CT, USA) was prepared, 100 µL of PBS was placed in the inner side of the well and 100 µL of spiked homogenate or plasma was placed in the outer side. Then, the chamber was covered with a sealing film (Platemax UC-500) and placed into the incubator with orbital shaker MaxQ4450 (Thermo Fisher Scientific, MA, USA) at 37 ºC and 200 rpm. At equilibrium after 6 h incubation, 50 µL of samples were taken from both sides of membrane and mixed with respective matrix, to avoid matrix-effect, when performing bioanalysis with LC-MS/MS. The 96-well plate was covered with an adhesive aluminium foil and stored at -20 ºC until analysis.

Fraction of unbound drug in brain homogenate could be evaluated as:

$$f_{u,hD} = \frac{C_{buffer}}{C_{brain}} \quad \text{[Eq 6]}$$

However, as homogenate is diluted (D, here 10) it is increasing the unbound fraction, assessed ratio (Eq.1.) must be corrected to yield an estimate of unbound fraction in undiluted tissue.[149]

$$f_{u,brain} = \frac{f_{u,hD}}{D + f_{u,hD} - D f_{u,hD}} \quad \text{[Eq 7]}$$

Fraction of unbound drug in plasma was calculated as:

$$f_{u,plasma} = \frac{C_{buffer}}{C_{plasma}} \quad \text{[Eq 8]}$$

The fraction of unbound drug has a numerical values from 0 to 1, 1 meaning there is no binding.

4.1.4.7 *In vitro* brain slice studies

To evaluate binding and intracellular brain distribution, the unbound volume of distribution in the brain ($V_{u,brain}$) was determined using the brain slice method.[150],[151] Six slices of 300 µm from the brain striatum area were cut with a vibrating blade microtome Leica VT1200 (Leica Microsystems AB, Sweden). The slices were incubated in a beaker with 15 mL of artificial extracellular fluid (aECF) pH 7.6 containing 200 nM of **(±)-56** and **(±)-57** (cassette A), **(-)-56** and **(-)-57** (cassette B), or **(+)-56** and **(+)-57** (cassette C), shaking at 45 rpm for 5 h at 37 ºC in an orbital shaker incubator MAXQ 4450 (Thermo Fischer Scientific, Nino Lab, Sweden) with constant O_2 flow of 75-80 mL/min. Samples of 200 µL of buffer at 0 and 5 h were taken and mixed with 200 µL of blank brain homogenate in artificial extracellular fluid (aECF) (1:4, w:v), as well as the six slices were weighed and homogenized in 9 parts of aECF. All the samples were stored at -20ºC until analysis.

$V_{u,\,brain}$ describes the relationship between the total drug concentration in the brain and the unbound concentration in the brain interstitial fluid (ISF).

$$V_{u,brain} = \frac{C_{total,brain}}{C_{u,brainISF}} \quad \text{[Eq 9]}$$

At equilibrium, it is assumed that the unbound drug concentration in the brain slice ECF is equal to the drug concentration in the buffer in the beaker.

Equilibrium → $C_{u,\ brainISF} = C_{buffer}$ [Eq 10]

$$V_{u,brain} = \frac{C_{T,brain}}{C_{u,brainISF}} = \frac{A_{brain} - V_i \cdot C_{buffer}}{C_{buffer}(1 - V_i)}$$ [Eq 11]

where Vi is the volume surrounding the slice layer of aECF and its value was determined as 0.094 mL·g brain^{-1}.[150]

4.1.5 Bioanalytical procedures

Compound of interest in all samples were analysed by liquid chromatography followed by detection with a tandem triple quadrupole mass spectrometer (LC-MS/MS) Micromass Quattro Ultima Pt (Waters, Milford, MA).

4.1.5.1 LC system

Liquid chromatography separation was performed using an Acquity UPLC system (Waters, Milford, MA) with a ACQUITY ULPC BEH XBridge C18 column (2.1 x 50 mm). The mobile phases used for the separation were A: MiliQ water containing 0.1% FA and B: ACN containing 0.1% FA. Flow rate was 0.3 mL/min and the volume of injection was 5 µL. Separation was performed using the gradient 10 – 95% B over 3.70 minutes. The gradient was then reversed back to 10 % B from 3.70 until 4.00 minutes and maintained at that percentage one more minute. The retention times for **(±)-56** and **(±)-57** were 2.02 and 1.89 minutes, respectively.

4.1.5.2 MS system

Positive electrospray ionisation was performed. The desolvation temperature was set to 450 ºC and the source temperature to 130 ºC. The desolvation gas (N_2) flow was maintained at 1000 L/h and the cone gas (N_2) flow was maintained at 50 L/h. The cone voltage was set to 60 V and the capillary voltage 3.50 kV. The analysis was performed in the multiple reaction mode (MRM) monitoring for **(±)-56** parent 574.2 to daughter 174.0 m/z transition, and for **(±)-57** parent 572.2 to daughter 174.0 m/z transition. Mass spectra were processed using MassLynx software, version 4.1 (Waters, Mildford, MA).

4.1.5.3 Sample preparation

Twenty-five µL of samples, standards, quality controls and respective blanks were precipitated with 75 µL of B and vortexed immediately. After 5 minutes centrifugation at 13 000 rpm in Scanspeed mini (Labogene, Lynge, Denmark), 50 µL of supernatant was added to a 150 µL of A in HPLC vials and vortexed. The samples were kept at 5 ºC in the Sample Organizer of the UPLC system until analysis.

In the case of equilibrium dialysis samples, an automated laboratory workstation Biomek4000 (Beckman Coulter Life science, Indianapolis, IN) was used. First, 96-well plate was vortexed using a Microplate Shaker (VWR International AB, Stockholm) at 1200 rpm, 5 minutes. After introducing the 96-well plate in the automated laboratory workstation, 30 µL of the samples were added to 90 µL of mobile phase B to precipitate them. Once finished, the plate was vortexed at 1200 rpm, 5 minutes and centrifuged at 1200 min^{-1}, 5 min, at room temperature using a centrifuge for plates SIGMA 4-16KS (Sigma Laborzentrifugen GmbH, Germany). Meanwhile, 150 µL of mobile phase A were put in another plate, and once the previous plate centrifuged, 50 µL of supernatant were added. The 96-well plate with 200 µL was frozen at -20ºC and was vortexed before analysis in the LC-MS system. For the equilibrium dialysis samples, the standard curve for both **(±)-56** and **(±)-57**were linear from 5 to 2000 nM for brain samples and 5 to 500 nM for plasma samples. The coefficient of determination (R^2) was higher than 0.995 for both compounds using a $1/x^2$ weighting factor.

4.2 Objective II. Development of second generation of MTDLs with improved physicochemical properties: 1-(2-(5-substituted-1*H*-indol-3-yl)ethyl)-3-(quinuclidin-3-yl)-derivatives

4.2.1 Chemistry

4.2.1.1 General procedure for (*R/S*)-1-(2-(5-substituted-1*H*-indol-3-yl)ethyl)-3-(quinuclidin-3-yl)thiourea/urea preparation

To a 0 ºC solution of 3-(2-isothiocyanatoethyl)-5-substituted-1*H*-indole or *N*-(2-(5-substituted-1*H*-indol-3-yl)ethyl)-1*H*-imidazole-1-carboxamide (1 eq) and DIPEA (3.5 eq) in DMF (10 mL/mmol), (*R*)- or (*S*)-3-aminoquinuclidine (1.5 eq) was added. It was allowed to warm up to room temperature and stirred until reaction completion. Then, DMF was evaporated. The residue was purified by column chromatography to afford the corresponding thiourea or urea product.

(*R*)-3-aminoquinuclidine (*R*)-60

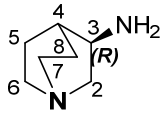

(*R*)-3-aminoquinuclidine dihydrochloride **(*R*)-59** (200 mg, 1.00 mmol) in saturated aqueous solution of KOH (1 mL, 7 M), and the resulting solution was stirred for 24 h. Then, the aqueous reaction solution was then extracted with $CHCl_3$ (10 x 2 mL), dried over Na_2CO_3, filtered and evaporated under reduced pressure. 120 mg of the desired compound **(*R*)-60** was quantitatively obtained without purification, as white solid and stored under Ar. ^{1}H NMR (250 MHz, MeOD) δ 3.13 (ddd, *J* = 13.4, 9.3, 2.2 Hz, 1H, H2a), 2.99 - 2.89 (m, 1H, H3), 2.86 - 2.59 (m, 4H, H7, H6), 2.35 (ddd, *J* = 13.5, 4.9, 2.2 Hz, 1H, H2b), 1.97 - 1.81 (m, 1H, H5a), 1.77 - 1.70 (m, 1H, H4), 1.69 - 1.64 (m, 1H, H8b), 1.59 (ddd, *J* = 8.1, 5.8, 2.9 Hz, 1H, H8a), 1.50 - 1.33 (m, 1H, H5b) ppm. The spectroscopic data matched with previously reported data.[152]

(*S*)-3-aminoquinuclidine (*S*)-60

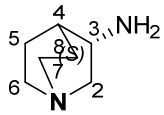

The reaction of (*S*)-3-aminoquinuclidine dihydrochloride **(*S*)-59** (200 mg, 1.00 mmol) in saturated aqueous solution of KOH (1 mL, 7 M) for 24 h, afforded, without purification, 120 mg (100%) of the desired compound **(*S*)-59** as a white solid. The NMR and mass spectra were identical to those reported for **(*R*)-59**

3-(2-isothiocyanatoethyl)-5-methoxy-1*H*-indole 63

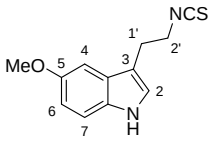

To a solution of 5-methoxy-tryptamine hydrochloride **53** (1 g, 5.26 mmol) in dry THF (20 mL) at 0 ºC, was slowly added 1,1'-thiocarbonyldiimidazole (TCDI) (987 mg, 5.26 mmol). After stirring for 1 h, warming to room temperature, additional TCDI (0.5 eq) was added at 30 min intervals until reaction completion at 2.5 h. Then, the reaction was concentrated *in vacuo* and purified by flash chromatography on silica gel (Pet.Et/CH_2Cl_2, 0-100 %), 797 mg (65 %) of the desired compound **63** as a light green oil. The spectroscopic data matched with previously reported data.[153] ^{1}H NMR (300 MHz, DMSO) δ 10.78 (s, 1H, NH), 7.25 (d, *J* = 8.7 Hz, 1H, H7), 7.18 (d, *J* = 2.5 Hz, 1H, H4), 7.08 (d, *J* = 2.5 Hz, 1H, H2), 6.73 (dd, *J* = 8.7, 2.4 Hz, 1H, H6), 3.90 (t, *J* = 6.6 Hz, 2H, 2xH2'), 3.78 (s, 3H, OC*H*$_3$), 3.06 (t, *J* = 6.6 Hz, 2H, 2xH1') ppm.

5-chloro-3-(2-isothiocyanatoethyl)-1*H*-indole 64

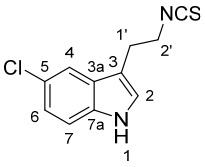

CS_2 (0.07 mL, 1.08 mmol) was added dropwise to a solution mixture of 5-Cl-tryptamine hydrochloride **61** (250 mg, 1.08 mmol), Et_3N (0.15 mL, 1.08 mmol) in THF (5.4 mL) at 0 °C over a period of 15 min. After stirring 30 min maintaining low temperature, H_2O_2 (0.015 mL, 1.62 mmol) was added dropwise. Then, the reaction mixture was neutralized with HCl 1 M, evaporated under reduced pressure and extracted with EtOAc (3x). The residue was purified by column chromatography on silica gel (Pet.Et/CH_2Cl_2, 30 - 100 %), 155 mg (61 %) of the desired compound **64** as a yellow oil. Rf 0.47 (Pet.Et:EtOAc 80:20) ^{1}H NMR (300 MHz, $CDCl_3$) δ 8.14 (s, 1H, NH), 7.51 (d, *J* = 2.2 Hz, 1H, H4), 7.31 (d, *J* = 8.6 Hz, 1H, H7), 7.17 (dd, *J* = 8.9, 2.1 Hz, 2H, H6, H2), 3.77 (t, *J* = 6.7 Hz, 2H, 2xH2'), 3.13 (t, *J* = 6.7 Hz, 2H, 2xH1') ppm. ^{13}C NMR (63 MHz, $CDCl_3$) δ 134.7, 128.0, 125.6, 124.5, 122.8, 118.0, 112.6, 111.2, 45.7, 26.4 ppm. HRMS (ES^+) Theoretical mass calc. for $C_{11}H_9ClN_2S$: 236.0175; found [$(M)^+$], 236.0178. IR (film) υ/cm^{-1} 3230, 2938, 2101, 2085, 1624, 1544, 1438, 1422, 1336, 1212, 1095, 1020, 922, 796.

3-(2-isothiocyanatoethyl)-1*H*-indole 65

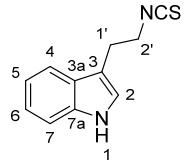

CS_2 (0.19 mL, 3.12 mmol) was added dropwise to a solution mixture of tryptamine hydrochloride **62** (500 mg, 3.12 mmol), Et_3N (0.44 mL, 3.12 mmol) in THF (31 mL) at 0 °C over a period of 15 min. After

stirring 30 min maintaining low temperature, H_2O_2 (0.15 mL, 4.68 mmol) was added dropwise. After 2 h, the reaction mixture was neutralized with HCl 1 M, evaporated under reduced pressure and extracted with EtOAc The residue was purified by column chromatography on silica gel (CH_2Cl_2, 100 %), 491 mg (78 %) of the desired compound **65** as an off-white solid. Rf 0.64 (CH_2Cl_2/MeOH 90:10) m.p. 43 - 45 ºC. ^{1}H NMR (250 MHz, $CDCl_3$) δ 8.09 (s, 1H, H1), 7.56 (d, *J* = 7.7 Hz, 1H, H4), 7.41 (dd, *J* = 7.9, 1.2 Hz, 1H, H7), 7.23 (d, *J* = 1.2 Hz, 1H, H2), 7.19 (dd, *J* = 5.0, 1.4 Hz, 1H, H6), 7.14 (dd, *J* = 5.4, 1.5 Hz, 1H, H5), 3.78 (t, *J* = 6.8 Hz, 2H, 2xH2'), 3.18 (t, *J* = 6.8 Hz, 2H, 2xH1') ppm.^{13}C NMR (63 MHz, $CDCl_3$) δ 174.1, 136.4, 126.9, 123.1, 122.5, 119.9, 118.4, 111.5, 111.4, 45.8, 26.7 ppm. HRMS (EI): Theoretical mass calc. for $C_{11}H_{10}N_2S$ 202.0565; found [$(M)^+$], 202.0571; for [$(M+H)^+$] 203.0643, found 203.0633. IR (film) υ/cm^{-1} 3390, 3041, 2919, 2858, 2174, 2078, 1616, 1547, 1452, 1422, 1354, 1334, 1091, 1070, 1006, 812, 745, 672.

***N*-(2-(5-methoxy-1*H*-indol-3-yl)ethyl)-1*H*-imidazole-1-carboxamide 66**

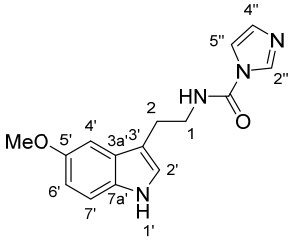

To a suspension of 5-MeO-tryptamine hydrochloride **53** (0.500 mg, 2.63 mmol) and DIPEA (1.6 mL, 9.2 mmol) in dry CH_2Cl_2 (10 mL) at 0 ºC, was slowly added 1,1'-carbonyldiimidazole (CDI) (0.660 mg, 3.94 mmol). After stirring for 1 h, warming to room temperature, additional CDI (0.5 eq) was added and stirred for 18 h. The residue was purified by flash chromatography on silica gel (CH_2Cl_2/MeOH, 0 - 2 %), giving 442 mg (65 %) g of the desired compound **66** as an off-white solid. Rf: 0.62 (CH_2Cl_2/MeOH 90:10) m.p. 153 - 155 ºC. ^{1}H NMR (250 MHz, MeOD) δ 8.17 (s, 1H, H2''), 7.54 (s, 1H, H4''), 7.19 (d, *J* = 8.8 Hz, 1H, H7'), 7.04 (s, 1H, H2'), 7.02 (d, *J* = 2.9 Hz, 2H, H4', H5'), 6.72 (dd, *J* = 8.8, 2.5 Hz, 1H, H6'), 3.71 (d, *J* = 3.5 Hz, 3H, OC*H*$_3$), 3.59 (s, 2H, 2xH1), 3.02 (s, 2H, 2xH2) ppm. HRMS (ES^+): Theoretical mass calc. for $C_{15}H_{16}N_4O_2$, 284.1273; found [$(M+H)^+$], 285.1348. IR (film) υ/cm^{-1} 3305, 3166, 2938, 1708, 1545, 1480, 1446, 1373, 1262, 1233, 1213, 1172, 928, 912, 829, 798, 742.

***N*-(2-(5-chloro-1*H*-indol-3-yl)ethyl)-1*H*-imidazole-1-carboxamide 67**

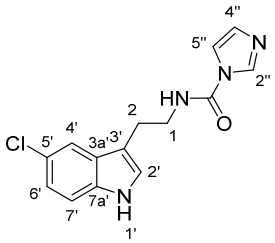

To a suspension of 5-Cl-tryptamine hydrochloride **61** (0.500 mg, 2.16 mmol) and DIPEA (1.9 mL, 10.8 mmol) in dry CH_2Cl_2 (8 mL) at 0 ºC, was slowly added CDI (0.542 mg, 3.24 mmol). After stirring for 1 h, warming to room temperature, additional CDI (0.5 eq) was added and stirred for 2 h. The residue was purified by flash chromatography on silica gel (CH_2Cl_2/MeOH, 0 - 2 %), giving 304 mg (49 %) g of the desired compound **67** as a white solid. Rf 0.56 (CH_2Cl_2/MeOH 90:10) m.p. 45 - 47 ºC ^{1}H NMR (250 MHz, MeOD) δ 8.13 (q, *J* = 1.3 Hz, 1H, H2'') , 7.48 (q, *J* = 1.8 Hz, 2H, H4', H5''), 7.22 (dd, *J* = 8.6, 1.6 Hz, 1H, H7'), 7.07 (d, *J* = 1.5 Hz, 1H, H2'), 6.99 (d, *J* = 2.0 Hz, 1H, H6'), 7.00 - 6.90 (m, 1H, H4''), 3.52 (dd, *J* = 8.1, 6.5 Hz, 2H, 2xH1), 2.96 (dd, *J* = 8.2, 6.1 Hz, 2H, 2xH2) ppm. ^{13}C NMR (63 MHz, MeOD) δ 150.7, 137.3, 136.4, 129.5, 125.0, 122.5, 118.6, 117.7, 113.5, 112.8, 42.8, 25.9 ppm. HRMS (ES^+): Theoretical mass calc. for $C_{14}H_{13}ClN_4O$, 288.0778; found [$(M+H)^+$], 289.0846. IR (film) υ/cm^{-1} 3303, 3180, 3019, 2936, 1704, 1543, 1451, 1433, 1281, 1258, 1226, 1042, 1024, 912, 888, 860, 798, 742.

***N*-(2-(1*H*-indol-3-yl)ethyl)-1*H*-imidazole-1-carboxamide 68**

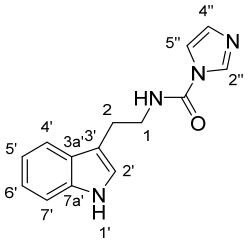

To a suspension of tryptamine hydrochloride **62** (0.500 mg, 3.18 mmol) and DIPEA (2.0 mL, 11.1 mmol) in dry CH_2Cl_2 (12 mL) at 0 ºC, was slowly added CDI (0.798 mg, 4.77 mmol). After stirring for 1 h, warming to room temperature, additional CDI (0.5 eq) was added and stirred for 20 h. The residue was purified by flash chromatography on silica gel (CH_2Cl_2/MeOH, 0 - 2 %), giving 302 mg (51 %) g of the desired compound **68** as an white solid. Rf 0.48 (CH_2Cl_2/MeOH 90:10) m.p. 153 - 155 ºC. ^{1}H NMR (250 MHz, DMSO-d_6) δ 10.83 (s, 1H, NH5), 10.83 (s, 1H, H1'), 8.64 (d, *J* = 6.4 Hz, 1H, NH), 8.19 (s, 1H, H2''), 8.06 (d, *J* = 8.1 Hz, 1H, H4'), 7.69 - 7.59 (m, 1H, H7'), 7.58 - 7.47 (m, 1H, H5''), 7.30 (dt, *J* = 14.7, 6.9 Hz, 1H, H5'), 7.19 (d, *J* = 10.5 Hz, 1H, H6'), 7.02 (q, *J* = 11.7, 9.4 Hz, 2H, H2', H4''), 3.52 (s, 2H, 2xH1), 2.96 (d, *J* = 6.7 Hz, 2H, 2xH2) ppm.^{13}C NMR (63 MHz, DMSO-d_6) δ 150.9, 136.3, 135.9, 130.2, 127.2, 124.6, 122.9, 122.8, 118.4, 118.3, 118.2, 116.6, 114.8, 111.3, 41.1, 24.9 ppm. HRMS (ES^+): Theoretical mass calc. for $C_{14}H_{14}N_4O$, 254.1168; found [$(M+H)^+$], 255.1252;

found [$(M+Na)^+$], 277.1184. IR (film) υ/cm^{-1} 3210, 3038, 1736, 1654, 1540, 1456, 1428, 1255, 1225, 1199, 1093, 1044, 1017, 737.

(*R*)-1-(2-(5-methoxy-1*H*-indol-3-yl)ethyl)-3-(quinuclidin-3-yl)thiourea (*R*)-69

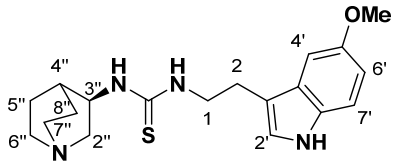

Following the *general procedure 4.2.1.2*, the reaction of **(*R*)-60** (90 mg, 0.44 mmol), DIPEA (0.15 mL, 0.88 mmol) and **63** (0.100 mg, 0.44 mmol) in DMF (4.4 mL), for 24 h afforded, after purification by flash chromatography on silica gel (CH_2Cl_2/MeOH/NH_4OH, 96:3:1-90:9:1), 98 mg (62 %) of the desired compound **(*R*)-69** as a white solid. Rf 0.06 (CH_2Cl_2/MeOH 90:10) m.p. 125 - 127 ºC. ^{1}H NMR (300 MHz, MeOD) δ 7.22 (dd, *J* = 9.0, 5.6 Hz, 1H, H7'), 7.18 (d, *J* = 3.2 Hz, 1H, H4'), 7.06 (d, *J* = 5.1 Hz, 1H, H2'), 6.75 (dd, *J* = 9.0, 3.2 Hz, 1H, H6'), 4.37 - 4.15 (m, 1H, H3''), 3.84 (s, 3H, OC*H*$_3$), 3.83 – 3.79 (m, 2H, 2xH1), 2.99 (t, *J* = 6.6 Hz, 2H, 2xH2), 2.85 (q, *J* = 10.9, 8.7 Hz, 4H, 2xH6'', H7'', H8''), 2.54 (d, *J* = 10.7 Hz, 1H, H2''a), 1.96 (s, 1H, H4''), 1.80 – 1.63 (m, 4H, H2''b, H5''a, H7'', H8''), 1.52 (dd, *J* = 15.5, 8.6 Hz, 1H, H5''b) ppm. ^{13}C NMR (76 MHz, MeOD) δ 183.6, 155.0, 133.4, 129.3, 124.4, 113.0, 112.9, 112.6, 101.7, 56.4, 55.8, 51.3, 47.7, 47.2, 46.1, 26.5, 26.2, 25.6, 20.3 ppm. HRMS (ES^+): Theoretical mass calc. for $C_{19}H_{26}N_4OS$, 358.1827; found [$(M)^+$], 358.1823. IR (film) υ/cm^{-1} 3237, 3053, 2926, 2869, 2321, 1993, 1656, 1616, 1539, 1482, 1452, 1438, 1379, 1341, 1309, 1213, 1167, 1025, 920, 792. $[\alpha]_D^{24}$= + 13.60 º (*c*. 1.25 mg/mL, MeOH) *ee* 97 % The enantiomers were separated by HPLC OVM Chiral Analytical Reverse Phase, buffer 20 mM KH_2PO_4 pH 5.9/ AcCN 95:5, retention time for (*R*), 18.497 (minor), 22.357 (major) and for racemic 19.223 min, 24.907 min. Compound purity was estimated by reversed phase C18 HPLC, with a UV detector at 254 nm, and the major peak area of tested compound was 100 % of the combined total peak area.

(*S*)-1-(2-(5-methoxy-1*H*-indol-3-yl)ethyl)-3-(quinuclidin-3-yl)thiourea (*S*)-69

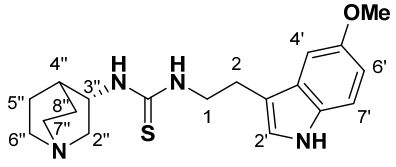

Following the *general procedure 4.2.1.2*, the reaction of **(*S*)-60** (86 mg, 0.42 mmol), DIPEA (0.25 mL, 1.5 mmol) and **63** (0.90 mg, 0.42 mmol) in DMF (4.2 mL), for 24 h afforded, after purification by flash chromatography on silica gel (CH_2Cl_2/MeOH/NH_4OH, 96:3:1-90:9:1), 127 mg (85 %) of the desired compound **(*S*)-69** as a white solid. $[\alpha]_D^{24}$= - 12.12 º (*c*. 1.32 mg/mL, MeOH) *ee* 94 % The enantiomers were

separated by HPLC OVM Chiral Analytical Reverse Phase, buffer 20 mM KH_2PO_4 pH 5.9/ AcCN 95:5, retention time for (*S*), 18.593 (major), 24.977 (minor) and for racemic 19.223 min, 24.907 min. Compound purity was estimated by reversed phase C18 HPLC, with a UV detector at 254 nm, and the major peak area of tested compound was 99 % of the combined total peak area.

(*R*)-1-(2-(5-chloro-1*H*-indol-3-yl)ethyl)-3-(quinuclidin-3-yl)thiourea (*R*)-70

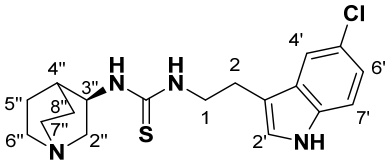

Following the *general procedure 4.2.1.2*, the reaction of **(*R*)-60** (57 mg, 0.45 mmol), DIPEA (0.18 mL, 1.03 mmol) and **64** (70 mg, 0.30 mmol) in DMF (3 mL), for 41 h afforded, after purification by flash chromatography on silica gel (CH_2Cl_2/MeOH/NH_4OH, 99:0:1-90:9:1), 84 mg (78 %) of the desired compound **(*R*)-70** as a white solid. Rf 0.03 (CH_2Cl_2/MeOH 90:5) m.p. 122 - 124 ºC. ^{1}H NMR (250 MHz, MeOD) δ 7.57 (dd, *J* = 2.1, 0.6 Hz, 1H, H4'), 7.27 (dd, *J* = 8.6, 0.4 Hz, 1H, H7'), 7.13 (s, 1H, H2'), 7.02 (dd, *J* = 8.6, 2.0 Hz, 1H, H6'), 4.48 - 4.29 (m, 1H, H3''), 3.75 (t, *J* = 6.8 Hz, 2H, 2xH1), 3.50 (dd, *J* = 13.5, 9.6 Hz, 1H, H2''b), 2.98 (t, *J* = 6.8 Hz, 6H, 2xH2, 2xH6'', H7'', H8''), 2.73 (d, *J* = 13.9 Hz, 1H, H2''a), 2.05 (d, *J* = 3.9 Hz, 1H, H4''), 1.81 (dd, *J* = 8.5, 5.5 Hz, 3H, H5''a, H7'', H8''), 1.61 (dd, *J* = 12.0, 6.8 Hz, 1H, H5''b) ppm. ^{13}C NMR (63 MHz, MeOD) δ 183.9, 160.0, 136.5, 130.2, 125.4, 122.4, 119.1, 113.5, 113.4, 55.7, 50.6, 47.6, 47.1, 46.3, 26.3, 25.7, 24.7, 19.7 ppm. HRMS (ES^+): Theoretical mass calc. for $C_{18}H_{23}ClN_4S$, 362.1332; found [$(M+H)^+$], 363.1407. IR (film) υ/cm^{-1} 3246, 2922, 2867, 2110, 1736, 1652, 1557, 1544, 1479, 1454, 1031, 862, 792. $[\alpha]_D^{24}$= + 4.59 º (*c*. 1.09 mg/mL, MeOH). Compound purity was estimated by reversed phase C18 HPLC, with a UV detector at 254 nm, and the major peak area of tested compound was 97 % of the combined total peak area.

(*S*)-1-(2-(5-chloro-1*H*-indol-3-yl)ethyl)-3-(quinuclidin-3-yl)thiourea (*S*)-70

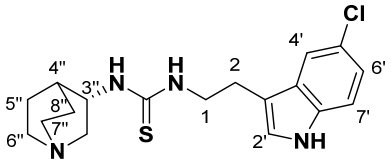

Following the *general procedure 4.2.1.2*, the reaction of **(*R*)-60** (57 mg, 0.45 mmol), DIPEA (0.18 mL, 1.03 mmol) and **64** (70 mg, 0.30 mmol) in DMF (3 mL), for 3 days 16 h afforded, after purification by flash chromatography on silica gel (CH_2Cl_2/MeOH/NH_4OH, 99:0:1-90:9:1), 68 mg (63 %) of the desired compound **(*S*)-60** as a white solid. $[\alpha]_D^{24}$= - 4.67 º (*c*. 1.07 mg/mL, MeOH). Compound purity was estimated

by reversed phase C18 HPLC, with a UV detector at 254 nm, and the major peak area of tested compound was 100 % of the combined total peak area.

(*R*)-1-(2-(1*H*-indol-3-yl)ethyl)-3-(quinuclidin-3-yl)thiourea (*R*)-71

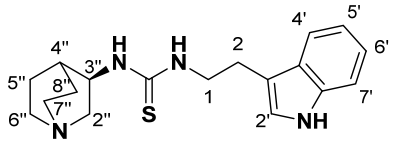

Following the *general procedure 4.2.1.2*, the reaction of **(*R*)-60** (30 mg, 0.24 mmol), DIPEA (0.15 mL, 0.84 mmol) and **65** (49 mg, 0.24 mmol) in DMF (1 mL), for 3 days 14 h afforded, after purification by flash chromatography on silica gel (CH_2Cl_2/MeOH/Et_3N, 98:1:1-90:9:1), 25 mg (32 %) of the desired compound **(*R*)-71** as a yellowish solid. Rf: 0.06 (CH_2Cl_2/MeOH 90:10) m.p. 131-133ºC. ^{1}H NMR (250 MHz, MeOD) δ 7.58 (dd, *J* = 7.6, 1.3 Hz, 1H, H4'), 7.30 (dt, *J* = 8.0, 1.0 Hz, 1H, H7'), 7.06 (dd, *J* = 8.6, 6.4 Hz, 2H, H2', H6'), 6.97 (ddd, *J* = 8.0, 7.0, 1.2 Hz, 1H, H5'), 4.30 (dd, *J* = 8.0, 4.8 Hz, 1H, H3''), 3.76 (t, *J* = 7.8, 4.9 Hz, 2H, 2xH1), 3.47 - 3.35 (m, 1H, H2''b), 3.00 (t, *J* = 6.9 Hz, 2H, 2xH2), 2.87 (t, *J* = 7.9, 7.5 Hz, 4H, 2xH6'', H7'', H8''), 2.59 (dd, *J* = 13.8, 7.5 Hz, 1H, H2''a), 1.98 (s, 1H, H4''), 1.75 (q, *J* = 10.2, 7.0, 5.6 Hz, 3H, H5''a, H7'', H8''), 1.56 (t, *J* = 15.3, 8.2 Hz, 1H, H5''b) ppm ^{13}C NMR (63 MHz, MeOD) δ 183.4, 138.2, 128.9, 123.7, 122.4, 119.7, 119.5, 113.2, 112.3, 55.6, 51.0, 47.7, 47.1, 46.2, 26.4, 26.1, 25.2, 20.0 ppm. HRMS (ES^+): Theoretical mass calc. for $C_{18}H_{24}N_4S$, 328.1722; found [$(M+H)^+$], 329.1804. IR (film) υ/cm^{-1} 3232, 3053, 2923, 2866, 2320, 1538, 1454, 1227, 1093, 1050, 985, 741. $[\alpha]_D^{24}$= + 6.67 º (*c*. 1.20 mg/ml, MeOH) Compound purity was estimated by reversed phase C18 HPLC, with a UV detector at 254 nm, and the major peak area of tested compound was 100 % of the combined total peak area.

(*S*)- 1-(2-(1*H*-indol-3-yl)ethyl)-3-(quinuclidin-3-yl)thiourea (*S*)-71

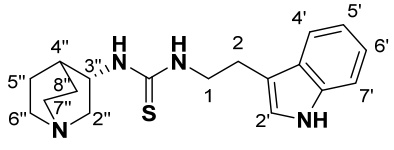

Following the *general procedure 4.2.1.2*, the reaction of **(*S*)-60** (62 mg, 0.49 mmol), DIPEA (0.31 mL, 1.71 mmol) and **65** (100 mg, 0.49 mmol) in DMF (2 mL), for 3 days 14 h afforded, after purification by flash chromatography on silica gel (CH_2Cl_2/MeOH/Et_3N, 98:1:1-90:9:1), 75 mg (47 %) of the desired compound **(*S*)-71** as a yellowish solid. $[\alpha]_D^{24}$= - 6.67 º (*c*. 1.20 mg/ml, MeOH) Compound purity was estimated by reversed phase C18 HPLC, with a UV detector at 254 nm, and the major peak area of tested compound was 98 % of the combined total peak area.

(*R*)-1-(2-(5-methoxy-1*H*-indol-3-yl)ethyl)-3-(quinuclidin-3-yl)urea (*R*)-72

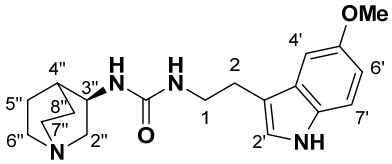

Following the general procedure for the *general procedure 4.2.1.2*, the reaction of **(*R*)-60** (30 mg, 0.24 mmol), DIPEA (0.15 mL, 0.84 mmol) and **66** (65 mg, 0.24 mmol) in DMF (1 mL), for 16 h afforded, after purification by flash chromatography on silica gel (CH_2Cl_2/MeOH/Et_3N, 95:5:1-80:19:1), 25 mg (30 %) of the desired compound **(*R*)-72** as a white solid. Rf 0.03 (CH_2Cl_2/MeOH 90:10) m.p. 117 - 119 ºC. ^{1}H NMR (250 MHz, MeOD) δ 7.19 (d, *J* = 8.7 Hz, 1H, H7'), 7.02 (d, *J* = 2.6 Hz, 2H, H2', H4'), 6.73 (dd, *J* = 8.8, 2.5 Hz, 1H, H6'), 3.90 - 3.81 (m, 1H, H3''), 3.80 (s, 3H, OC*H*$_3$), 3.41 (t, *J* = 6.6 Hz, 3H, H2''b, 2xH1), 2.87 (q, *J* = 7.0 Hz, 2H, H7'', H8''), 3.05 - 2.92 (m, 2H, 2xH6''), 2.88 (q, *J* = 7.0 Hz, 2H, 2xH2), 2.53 (dd, *J* = 13.8, 5.0 Hz, 1H, H2''a), 1.89 (q, *J* = 3.0 Hz, 2H, H4'', H5''a), 1.82 (dd, *J* = 11.6, 3.8 Hz, 2H, H7'', H8''), 1.61 (m, 1H, H5''b) ppm. ^{13}C NMR (63 MHz, MeOD) δ 160.8, 155.0, 133.5, 129.2, 124.4, 113.2, 112.9, 112.5, 101.5, 56.3, 56.0, 47.7, 47.3, 47.1, 41.8, 27.1, 26.9, 25.1, 19.7 ppm. HRMS (ES$^+$): Theoretical mass calc. for $C_{19}H_{26}N_4OS$, 342.2056; found [(M+H)$^+$], 343.2147. IR (film) υ/cm^{-1} 3247, 2929, 2875, 1648, 1556, 1483, 1440, 1213, 1172, 1027, 920, 795. $[\alpha]_D^{25}$= + 4.90 º (c. 1.02 mg/mL, MeOH) Compound purity was estimated by reversed phase C18 HPLC, with a UV detector at 254 nm, and the major peak area of tested compound was 97 % of the combined total peak area.

(*S*)-1-(2-(5-methoxy-1*H*-indol-3-yl)ethyl)-3-(quinuclidin-3-yl)urea (*S*)-72

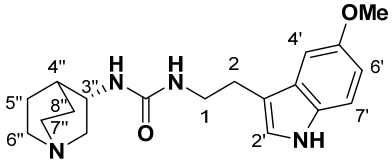

Following the *general procedure 4.2.1.2*, the reaction of **(*S*)-60** (28 mg, 0.22 mmol), DIPEA (0.14 mL, 0.80 mmol) and **67** (60 mg, 0.20 mmol) in DMF (0.8 mL), for 16 h afforded, after purification by flash chromatography on silica gel (CH_2Cl_2/MeOH/Et_3N, 95:5:1-80:19:1), 45 mg (66 %) of the desired compound **(*S*)-72** as a white solid. $[\alpha]_D^{24}$= - 19.0 º (*c*. 1.00 mg/mL, MeOH) Compound purity was estimated by reversed phase C18 HPLC, with a UV detector at 254 nm, and the major peak area of tested compound was 100 % of the combined total peak area.

(*R*)-1-(2-(5-chloro-1*H*-indol-3-yl)ethyl)-3-(quinuclidin-3-yl)urea (*R*)-73

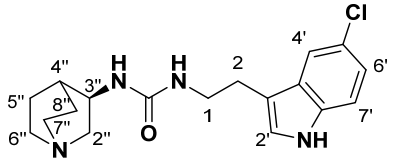

Following the *general procedure 4.2.1.2*, the reaction of **(*R*)-60** (40 mg, 0.31 mmol), DIPEA (0.2 mL, 0.84 mmol) and **67** (80 mg, 0.28 mmol) in DMF (1.1 mL), for 5 days afforded, after purification by flash chromatography on silica gel (CH_2Cl_2/MeOH/Et_3N, 95:4:1-80:19:1), 30 mg (31 %) of the desired compound **(*R*)-73** as a white solid. Rf 0.03 (CH_2Cl_2/MeOH/Et_3N, 95:5:1-80:19:1) m.p. 139 - 141 ºC. ^{1}H NMR (250 MHz, MeOD) δ 7.50 (dd, J = 2.1, 0.6 Hz, 1H, H4'), 7.26 (dd, J = 8.6, 0.6 Hz, 1H, H7'), 7.09 (s, 1H, H2'), 7.00 (dd, J = 8.6, 2.1 Hz, 1H, H6'), 3.79 (dd, J = 8.3, 4.4 Hz, 1H, H3''), 3.37 (t, J = 6.8 Hz, 2H, H1), 3.34 (dt, J = 3.3, 1.6 Hz, 2H, H2''b, H7''), 3.01 - 2.79 (m, 6H, 2xH2, H4'', H6''a, H7'', H8''), 2.60 - 2.45 (dd, J = 14.0, 1.8, 1H, H2''a), 1.85 (d, J = 3.1 Hz, 1H, H6''b), 1.75 (dd, J = 13.2, 6.9 Hz, 2H, H5''a, H8''), 1.62 - 1.44 (m, 1H, H5''b) ppm. ^{13}C NMR (63 MHz, MeOD) δ 160.7, 136.5, 130.2, 125.3, 122.4, 118.9, 113.5, 113.4, 56.1, 47.8, 47.4, 47.1, 42.0, 27.0, 26.9, 25.3 ppm. HRMS (ES^+): Theoretical mass calc. for $C_{18}H_{23}ClN_4O$, 346,1560; found [$(M+H)^+$], 347.1645. IR (film) υ/cm^{-1} 3250, 2930, 2871, 1638, 1556, 1454, 1314, 1251, 1227, 1098, 1052, 891, 793. $[\alpha]_D^{25}$= + 13.86 º (*c*. 1.01 mg/mL, MeOH) Compound purity was estimated by reversed phase C18 HPLC, with a UV detector at 254 nm, and the major peak area of tested compound was 100 % of the combined total peak area.

(*S*)-1-(2-(5-chloro-1*H*-indol-3-yl)ethyl)-3-(quinuclidin-3-yl)urea (*S*)-73

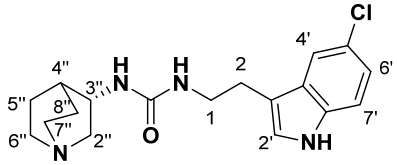

Following the *general procedure 4.2.1.2*, the reaction of **(*S*)-60** (32 mg, 0.25 mmol), DIPEA (0.12 mL, 0.68 mmol) and **67** (50 mg, 0.17 mmol) in DMF (0.7 mL), for 14 h afforded, after purification by flash chromatography on silica gel (CH_2Cl_2/MeOH/Et_3N, 95:5:1-80:19:1), 40 mg (68 %) of the desired compound **(*R*)-73** as a white solid. $[\alpha]_D^{25}$= - 12.75 º (*c*. 1.02 mg/mL, MeOH) Compound purity was estimated by reversed phase C18 HPLC, with a UV detector at 254 nm, and the major peak area of tested compound was 96 % of the combined total peak area.

(*R*)-1-(2-(1*H*-indol-3-yl)ethyl)-3-(quinuclidin-3-yl)urea (*R*)-74

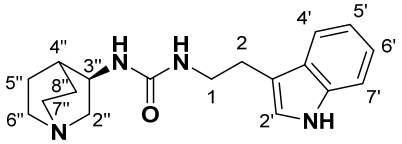

Following the *general procedure 4.2.1.2*, the reaction of **(*R*)-60** (55 mg, 0.26 mmol), DIPEA (0.13 mL, 0.84 mmol) and **68** (34 mg, 0.18 mmol) in DMF (1.1 mL), for 24 h afforded, after purification by flash chromatography on silica gel (CH_2Cl_2/MeOH/Et_3N, 95:5:1-90:9:1), 50 mg (62 %) of the desired compound **(*R*)-74** as a white solid. Rf 0.03 (CH_2Cl_2/MeOH 90:10) m.p. 161 - 163 ºC. ^{1}H NMR (250 MHz, MeOD) δ 7.55 (dd, *J* = 8.2, 1.3 Hz, 1H, H4'), 7.30 (dt, *J* = 8.2, 2.8 Hz, 1H, H7'), 7.04 (m, 2H, H2', H6'), 6.97 (tdd, *J* = 7.4, 2.3, 1.0 Hz, 1H, H5'), 4.06 - 3.91 (m, 1H, H3''), 3.79 - 3.63 (m, 1H, H2''b), 3.49 - 3.28 (m, 4H, 2xH1, H6''b, H7''), 3.01 (d, *J* = 9.3 Hz, 1H, H4''), 2.95 - 2.82 (m, 4H, 2xH2, H6''a, H8''), 2.75 (t, *J* = 7.7 Hz, 1H, H5''a), 2.37 (dd, *J* = 13.5, 5.4 Hz, 1H, H2''a), 2.14 - 1.96 (m, 2H, H7'', H8''), 1.67 (m, 1H, H5''b) ppm.^{13}C NMR (63 MHz, MeOD) δ 159.5, 137.2, 127.9, 122.6, 121.3, 118.6, 118.4, 112.3, 111.3, 55.4, 46.9, 46.2, 45.9, 40.9, 26.3, 26.1, 23.0, 19.5 ppm. HRMS (ES^+): Theoretical mass calc. for $C_{18}H_{24}N_4O$, 312.1950; found [$(M+H)^+$], 313.2017; found [$(M+H+CH_3)^+$], 327.2171. IR (film) υ/cm^{-1} 3235, 2941, 2311, 1738, 1624, 1544, 1484, 1452, 1439, 1378, 1351, 1213, 1172, 1064, 1022, 923, 797. $[\alpha]_D^{25}$= + 7.84 º (*c*. 1.02 mg/mL, MeOH) Compound purity was estimated by reversed phase C18 HPLC, with a DAD detector in line with the spectrophotometer from 200 to 450 nm, and the major peak area of tested compound was 99 % of the combined total peak area.

(*S*)-1-(2-(1*H*-indol-3-yl)ethyl)-3-(quinuclidin-3-yl)urea (*S*)-74

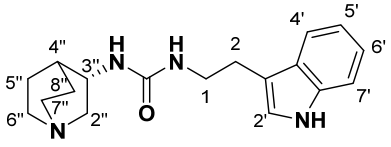

Following the *general procedure 4.2.1.2*, the reaction of **(*S*)-60** (55 mg, 0.26 mmol), DIPEA (0.18 mL, 1.04 mmol) and **68** (44 mg, 0.26 mmol) in DMF (1.1 mL), for 24 h afforded, after purification by flash chromatography on silica gel (CH_2Cl_2/MeOH/Et_3N, 95:5:1-90:9:1), 20 mg (25 %) of the desired compound **(*S*)-74** as a white solid. $[\alpha]_D^{25}$= - 12.75 º (*c*. 1.02 mg/mL, MeOH) Compound purity was estimated by reversed phase C18 HPLC, with a UV detector at 254 nm, and the major peak area of tested compound was 96 % of the combined total peak area.

4.2.2 Pharmacological evaluation

4.2.2.1 Determination of Nrf2 induction activity

Protocol described in *Section 4.1.2.3.*

4.2.2.2 Oxygen Radical Absorbance Capacity (ORAC) assay

Protocol described in *Section 4.1.2.4.*

4.2.2.3 Calcium fluorimetry.

For measurement of cellular response stimulating nicotinic receptors with ACh, or α7-nAChR selective agonist PNU282987, protocol described in *Section 4.1.2.6* was followed. For testing novel compounds as agonists, they were injected at different concentrations (0.3, 1, 3, 10, 30 μM) to cells incubated 10 min with PNU120596 at 10 μM prior injection. In addition, injection over KH and MLA was performed for better understanding of the selective α7-nAChR activation.

4.2.2.4 SH-SY5Y Per se toxicity studies

Protocol described in *Section 4.1.2.9.*

4.2.2.5 Cell viability assessment by MTT method

Protocol described in *Section 4.1.2.10.*

4.2.2.6 SH-SY5Y *in vitro* neuroprotection studies

Protocol described in *Section 4.1.2.11.*

4.2.2.7 Docking studies on α7-nAChR

Protocol described in *Section 4.1.3.3.*

4.3 Statistical analysis

Results obtained in this Thesis are expressed as mean ± standard error of the mean (SEM). Analysis of the effect of different compounds were performed using paired and unpaired *Student's t-test* between two groups or one-way ANOVA followed by Newman-

Keuls post-hoc test when three groups are implicated. Statistically significant results were considered when $p < 0.05$.

5 Results and Discussion

5.1 Objective I: design, synthesis, pharmacodynamic and pharmacokinetic evaluation of multitarget directed ligands as antioxidants, Nrf2 inducers and α7-nAChRs modulators.

5.1.1 Design of novel Nrf2 inducers and α7-nAChRs ligands as multitarget drugs for AD

New multitarget ligands were proposed to be able to reduce two contributors to AD progression, oxidative stress and cholinergic system hypofunction to, eventually, promote neuroprotection. The first can be address by inducing the main mechanism of cells self-defence against oxidative stress to balance out the excess of ROS and RNS: the antioxidant enzyme system regulated by the transcription factor Nrf2. Notwithstanding, we can complement the Nrf2 capacity with further scavenger effect by including a melatonin scaffold analogue on the molecule.[38]

The design of the new MTDLs was based on the existence of Nrf2 inducers by dissociation of Nrf2-Keap1 complex. As explained in *Section 2.10.3*, Nrf2-EpRE pathway can be induced by different manners, being the most explored the use of organic compounds with a noticeable electrophilic character. However, they generally present high carcinogenicity and/or genotoxicity which hinder their use as therapeutic agents. Thus, the development of new Nrf2 inducers with low or none toxicity, and similar or even higher potency, would be very beneficial.

As depicted before, the second activity of our drug design program is the potentiation of the cholinergic system. In this regard, several targets can be considered like AChE inhibition and nAChRs potentiation. As already mentioned in *Section 2.5*, current treatments for AD are AChEi, which main purpose is to prevent cholinergic system atrophy by maintaining ACh levels in the synaptic cleft. Nevertheless, this class of drugs are symptomatic. Thus, modulation of nAChRs is an interesting strategy to achieve DMTs, since they initiate intracellular signalling cascades promoting neuronal survival.

Considering the structure of known nAChRs ligands and other active molecules, all of them possess a stereogenic quaternary centres as a common feature. This is the case

of alkaloids with 5,6,6-spiro-azatricyclic system such as lycorine **74,** (grow and metathesis inhibitor), fasicularin **75** (DNA alkylating agent) lepadiformine **76** (antiarrhythmic properties) and cylindricine K **77** (no biological activity reported yet). Specifically, nicotine **78**, cytisine **79** and epibatidine[154] **80**, have provided structures and key tools to understand nAChRs **(Figure 13)**. In general, alkaloids with activity in nAChRs share common structural features such as polycyclic scaffolds, rings with a nitrogen-bridged atom and enantiopure chiral quaternary carbons. Galantamine **4** (**Figure 1**) already mentioned in *Section 2.5.*, is a distinguished example of isoquinoline class of alkaloid obtained from *Galanthus nivalis* and other plants with AChE and α7-nAChRs activity. It is a PAM of α7-nAChRs at low concentrations (0.02-2 μM) whereas at higher concentrations (> 10 μM) it is a non-competitive antagonist.[155] Similar properties have been found for codeine, and both alkaloids contain chiral quaternary carbons and fused cycles.[156]

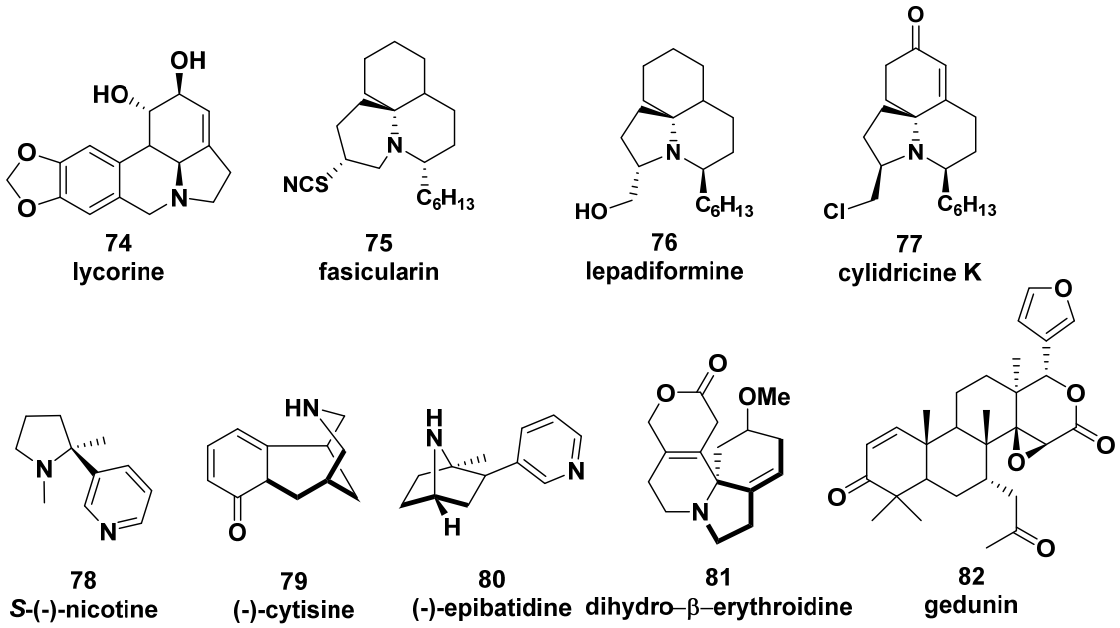

Figure 13. Tridimensional structure of alkaloids with 5,6,6-spiro-azatricyclic structure and known nicotinic ligands. Gedunin, a potent Nrf2 inducer alkaloid.

Based on the structure of I) alkaloids with nAChRs activity, II) Michael acceptors with Nrf2 induction activity and III) melatonin, a natural antioxidant with neuroprotective properties, a new family of MTDLs was designed to contain following structural features, (**Figure 14**):

- An alkaloid-like polycyclic moiety designed to modulate nAChRs response.
- Two Michael acceptors sterically impeded embedded into the tricyclic structure designed to avoid mixed interactions with different nucleophiles present in cell, and hence, to reduce their toxicity.
- A melatonin-derived moiety designed to scavenge ROS conferring a potent antioxidant effect.

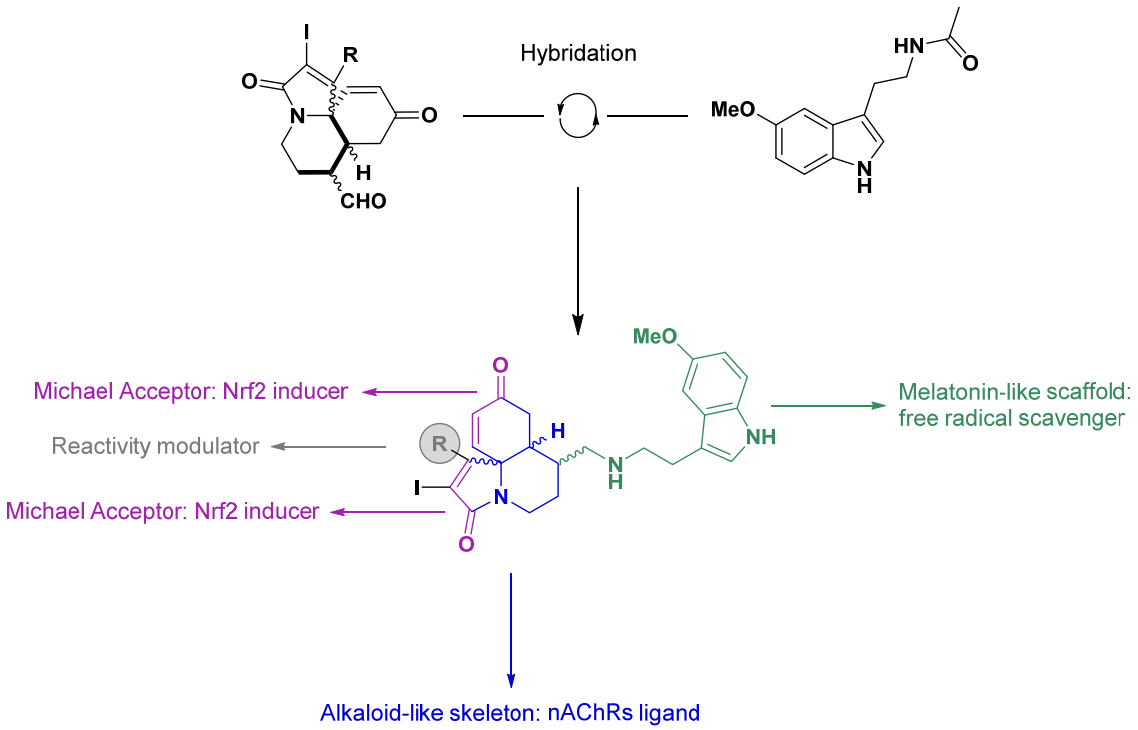

Figure 14. Rational design of novel hybrid compounds with multitarget activities. In blue, a twisted and rigid tricyclic structure with a bridged nitrogen atom included to modulate nAChRs; in purple, two α,β-unsaturated systems embedded in the complex structure and sterically hindered to moderately induce Nrf2-EpRE pathway; in green, an indole skeleton with substituents present in melatonin to afford a ROS scavenging activity; in red, different substituents to modulate reactivity.

Therefore, a complex tridimensional tetrahydropyrroloquinolindienone containing three contiguous stereocentres, a chiral quaternary carbon, a bridged-nitrogen atom and two α-β-unsaturated systems, was included mimicking two alkaloids cylindricine K **77** and gedunin **82**, **Figure 13**. Moreover, the particular tricyclic structure resembles to dihydro-β-erythroidine **81** (DHβE), a well-known selective α4β2 antagonist erythrine alkaloid, suggesting a potential nAChRs activity. The cyclohexanone scaffold

present in the natural product gedunin **82**, a potent Nrf2 inducer with neuroprotective properties,[157] was intentionally designed to release Nrf2 transcription factor by directly reaction with sulfhydryl groups of Keap1 cysteines. Five electronic and size different R substituent groups like phenyl (Ph), *m*-fluorophenyl (*m*-F-Ph), propyl (Pr), cyclopropyl (CyPr) and cyclohexyl (CyHx) were included to modulate reactivity towards Nrf2 induction and nAChR modulation. Afterwards, the remaining indole moiety would be able to act as a potent free radical scavenger showing a mechanism of action similar to the known "melatonin antioxidant cascade".

These compounds are conceived to be directed to different therapeutic targets which act synergically at complementary points of the pathological network. Thus, activating the endogen survival cell routes, could prevent or, at least, slow down the neurodegeneration process.

5.1.2 *In silico* physicochemical properties

Physicochemical properties are a consequence of the molecular structure. In this regard, the *Rule of 5* developed by Lipinski and co-workers[158] is a valuable tool for medicinal chemists. These terms are important to determine a potential drug candidate to avoid issues with oral absorption and permeability. Thus, to predict the druglikeness of the new compounds **54** (Ph), **55** (*m*-F-Ph), **56** (Pr), **57** (CyPr) and **58** (CyHx), some physicochemical descriptors related with size (MW), hydrogen bonding donor/acceptor (HBD/HBA) character, number of rotatable bonds (RB), topological polar surface area (TPSA), lipophilicity (clogP), acid-base character (pK_a), as well as blood brain barrier (BBB) permeation were calculated using both SwissADME[159] and Chemicalize from ChemAxon[160] free platforms, (**Table 1**).

Table 1. Druglike physicochemical properties of compounds **46-50**

Cpd	MW (g/mol)	HBA	HBD	RB	TPSA (Å^2)	pK$_a$ [a]	clogP [b]	S [c] (mg/mL)	P-gp substrate	BBB permeant
54	607.48	4	2	7	74.43	10.4	4.20	$3.03 \cdot 10^{-7}$	Yes	No
55	625.47	5	2	7	74.43	10.4	4.49	$1.73 \cdot 10^{-7}$	Yes	No
56	573.47	4	2	8	74.43	10.4	3.91	$5.39 \cdot 10^{-6}$	Yes	Yes
57	571.45	4	2	7	74.43	10.4	3.60	$2.11 \cdot 10^{-5}$	Yes	Yes
58	613.53	4	2	7	74.43	10.4	4.55	$3.75 \cdot 10^{-6}$	Yes	No

All parameters were calculated using SwissADME platform (http://www.swissadme.ch/index.php) and [a]Chemicalize free software tool https://chemaxon.com/products/chemicalize [b]Consensus log Po/w is the arithmetic mean of the values predicted by the five methods (iLOGP, XLOGP3, WLOGP, MLOGP, SILICOS-IT). [c]SwissADME SILICOS-IT prediction.

All derivatives have a MW higher than 500 g mol^{-1} in the following order: *m*-F-Ph **55** > CyHx **58** > Ph **54** > Pr **56** > CyPr **57**. The number of HBD is 2 for all and the HBA less than 10. Also, number of rotatable bonds are less than 10 and the topological polar surface is between optimal range, 60 to 70/90 Å^2.[161] Compounds with large substituent (Ph **54**, *m*-F-Ph **55** and CyHx **58**) are more lipophilic (clogP > 4) than compounds with small substituents (Pr **56** and CyPr **57**, cLogP: 3.91 and 3.60 respectively). Lipophilic molecules are more prone to be able to cross cellular membranes passively. However, the high lipophilic character of the compounds is reflected in low water solubility (S < 0.01 mg/mL) which is an issue for their transport through blood strain. All compounds present a predicted pKa of 10.4. That strong basicity entails protonated compounds at physiological pH, favouring their solubility in aqueous media. Therefore, a tight equilibrium between those properties makes the small size compounds, **56** and **57**, might be able to cross the BBB passively, although they are predicted to be P-glycoprotein (P-gp) substrates (an efflux transporter of the BBB) as well as bigger derivatives.

5.1.3 Synthesis of 2-iodo-7-(((2-(5-methoxy-1*H*-indol-3-yl)ethyl)amino)methyl)-1-alkyl/aryl-6,7,7a,8-tetrahydro-3*H*-pyrrolo[2,1-*J*]quinoline-3,9(5*H*)-dione (54-58)

Quaternary stereocentres-containing molecules that dispose orthogonal functionality for later manipulation are of great value in organic chemistry.[162] Since most of the cases one of the two enantiomers has more potency of binding to its target than the other,[163] we proposed an enantioselective synthesis of compounds of **Family A** named 2-iodo-7-(((2-(5-methoxy-1*H*-indol-3-yl)ethyl)amino)methyl)-1-alkyl/aryl-6,7,7a,8-tetrahydro-3*H*-pyrrolo[2,1-*J*]quinoline-3,9(5*H*)-dione. Thus, both enantiomers as well as racemic mixture of each derivative could be achieve after a seven-step linear process. Finally, it was evident to propose a reductive amination between it and tricyclic aldehyde as latest reaction illustrated in retrosynthetic scheme, (**Scheme 1**). Then, our efforts were focused on the synthesis of the tricyclic aldehyde scaffold **48-52**. In this case, the synthesis was based on electrophile-triggered catalytic enantioselective dearomatization (ECED) strategy developed by León and colleagues in 2011.[114] Two consecutive steps form the tricyclic lactam **48-52** which includes an enantiomerically pure quaternary carbon and two chiral tertiary centres. Also, it contains an aldehyde, a cyclohexanone functionality and a vinyl iodide, all, very versatile functional groups that could be subjected to orthogonal transformations.

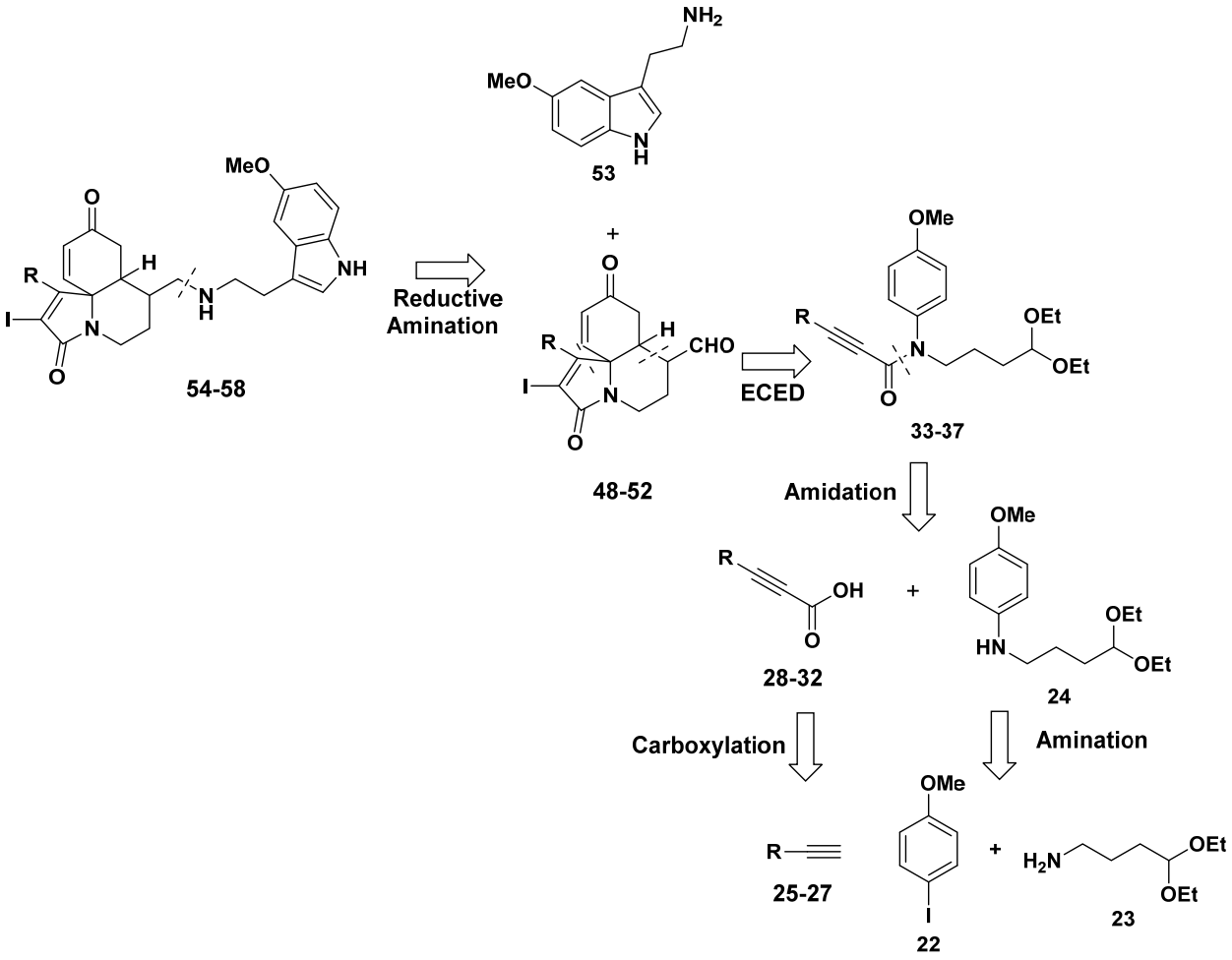

Scheme 1. Retrosynthetic scheme with key reactions to obtain compounds of **Family A**.

The synthesis started with the preparation of the *N*-(4,4-diethoxybutil)-4-methoxyaniline **24** employing an Ullmann-like amination of 4-iodoanisole **22** with 4,4-diethoxybutan-1-amine **23**, using CuI as catalyst, L-proline as ligand and K_2CO_3 as base at 80 ºC for 26 h in DMSO in a 85 % yield. Carboxylic acid is essential to contain an alkyne group contiguously since it is necessary to perform ECED transformation. However, the variety of commercially available starting materials is reduced. 3-(*m*-fluorophenyl)-propiolic acid **29**, 3-cyclopropylpropiolic acid **31** and 3-cyclohexylpropiolic acid **32** were easily and quantitatively prepared from acetylide anion generated during an hour with n-BuLi in dry Et_2O at -78ºC, and excess of solid carbon dioxide (dry ice).

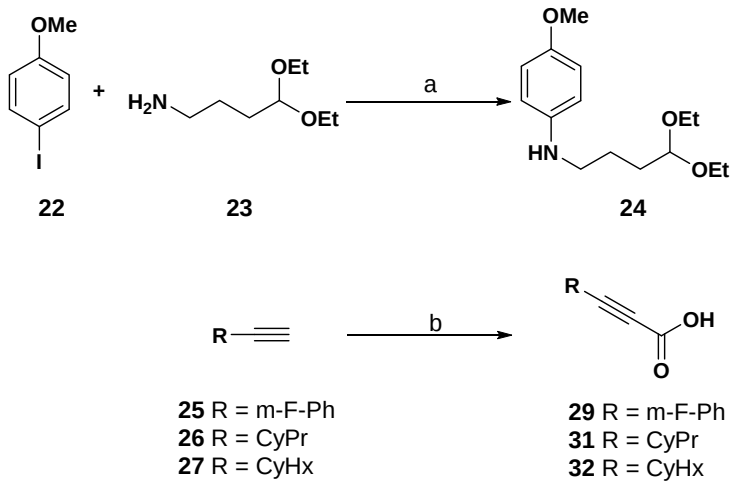

Scheme 2. Synthesis of starting materials amine and carboxylic acids derivatives for amide coupling. Starting materials and reaction conditions: a) L-proline, CuI, K_2CO_3, DMSO, 80 ºC, 26 h. b. CO_2, Et_2O, -78 ºC, 1 h.

Amide bond formation was achieved by activation of carboxylic acid with a coupling agent to covert –OH in a good leaving group susceptible to be released by amine addition. In this case, following previous reported conditions,[114] 1-Ethyl-3-(3-dimethylaminopropyl)carbodiimide (EDCI) coupling agent and 1-hydroxy-1*H*-benzotriazol (HOBT) additive were employed with 3-phenylpropiolic **28** and 3-cyclopropylpropiolic acid **31** in CH_2Cl_2 at room temperature overnight, yielding 95 % and 44 % of respective amides. Unexpected moderate yield was obtained with CyPr derivative, in fact, 26 % of starting amine **24** was recovered. Thus, we used 1-[Bis(dimethylamino)methyleny]-1H-1,2,3-triazolo[4,5-b]pyridinium3-oxyhexafluorophosphate (HATU) as catalyst and Et_3N in CH_2Cl_2. As a result, reactions were accelerated and planar amide derivatives **33-37** were obtained with excellent yields, **Table 2**. Thereafter, acetal protection was removed with HCl 2 N solution in THF at room temperature during 1 h (Pr **35** and CyPr **36**), 1.20 h (CyHx **37**), 2 h (Ph **33**) and 4 h (*m*-F-Ph **34**) obtaining desired aldehydes **38-42** quantitatively.

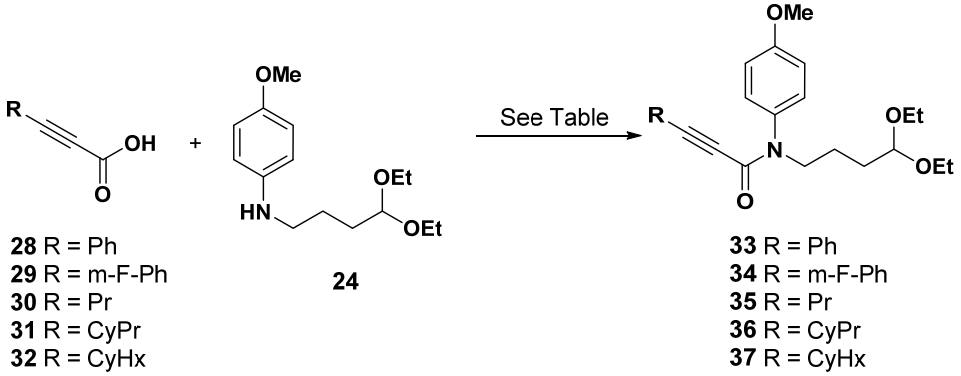

Table 2. Amidation reaction between common amine precursor and 3-substitutedpropiolic acids.

Compound	R	Conditions	t (h)	Yield (%)
33	Ph	EDCI, HOBT, CH_2Cl_2, 25ºC	16	95
36	CyPr	EDCI, HOBT, CH_2Cl_2, 25ºC	17	44
33	Ph	HATU, Et_3N, CH_2Cl_2, 0ºC to rt	1.40	95
34	*m*-F-Ph	HATU, Et_3N, CH_2Cl_2, 0ºC to rt	4	97
35	Pr	HATU, Et_3N, CH_2Cl_2, 0ºC to rt	1.20	92
36	CyPr	HATU, Et_3N, CH_2Cl_2, 0ºC to rt	2	91
37	CyHx	HATU, Et_3N, CH_2Cl_2, 0ºC to rt	2	97

ECED is based on the fact that dearomatization of *ortho*- or *para*-phenols leads to 2,4- or 2,5-cyclohexadienones since one planar sp^2-hybridized carbon transforms into sp^3-hybridized carbon, opening the opportunity to induce asymmetry. As dearomatizated phenols are thermodynamically unfavoured, appropriate reaction conditions oxidation, are necessary to isolate dearomatized product.[164] In our particular case, firstly, we induced the dearomatization of planar alkyne-containing anisidine derivatives **43-47** adding dropwise a potent electrophile, iodide monochloride, at -78 ºC in CH_2Cl_2. ICl reacts with the alkyne moiety generating an iodirenium intermediate which rapidly experiences a 5-*endo*-dig Larock *ipso*-iodocyclization, as shown in **Scheme 3**, yielding achiral *meso*-iodo-substituted spirocyclic cyclohexanodienones **43** (73 %) **44** (46 %) **45** (72 %) **46** (69 %) **47** (73 %). Much attention should be paid regarding the careful addition of the electrophile in order to prevent the formation of byproducts.

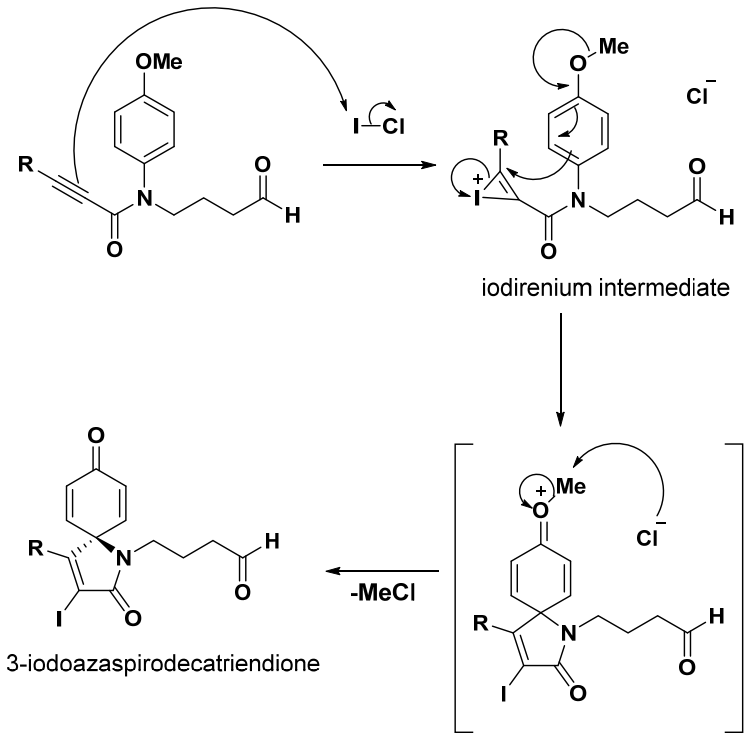

Scheme 3. Electrophilic-triggered dearomatization (ECED) mechanism of alkyne-containing anisidine derivatives through a 5-*endo*-dig *ipso*-iodocyclization of Larock leads to a *meso*-iodo-substituted spirocyclic cyclohexanodienones.

Azaspirocyclohexanodienone is an achiral compound, presenting enantiotopic hydrogens at cyclohexanodienone ring. Therefore, by using the sterically bulky and enantiomerically pure catalyst (*R*)- or (*S*)- diphenylprolinol trimethylsilylether (Hayashi-Jørgensen catalyst), enantioselective desymmetrising induction can be performed. Thus, aldehyde reacts with Hayashi-Jørgensen catalyst forming an enamine, which, by an *endo*-like attack onto the *Si* face of the α,β-unsaturated system,[165] undergoes an intramolecular Michael addition placing simultaneously three chiral centers with enantiopure configuration in one step, **Scheme 4**.

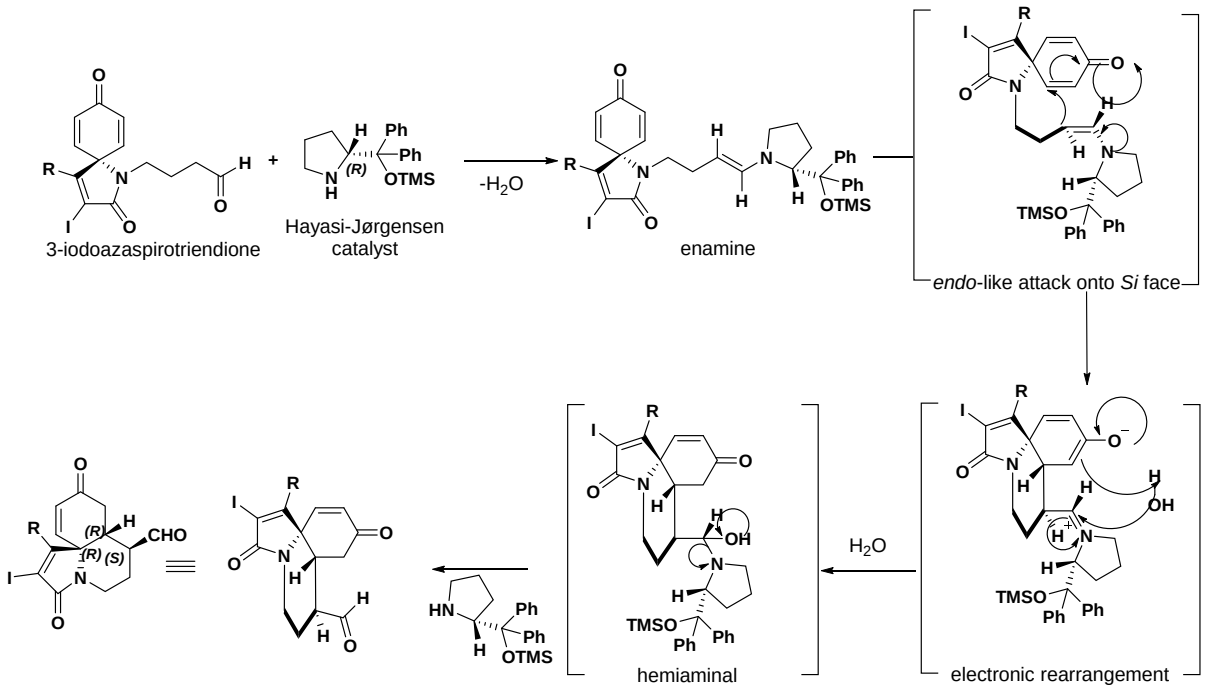

Scheme 4. ECED desymmetrization process. Organocatalytic enantioselective intramolecular Michael addition through an *endo*-like attack towards *Si* face α,β-unsuturated system.

Thus, the (*R*) enantiomeric form of Hayashi-Jørgensen catalyst produced [7(*S)*, 7a(*R)*, 11a(*R*)] configuration levorotatory **(-)** enantiomer (**Scheme 4**), while *S* form provided the opposite configuration [7(*R)*, 7a(*S)*, 11a(*S*)] dextrorotatory **(+)** derivatives (**Scheme 5**). The mixture of both catalysts led to racemic mixtures **(±)-.**

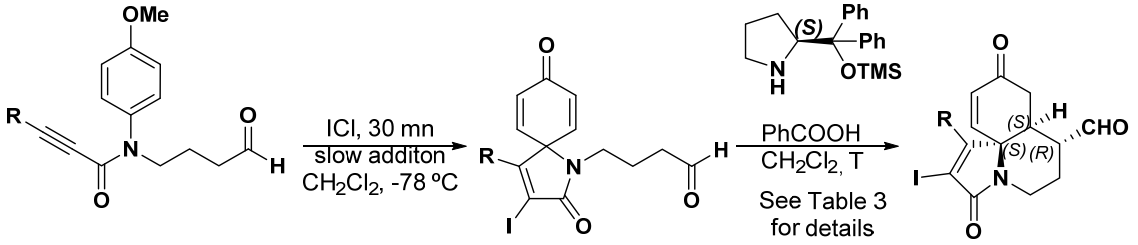

38 R = Ph
39 R = *m*-F-Ph
40 R = Pr
41 R = CyPr
42 R = CyHx

43 R = Ph
44 R = m-F-Ph
45 R = Pr
46 R = CyPr
47 R = CyHx

(+)-48 R = Ph
(+)-49 R = m-F-Ph
(+)-50 R = Pr
(+)-51 R = CyPr
(+)-52 R = CyHx

Scheme 5. ECED desymmetrization process illustrated with (*S*)-catalyst form, followed by reductive amination to obtain **Family A** dextrorotatory derivatives with [7(*R)*, 7a(*S)*, 11a(*S*)] configuration. Configuration of levororatory derivatives is the opposite, [7(*S)*, 7a(*R)*, 11a(*R*)].

Optimization of reaction conditions are presented herein in the **Table 3**. In general, -20 ºC and a dilution of 35 mL/mmol in CH_2Cl_2 using a 20 % mol of both

catalysts gave moderate to high yields, ranging from 60 % to 90 %, and *ee*, determined on final compounds, being from 81 % (**(+)-58**) to 92% for (**(-)-57)**.

Table 3. Optimized conditions ECED process with different substituents and subsequent reductive amination with 5-MeO-tryptamine to obtain final derivatives, 2-iodo-7-(((2-(5-methoxy-1*H*-indol-3-yl)ethyl)amino)methyl)-1-alkyl/aryl-6,7,7a,8-tetrahydro-3*H*-pyrrolo[2,1-*J*]quinoline-3,9(5*H*)-diones **54-58**.

Cat.	ECED product	t (days.h)	Yield (%)	Final product	t (h)	Yield (%)	*ee* (%)
RAC	**(±)-48**	3.21	57	**(±)-54**	20	71	-
R	**(-)-48**	3.21	89	**(-)-54**	20	66	89
S	**(+)-48**	2.15	79	**(+)-54**	20	72	87
RAC	**(±)-49**	1.15	90	**(±)-55**	20	52	-
R	**(-)-49**	1.15	85	**(-)-55**	21	73	91
S	**(+)-49**	4.22	88	**(+)-55**	23	52	89
RAC	**(±)-50**	2.19	72	**(±)-56**	24	75	-
R	**(-)-50**	5.13	80	**(-)-56**	22	79	85
S	**(+)-50**	4.19	81	**(+)-56**	18	70	88
RAC	**(±)-51**	1.15	60	**(±)-57**	16	51	-
R	**(-)-51**	3.18	85	**(-)-57**	21	64	92
S	**(+)-51**	3.18	86	**(+)-57**	21	72	86
RAC	**(±)-52**	4.20	74	**(±)-58**	23	59	-
R	**(-)-52**	3.21	89	**(-)-58**	24	43	84
S	**(+)-52**	2.17	70	**(+)-58**	20	54	81

Final compounds **54-58** were synthetized by a reductive amination. Reaction of aldehydes **48-52** with 5-MeO-tryptamine **53** led to the formation of an imine intermediate which was transformed into an amine after the addition of sodium triacetoxyborohydride

giving moderate to high yields, **Scheme 6**. *ee* and purities were obtained by liquid chromatography (LC) technique. Retention times of each derivative and the specific conditions for each measurement are detailed in **Table A1, Appendix A**.

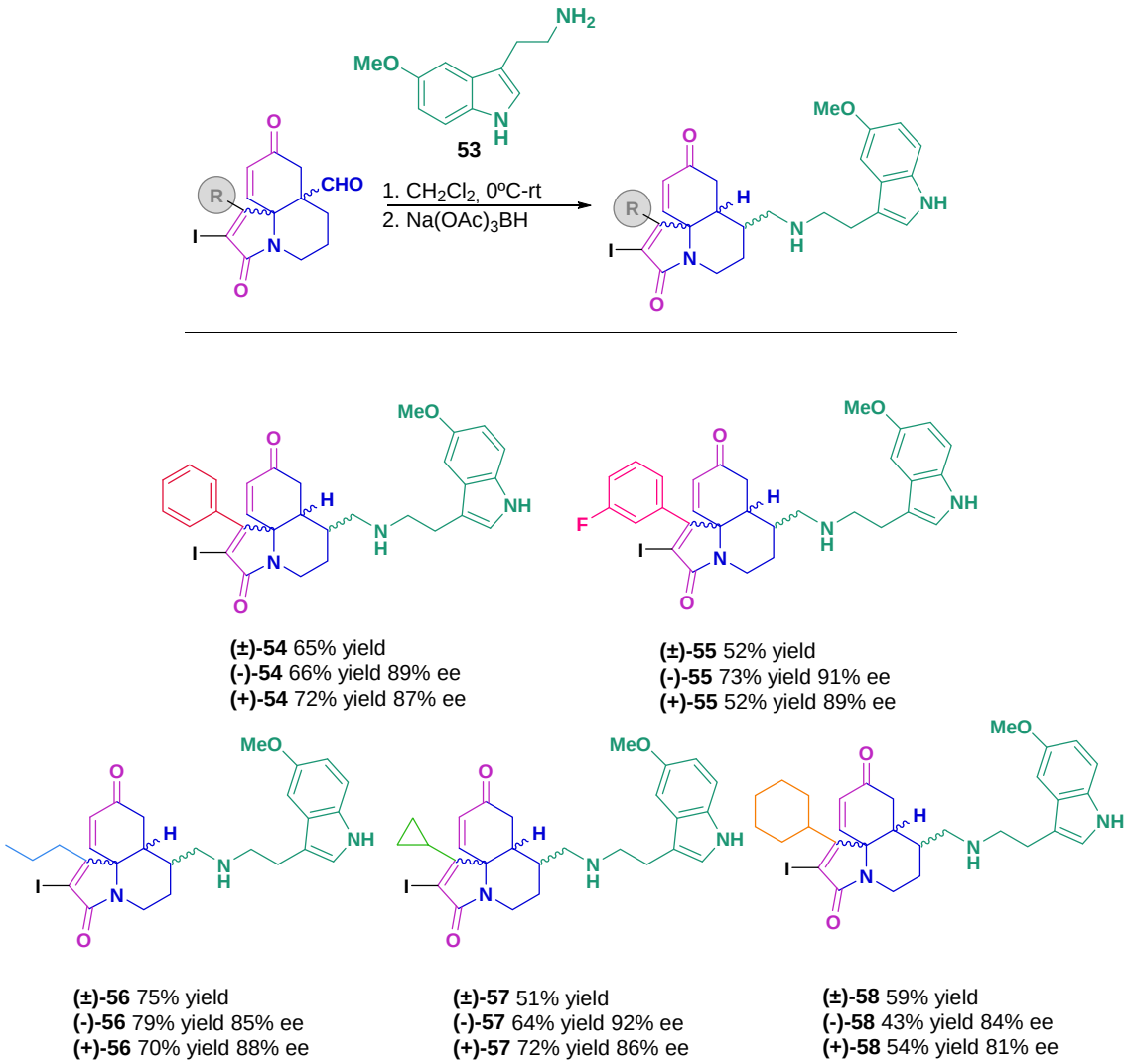

Scheme 6. Reductive amination to obtain **Family A** compounds. Structure of final compounds with yields and enantiomeric excesses.

5.1.4 *In vitro* pharmacological evaluation

New MTDLs of **Family A** were screened for the activities expected. Therefore, we aimed to evaluate the Nrf2 induction capacity, the free radical scavenger activity and the modulation of cholinergic system. As consequence of these activities, we also assessed their potential neuroprotective profile.

5.1.4.1 New MTDLs have Nrf2 transcription factor induction effect

Nrf2 induction, was evaluated in AREc32 cell line. This cells are MCF-7 human cells stably transfected with 8x luciferase reporter gen inserted after EpRE sequences.[117] Thus, in the presence of electrophiles or oxidative stress, Nrf2 translocates to the nucleus where it binds to EpRE sequences, promoting its expression, which is directly proportional to the luciferase expression, easily measured by luminescence assay. Compounds at four concentrations (1, 5, 10, 15 μM) and the positive control *tert*-butylhydroquinone (TBHQ) at 10 μM were incubated for 24 h and then, luciferase activity was measured. The values were normalized to basal luminescence considered as 1. Nevertheless, in order to compare among compounds and experiments, the concentration that double the basal activity of luciferase (CD) was calculated. In parallel, we assessed the *per se* toxicity of derivatives in this cell line (**Table A2, Appendix A**).

Data are shown in **Table 4** as CD values. Compounds with an aromatic ring, **54** (Ph) and **55** (*m*-F-Ph), showed CD values below 5 μM, being potent Nrf2 inducers, in the same extent as TBHQ. Conversely, compounds with aliphatic substituent, **56** (Pr) and **57** (CyPr), were statistically less potent than TBHQ, being moderate Nrf2 inducers. **(-)-56** and **(±)-56** have similar values, and, surprisingly, they are statistically more potent inducers than **(+)-56**. CyHx **58** were extremely toxic at 10 μM (65 to 70 % death, (**Table A2**), and in lower tested concentrations, they were not able to induce the double activity of luciferase, most probably because of steric hindrance since it is the largest substituent.

Table 4. Nrf2 transcription factor induction by compounds and TBHQ, reference compound, as relative CD values, and antioxidant capacity of compounds **54-58** measured as ORAC values.

Compound	CD[a] (μM)	TEq[b]
TBHQ	1.9 ± 0.5	
Melatonin		2.68 ± 0.13***
(±)-54	3.3 ± 0.9	2.26 ± 0.09**#
(-)-54	2.8 ± 1.1	2.38 ± 0.16**
(+)-54	3.9 ± 1.0	2.33 ± 0.31*
(±)-55	2.4 ± 0.5	2.24 ± 0.16**#
(-)-55	2.7 ± 0.8	2.36 ± 0.09**#$
(+)-55	3.5 ± 0.4	2.01 ± 0.14***###
(±)-56	6.1 ± 1.5	2.79 ± 0.11***
(-)-56	5.9 ± 0.6	2.96 ± 0.41***#
(+)-56	8.8 ± 0.6	2.27 ± 0.15**#$$
(±)-57	8.8 ± 0.2	2.68 ± 0.06***
(-)-57	9.6 ± 0.7	2.76 ± 0.23*
(+)-57	8.6 ± 0.4	3.11 ± 0.05***##
(±)-58	&	1.74 ± 0.14**###
(-)-58	&	1.82 ± 0.13**###
(+)-58	&	1.82 ± 0.09***##

Data are shown as mean ± SEM of duplicates of three experiments at four (Nrf2) and six (ORAC) different concentrations. [a]CD: Concentration to double the activity of luciferase. Unpaired *Student's t-test* $^{\#}p < 0.05$, $^{\#\#}p < 0.01$, $^{\#\#\#}p < 0.001$ with respect to TBHQ. Unpaired *Student's t-test* $^{\$}p < 0.05$ between derivatives. & CD could not be calculated due to lack of concentration-response dependency. [b]Paired *Student's t-test* $^{*}p < 0.05$, $^{**}p < 0.01$, $^{***}p < 0.001$ with respect to trolox. Unpaired *Student's t-test* $^{\#}p < 0.05$, $^{\#\#}p < 0.01$, $^{\#\#\#}p < 0.001$ with respect to melatonin; $^{\$}p < 0.05$, $^{\$\$}p < 0.01$ between enantiomers.

5.1.4.2 New MTDLs possess a free radical scavenger effect

The melatonin indole scaffold is able to reduce ROS/RNS by donation of a single electron, causing radical chain reactions of which metabolites, AMFK and AMK among others, propagate the scavenger effect.[100] Intentionally designed to that effect, we expected our compounds to be able to scavenge free radicals, at least at the same extent as melatonin. Thus, the free radical scavenger effect of the derivatives was studied using

ORAC-fluorescein test.[118] This assay is based on the inhibition of the peroxyl $RO_2^{\cdot}$-induced-oxidation initiated by thermal decomposition of AAPH. AAPH decomposes, generating peroxyl ($RO_2^{\cdot}$) and alkoxyl ($RO^{\cdot}$) radicals[166] which react with the fluorescent probe, FL, which will extinguish fluorescence signal. The addition of an antioxidant compound will avoid fluorescence loss. Compounds were tested at five different concentrations using trolox, a well-known antioxidant derived from vitamin E as reference, and melatonin, as positive control. Then, data are collected throughout time and it is compared with trolox, expressing results as trolox equivalents (TEq)

All new compounds showed higher scavenger capacity than trolox and both Ph enantiomers **(-)-54** and **(+)-54** and small sized derivatives Pr **(±)-56**, CyPr **(±)-57** and **(-)-57**, at the same extent as melatonin, **Table 4**. Markedly, Pr **(-)-56** and CyPr **(+)-57** were the best scavengers. By contrast, Ph **(±)-54**, *m*-F-Ph **55** and CyHx **58** as well as Pr **(+)-56**, had statistically significant less scavenger activity than melatonin. Furthermore, there was no difference among enantiomers and racemic mixture with the exception of **(+)-55** and **(-)-56**, which showed higher values than their enantiomers.

5.1.4.3 New MTDLs are able to selectively modulate α7-nAChRs

SH-SY5Y cell line was employed since expresses α3, α5, α7, β2 and β4 subunits of nAChRs.[121] nAChRs are ligand-gated ion channels that mediate the flow of Na^+, K^+ and Ca^{2+}, when they are activated by an agonist.[50] Thus, intracellular calcium fluorimetry-based measurement was performed in order to assess if the compounds were able to modulate the nAChRs response.

Firstly, ACh 100 μM was employed as non-specific agonist of nAChRs and compounds at 10 μM were incubated for 10 minutes in SH-SY5Y. An increase of fluorescence consistent with an increase of cytosolic Ca^{2+} concentration was observed when 100 μM of ACh was added. In the presence of compounds **54**, **55** and **58**, the percentage of response normalized to ACh was decreased in a range between 37 % (**(+)-58**) and 45 % (**(-)-54**), whereas Pr derivatives **56** blocked less, 23 % **(±)-56**, 31 % **(-)-56** and 22 % **(+)-56**, and no significant blockade was seen for CyPr **57** (**Table 5**).

Then, we were interested in their potential selectivity over the different nAChRs subtypes. Thus, we used specific agonists or cell lines overexpressing the receptor, to assure that the monitored response is related to the receptor of study.

To evaluate their activity over α7-nAChRs, we used the agonist *N*-(3*R*)-1-azabicycle[2.2.2]oct-3-il-4-chlorobenzamide (PNU282987), extensively employed as pharmacological tool because of its high affinity (K_i = 27 nM) and selectivity towards α7-nAChRs among other nAChRs (only negligible antagonist activity over α3β4 subtype, $IC_{50} \geq 60$ μM).[41] Due to the distinctive feature of rapid desensitization of these receptors, we used a type II selective allosteric modulator to increase Ca^{2+} transients in cell population-based assays. Thus, SH-SY5Y pre-incubated with the PAM PNU120596 at 10 μM gave an increment of fluorescence according to increase of concentrations of cytosolic Ca^{2+} after the injection of 10 μM PNU282987. Strikingly, when the compounds were co-incubated with PNU120596 at 10 μM, the fluorescence signal was significantly reduced. **56** and **57** derivatives blocked the Ca^{2+} entry ranging from 28 % **(-)-57** to 63 % **(-)-56**. By contrast, **54** (Ph), **55** (*m*-F-Ph) and **58** (CyHx) inhibited the increase of fluorescence in the same extent as the selective α7-nAChR antagonist MLA at 100 nM, (92 - 93 %, 87 - 94 % and 90 - 93 %, respectively, **Table 5**) of the normalized response of the combination of agonist and PAM.

Finally, we employed SH-EP overexpressing human α4β2-nAChRs ($SH_{\alpha4\beta2}$) cell line to test whether **54-58** were modulators of this receptor subtype. Comparatively to first screening, we performed the same protocol, stimulating $SH_{\alpha4\beta2}$ with ACh at 100 μM. As shown in **Table 5**, only three compounds, **(±)-54**, **(±)-56** and **(±)-57** blocked the Ca^{2+} entry significantly (24 %, 13 % and 31 %,respectively), although the calculated IC_{50} values were higher than 30 μM for all of them.

Table 5. Normalized response percentages of compounds at 10 μM obtained after injection of agonists, ACh at 100 μM and PNU282989 at 10 μM.

Cell line	SH-SY5Y				SH-EP$_{\alpha4\beta2}$
Compound	**%Normalized response ACh (100 μM)[a]**	**%Normalized response PNU28+PNU12 (10 μM)[b]**	**IC_{50} (μM)**	**Hill Slope**	**%Normalized response ACh (100 μM)[c]**
ACh	100		-		100
PNU28+PNU12		100			
MLA	69.1 ± 7.4***	4.11 ± 0.9***			
(±)-54	61.6±6.4***	7.2 ± 2.5***	2.69 ± 0.57	2.2	75.7±6.2**
(-)-54	55.2±10.6***	6.8 ± 4.2***	0.50 ± 0.08	0.7	91.0 ± 9.4
(+)-54	56.5 ± 5.6***	7.9 ± 2.9***	0.93 ± 0.02	0.9	104.8 ± 15.3
(±)-55	60.0 ± 7.1***	6.4 ± 1.9***	1.78 ± 0.30	2.0	84.5 ± 11.2
(-)-55	60.5 ± 8.3***	8.2 ± 1.4***	1.51 ± 0.18	1.5	78.0 ± 11.2
(+)-55	53.8 ± 8.3***	12.6 ± 2.4***	1.26 ± 0.14	1.4	98.1 ± 14.6
(±)-56	77.7 ± 4.4***	57.1 ± 8.1**	7.77 ± 1.69	1.9	86.6 ± 5.7*
(-)-56	69.7 ± 5.5***	37.4 ± 9.6**	6.46 ± 0.87	2.4	82.7 ± 18.4
(+)-56	79.1 ± 5.4**	64.2 ± 6.6**	7.35 ± 2.30	1.8	90.5 ± 4.1
(±)-57	93.9 ± 7.5	60.8 ± 2.3***	9.05 ± 1.52	1.9	68.6 ± 4.4***
(-)-57	92.4 ± 5.4	72.3 ± 3.2**	13.27 ± 1.20	2.2	106.0 ± 24.6
(+)-57	89.7 ± 8.5	39.3 ± 14.0*	9.10 ± 0.72	2.3	105.5 ± 10.2
(±)-58	58.8 ± 9.5**	7.3 ± 0.5***	1.41 ± 0.47	2.6	86.7 ± 9.0
(-)-58	61.8 ± 10.1**	7.8 ± 1.7***	0.93 ± 0.41	1.0	98.3 ± 24.2
(+)-58	63.2 ± 9.2**	10.0 ± 2.7***	1.32 ± 0.26	1.8	123.8 ± 21.5

Data are shown as mean ± SEM of duplicates of at least three independent experiments. IC50 and Hill Slope values were obtained from the blockade of PNU282989 response, and are showed as mean value of three independent experiments. [a]Paired Student's *t-test*. $^{**}p < 0.005$, $^{***}p < 0.0001$ compared to ACh. [b]Paired *Student's t-test*. $^{*}p < 0.02$, $^{**}p < 0.005$, $^{***}p < 0.0001$, compared to PNU282987+PNU120596 [c]*Student's t-test*. $^{*}p < 0.05$, $^{**}p < 0.01$, $^{***}p < 0.001$ compared to ACh.

In light of these results, all the compounds were clearly able to selectively modulate α7-nAChRs. The blockade of the effect of an agonist could be mediated by an antagonist, a partial agonist or a NAM.[58] Thus, we decided to perform concentration-

response curves of the compounds. It is worth to note that IC_{50} values were in lower micromolar and submicromolar range for derivatives with large substituent group, with no differences between enantiomers. By contrast, IC_{50} values of **56** (Pr) and **57** (CyPr) ranged from 6.4 up to 13.2 μM with differences between both enantiomers. Curiously, not the same enantiomers were the most potent, in other words, **(-)-56** presented an IC_{50} = 6.37 μM whereas 8.99 μM was for **(+)-57**. In this case, the spatial disposition of the substituents seems to influence the stability of the interactions between ligand and receptor, giving the slightly different potency. Moreover, all Hill coefficients where higher than one, indicating a positive cooperative binding, which means that the binding of the first molecule to the receptor changes the affinity for the second coming molecule. Therefore, a small change in ligand concentration is reflected in a large change in concentration of the ligand-receptor complex.

As stated in *Section 2.9.2*, a partial agonist blocks the effect of a full agonist in a concentration dependent manner. Thus, as we have seen that higher concentrations of compounds produced higher reduction in the fluorescence, it suggests that they could probably act as a partial agonist.

Therefore, we can assure that the novel MTLDs can selectively block the response of the α7 nicotinic agonist PNU282987 at 10 μM, as at that concentration they did not significantly show modulation of α4β2-nAChRs. Nevertheless, we cannot know what kind of ligand they are. More sophisticated electrophysiological studies are needed to understand the behaviour of compounds and are currently carrying out by our collaborators from the department of pharmacology and physiology of the faculty of medicine in the Universidad Autónoma de Madrid.

5.1.4.4 Docking and molecular dynamic studies on α7-nAChRs

Meanwhile the electrophysiological studies are ongoing, we tried to computationally assess which type of ligand we created. The aforementioned results pointed out that **54-58** could be partial agonists since they inhibited the response of the selective agonist α7-nAChR, PNU282989 and they did not show an increase of intracellular Ca^{2+} in the absence of PAM or presence of antagonists. Whether our hypothesis was true, they should bind to the orthosteric site as described in *Section 2.9.2*.

Therefore, we performed computational studies on the orthosteric site as following described.

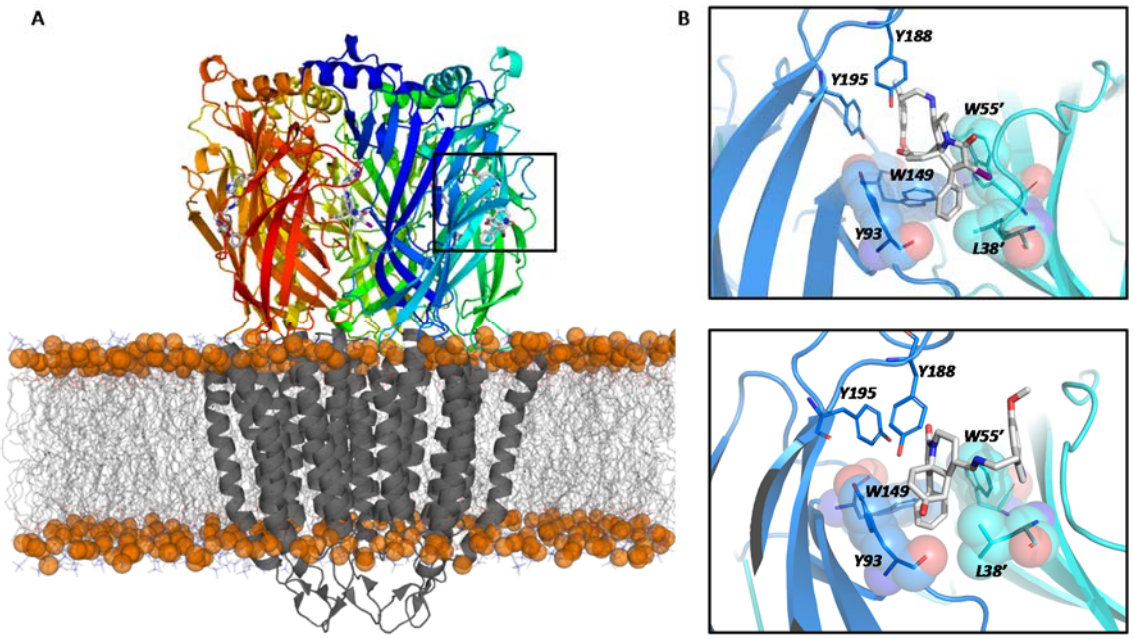

Figure 15. **A)** α7-nAChR extracellular and transmembrane domains embedded in a lipidic bilayer. The extracellular domain used for homology modelling, docking studies and molecular dynamics simulations is colored while transmembrane domain is shown in gray. The orthosteric site is indicated and occupied with compound **(-)-54** represented as white sticks. **B)** Representative binding modes of compounds **(-)-54** (top right) and **(+)-54** (bottom right) extracted from the molecular dynamics simulation. Residues conforming the hydrophobic pocket are displayed as spheres.

Due to the lack of an experimentally determined structural model of the α7-ECD a pentameric homology model was built, **Figure 15**. After ensuring that docking employing our model was able to reproduce the crystallographic binding pose of known ligands such as nicotine[167,] or epibatidine,[168] compounds **(-)-54, (+)-54, (-)-55, (+)-55, (-)-56, (+)-56, (-)-57, (+)-57, (-)-58** and **(+)-58** were docked at the orthosteric site using a consensus docking approach based on a combination of Glide and AutoDock4. With this strategy, we were able to find a common binding mode for all compounds with dextrorotatory configuration. Regarding compounds with levorotatory configuration, two possible binding modes were predicted by the docking analysis, which only differed in a rotation of the main core of ~110 Å around the ligand longitudinal axis. Interestingly, the predicted binding pose of levorotatory compounds was completely inverted in

comparison with the ones with dextrorotatory configuration. In order to take into account protein flexibility and to ensure that the predicted binding modes were stable, we performed molecular dynamics simulations of 300 ns of the full pentameric model with all five orthosteric sites occupied by the ligand. Due to the high computational cost, only simulations of compound **(-)-54** (which only one binding mode was predicted by the docking study), which exhibits the more potent α7 agonist activity, and its enantiomeric counterpart **(+)-54** were performed.

Regarding compound **(-)-54**, after an initial rearrangement a stable binding mode is observed at each binding site, with exception of a subtle deviation at the orthosteric site from 240 to 285 ns, after which the previous conformation is recovered (**Figure 16**). Interactions between compound **(-)-54** and the α7 ECD are essentially hydrophobic at all five subunits, with no stable polar interactions driving the binding. Notable differences are observed in the binding mode found at each site, especially at site D as can be deduced from the ligand-protein contact map (**Figure 17**). However, residues Y93, W149, Y188, Y195, L38', W55' and L119 are in close contact with **(-)-54** at all five subunits for over 80 % of the last 200 ns of simulation, suggesting that these residues might be critical for the binding. Site D is the only exception as it does not display contacts with L38' so frequently (see below). Y93, W149, L38' and W55' conform a hydrophobic pocket in which **(-)-54** inserts its Ph group and part of the core. In sites C and E, G167' is also involved in the formation of the pocket functioning as a cap of the cavity and fully surrounding the Ph group. In fact, as soon as **(-)-54** introduces the aromatic group in this cavity it is strongly stabilized, being RMSD fluctuations caused exclusively by the linker and indole mobility. At site D the Ph moiety and core are not fully introduced in the hydrophobic pocket but rather located on the entrance of the cavity maintaining contacts with Y93 and W55' while the main core is stacked with W149, which explains its lower contact frequency with L38'. This conformation is presumably achieved due to the hydrogen bond established between the charged amine group of **(-)-54** and the backbone carbonyl oxygen of W149. A similar orientation was observed at site E for the first part of the simulation, but after 225 ns the Ph group is also inserted in the hydrophobic pocket where remains until the end of the simulation. Y188 and Y195 are also in close contact with **(-)-54** in all five subunits despite not being involved in the architecture of the

hydrophobic pocket. They establish interactions of different nature at each subunit that involve different atoms of the ligand. In some cases, the main interaction consists on CH-π interactions with methylene hydrogens, π - π interactions with indole or a tightly packaging with the core. Regarding the indole moiety root mean square fluctuation (RMSF) calculations (data not shown) showed that it was the region of the molecule with higher mobility at sites A, B, C and E due to the lack of strong interactions with protein residues. L109' and L119' establish hydrophobic contacts with indole or contiguous methylene at most subunits, being these, the more prominent stabilizing interactions for these moieties (**Figure 16**). Only exception is site D in which the indole moiety was stabilized by a CH-π interaction between the methylene contiguous to the indole moiety and Y188 and Y195, the hydrophobic interaction with L109' and an intramolecular cation-π interaction with the charged amine that leads to **(-)-54** adopting a bend conformation which is also observed at site C. The methoxy or amine groups of the indole do not stablish polar interactions with protein residues in any of the five orthosteric sites. Despite interacting with some residues at subunits D and E, interactions with the charged amine moiety located at the linker do not seem to be critical for the binding. This is well represented at site B where it does not interact with any residue and the ligand remains stable at the binding site. **(-)-54** main core is stacked by different residues at each subunit with no stable polar interactions between carbonyl groups and protein residues. Overall, these results show that compound **(-)-54** is able to bind strongly to α7 orthosteric site primarily by means of hydrophobic interactions. Concretely, our simulations show that the insertion of the Ph group in the hydrophobic pock *et al*ongside the interaction of the core with the aromatic residues of the pocket might be the critical element for the binding of this compound.

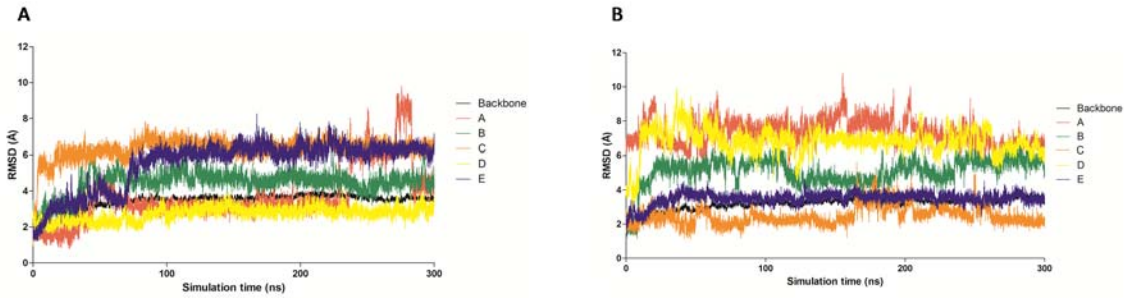

Figure 16. RMSD evolution of protein backbone and ligand heavy atoms along the simulation of compounds **(-)-54** (**A**) and **(+)-54** (**B**). Image was generated with Gnuplot.

In fact, the key role of the Ph and core moieties is also supported by the results of the molecular dynamics simulations of **(+)-54**. In a similar fashion to **(-)-54**, it remained bound to the orthosteric site at all five sites mainly via hydrophobic interactions. As can be deduced from the contact map, there are notable differences in the residues involved in the recognition of **(-)-54** and **(+)-54** as exemplified by L109'. This is caused by the inversed conformation of **(+)-54** in the binding site, locating its linker and indole moiety far from this residue **(Figure 15 B).** However, it is remarkable that despite starting the simulation from a totally inverted binding pose from the one of **(-)-54**, residues Y93, W149, Y188 and W55' are also in close contact with **(+)-54** over 80 % of the time during the last 200 ns at all subunits **(Figure 17)** further increasing our conviction that these residues are the key structural element for the binding of our compounds. Even more interestingly, these close contacts are given by the allocation the Ph group and part of the core in the same hydrophobic pocket conformed by Y93, W149 and W55'. Only exception is found at site C, in which the hydrophobic pocket deepness is notably reduced due to the establishment of a π-π interaction between W149 and W55', which leads to the ligand placing a part of the core and linker in the 'reduced' cavity while the Ph moiety is placed above the cavity, closer to L119' and the backbone of S150 and Y151. In sites A and B the ligand adopted a bend conformation and even the indole moiety entered the hydrophobic pocket. Similarly to the binding mode found for **(-)-54**, L38' is also involved in the establishment of this cavity (sites A, B and D). In this case, G167' only acts as the cap of the cavity at site B. Y188 is found stacked with the main core of **(+)-54** with exception of subunit A in which it establishes T-shaped π-π interactions with the indole for most part of the trajectory. RMSF of **(+)-54** during the last 200 ns of simulations follows the same trend observed for **(-)-54**. The Ph group and main core of the molecules remain stable at the binding site while the linker and indole positions exhibit a higher fluctuation due to the lack of strong interactions, illustrating that the anchoring to the orthosteric site is again provided by the main core and the Ph group.

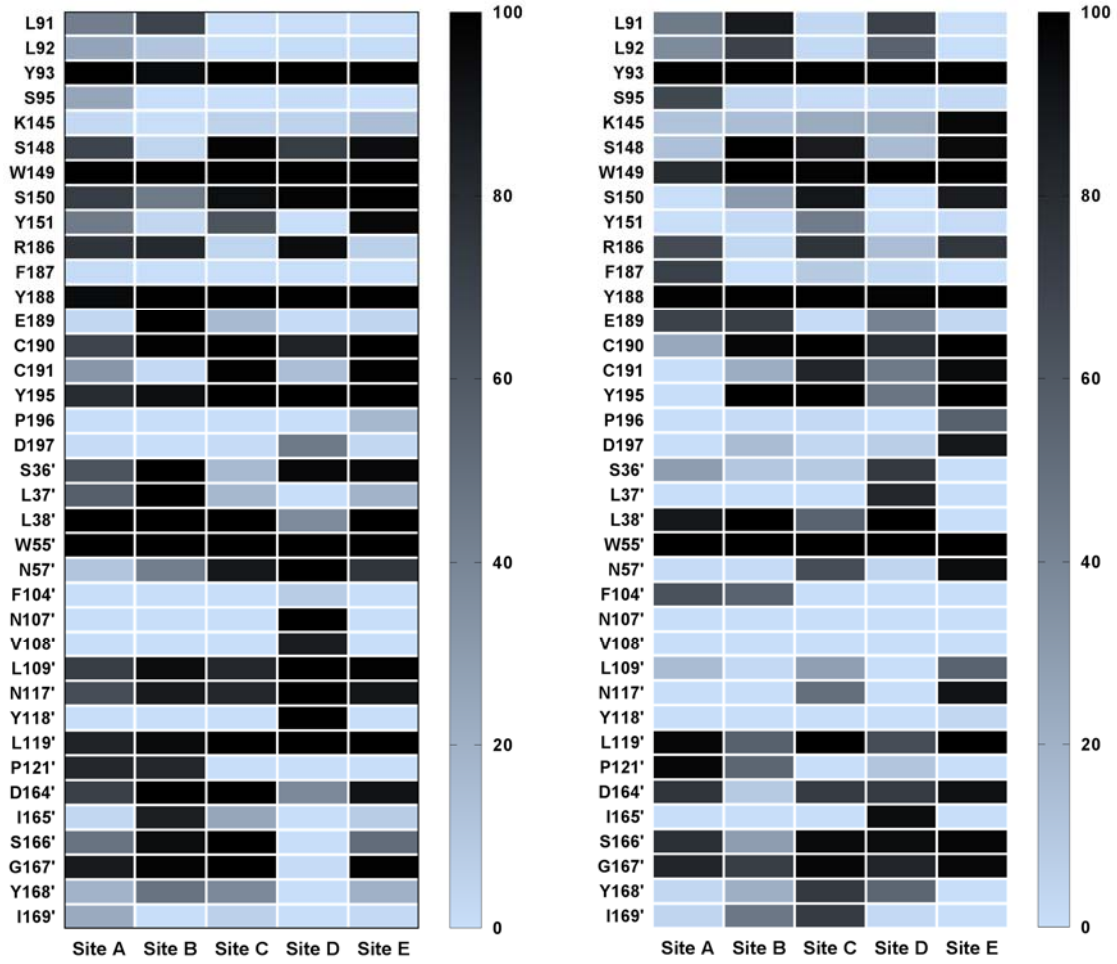

Figure 17. Protein-ligand contact frequency map of compound **(-)-54** (left) and **(+)-54** (right) at each orthosteric site. Colors represent the percentage of frames in which there is a distance below 5 Å between a certain residue and the ligand. Values were calculated for the last 200 ns of the simulation. Residues that are in close contact with the ligands in all subunits due to proximity to a key residue are not discussed in the text.

5.1.4.5 New compounds inhibit AChE activity selectively.

As depicted in the *Section 2.6.1*, progressive atrophy of cholinergic function is produced owing to a reduced ACh release together with diminished binding and expression of mAChRs and nAChRs among other facts.[21] Consequently, the restoration of the cholinergic neurotransmission was first exploited, as palliative treatment, by inhibiting AChE.[12] AChE is the enzyme in charge of hydrolyze ACh in the synaptic cleft and finish the neurotransmission. Apart from its catalytic site, AChE has a peripheral anionic site (PAS) where not only quaternary ligands bind, but also Aβ.[169]

The new compounds were evaluated as potential AChEis following Ellman's method.[124] To obtain inhibition curves which allowed to calculate the IC_{50} values, five (AChE) and six (BuChE) different concentrations were prepared and measured their enzymatic activity.

Table 6. AChE and BuChE inhibition by compounds **54-58.** K_i values obtained employing Lineweaver-Burk reciprocal linearization plot. Effects on the V_{max} and K_m values of the enzyme exerted by compounds compared to control values without inhibitor.

Cpd	IC_{50} (μM) *Ee*AChE	IC_{50} (μM) *Eq*BuChE	Selectivity (*Eq*BuChE/ *Ee*AChE)	K_i (μM)	V_{max}[a]	K_m[a] (mM)
Control					0.24 ± 0.01	0.47 ± 0.04
(±)-54	11.5 ± 1.9	>100	>8.8	7.9 ± 1.8	0.33 ± 0.03***	0.68 ± 0.34***
(-)-54	18.7 ± 2.8	>100	>5.3	12.7 ± 2.1	0.22 ± 0.04*	1.57 ± 0.26***
(+)-54	12.4 ± 1.8	>100	>8.1	9.9 ± 2.4	0.16 ± 0.04***	0.51 ± 0.17***
(±)-55	16.0 ± 4.7	>100	>6.3	6.3 ± 1.3	0.11 ± 0.04***	0.27 ± 0.02
(-)-55	14.4 ± 2.9	>100	>6.9	10.2 ± 2.0	0.25 ± 0.07***	2.25 ± 0.97***
(+)-55	15.8 ± 2.5	>100	>6.3	15.3 ± 0.4	0.22 ± 0.06***	1.45 ± 0.4***
(±)-56	6.5 ± 0.5	>100	>15.4	2.7 ± 0.8	0.18 ± 0.04***	0.62 ± 0.46*
(-)-56	8.1 ± 1.7	>100	>12.3	5.7 ± 1.2	0.15 ± 0.05***	0.89 ± 0.21***
(+)-56	6.3 ± 1.2	>100	>15.9	3.6 ± 0.5	0.22 ± 0.08***	0.56 ± 0.04***
(±)-57	7.6 ± 0.3	64 ± 16	>8.4	7.5 ± 1.2	0.18 ± 0.04***	0.28 ± 0.10***
(-)-57	8.8 ± 0.8	>100	>11.4	9.1 ± 2.2	0.24 ± 0.04***	0.63 ± 0.13***
(+)-57	8.5 ± 0.7	>100	>11.8	0.76 ± 0.02	0.21 ± 0.06***	0.86 ± 0.12***
(±)-58	10.1 ± 1.5	>100	>9.9	4.1 ± 0.2	0.12 ± 0.03***	0.58 ± 0.26***
(-)-58	7.8 ± 1.0	2.3 ± 0.1	>0.3	8.0 ± 0.1	0.18 ± 0.05***	0.39 ± 0.09***
(+)-58	13.2±9.2**	>100	>7.2	12.7 ± 0.7	0.22 ± 0.06***	0.64 ± 0.05***

Data are shown as mean ± SEM of at least three experiments at five (AChE) and six (BuChE) different concentrations. [a]*Student's t-test*, unpaired $^{*}p < 0.01$, $^{***}p < 0.0001$

Regarding AChE, compounds **56** (Pr) and **57** (CyPr) showed IC_{50} values lower than 10 μM. Conversely, derivatives **54** (Ph), **55** (*m*-F-Ph), **58** (CyHx) showed IC_{50} values from 10.1 μM to 18.7 μM, with the exception of (-)-**58** (7.8 μM), as shown in **Table 6**.

In addition, there are no differences between enantiomers although the same tendency seeing in other pharmacological activities is also herein presented. Levorotarory enantiomers of Ph and Pr, (-)-**54** and (-)-**56,** tend to be less potent inhibitors than dextrorotatory derivatives (+)-**54** and (+)-**56**. On the contrary, levorotatory enantiomers of *m*-F-Ph (-)-**55** and CyHx (-)-**58** exerted higher potency than dextrorotatory ones (+)-**55** and (+)-**58**. **57** enantiomers present same values.

As described, the majority of compounds were more potent inhibitors for AChE than BuChE (IC_{50} > 100 μM). This selectivity may indicate that the compounds bind to the PAS instead of catalytic site, as BuChE does not have it.[170] Compounds like propidium iodide, a well-known PAS ligand, impedes Aβ aggregation by interrupting the binding between Aβ and PAS.[171] In this line, we wanted to explore the mechanism of AChE inhibition. Following Michaelis-Menten enzymatic kinetics, competitive, non-competitive, uncompetitive or mixed mechanisms can be differentiated analyzing data according to the Lineweaver-Burk method.[172] For this purpose, five different concentrations of substrate and seven of compounds were used. Then, K_i values were obtained by plotting the slopes of the double reciprocal linear regression versus the concentration of the compounds, as detailed in *Section 4.1.2.8*.

Generally for all compounds, K_i values were in low micromolar range, indicating a weak inhibition potency probably owing to the easy dissociation of the enzyme-inhibitor complex. Markedly, the dextrorotatory compounds **(+)-56** and **(+)-57** showed the best values of IC_{50} and K_i, respectively. With these kinetic studies we could assess the mechanism of inhibition of compounds. V_{max} and K_m were calculated from fitting Lineweaver-Burk plot of hydrolysis rate against substrate concentration in the presence of inhibitor. This allowe us to compare V_{max} and K_m in the absence or presence of compounds **54-58**. V_{max} decreased whereas K_m increased for all derivatives, indicating a mixed mechanism of action, **Table 6**.[173] Therefore, consistently with higher selectivity for AChE rather than BuChE, the outcome supports the hypothesis of binding to PAS.

5.1.4.6 New MTDLs exhibit a promising neuroprotective profile.

Novel derivatives exhibited moderate to potent Nrf2 induction, and greater scavenger capacity than trolox. Additionally, they were able to modulate cholinergic

system by inhibition of AChE and by modulating a7-nAChRs. In light of our initial hypothesis by acting on multiple targets, we expect to promote neuroprotection. Thus, we were interested in exploring the neuroprotective profile of our compounds. As mentioned in the *Section 2.6.4*, oxidative stress is not only a very early contributor but also a consequence of AD.[43] Therefore, we studied the neuroprotective properties of novel compounds in a well-established in-house oxidative stress model using R/O cocktail, blockers of mitochondrial complexes I and V, respectively, in SH-SY5Y neuroblastoma cell line.[102] Additionally, tau pathology, has been recently pointed as key player of AD triggering,[31] due to the toxicity of P-tau and the fact that free tau oligomers propagate trans-synaptically.[32] OA, a serin/threonin phosphoprotein phosphatases PP1 and PP2A inhibitor marine toxin, provokes a tau hyperphosphorylation in *in vitro*[174] as well as *in vivo*[175] Hence, OA is accepted and commonly used as *in vitro* model which reproduces tau hyperphosphorylation and oxidative stress to induce cell death.[126]

Per se toxicity of compounds were first performed to address the optimal concentration to do the screening. Concentration curves ranged from 1 to 30 μM were done incubating compounds 24 h to obtain the concentration that reduces the 50 % of cell viability (LC_{50}). Small sized derivatives **56** and **57** were less toxic (LC_{50} > 30 μM) than most voluminous compounds **54**, **55** and **58**. **54** (Ph), and **55** (*m*-F-Ph) derivatives had a LC_{50} around 19 μM, while **58** (CyHx) were the most toxic compounds with LC_{50} around 2 μM, (**Table A3, Appendix A**). Thus, 1 μM was selected to perform the screening in neuroprotection studies.

5.1.4.6.1 Oxidative stress model

As the compounds were designed to being ROS scavengers and antioxidants, neuroprotection studies against oxidative stress conditions were performed, following a pre-treatment of compounds for 24 h and immediately co-treatment using R/O combination at 30 μM and 10 μM, respectively for additional 24 h. All compounds were neuroprotectants in the same extent as melatonin, the positive control, **Table 7**. The three exceptions **(+)-54**, **(+)-57** and **(+)-58**, might be due to experimental error, since there was no significant difference between the racemic mixture and the other enantiomer. The best outcome was achieved by **(±)-56** (Ph) with a 61 %.

Table 7. Percentage of survival and neuronal protection produced by compounds and melatonin, at 1 μM against toxic cocktail rotenone 30μM and oligomycin A 10 μM as oxidative stress model, and against okadaic acid 20 nM, as tauophaty model.

Compound	RO Pre- & Co-incubation		OA Pre- & Co-incubation	
	% Survival	% Protection	% Survival	% Protection
Basal	100		100	
Toxic	58.0 ± 7.0$^{###}$		46.1 ± 4.4$^{###}$	
Melatonin	75.8 ± 5.0*	43 ± 4	75.9 ± 3.8***	54 ± 5
(±)-54	73.0 ± 6.1*	38 ± 5	73.7 ± 4.1***	45 ± 8
(-)-54	77.3 ± 5.6*	48 ± 8	74.6 ± 3.4***	49 ± 6
(+)-54	72.5 ± 8.5	38 ± 7	73.4 ± 2.4**	42 ± 7
(±)-55	76.5 ± 5.3*	43 ± 13	66.5 ± 3.4**	30 ± 9
(-)-55	75.9 ± 6.2*	45 ± 12	68.3 ± 5.1**	37 ± 8
(+)-55	76.3 ± 2.6*	47 ± 9	71.4 ± 4.1***	41 ± 8
(±)-56	82.1 ± 6.2**	61 ± 10	70.6 ± 4.2**	43 ± 7
(-)-56	77.5 ± 6.5*	49 ± 9	71.3 ± 6.2***	42 ± 11
(+)-56	75.2 ± 4.5*	42 ± 6	75.6 ± 4.8***	50 ± 10
(±)-57	77.1 ± 5.3*	46 ± 4	66.1 ± 5.8***	43 ± 9
(-)-57	79.4 ± 7.0*	53 ± 13	73.6 ± 3.7***	45 ± 7
(+)-57	74.1 ± 13.5	52 ± 19	74.9 ± 5.3***	47 ± 10

(±)-58	75.9 ± 9.8*	49 ± 13	58.3 ± 10.4	32 ± 9
(-)-58	78.3 ± 5.6*	49 ± 10	54.7 ± 8.8	26 ± 8
(+)-58	72.3 ± 8.1	38 ± 6	59.6 ± 8.7	22 ± 11

Data are expressed as mean ± SEM of five experiments by triplicate. One way ANOVA Newman Keuls post test $^{###}p < 0.001$; compared to basal. $^{**}p < 0.01$; $^{***}p < 0.001$; compared to toxic.

5.1.4.6.2 Tau hyperphosphorylation model

Compounds were also designed to modulate α7-nAChRs whose stimulation plays an important role inducing neuroprotective effects.[64] Hence, neuroprotection studies in a tauopathy model were perform following a similar procedure of pre- and co-incubation treatment of compounds for 24 h and 18 h, respectively at 20 nM of OA. With the exception of CyHx derivatives **58**, all compounds could revert the toxicity exerted by OA in the same extent as melatonin, **Table 7**. In this case, the best neuroprotectant effect was exerted by the dextrorotatory enantiomer **(+)-56** (Pr).

5.1.4.7 Mechanism of action of compounds SA35-SA49

Taking into account all the activities measured, **56** (Pr) and **57** (CyPr) derivatives presented the most favourable properties regarding toxicity (LC_{50} > 15 μM and > 30 μM in AREc32 and SH-SY5Y cell lines, respectively), great scavenger capacity in the same extent as melatonin, moderate induction of Nrf2, IC_{50} < 10 μM for AChE, and modulation of α7-nAChR. Regarding physicochemical properties, **56** and **57** are the smallest of the **Family A**, less lipophilic and higher water soluble than the large derivatives. Once discarded **54**, **55** and **58**, among **56** and **57**, although differences were very subtle, the racemic of Pr derivatives **(±)-56** was finally selected as hit compound to investigate its mechanism of action, since it presented the highest percentage of neuroprotection in oxidative stress model (61 %) and quite high (43 %) in the tauopathy model.

Multiple studies demonstrated the implication of nAChRs in neuronal survival against toxic insults, as previously mentioned in *Section 2.9.3.* In fact, previous studies in our *Instituto Teófilo Hernando*, showed that cell death exerted by OA at 30 nM was avoided by PNU282989 at 10 μM, pre-incubated 24 h. The neuroprotectant effect was Ca^{2+}-independent and mediated by JAK2/STAT3 pathway and PI3K/Akt survival route.

Conversely, the same study also demonstrated that the protection offered by the selective agonist for α4β2-nAChRs, 5IA85380, was Ca^{2+}-dependent regulated by extracellular regulated kinase 1/2 (ERK1/2) as well as by PI3K/Akt/Nrf2/HO-1 pathway.[64] Activation of this survival route, led to indirect induction of Nrf2 transcription factor, since GSK3-β is downregulated.

Compound **(±)-56** was able to prevent cell death against OA in a 43 %. Since it is a MTDL, we wanted to explore which target was the responsible of the protective actions. **(±)-56** induced Nrf2 in AREc32 cell line. In agreement with that observation, we pharmacologically inhibited Nrf2 with 10 μM of trigonelline (TR) and 10 μM tin protoporphyrin (SnPP), an inhibitor of the antioxidant enzyme HO-1.[176] In both cases neuroprotection elicited by **(±)-56** was reduced significantly, (**Figure 18, A-B**).

Activation of MT1 receptors of melatonin converge also in the activation of pro-survival pathways.[102] Therefore, we treated cells with 3 μM luzindole (LZ), an antagonist of MT1 and MT2,[177] and neuroprotection was prevented, (**Figure 18, C**).

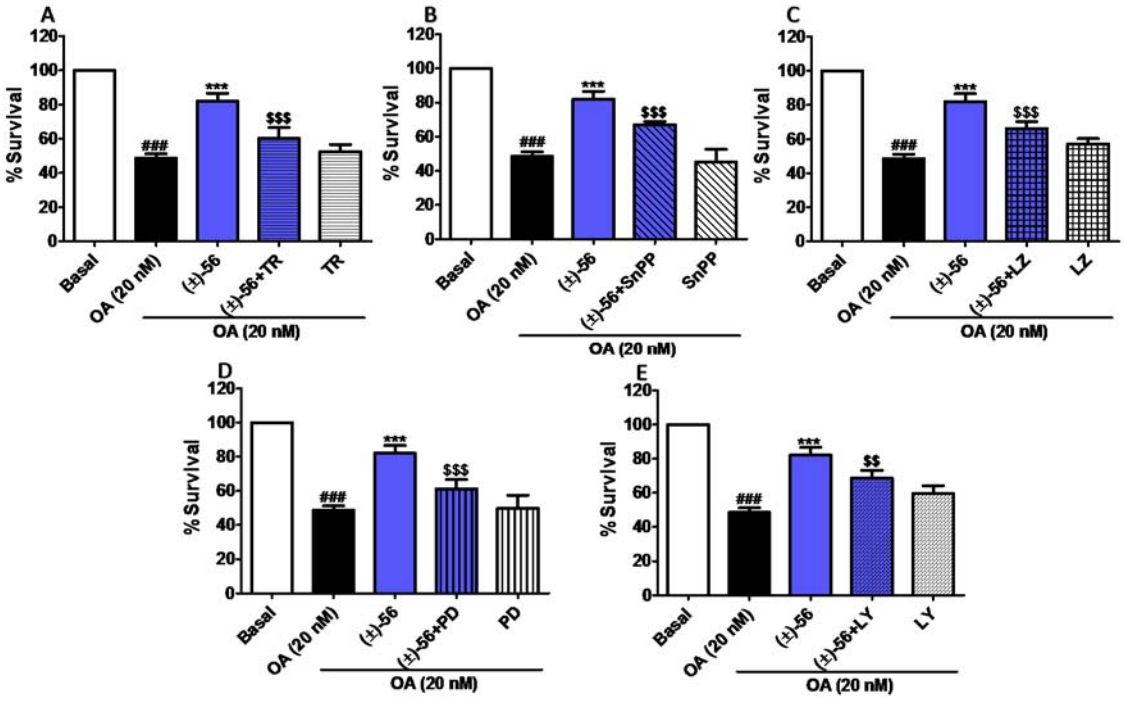

Figure 18. The neuroprotection exerted by **(±)-56** was mediated by of Nrf2-EpRE/HO-1 induction, melatonin receptors and activation of α7-nAChRs. SH-SY5Y cells were pre-incubated for 24 h with 1 μM **(±)-56**, following 18 h co-incubation with OA in the absence or presence of trigonelline (10 μM), SnPP (10 μM), luzindole (10 μM), PD98059 (10 μM) or LY294002 (3 μM). Data are depicted as mean ± SEM of eight experiments by triplicate. $^{###}p < 0.001$ with respect to

basal; $^{***}p < 0.001$ with respect to OA; $^{\$\$}p < 0.01$ and $^{\$\$\$}p < 0.001$ with respect to **SA41**-treated cells-

Finally, several neuroprotective signalling pathways can be triggered by the activation of α7-nAChRs. LY2940002, an inhibitor of PI3K,[178] and PD98059, an inhibitor of p-ERK1/2,[179] were employed to explore them, and both seemed to be implicated in the protection effect (**Figure 18, D-E**).

Thus, we can conclude that the induction of Nrf2-EpRE pathway as well as the activation of melatonin receptors and α7-nAChRs, and are implicated in the neuroprotective effect elicited by the compounds of **Family A**. These promising results gave us courage to further study the PK and brain distribution profile of compounds **56-57.**

5.1.5 *In vivo* pharmacokinetic and brain distribution studies

As every single drug exhibits undesired effects, it is necessary to know the equilibrium between the beneficial and detrimental effects to achieve a successful therapy. This knowledge can be assess performing PK studies, which describe the drug absorption, distribution and elimination mechanisms and kinetics in the body. Therefore, by analysing the temporary changes of the molecule and its metabolites in blood, plasma, or urine, following an intravenous administration, the disposition characteristics can be obtained.[180] Furthermore, some compounds can bind to plasma proteins (serum albumin, lipoprotein, glycoprotein and α, β and γ globulins), and that protein binding can influence its half-life.[181,149] Thus, it is necessary to determine the plasma drug concentration ($C_{tot,plasma}$), and once it is obtained, is possible to estimate tissue distribution.

Due to the new derivatives were designed to exert a neuroprotective effect, next step was to study the CNS distribution. To reach CNS, the compounds must overcome the BBB which main functions rely, not only in taking up nutrients and components for brain function and discarding waste products from brain activity, but also it protects the brain from xenobiotics and other biochemical environment changes.[182]

As knowledge about the extent of BBB transport of new chemical entities is crucial for successful CNS drug development, we performed *in vivo* PK studies with focus on unbound drug, and we characterized the neuroPK for selected lead compounds. The

selection of leads was based on ranking of compounds according to their pharmacodynamics and toxicity. **56** (Pr) and **57** (CyPr) were chosen as they have showed greater scavenger activity, moderate Nrf2 induction, better neuroprotectant effect and lower toxicity effect than the large derivatives **54**, **55** and **58**, (**Tables 4, 7 and A3)**.

5.1.5.1 Pharmacokinetic study

For PK study, we used 1 mg/Kg dose in 17.5 % DMSO and 0.1 % of FA in 0.9 % saline. The DMSO concentration was lower of that used for melatonin where was i.v. administered in rats as a solution of 25 % DMSO in water.[183] Nevertheless, total solubilization was not achieved and the real dose given as i.v. short infusion was 0.6 mg/Kg for both **(±)-56** and **(±)-57**. Total plasma concentrations were measured at 0, 2.5, 5, 9, 15, 30, 60, 120, 240, 420 min and 24 h after administration and are shown in **Figure 19**. The systemic PK parameters were obtained using non-compartmental analysis from the area under the plasma total drug concentration-time curve[184] and compared with structural related melatonin (**Table 8**).

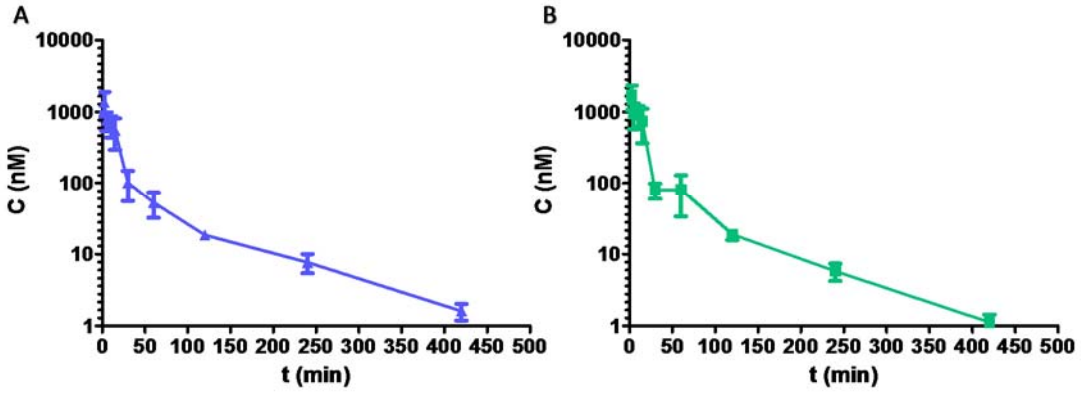

Figure 19. Total plasma **(±)-56** (blue, A) and **(±)-57** (green, B) concentration - time profiles after intravenous short infusion to SD rats (n = 3 for each compound) of 0.6 mg/kg of **(±)-56** and **(±)-57**, respectively.

Maximal total plasma concentration (C_{max}) of **(±)-56** and **(±)-57** observed at 4.8 min was 680 and 830 ng/mL, respectively at 5 min after IV bolus. Apparent volume of distribution at steady state (V_{ss}) of **(±)-56** was 1.4-fold times and 2.3-fold times larger than **(±)-57** and melatonin, respectively, (**Table 8**), indicating higher disposition into peripheral tissues for **(±)-56**. Even so, both compounds have a moderate distribution, as V_{ss} values are between 0.6 and 5 L/kg.[185] Both compounds exhibited high apparent total

body clearance (Cl) values 0.057 and 0.051 L/min·kg for **(±)-56** and **(±)-57**, indicating fast elimination of the compounds from the plasma. This leaded to short elimination half-lives, 76.5 min and 72.7 min for **(±)-56** and **(±)-57**, respectively, although they are about 4-fold times longer than the half-life of parent compound melatonin. However, to put in context our results, morphine, also an alkaloid, one of the most commonly used analgesics for severe pain, has an extensive distribution throughout the peripheral tissues as V_{ss} is 9 L/Kg, but it is cleared from blood faster than **(±)-56** and **(±)-57**, as Cl is 412.6 mL/min·kg, which is reflected in 15 min half-live.[186]

Table 8. Summary of systemic pharmacokinetic parameters obtained following intravenous infusion of **(±)-56** and **(±)-57** to Sprague-Dawley rats. Pharmacokinetic parameters of melatonin obtained from Yeleswaram, K. *et al*.[183]

Parameter	Units	(±)-56	(±)-57	Melatonin
D	mg/kg	0.61 ± 0.13	0.61 ± 0.11	5.00
$AUC_{0-\infty}$	mg/L·min	10.8 ± 2.9	12.2 ± 2.7	142.8
Cl	L/min·kg	0.057 ± 0.008	0.051 ± 0.008	0.035
$t_{1/2}$	min	76.5 ± 10.6	72.7 ± 4.7	19.8
V_{ss}	L/kg	2.37 ± 0.33	1.74 ± 0.26	1.05
V_z	L/kg	6.03 ± 0.77	5.28 ± 0.73	No data

Data are shown as mean value ± SD.

5.1.5.2 Neuropharmacokinetics

The characterization of the neuroPK of selected compounds was performed using CMA. Thus, key parameters describing plasma protein binding, intra-brain distribution and the extent of BBB transport of **56** and **57** derivatives are presented in **Table 9** and discussed below.

Table 9. Key pharmacokinetic parameters with focus on CNS distribution of **56** (Pr) and **57** (CyPr) derivatives.

PK parameter	Compounds					
	(±)-56	**(-)-56**	**(+)-56**	**(±)-57**	**(-)-57**	**(+)-57**
$f_{u,plasma}$	0.14 ± 0.01	0.13 ± 0.05	0.13 ± 0.01	0.18 ± 0.02	0.13 ± 0.01	0.16 ± 0.03
$f_{u,brain}$	0.015 ± 0.001	0.014 ± 0.001	0.013 ± 0.001	0.016 ± 0.001	0.017 ± 0.002	0.015 ± 0.001
$V_{u,brain}$[a]	195 ± 38	224 ± 4	262 ± 39	106 ± 17	121 ± 4	160 ± 23
$K_{p,uu,cell}$	2.93	3.19	3.41	1.70	2.09	2.40
$K_{p,brain}$	0.97 ± 0.06			0.27 ± 0.13		
$K_{p,uu,brain}$	0.036			0.014		

Data are shown as mean value ± SD. [a]Units:mL/brain^{-1}

5.1.5.3 Plasma protein binding

The unbound fraction in plasma ($f_{u,plasma}$) was determined employing the equilibrium dialysis technique for the racemic mixture **(±)-56** and **(±)-57** as well as levorotatory enantiomers, **(-)-56** and **(-)-57** and dextrorotatory enantiomers **(+)-56** and **(+)-57**. $f_{u,plasma}$ of all studied compounds was low **(Table 9)**, which means that the compounds have high plasma protein binding ranging from 82 % to 87 %. There is a significant difference of low $f_{u,plasma}$ for Pr **56** series **(Figure A1, Appendix A)**, indicating 1.25-fold higher plasma protein binding in comparison with the **57** CyPr derivatives, which could be a reflection of higher lipophilicity of that group of compounds (see *Section 5.1.4,* **Table 1**). Moreover, in both series, there is a difference between levorotatory and dextrorotatory enantiomers. However, in Pr derivatives $f_{u,plasma,}$ of **(-)-56** is higher than **(+)-56** whereas in CyPr series is the opposite.

5.1.5.4 Intra-brain distribution

Employing the brain slices methodology,[150,151] the unbound volume of distribution in the brain ($V_{u,brain}$, mL/brain^{-1}) was obtained for all six compounds**.** $V_{u,brain}$ represents the relationship between the total compound concentration in the brain and unbound compound concentration in brain interstitial fluid at equilibrium. The $V_{u,brain}$ values obtained were significantly higher than 1 mL/brain^{-1} **(Table 9)**, i.e. exceeding the total volume of water in the brain tissue, indicating extensive distribution into the brain

parenchymal cells. It is worth to point out that Pr derivatives **56** have statistically significant higher values than CyPr derivatives **57**, **(Figure A2, Appendix A)**. In both series, the dextrorotatory enantiomers **(+)-56** and **(+)-57** have greater $V_{u,brain}$ than the levorotatory ones.

When studying brain tissue binding using brain homogenate method, fraction of unbound drug ($f_{u,brain}$) for all investigated compounds was similarly low indicating high affinity to brain tissue. In addition, it was in average one order of magnitude difference between $f_{u,brain}$ and $f_{u,plasma}$ **(Table 9)**, indicating that compounds are more highly prone to bind to brain parenchyma than to plasma proteins.

For thorough understanding of intracellular target exposure in the brain, unbound intracellular to extracellular concentration ratio, $K_{p,uu,cell}$, was estimated. It varied between 1.70 for **(±)-57** and 3.41 **(+)-56** (**Table 9**), suggesting higher accumulation inside cells for Pr than CyPr derivatives. In addition, it is remarkable that dextrorotatory enantiomer **(+)-57** has 30 % higher $K_{p,uu,cell}$ than its racemic mixture (**Figure A3, Appendix A**).

5.1.5.5 Extent of BBB transport

As a critical part of CMA, *in vivo* neuroPK studies were performed in rats with each racemic mixture of Pr and CyPr derivatives. To reduce the animal use, the intravenous 4 h slow rate infusion, assuring achievement of steady state total plasma concentration, was designed. At the end of infusion total concentration of compound was measured in plasma and brain, in order to obtain the partition coefficient $K_{p,brain}$. As it could be seen from **Table 9**, **(±)-56** has 3.6-fold higher $K_{p,brain}$ than **(±)-57**. However, this number might be misleading and may reflect not the superiority in the extent of BBB transport but rather the high affinity of (±)**-56** to plasma and brain tissues. Hence, the assessment of unbound brain to plasma concentration ratio, $K_{p,uu,brain}$, describing the extent of unbound compound transport across BBB, has been evaluated using CMA,[148] through a combination of the experimentally determined $K_{p,brain}$, $V_{u,brain}$ and $f_{u,plasma}$. Results indicate that both compounds are efficiently effluxed at the BBB, as $K_{p,uu,brain}$ values were lower than unity.[146]

5.1.6 Discussion of results from objective I

Despite enormous scientific and economic efforts have been done last decades, we are still lack of efficacious treatments to stop AD progression. This fact brings to light the urgent necessity of finding new DMTs.

The Thesis objective was the synthesis and preclinical development of a new family of MTDLs focused on stopping the neurodegeneration process. We chose the MTDLs approach because of the multifactorial character of the disease. We, as many other researchers[187,188,189] believe that acting simultaneously on several targets, would be a better strategy to preserve neurons viability. For that reason, we fixed our attention in reducing the exacerbated oxidative stress presented in AD brains and activating endogen intracellular pro-survival routes to prevent the death of cholinergic neurons. Thus, our main purposes were to obtain an antioxidant effect by exerting a potent free radical scavenger activity and by inducing Nrf2-EpRE pathway, and restoring the malfunctioning cholinergic system, by inhibiting AChE and modulating α7-nAChRs.

The design of the new **Family A** compounds **54-58** was based on rational target selection, including connected pharmacophores able to modulate them. Thus, the molecules of **Family A** are characterized by twisted and rigid tricyclic structure with a bridged nitrogen atom and three chiral centres, features of alkaloids capable to modulate cholinergic response; two Michael acceptors sterically hindered to moderately induce Nrf2-EpRE pathway and an indole scaffold with substituents present in melatonin to obtain ROS scavenging effect.

The synthesis of targeted molecules was carried out in a seven step convergent linear process, following the previously reported procedure by Leon.[114] Nevertheless, the critical reaction was undoubtedly the ECED, because of the introduction of the chirality in the molecules, induced by Hayashi-Jørgensen catalyst.[190,191] This catalyst is highly efficient in terms of reactivity and stereoselectivity, and it allowed us to obtain moderate to high yields (57 - 90 %), in line with similar previously reported derivatives,[114] and high to excellent *ee* (81 - 92 %), although slightly lower in comparison to them. Final compounds **54-58** were obtained by reductive amination between the aldehyde and the 5-methoxy-tryptamine, also with moderate to good yields ranging from 43 to 79 %. The variability in the yields seemed not to be dependent on the substituent, since within series,

we obtained heterogeneous yields. The most probable explanation might be related to the reversibility of the imine formation, since whether the water byproduct was not properly removed, imine hydrolysis would ocurr.[192] Even so, herein we have obtained a new class of chiral molecules, synthetized with affordable starting materials with an overall good yields and *ee* after seven steps.

Family A compounds are characterized by two Michael acceptors: the 2,1-α,β-unsaturated system and the 10,11-α,β-unsaturated system. The former is an α,β-unsaturated lactame, usually less reactive towards a Michael addition than other α,β-unsaturated systems.[193] However, the presence of the substituents in β-carbon, modulates its electronic character, being more electronegative with alkyl-containing substituents (**56-58**), and thus, making them less reactive than aryl-containing compounds (**54-55**). We postulate that the MOA of Nrf2 induction would be the 1,4-Michael addition of the thiol groups of the Keap1 cysteines to the α,β-unsaturated systems.[194] **54** (Ph) and **55** (*m*-F-Ph), presented a bell shaped concentration-Nrf2 induction response curves (data not shown), indicating higher potency (**Table 4**). Conversely, alkyl-containing derivatives **56** (Pr) and **57** (CyPr) showed moderate induction of Nrf2 in a concentration-dependent manner. **58** (CyHx) despite of also presenting a bell-shaped concentration-Nrf2 induction curves, they did not induce Nrf2 more than the double of luciferase due to their high toxicity (**Table A2, Appendix A)**. Thus, the potency of the Nrf2 induction effect could be explained by the electronic properties of the substituents since the aryl-containing 2,1-α,β-unsaturated system is more reactive than alkyl-containing compounds. Moreover, the Nrf2 induction could be explained by the ability of substituents to interact more stably with Keap1. The entrance of Keap1 pocket is surrounded by hydrophobic residues, mainly composed by tyrosines (Tyr572, Tyr525, and Tyr334) and phenylalanine (Phe478).[195] **54** and **55** are very lipophilic (clogP = 4.20 and 4.49, respectively) and might probably establish stronger hydrophobic interactions with aforementioned residues than **56** and **57.** In addition, Ph **54** and *m*-F-Ph **55** could further establish π-π stacking interactions with the aromatic rings of tyrosines and/or phenylalanine, which could explain the higher Nrf2 induction potency of these compounds.

The indole moiety mimicking melatonin struture was included to act as radical scavenger. Indeed, all new compounds possessed higher scavenger capacity than trolox,

in the same extent as melatonin, except for Ph **(±)-54**, *m*-F-Ph **55**, and CyHx **58** which exerted a less potent effect. As α,β-unsaturated systems can also undergo radical additions, their participation could explain the differences in TroloxEq among derivatives. The better antioxidant activity was generally presented by small alkyl derivatives, **56** and **57**. After the addition of the ROS to β-carbon, a new radical would be generated involving the carbonyl group. Then, as Pr and CyPr are the weakest inductive electron donating groups, they could not stabilize the radical carbocation generated, making it more reactive towards radical chain reaction than, for instance, *m*-F-Ph or Ph which might be able to stabilize the carbocation by resonance effect.

The α7-nAChR is unique within nAChR family because has a dual ionotropic and metabotropic nature. Taking advantage of the ionotropic part, we performed intracellular Ca^{2+} measurements in SH-SY5Y to evaluate whether the compounds were able to modulate these receptors. Indeed, after stimulation with ACh, a partial blockade of the response was observed. Then, to evaluate the capacity of these compounds to modulate specifically α7-nAChR, we studied their effect in cells stimulated with the selective α7-nAChR agonist PNU282989. The presence of the PAM PNU120596 was needed, as the Ca^{2+} entrance is not observed with the agonist alone because of high desensitation of the receptor.[52] We could see how all the compounds were clearly able to selectively modulate α7-nAChRs, since the signal elicited by the agonist and the PAM was almost completely reduced in the presence of the big compounds **54**, **55** and **58**. It is worth noting that IC_{50} values were in lower micromolar and submicromolar range for these derivatives (**Table 5**), with subttle differences between enantiomers. By contrast, the IC_{50} values were higher for **56** and **57**, and in turn, marked differences between both enantiomers were observed. The distinct behaviour of the enantiomers, as well as the differences in IC_{50} values, could be explained based on results from the docking and molecular dynamic studies.

Overall, the computational study conducted on the binding mode of this family, choosing the most potent derivative **(-)-54**, suggests that the insertion of the Ph group and tricyclic core in the hydrophobic pocket conformed by Y93, W149, L38' and W55'[196] is the key structural determinant for the binding of this compounds to the α7-nAChR orthosteric site. In addition, Y188 and Y195 residues have a prominent role in the recognition process, by interaction with methylene groups of linker chain (**Figures 15**

and 17). Moreover, the predicted more stable poses of the enantiomers were completely inverted. These results are in good agreement with the structure-activity relationship of the **Family A** compounds with both levo- and dextrorotatory enantiomers, helping to explain the differences observed among the family. Our structural study suggests that the bigger volume and lipophilic character of Ph, *m*-F-Ph, and CyHx in comparison with Pr and CyPr substituents results, in a stronger stabilization of the ligand at the orthosteric site by interaction with the residues conforming the hydrophobic pocket. We expect that ongoing simulations with compounds **(-)-56** and **(+)-56** further confirm this idea.

The blockade of the effect of an agonist could be mediated by an antagonist, a partial agonist or a NAM.[58] Since molecular dynamic studies of **(-)-54** showed a high stabilization of the compound in the orthosteric site, NAM possibility is discarded. However, electrophysiological studies at single channel[197] are needed to elucidate if **Family A** compounds are partial agonists or antagonists, and studies that were ongoing during the writing of this Thesis.

Regarding AChE inhibition studies, all derivatives were able to selectively inhibit AChE through a mixed-type mechanism, indicating that they bind to the PAS (**Table 6**). The main interactions at PAS are mainly contributions from π-π stacking,[169] therefore, we would expect that aromatic derivatives were more potent inhibitors. Nevertheless, **54** and **55**, have greater IC_{50} values than **56** and **57,** whose IC_{50} is lower than 10 μM. IC_{50} values of **58** are in between. Therefore, a plausible reasoning of the different tendency would be related to the steric hindrance of the substituents, rather than the electronic properties. The main interactions established would be π-π stacking between the indole ring and aromatic residues of the PAS, placing molecules in a position that makes the most voluminous substituents able to collide with another part of the protein, leading to weaker interactions, and finally, less inhibition potency. In line with the cholinergic hypothesis (*Section 2.6.1*), **Family A** compounds might enhance the cholinergic neurotransmission by increasing the amount of ACh in the synaptic cleft, and besides, they could also interfere in the Aβ-aggregation induced by the PAS of AChE.[198]

Notwithstanding the obtained differences in the potency among the derivatives, we achieved a new class of compounds capable of induce Nrf2, exert a radical scavenging effect, inhibit AChE and modulate α7-nAChR. Thus, we, actually, created a new class of

MTDLs. Hence, following the hypothesis of acting on several targets, might be act with synergy and prevent cellular death,[44] we determined the neuroprotective profile of **Family A**. The oxidative stress might be an early contributor of the AD where unbalance of free radicals is produced.[37] Thus, we tested our compounds at 1 μM in the R/O model, and they could revert the cell death induced by the toxic cocktail. We used melatonin for comparative purposes due to its well-known scavenger and antioxidant effects,[99] and all derivatives showed a potency similar to that of melatonin (**Table 7**), distinguishing **(±)-56** (Pr) with a 61 % of protection. This suggests that the inclusion of the indole moiety as well as the α,β-unsaturated systems was successful for achieving a good antioxidant activity. Also, under the tau hypothesis, tauopathy may be also an early contributor of AD, since NFT formation preceds Aβ plaques deposition.[32] Thus, we employed a tau hyperphosphorylation model to screen our compounds. Although CyHx derivatives **58** were not able to revert the cell death induced by OA, similar neuroprotection percentages as melatonin were obtained for derivatives **54-57** (**Table 7**). Hence, **Family A** compounds would have a preventive role in tau aggregation, likewise melatonin. [99]

In order to understand the MOA of this class of compounds, **(±)-56** was selected because of highest neuroprotectant effect. Nrf2-EpRE pathway activation leads to the constitutive and inducible expression of phase II antioxidant and anti-inflammatory protein, such HO-1.[82] This MOA is presented in our in-house-library compound ITH12674, which elicits a 72% neuroprotective effect against oxidative stress conditions at 1 μM.[153] With the aim to reveal whether Nrf2 and HO-1 were involved in the neuroprotection effect promoted by **(±)-56**, we pharmacologically inhibited them, leading to a significant reduction of the protection (**Figure 18, A and B**), indicating that the Michael acceptors are acting as Nrf2 inducers. As already mentioned, melatonin has pleiotropic effects; one of them, the activation of the antiapoptotic ERK/MAPK signalling pathway, is mediated by its receptors MT1 and/or MT2.[199] Thus, when we employed luzindole, an inhibitor of MT1/MT2, and PD98059, an inhibitor of ERK1/2, we observed a prevention of the protective actions elicited by **(±)-56** (**Figure 18, C and D**) suggesting the participation of the indole moiety as a ligand of MT. Finally, the activation of α7-nAChRs by, for instance selective agonist PNU282989, promotes 50% of neuroprotection in R/O stressed SH-SY5Y cells by the induction of the Jak2/PI3K/Akt signalling

pathway.[63] In line with this, we used an inhibitor of PI3K, which markedly antagonized the protective effect given by **(±)-56** (**Figure 18 E**), which leads to confirm that **(±)-56**, whether it acts as a partial agonists or an antagonist, it might be a selective α7-nAChRs ligand.

Overall results indicate that, the less lipophilic and voluminous derivatives, **56** (Pr) and **57** (CyPr) presented the less potent Nrf2 induction, the less potent α7-nAChRs modulation, the more potent AChE inhibition and the highest scavenger capacity of the **Family A**, which correlated with higher neuroprotectant properties.

Following the steps of drug discovery process, to choose the lead compound, is important to know the PK parameters as regards potential preclinical development of the compounds. The PK profile of selected hits **(±)-56** (Pr) and **(±)-57** was similar, reaching the maximum plasma concentration at 5 min after IV bolus. The estimated primary PK parameters that indicate extensive distribution into peripheral tissues (high V_z) for both compounds and fast elimination of the compounds from the plasma. High Cl is reflected in moderately low elimination half-lives, which is good in order to prevent insufficient drug distribution and undesired side effects. Interestingly, they are *ca.* four times longer than the half-life of melatonin, what may indicate more plasma protein binding which would act as a depot. Indeed, plasma protein binding of **56** and **57** compounds is high, with the lowest value being 0.128 for **(+)-56** and the highest 0.176 for **(±)-57**. The significantly different lower values of $f_{u,plasma}$ for Pr rather than CyPr derivatives, could probably be due to their higher lipophilicity, and therefore, would interact more strongly with the hydrophobic binding site of albumin. Interestingly, there were differences in enantiomer binding to plasma proteins for both derivatives (**Figure A1, Appendix A),** which could lead to stereoselectivity in brain distribution, as K_p is governed by brain and plasma protein binding as well as transport across BBB (Eq.4, *Section 4.1.*).

CNS total compound concentration accounts free compound and bounded compound to specific targets and non-specific tissue components. Regarding intra-brain distribution, non-specific binding to the brain tissue is quantitatively significant for all compounds, being $f_{u,brain,}$ 10-fold lower than $f_{u,plasma}$. Even so, we used brain slice methodology to determine the accumulation of compounds in the brain related to unbound compound in brain ISF, since it is a more valid approach than brain homogenate method

because conserves cell membranes integrity.[151] Thus, we assessed $V_{u,brain}$ (**Table 9,** *Section 5.1.4.2*), and it is worth noting that Pr derivatives **56** have statistically significant higher $V_{u,brain}$ values than CyPr derivatives **57**. This outcome could be explained because of a higher lipophilicity of Pr derivatives, which have higher affinity for phospholipids of membranes, leading to a higher non-specific binding to brain tissue, and therefore, high total brain concentrations despite of low unbound compound. Regardless the substituent, dextrorotatory compounds showed the highest $V_{u,brain}$ within series, most probably due to differences in the interaction with plasma membrane. Determining $V_{u,brain}$, not only we could assess significantly high distribution into the brain parenchymal cells, but also, additional mechanisms such as active uptake into the cells and lysosomal trapping. In this regard, the estimated $K_{p,uu,cell}$ values were greater than unity for all investigated compounds. This means that there is an intracellular accumulation of the compounds, more pronounced for **56** Pr derivatives. Again, the highest intracellular unbound concentration estimated were for dextrorotatory **(+)-56** and **(+)-57**, indicating that it is a result of both pH-gradient-driven and other unknown active processes, probably favoured by stereoselective binding to the transporters. On the other hand, the estimated $K_{p,uu,cyto,pred}$ 1.74 and $K_{p,uu,lyso,pred}$ 131.72[148] support the hypothesis of lysosomal trapping phenomenon, driven by the basicity of the compounds.

Finally, in light of compilation of all PK and intra-brain distribution and extent parameters, we could conclude that once all investigational compounds cross the main obstacle BBB, they will have no restriction to distribute within the brain and will tend to accumulate inside the cells. Neverheless, **(±)-56** or **(±)-57** are actively effluxed from brain to plasma, and, unfortunately, only 3.6 % and 1.4 % of unbound **(±)-56** or **(±)-57** will reach brain interstitum. This might be because these compounds are substrates of efflux transporter(s) such as P-gp, as they present two type II units of electron donating groups.[200] The latter is a very well-known hurdle in CNS drug development and requires chemical modifications to obtain improved $K_{p,uu,brain}$ values, along with optimization of their PD properties.

Family A compounds are a new class of chiral MTDLs able to induce Nrf2, modulate α7-nAChRs, inhibit AChE and possess a radical scavenger effect, and the utmost importance, they prevent cell death. Despite achieving all the desired activities,

the main drawback of **Family A** compounds was the neuro-PK. Hence, we set out to improve that disadvantage in a second generation of MTDLs.

5.2 Objective II: design, synthesis and pharmacological evaluation of quinuclidine derived multitarget directed ligands.

5.2.1 Introduction

For a successful CNS effect, drug must have the ability to be delivered to the region of interest in the brain with enough concentration. The presence of the BBB blocks the entrance of many drugs to the CNS since it is a selective permeable membrane rich in efflux transporters such as P-gp, and it represents the main impediment for new CNS drug therapy development.[14]

The main drawback of **(±)-56** and **(±)-57** is that they were actively effluxed from the brain to blood, since the estimated $K_{p,uu,brain}$ was less than one, implicating reduced brain concentrations and proportionally higher dose requirements. However, high doses could lead to toxicity instead of therapeutic effect. Moreover, the requirement of a highly concentrated infusion solution for administration, would be an issue for formulation, due to low water solubility. Thus, we could modify the substitution pattern while maintaining the essential structure of **Family A**, in order to improve solubility and extent in the brain.

As has been noted, CNS drugs are even more challenging because of distinctive features of BBB, making physicochemical properties even more restrictive. Indeed, four years after his rule, Lipinski studied the structure of 1500 marketed CNS drugs which had already knowledge of good brain penetration and orally bioavailability, establishing narrow ranges for potential CNS therapeutics in comparison to general non-CNS targeted drugs (**Table 10**). Compared CNS marketed drugs with non-CNS drugs, revealed that CNS drugs tend to have lower MW, be less polar, less flexible, lower TPSA, with a pKa between 7.5-10.5, and aqueous solubility higher than 60 μg/ml, in comparison to non-CNS drugs.[161]

Table 10. Comparison of Rule of 5 for general non-CNS drug candidate and Rule of CNS drug candidates.

Physicochemical property	*Rule of 5*	*Rule of CNS*
MW	≤ 500	≤ 400
HBA	≤ 10	≤ 7
HBD	≤ 5	≤ 3
clogP	≤ 5	≤ 5
RB	≤ 10	≤ 8

Notwithstanding these mnemonics have provided a relevant and helpful tool for to predict brain penetration and bioavailability for novel molecular entities, it should be noted that only considers passive membrane transportation. Taking into account that molecules can be actively transported across BBB, as a consequence, violation of one or two of these rules does not mean a failed compound. Therefore, we must be cautious before rejecting potential candidates.[201]

During many years, the brain-to-plasma concentration ratio, K_p, also known as logBB, was taken to determine structure-brain exposure relationships. Nevertheless, as K_p accounts the plasma and brain protein binding, it is not a suitable parameter for prediction of the BBB transport and the extent of distribution of the free drug within the brain.[202] Then, lipophilicity was pointed out as main physicochemical parameter for successful CNS permeability, also known as logPS. Permeability is defined as the rate of the transport across the BBB, therefore, lipophilicity does not account for unbound brain exposure. Although, of course, if a drug readily reaches brain, as a result of high passive diffusion, could counteract the effect of active transport and leading to increased CNS exposure.

Hence, accordingly to the fact that $K_{p,uu,brain}$ is the highest relevant parameter which defines brain exposure, Friedén and co-workers, evaluated the relationship between structure and free brain exposure by determining $K_{p,uu,brain}$ of 41 marketed CNS drugs.[203] They found that HBA capacity dominated the extent of brain exposure and, conversely, lipophilicity had no correlation. In line with this study, Loryan and colleagues

determined the molecular descriptors for $K_{p,uu,brain}$, $V_{u,brain}$ and $K_{p,uu,cell}$. For $K_{p,uu,brain}$, besides HBA, TPSA is a significant descriptor. Thus, if two HBA are removed leading to a low hydrogen bond capacity and lower polarity, an increase of $K_{p,uu,brain}$ will be achieved. By contrast, higher $V_{u,brain}$ values depends on higher logP, and number and distribution of HBA. Finally, high $K_{p,uu,cell}$ will be determined by higher pK_a, (higher basicity) as well as higher molecular surface area related to HBD.[204]

Taking into account the low $K_{p,uu,brain}$ for **Family A**, it could be modified considering the described molecular descriptors. Thus, the second chapter of this Thesis was focused on the design of a second generation of MTDLs, with the aim to improve physicochemical properties, maintaining the activities observed on **Family A**.

5.2.2 Design of novel MTDLs with improved CNS profile

As previously mention, HBA is the main physicochemical property which influences in brain exposure. Thus, since **56** and **57** possess four HBA, (*Section 5.1.2,* **Table 1**), we planned the reduction of HBA groups in **Family B** derivatives In addition, lipophilicity is one of the key factors in drug discovery and lead optimization process which govern permeability, solubility, plasma and tissue protein binding, metabolism and toxicity of the compounds.[205] **Family A** compounds are moderate-to-highly lipophilic with clogP ranging from 3.60 to 4.55. Despite of **56** and **57** have lower clogP values, we have demonstrated that they were poor water soluble and presented high plasma and non-specific brain protein binding affinities. In **Family A** compounds, the complex tetrahydropyrroloquinoline tricycle, is, indeed, responsible of high clogP values, therefore, we envisaged the replacement of this moiety by a less lipophilic structure.

In this regard, focused on the search for α7-nAChRs ligand, we studied the structural requirements of known α7-nAChR ligands, extracting several conclusions. There are three key pharmacophoric elements: 1) a cationic centre, considered an essential pharmacophore for this type of receptors because mimics the endogen ligand, ACh; 2) a hydrophobic element containing π-electron density, which is important for establishing π-π stacking interactions with the binding site, giving selectivity for α7 subtype; and 3) a HBD/HBA, acting as a linker between them (**Figure 20**).

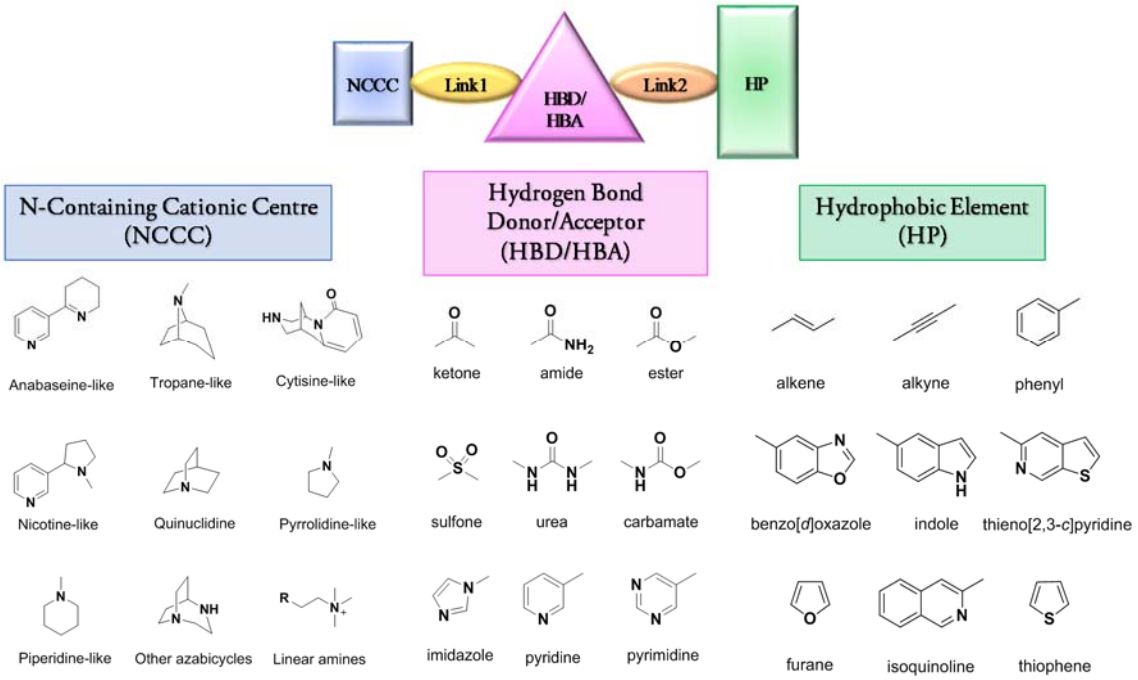

Figure 20. General structure for α7-nAChR ligands and some examples of the three key pharmacophoric elements: N-containing cationic centre, a hydrogen bond acceptor and a hydrophobic element. (Modified from Mazurov *et al.*)[206]

Our design included a rigid basic amine moderately bulky, to reduce the final molecule size of new molecules. Finally, chirality implies different potency towards the receptor and, as demonstrated previously for **Family A** compounds, the enantiomers might have differential affinity to plasma or tissue proteins that could lead to different distribution within brain

After deep bibliographic reviewing, we found a wide structural diversity of nAChRs activators such as nicotinic-, cytisine- and tropane-like scaffolds, anabaseines, pyrrolidines, piperazines, linear amines and many different azabicycles (**Figure 20**). Among them, the most common used for selective α7-nAChRs ligands, 1-azabicyclo[2,2,2]octane (quinuclidine), **Figure 20**.[207] Quinuclidine possesses a bridged nitrogen atom with minimal steric hindrance and maximal availability of lone electronic pair, conferring strong basicity with a pK_a around 10-11, prompting it to be protonated at physiological pH. For instance, already mentioned in *Section 2.9.5*, the most extensively used agonist of α7-nAChRs, PNU282987 (**11, Figure 21**), belongs to this class of compounds. PNU282987 readily crosses BBB and has neuroprotective properties in both *in vitro* and *in vivo* studies.[63,64] However, its clinical use is hampered because its

significant activity on hERG channel, which is associated with risk of cardio arrhythmic properties.[78] Under those evidences, we chose 3-aminoquinuclidine scaffold as a chiral alternative of complex tetrahydropyrroloquinoline structure present in **Family A**.

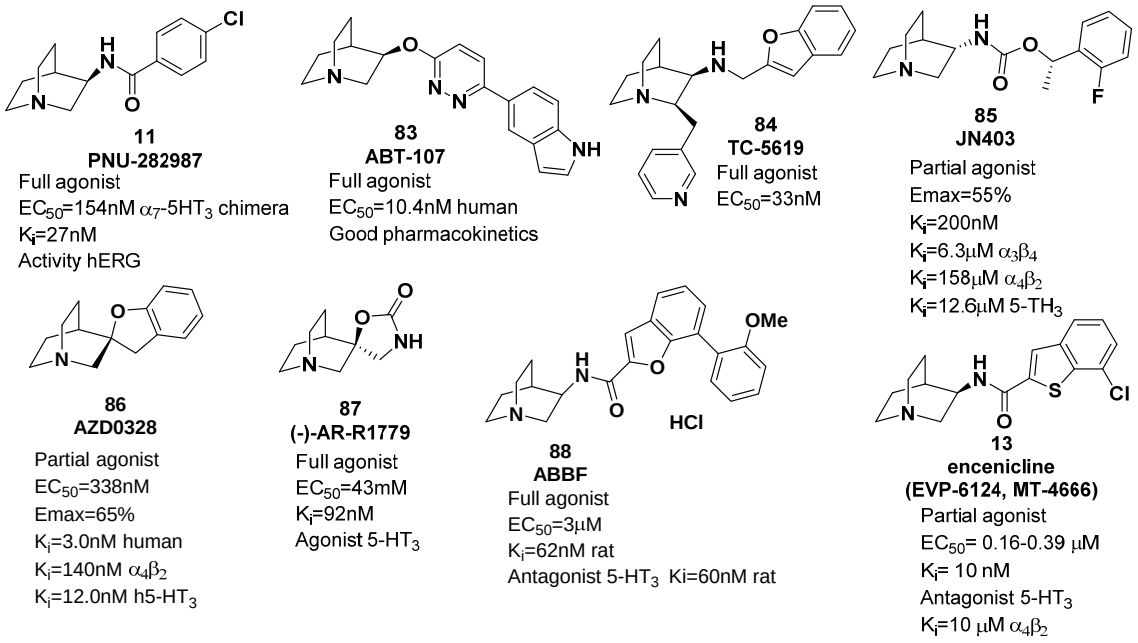

Figure 21. Selected examples of full and partial agonists of α7-nAChRs containing quinuclidine scaffold as cationic centre.

Apart from cationic nitrogen centre, to maintain α7-nAChR activity, novel designed compounds should have a hydrophobic element and a HBA or HBD group. **Family A** compounds (**Figure 22**) already present these features. Thus, the hydrophobic element, the indole scaffold in **Family A**, will be conserved, not only for the α7-nAChR pharmacophore requirement, but also for retaining the antioxidant activity. Besides, indole ring allows the possibility to explore the influence of different substituents. By including different electronic properties, the physicochemical features will be affected and, also, they may modulate differently the biological response.

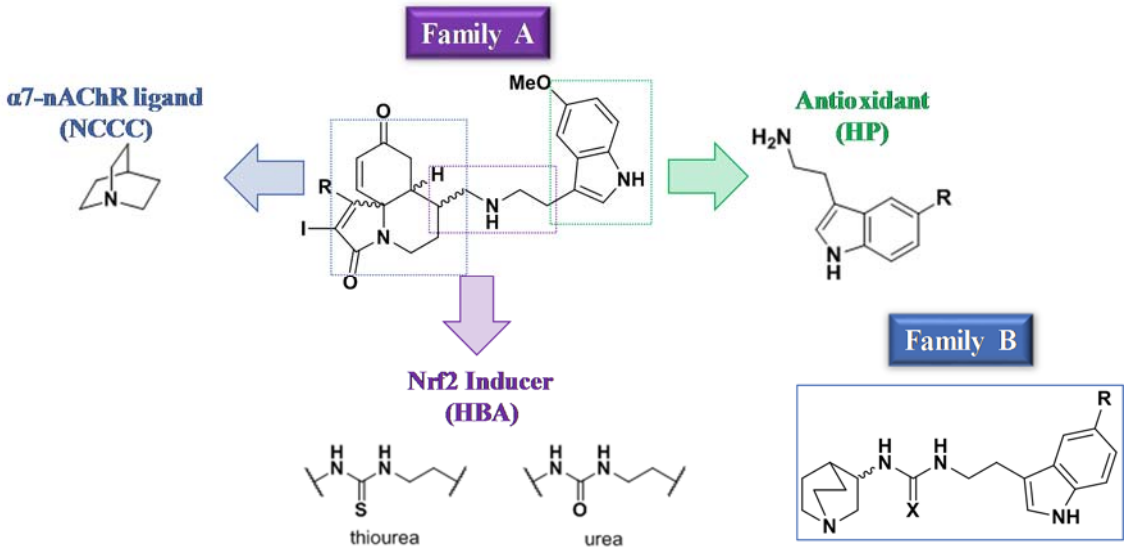

Figure 22. Inspiring design of **Family B** modifying **Family A** general structure.

Lastly, among the long list of HBA possibilities like amides, carbamates, esters, heterocycles, ketones, sulphonamides, etc **(Figure 20)**, we completed the α7-pharmacophore including a HBA with the idea of obtaining as well the ability to induce Nrf2 transcription factor. As stated in the Introduction (*Section 2.10.3*), there are covalent (electrophilic) and non-covalent (PPI) types of Nrf2 inducers. The Nrf2 inducers of Family A belong to the first class, an α,β-unsaturated carbonyl and a substituted α,β-unsaturated lactame sterically hindered to prevent promiscuity within nucleophiles in the cell. Thus, to investigate different inducers from electrophiles, we wanted to open the possibility to explore new compounds as PPI inhibitors. This type of inducers has emerged recently and is gaining much more attention due to their significant improvement of selectivity over electrophiles.[96] Thus, among the 5 classes described[84], we focused our interest on urea derivatives, since urea is present as HBA in known α7-nAChR ligands like PNU120596. Moreover, we included the thiourea functional group for comparative purposes. Despite establishing weaker hydrogen bonds than ureas, thioureas are likely to accept more than one HBD which promotes a preferably anti-conformation instead of usually adopted syn-conformation by ureas. Although none thiourea derivative has been reported as Nrf2 inducer, the interest of this kind of derivatives is high, since it has been demonstrated that thioureas have AChE inhibition,[171] Cu^{2+} chelation and ROS scavenging

activities,[208] and together with ureas, they are capable of reduce NO production,[209] being all these biological activities, interesting for AD treatment.

Hence, the second generation of compounds (**69-74**) was designed as MTDLs linking three pharmacophores, a cationic centre provided by quinuclidine, a HBA and a HP, to generate a small chemical library of twelve compounds classified in two classes of derivatives depending on the HBA inserted: thioureas or ureas. In turn, each derivative provides different compounds regarding the substituent included in the indole ring, either MeO, Cl or unsubstituted. In addition, both enantiomers were obtained separately increasing the structure-activity relationship possibilities, **Figure 22**.

5.2.3 *In silico* physicochemical properties

Likewise to Family A, we used SwissADME[159] and Chemicalize from ChemAxon[160] free platforms, to predict the physicochemical descriptors needed were predicted to determine the druglikeness of the new compounds, **Table 11**.

Table 11. Druglike physicochemical properties of compounds **69-74**[a]

Cpd	MW (g/mol)	HBA	HBD	RB	TPSA (Å^2)	pK_a	clogP[b]	S[c] (mg/mL)	BBB permeant	Pgp-substrate
69	358.5	2	3	7	52.32	8.05	2.58	$2.04 \cdot 10^{-3}$	No	Yes
70	362.9	1	3	6	43.09	8.06	3.06	$6.76 \cdot 10^{-4}$	Yes	Yes
71	328.5	1	3	6	43.09	8.05	2.54	$2.40 \cdot 10^{-3}$	Yes	Yes
72	342.4	3	3	7	69.39	8.04	2.06	$3.03 \cdot 10^{-5}$	Yes	Yes
73	346.9	2	3	6	60.16	8.04	2.57	$1.00 \cdot 10^{-5}$	Yes	Yes
74	312.4	2	3	6	60.16	8.04	2.05	$3.57 \cdot 10^{-3}$	Yes	Yes

[a]All parameters were predicted using SwissADME platform (http://www.swissadme.ch/index.php) and Chemicalize free software tool (https://chemaxon.com/products/chemicalize). [b]Consensus log $P_{o/w}$ is the arithmetic mean of the values predicted by the five methods (iLOGP, XLOGP3, WLOGP, MLOGP, SILICOS-IT). [c]SwissADME SILICOS-IT prediction.

The second generation of MTDLs is characterized by considerably smaller size of compounds in comparison to **Family A**, as MW ranged from 309 to 363 Da. Accordingly to *Rule of CNS*, we tried to keep the number of HBDs low to avoid interactions between

the compounds and the polar heads of the phospholipids of the membranes, (*Section 5.2.1*, **Table 10**). Thus, both derivatives thioureas **69-71** and ureas **72-74** have one HBD more than molecules from **Family A**. Whereas, since $K_{p,uu,brain}$ was described to be dependent of HBA, we reduced and included more variability in the number of HBAs. As can be seen in **Table 11**, HBAs vary from one in **70** and **71**, two in **69**, **73**, **74** to three in **72** to check the repercussion in this parameter.

As already pointed out in *Section 5.2.1*, lipophilicity does not affect the concentration of unbound drug within brain, but it is important for the rate of transport, as well as for $V_{u,brain}$. clogP values (2.05-3.06) are significantly lower compared to those calculated for **Family A**, being in the optimal range for CNS successful drugs. Solubility is inversely correlated to lipophilicity, thus, compounds of **Family B** are more soluble than **Family A** derivatives, estimating solubility of ureas higher than thioureas. Within derivatives, Cl-containing compounds are less polar and, therefore, less water soluble, whereas MeO-containing molecules are more hydrophilic.

However, although lipophilicity was classically considered the key factor for membranes penetration rate, it has been demonstrated that TPSA is better correlated.[203] Most of new compounds have a TPSA ranging between 43 $Å^2$ and 69 $Å^2$, lower than 74 $Å^2$ calculated for **Family A**, being, also in the optimal range to reach CNS.[161] The decrease of the TPSA is related to less flexibility, in terms of RBs, and hydrogen bond capacity. Except two MeO-containing derivatives **69** and **72** which count 7 RBs as **Family A**, **70-71/73-74** have 6 RBs, values presented by most of centrally acting drugs.[210]

Finally, all of new quinuclidine-based MTLDs are basic compounds. They are prone to be protonated at physiological pH, allowing interaction with phospholipid heads, favouring passive diffusion, and therefore, they will, presumably, have higher distribution inside cells (higher $K_{p,uu,cell}$).

Notwithstanding better physicochemical properties achieved in **Family B** in comparison to **Family A** compounds, they are as well predicted to be Pgp-substrates. However, it is possible that improved physicochemical properties could lead to an enough unbound compound within brain being able to exert their pharmacological response.

5.2.4 Synthesis of Family B 1-(2-(5-substituted-1*H*-indol-3-yl)-ethyl-3-(quinuclidine-3-yl) derivatives

(5-substituted-1*H*-indol-3-yl)-*N*-(quinuclidin-3-yl)-derivatives synthetic approach is shorter than **Family A** derivatives. Similarly to **Family A**, as some different 5-substituted-tryptamines and indoles as well as enantiomerically pure (*R*)- or (*S*)-3-amino-quinuclidine dihydrochloride are commercially available, the objective of the synthesis was reduced to include the linker between both units as illustrated in retrosynthetic (**Scheme 7**). 5-MeO-tryptamine **53** and 5-Cl-tryptamine **61** dihydrochlorides present different electronic properties to analyse structure-activity relationship. The preparation of thiourea, **69-71**, and urea, **72-74**, derivatives required just two steps, the synthesis of intermediary isothiocyanate **63-65** or carbonylimidazolide **66-68**, and its coupling with the primary amine of both (*R*)- and (*S*)-3-aminoquinuclidines **(*R*)-60** and **(*S*)-60**.

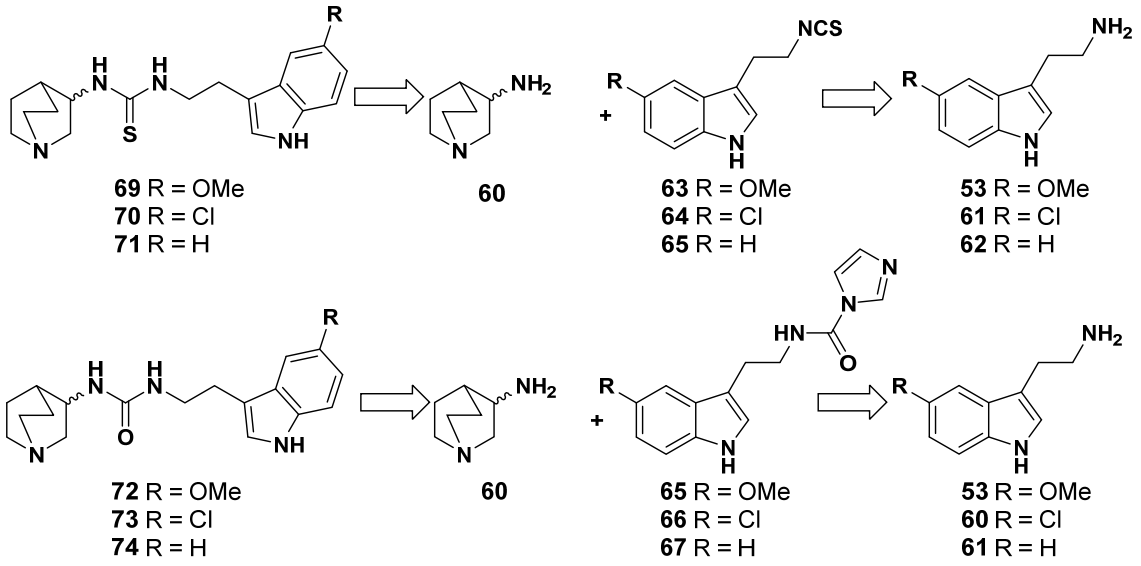

Scheme 7. Retrosynthetic scheme for the synthesis of **Family B** compounds.

The synthesis of thioureas involves an intermediate of isothiocyanate which easily reacts with amines. Compound 3-(2-isothiocyanatoethyl)-5-methoxy-1*H*-indole **63** was previously included in our in-house-chemical library. We described its Nrf2 induction and free radical scavenger activity with neuroprotectant and anti-inflammatory properties.[153] Firstly, the isothiocyanate with R substituent group MeO- **63** and Cl- **64** were prepared using a previously optimized protocol in our group, employing commercial

5-MeO-tryptamine **53** and 5-Cl-tryptamine **61** dihydrochlorides and TCDI in THF from 0 ºC to room temperature. After, 2.5 and 19.5 h of reaction, respectively, corresponding isothiocyanates were obtained as pale green and light yellow oils, in 65 % and 61 % yield, respectively. However, imidazole is formed in high quantities interfering with their purification due to their similarities in polarity. Thus, we modified our synthetic approach by the use of CS_2 which reacts with the primary amine of 5-Cl **61** or 5-H-tryptamine **62** in the presence of Et_3N employing THF as solvent at 0 ºC. This generates a carbamodithioate triethylammonium salt that undergoes a dimerization and oxidation after the dropwise addition of 30 % H_2O_2 during 2 h yielding compounds **64** and **65** in 61 % and 78 %, respectively, (**Scheme 8**). This protocol allowed us to obtain these compounds without secondary products interference in the purification process.

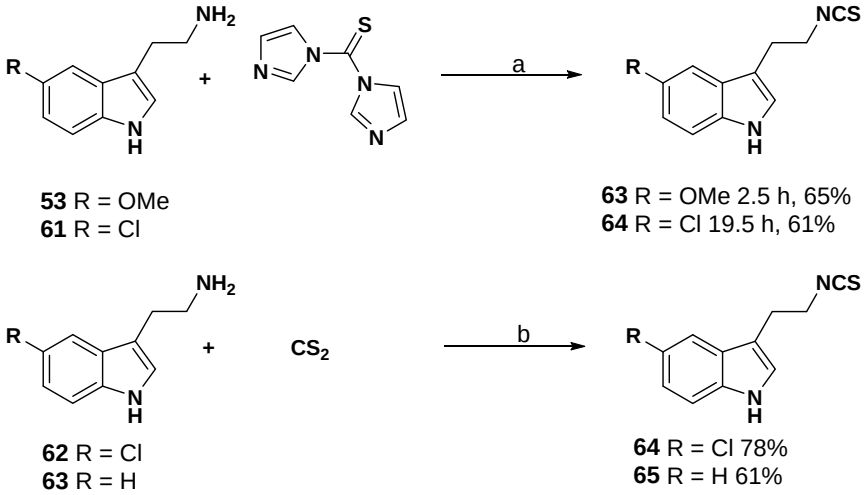

Scheme 8. Reaction conditions for isothiocyanate preparation I: a. TCDI, THF, 0 ºC-rt and for isothiocyanate preparation II: b. CS_2, 30 % H_2O_2, Et_3N, THF, 0ºC-rt, 2 h.

Thus, once obtained the isothiocyanates **62-64**, MeO-thioureas were synthetized firstly by using commercial (*R*)- or (*S*)-3-amino-quinuclidine dihydrochloride in the presence of DIPEA in anhydrous DMF from 0 ºC to room temperature, for 24 h to obtain the dextrorotatory compound obtained from (*R*) enantiomer (62 % yield) and the levorotatory derived from (*S*) enantiomer (85 % yield), (**Scheme 9**).

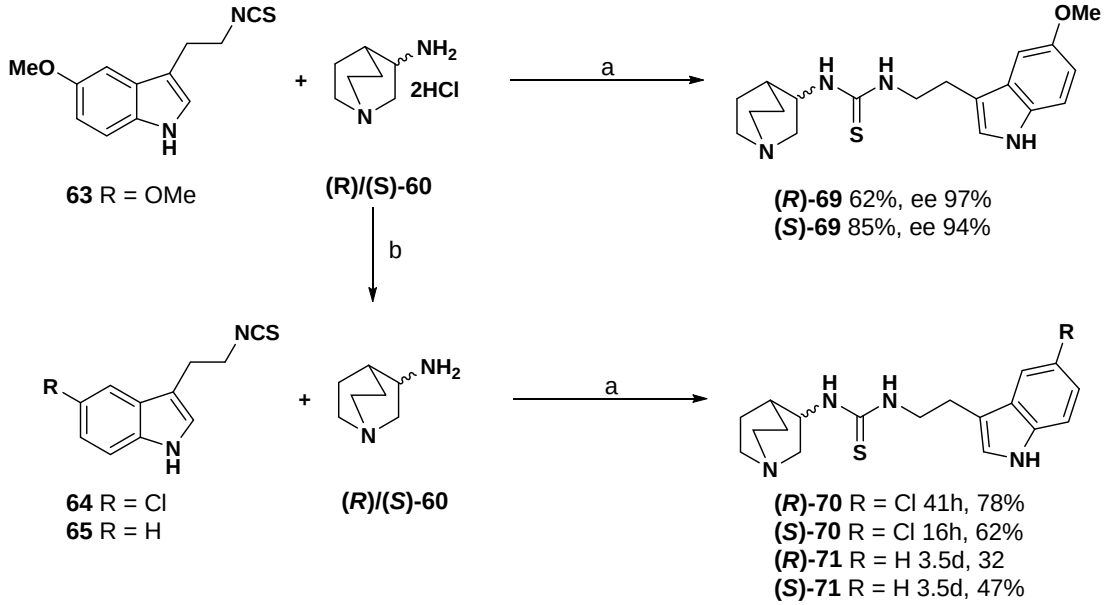

Scheme 9. Reagents and reaction conditions for thiourea derivatives **69-70** synthesis: a. DIPEA, DMF, 0 ºC - rt and for quinuclidine hydrochloride hydrolysis: b. KOH_{sat}, rt, 24 h.

However, as the 3-amino-quinuclidine dihydrochlorides were not fully soluble in the reaction media, the hydrolysis of hydrochlorides was performed before thiourea formation of **70** and **71** compounds. For this purpose, stirring hydrochlorides with saturated solution of KOH for 24 h gave free amine quantitatively **(*R*)/(*S*)-60**. Then, above mentioned conditions for thiourea synthesis were used for both substituents with yields ranging from 32 % to 78 % (**Scheme 9**).

Regarding urea derivatives, combination of 5-substituted-tryptamine hydrochlorides, DIPEA and CDI in dry CH_2Cl_2 from 0 ºC to room temperature, afforded, the corresponding carbonylimidazolide intermediates **67-69** in moderate yields (**Scheme 10**).

Finally, urea derivatives were obtained by overnight reaction of 3-aminoquinuclidine **(*R*)-60** or **(*S*)-60**, DIPEA and *N*-(2-(5-substituted-1*H*-indol-3-yl)ethyl)-1*H*-imidazole-1-carboxamide **67-69** in DMF leading to low to moderate yields as depicted in **Scheme 10**. Notwithstanding that we started with enantiomerically pure quinuclidines and the possibility of epimerization of the chiral centre was very low, we would like to check that the *ee* was conserved. Thus, we determined the *ee* of **(*R*)-68** and **(*S*)-68**, 97 % and 94 %, respectively **(Scheme 9)**, using the same chiral column of **Family A** but different conditions (*Section 4.2.1.1*).

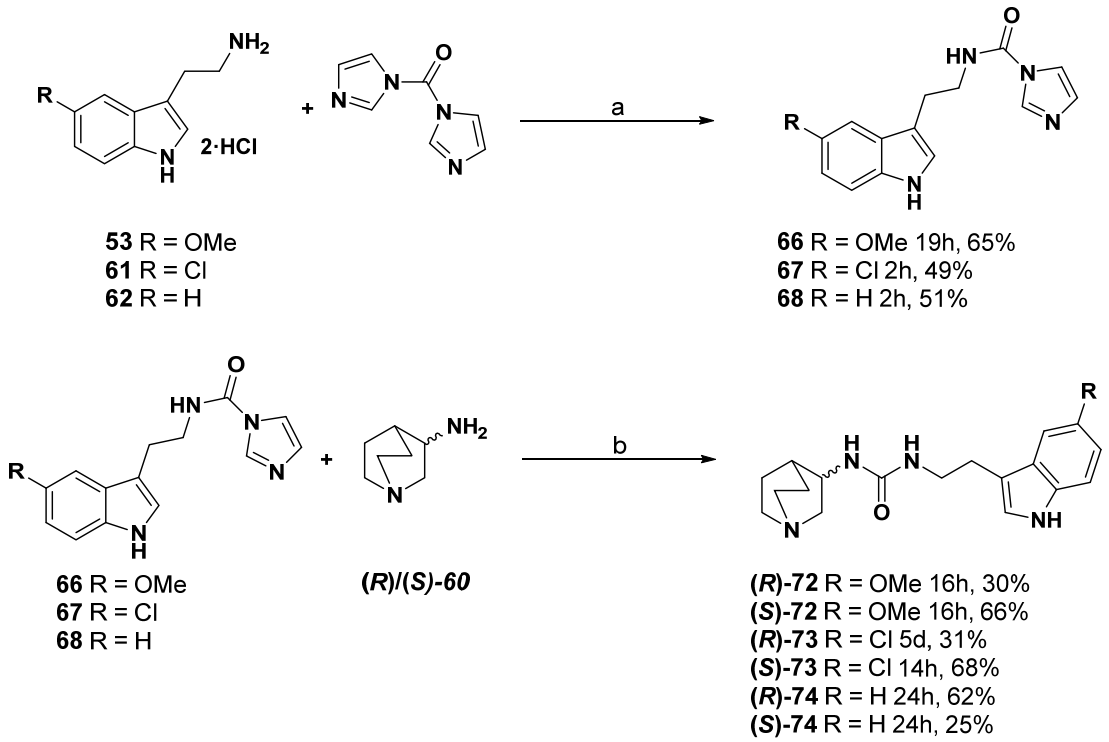

Scheme 10. Reaction conditions for carbonylimidazolide preparation: a. DIPEA, CDI, CH_2Cl_2, 0 ºC - rt, and for urea synthesis: b. DIPEA, DMF, 0 ºC - rt.

5.2.5 *In vitro* pharmacological evaluation.

Comparatively to **Family A**, after structural characterization and determination of purity, compounds of **Family B** followed the similar pharmacological screening procedure, assessing the induction of Nrf2 transcription factor, free radical scavenger activity, the modulation of the nAChRs, and, as a result of combined activities, the potential neuroprotective profile of the derivatives. Protocols and procedures were the same employed to evaluate **Family A** compounds, unless changes mentioned.

5.2.5.1 Evaluation of Nrf2 induction

As already indicated in *Section 5.1.4.1.*, the evaluation of the capability of compound to induce Nrf2 transcription factor was conducted in AREc32 cell line. In this case compounds were incubated at five concentrations (1, 3, 10, 30, 60 μM) together with the positive control TBHQ at 10 μM for 24 h and then, both, luciferase activity and survival were measured. Unexpectedly and unfortunately, none of the compounds were able to double the luciferase activity at tested concentrations (CD > 60 μM). The only

good result here was related to toxicity. Compounds of **Family B** were much less toxic than the ones of Family A in AREc32 cell line, since LC_{50} values were above 60 μM for all compounds, except for **70** (Cl-thioureas) which have a LC_{50} of 34.4 ± 4.1 for **(*R*)-70** and 30.1 ± 4.9 for **(*S*)-70**.

5.2.5.2 Quinuclidine-derived MTDLs are free radical scavengers

The indole moiety was maintained in **Family B**, thus we expected that the compounds **69-74** would conserve the ROS/RNS scavenger activity. To confirm our assumption, compounds and positive control melatonin were evaluated at the concentrations of 0.03, 0.1, 0.3, 1, and 3 μM using ORAC-fluorescein test.[118] Indeed, all **Family B** compounds possessed a potent scavenger activity, in the same extent as melatonin, with the exception of **(*R*)-69** and **(*S*)-72**, which have less potency, must probably due to experimental issues (**Table 12)**.

Table 12. Oxygen free radical absorbance capacity as Trolox equivalents of the compounds as well as melatonin, as positive control.

Compound	TEq	Compound	TEq
Melatonin	$3.42 \pm 0.15^{***}$		
(*R*)-69	$2.78 \pm 0.02^{***\#}$	**(*R*)-72**	$3.57 \pm 0.16^{***\$}$
(*S*)-69	$3.36 \pm 0.16^{***\$}$	**(*S*)-72**	$2.50 \pm 0.13^{**\#\#}$
(*R*)-70	$3.31 \pm 0.16^{***}$	**(*R*)-73**	$3.77 \pm 0.14^{**}$
(*S*)-70	$3.24 \pm 0.25^{**}$	**(*S*)-73**	$3.62 \pm 0.19^{**}$
(*R*)-71	$3.53 \pm 0.20^{**}$	**(*R*)-74**	$3.62 \pm 0.16^{**}$
(*S*)-71	$3.44 \pm 0.14^{***}$	**(*S*)-74**	$3.28 \pm 0.25^{*}$

Data are shown as mean ± SEM of duplicates of four experiments at five different concentrations. Paired *Student's t-test* $^{*}p < 0.05$, $^{**}p < 0.01$, $^{***}p < 0.001$ with respect to trolox. Unpaired *Student's t-test* $^{\#}p < 0.05$, $^{\#\#}p < 0.01$, with respect to melatonin; $^{\$}p < 0.05$, $^{\$\$}p < 0.01$ between enantiomers.

5.2.5.3 Selective modulation of α7-nAChRs exerted by Family B

With the aim to determine if **69-74** were able to modulate nAChRs response, ACh 100 μM was injected to SH-SY5Y cell line incubated with compounds at 10 μM. Indeed, a significant decrease of fluorescence was observed for all derivatives, with the exception of **(*S*)-72**, **(*R*)-74** and **(*S*)-74**. In general, thiourea derivatives **69-71** tended to block Ca^{2+} entry more efficiently than urea **72-74** derivatives, clearly seeing for **(*R*)-71** and **(*R*)-74**. Nevertheless, both series shared that **70** and **73** (Cl-substituted) presented the lowest

values of relative response to ACh (**Table 13**), compared to **69** and **72** (MeO) or **71** and **74** (unsubstituted). Interestingly, **(*S*)-70** and **(*S*)-73** blocked more than *R* enantiomer, whereas the contrary tendency was observed for other derivatives.

Table 13. Response percentages of **69-74** at 10 μM obtained normalized to agonist ACh at 100 μM in SH-SY5Y and SH-$EP_{\alpha4\beta2}$, compared to agonist PNU282989 and positive allosteric modulator PNU120596 both at 10 μM in SH-SY5Y, which have been normalized 100% response.

		SH-SY5Y	$SH\text{-}EP_{\alpha4\beta2}$
Cpd	**% Relative response ACh (100 μM)**	**%Relative response PNU28+PNU12 (10 μM)**	**% Relative response ACh (100 μM)**
Meca	$52.7 \pm 6.8^{*}$	-	$86.8 \pm 2.5^{*}$
MLA	$69.1 \pm 7.4^{*}$	$6.6 \pm 0.9^{***}$	-
(*R*)-69	$62.3 \pm 2.4^{***}$	$2.7 \pm 0.9^{***}$	97.4 ± 7.7
(*S*)-69	$68.8 \pm 6.5^{*}$	$3.0 \pm 1.2^{***}$	98.4 ± 9.3
(*R*)-70	$60.4 \pm 5.2^{**}$	$1.8 \pm 0.4^{***}$	102.0 ± 8.4
(*S*)-70	$37.7 \pm 12.5^{*}$	$2.2 \pm 0.6^{***}$	105.7 ± 8.1
(*R*)-71	$56.8 \pm 12.1^{*}$	$3.2 \pm 1.4^{***}$	97.5 ± 5.1
(*S*)-71	$77.6 \pm 4.0^{**}$	$3.0 \pm 0.8^{***}$	94.1 ± 5.6
(*R*)-72	$82.6 \pm 5.5^{*}$	$2.7 \pm 0.3^{***}$	97.1 ± 9.0
(*S*)-72	88.6 ± 4.9	$3.2 \pm 0.2^{***}$	96.1 ± 16.2
(*R*)-73	$73.0 \pm 5.5^{*}$	$2.0 \pm 0.3^{***}$	99.6 ± 4.6
(*S*)-73	$61.7 \pm 8.5^{*}$	$2.1 \pm 0.4^{***}$	96.8 ± 11.6
(*R*)-74	87.2 ± 13.1	$30.0 \pm 7.3^{***}$	132.2 ± 20.9
(*S*)-74	87.0 ± 6.4	$2.2 \pm 0.3^{***}$	108.5 ± 10.9

Data are shown as mean ± SEM of duplicates of four independent experiments**.** Paired *Student's t-test*., $^{*}p < 0.05$; $^{**}p < 0.01$;$^{***}p < 0.001$; with respect to agonist.

To evaluate which subtype of receptors were implicated, compounds were tested in SH-EP1 cells overexpressing α4β2 ($SH_{\alpha4\beta2}$) stimulated with ACh at 100 μM. As showed in the **Table 13** none of the compounds change the Ca^{2+} entry compared to agonist. These results demonstrate that these compounds do indicating they do not modulate α4β2-nAChRs, at least at 10 μM.

To verify if the compounds **69-74** were selective for α7 subtype, they were screened adding 10 μM PNU282987 in SH-SY5Y cells 10 minutes after co-incubation of

compounds with PAM PNU120596 at 10 µM. Very successfully, all of them blocked the Ca^{2+} entry in the same extent as MLA, indicating they are able to bind to α7-nAChRs, **Table 13**.

As previously mentioned, when a ligand blocks the effect of an agonist, this effect could be related to an antagonistic or agonistic effect.[58] Since compounds belonging to **Family B** were designed including specifically the quinuclidine moiety to be selective agonists of α7-nAChRs, we explored the agonism concept. SH-SY5Y cells were stimulated with compounds at 30 µM but no increase of fluorescence intensity was produced. By contrast, the fluorescence was extremely increased when concentration-response curves at five concentrations (0.3, 1, 3, 10, 30 µM) were performed in the presence of PNU120596 at 10 µM (**Figure 23**). Such potentiation of signal was completely blocked by MLA (**Figure B1, Appendix B**), indicating the compounds are acting as α7-nAChRs selective agonists.

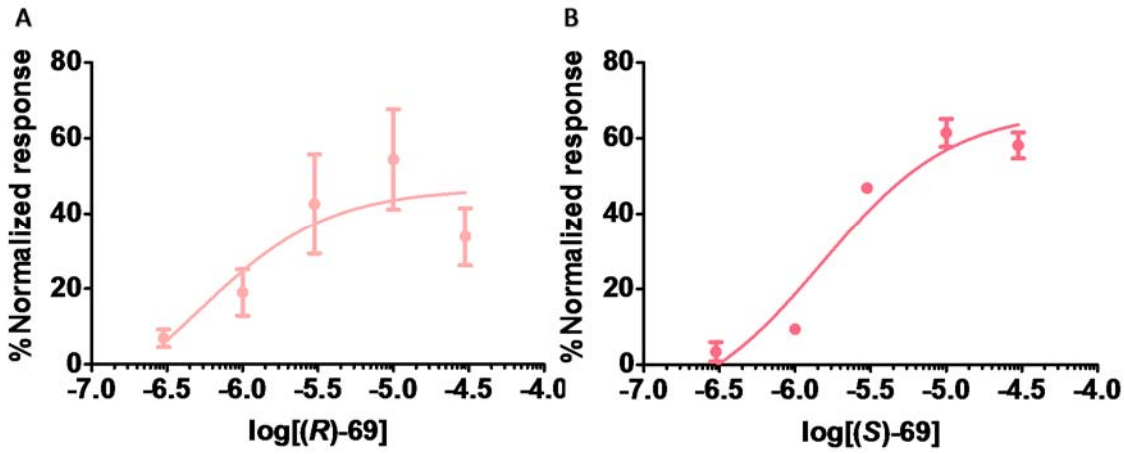

Figure 23. Representative concentration-response curves (0.3 - 30 µM) of thioureas **A) (*R*)-69** and **B) (*S*)-69**, in the presence of PNU120596 (10 µM) normalized to combination of PNU282989 and PNU120596 (both 10 µM) in SH-SY5Y.

Compounds **69-74** activated the α7-nAChRs in a concentration-dependent fashion, with EC_{50} values in the low micromolar range from 1.1 µM of **(*R*)-73** to 11.1 µM of **(*S*)-72** as showed in **Table 14**. However, most of compounds displayed a reduction in Ca^{2+} entry at 30 µM, with the exception of the *S*-enantiomers of MeO derivatives **(*S*)-69** and **(*S*)-72**. Representative concentration-response curves normalized to control agonist PNU282989 are displayed in **Figure 23**, showing that the maximum response of compounds did not reach the 100%, suggesting they are partial agonists.

Table 14. EC_{50} elicited by compounds of **Family B** and derived Hill slope.

Compound	EC_{50} (μM)	Hill Slope
(*R*)-69	2.4 ± 0.1	12.9
(*S*)-69	1.9 ± 0.4	3.1
(*R*)-70	1.2 ± 0.4	7.3
(*S*)-70	1.2 ± 0.2	14.5
(*R*)-71	2.4 ± 0.9	12.8
(*S*)-71	5.2 ± 1.7	4.6
(*R*)-72	3.1 ± 0.2	1.6
(*S*)-72	11.1 ± 3.4	1.7
(*R*)-73	1.1 ± 0.1	10.9
(*S*)-73	2.0 ± 0.3	1.8
(*R*)-74	7.3 ± 3.1	7.5
(*S*)-74	2.1 ± 0.4	1.5

Data are expressed as mean value ± SEM of three independent experiments in SH-SY5Y.

5.2.5.4 Docking study of (*S*)-69 on α7-nAChRs

Similarly to compounds of **Family A** we tried to elucidate the binding mode of **Family B** derivatives to the orthosteric site of the α7-nAChR. **(*S*)-69** was selected as hit compound because of its response-concentration dependency, low EC_{50} and low toxicity values. For this purpose, we followed a similar consensus docking approach discussed in *Section 4.1.3*, using the same homology model of the ECD of α7-nAChR. Only differences were introduced in the AD4 searching algorithm by increasing a logarithmic unit the maximum number of energy evaluations and modifying the number of runs from 10 to 50. These modifications were necessary due to the lack of a consensus pose between Glide and AD4 with the parameters previously employed for compounds of **Family A**.

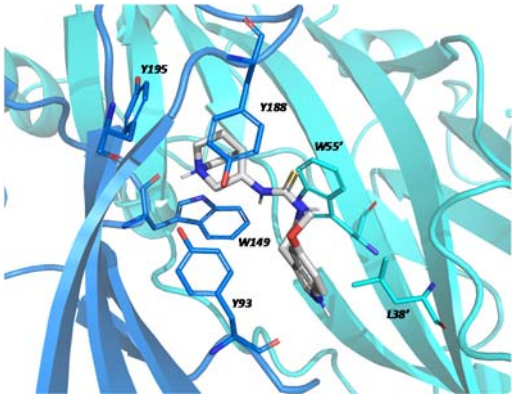

Figure 24. Predicted binding mode of **(*S*)-69** by docking. Residues in close proximity to the ligand are labelled and its interactions discussed in the text.

Following this approach, we were able to reach a unique predicted binding pose (**Figure 24**). Our study suggests that compound **(*S*)-69** places the charged tertiary amine in a similar spatial location than the one found for several nAChR ligands that have been crystallized with AChBP.[211,168,167]In detail, quinuclidine is disposed close to Y93 hydroxyl, W149 carbonyl oxygen and indole as well as to Y195 aromatic sidechain. There, the charged amine could interact via cation-π interactions with the aromatic residues or establish H-bonds with the backbone carbonyl oxygens, interactions that have been found in ligands of nAChR and have been proposed as critical for the interaction of these compounds, as mentioned earlier. Also, hydrophobic interactions are found between the quinuclidine and Y188 sidechain. The thiourea linker does not establish any interaction but due to its location, it could be expected to stabilize the interaction with the α7-nAChR by means of amide NH-π interactions with Y93 and W55'. Finally, the indole moiety is placed in a hydrophobic hall conformed by L38' and Y93 sidechain. A similar position for the indole moiety was predicted in the docking study for dextrorotatory **(+)-** compounds of **Family A**. However, molecular dynamics simulations conducted on compound **(+)-54** showed that these interactions were not stable, with the indole group exhibiting a high mobility and thus, suggesting that it is not a critical element for the binding.

5.2.5.5 Family B compounds present an encouraging neuroprotective profile

Compounds of the second generation despite they did not unfortunately exhibit Nrf2 induction, they conserved the greater scavenger capacity as compounds of first

generation. Furthermore, they were able to modulate cholinergic system by activating α7-nAChRs. Thus, to verify that the combination of those activities could rescue neuronal death, the neuroprotective profile of compounds was assessed following the same protocols as used for **Family A**, the oxidative stress and tau hyperphosphorylation models.

Prior to those studies, *per se* toxicity of the compounds was evaluated in SH-SY5Y during 24 h. LC_{50} values were obtained from the concentration-response curves ranged from 1 to 30 μM. Fortunately, the new compounds showed low toxicity as LC_{50} was higher than 30 μM. Only Cl-substituted thioureas **70** presented more toxicity with LC_{50} 22.0 ± 1.4 μM for **(*R*)-70** and 19.0 ± 1.0 for **(*S*)-70**, having no differences between them. Henceforth, all compounds were tested at 1 μM.

5.2.5.5.1 Oxidative stress model:

Given that the compounds were ROS scavengers, neuroprotection studies against OS conditions were performed. Treatment of SH-SY5Y cell line with a combination concentration of R/O 30 μM and 10 μM, respectively, for 24 h. When pre-incubated compounds at 10 μM for 24 h before R/O addition, and co-incubating with it 24 h after, an increase of cell viability was observed. All compounds achieved a significant protection against the injury induced by R/O, ranging from 21 % of **(*R*)-72** to 50 - 55 % for chloride thioureas **(*R*)-70** and **(*S*)-70**, respectively, **Table 15**. However, they do not differ from melatonin. In the urea series, there is a tendency of different neuroprotection activity regarding the substituent bearing in the indole, in the following *in crescendo* order: MeO containing ureas **72** < Cl-containing ureas **73** < unsubstituted ureas **74**. Furthermore, in both series, MeO derivatives showed the lower values. No statistically significant differences were observed between enantiomers.

Table 15. Percentage of survival and neuronal protection produced by compounds and melatonin, at 1 μm against toxic cocktail rotenone 30 μM and oligomycin A 10 μM as oxidative stress model, and against okadaic acid 20 nM, as tauophaty model.

Compound	RO Pre- & Co-incubation		OA Pre- & Co-incubation	
	%Survival	%Protection	%Survival	%Protection
Basal	100		100	
Toxic	49.8 ± 3.8$^{###}$		55.8 ± 4.1$^{###}$	
Melatonin	72.0 ± 6.0***	46 ± 13	82.5 ± 4.8***	62 ± 11
(*R*)-69	61.8 ± 3.6**	23 ± 5	86.8 ± 2.6***	63 ± 7
(*S*)-69	62.4 ± 0.3**	34 ± 13	90.2 ± 6.1***	76 ± 19
(*R*)-70	77.1 ± 11.1**	55 ± 21	91.4 ± 6.7***	79 ± 16
(*S*)-70	74.3 ± 10.7**	50 ± 23	76.4 ± 7.9**	50 ± 15
(*R*)-71	75.3 ± 8.4***	52 ± 17	71.1 ± 7.4*	37 ± 8
(*S*)-71	69.1 ± 6.5**	40 ± 14	87.8 ± 6.3**	73 ± 17
(*R*)-72	60.7 ± 2.9**	21 ± 7	89.3 ± 3.7***	79 ± 8
(*S*)-72	64.5 ± 3.2**	29 ± 5	80.6 ± 7.1**	62 ± 15
(*R*)-73	60.7 ± 5.4**	33 ± 5	90.5 ± 8.5***	85 ± 16
(*S*)-73	65.7 ± 2.0**	30 ± 7	82.9 ± 14.8***	74 ± 24
(*R*)-74	71.2 ± 8.8***	41 ± 17	78.1 ± 11.6*	55 ± 23
(*S*)-74	73.1 ± 3.3***	45 ± 16	89.4±18.5	79 ± 38

Data are expressed as mean ± SEM of at least four experiments by triplicate. One way ANOVA Newman Keuls post test $^{###}p < 0.001$; compared to Basal. $*p < 0.05$, $**p < 0.01$; $***p < 0.001$; compared to toxic.

5.2.5.5.2 Tau hyperphosphorylation model:

Similar procedure of pre- and co-incubation treatment of compounds for 24 h and 18 h, respectively, with an OA concentration of 20 nM was carried out in SH-SY5Y cells. Once again, all compounds could successfully revert the toxicity exerted by OA, 44 % of cell death, in the same extent as melatonin, **Table 15**. The survival percentages were slightly higher for MeO and Cl than for unsubstituted compounds, although, again, no significant difference was observed.

Survival percentages of enantiomers of thiourea derivatives **69-71** were comparable between models. Curiously, the enantiomers of urea derivatives showed an opposed potency. For example, *S*-enantiomer of Cl-urea **(*S*)-73** had higher protection percentage, 84 %, than *R* enantiomer **(*R*)-73**, 59 % in oxidative stress model, whereas the opposite occurred in the tauopathy model, **(*R*)-73** 85 % versus **(*S*)-73** 74 %. As the differences were not statistically significant, these might be related with experimental variability.

5.2.6 Discussion of results derived from objective II

The second generation of MTDLs was designed taking into account knowledge obtained from the experiments regarding **Family A** compounds. The main objective was to improve the physicochemical properties to obtain molecules that could be available within brain in their unbound form, to exert their maintained biological activities. For that reason, focused on our main target, α7-nAChRs modulation, we modified our **Family A** in two out of three required pharmacophores: the cationic centre and the HBA linker, keeping the indole moiety invariable. Thus, comparatively to molecules of **Family A**, all the molecules belonging to **Family B** contain a bridged-nitrogen atom and a chiral quaternary carbon, provided by quinuclidine scaffold, included to activate α7-nAChRs.

The diversity of the chemical library comes from the other two elements, HBA linker and HP unit. In the latter, the indole skeleton was maintained from **Family A**, as it provided a potent free radical scavenger activity with antioxidant function similar to melatonin. However, apart from MeO substituent, a typical electron donating group, at

5th position, we decided to incorporate a Cl, as electron withdrawing group, and an unsubstituted indole, to test if electronic differences have an impact on the structure-activity relationship.

Considering that numerous quinuclidine-derived molecules have been reported with many different HBA groups, apart from including already known linkers like ureas, we included less common HBA linkers such as thioureas, since they have been reported as a critical group for metal chelation, AChE inhibition and antioxidant properties.[208] Besides, the compounds were designed with the intention, not only to act as HBA for α7-nAChRs, but also to release Nrf2 transcription factor by impeding Keap1-Nrf2 interaction. Additionally, and taking into account that the clinically relevant parameter $K_{p,uu,brain}$ only depends on the HBA capacity of the molecules, these functional groups were included to obtain compounds with variable number of HBAs, from one to three. Hence, it would be expected that the derivatives with less number of HBA, have minor possibilities of interaction with efflux transporters and, therefore, have higher $K_{p,uu,brain}$.[203]

Additionally, flexibility, described in terms of number of RB, together with HBA, affects TPSA, which has a better correlation to BBB permeation than classically described lipophilicity.[210] In this regard, molecules belonging to **Family B** have TPSA values in the optimal range described for CNS drugs, lower than 60-70 $Å^2$.[161] In the optimal range for CNS drugs are also their clogP (2.05-3.06) values (**Table 11**). Conversely to **Family A** hits, clogP are markedly minor, favouring not only water solubility, but also making **69-74** less prone to non-specific binding, mainly affecting $V_{u,brain}$ parameter. Regarding intra-cellular distribution, it is most likely that derivatives from **Family B** can accumulate inside cells, since they are basic compounds, especially ureas **72-74**. The overall view of physicochemical properties led us to think that the second generation of MTDLs could have better brain extent and distribution than first ones.

To carry out the synthesis of quinuclidine-derived MTDLs, a short synthetic route and availability of starting materials were taken into consideration to facilitate the subsequent synthetic scale up, in case that some of them result interesting for further preclinical and clinical investigations. Thus, by combining enantiomerically pure 3-amino-quinuclidines with 5-substituted-tryptamines through different linkers, a wide variety of compounds in a short step process could be obtained. The outlined synthesis

was similar for both derivatives, thioureas and ureas, involving a two-step process. First, the preparation of isothiocyanates **63-65** and carbonylimidazolides **66-68** intermediates, gave comparable fast reactions and moderate to good yields, indicating they are suitable for the synthesis of a wide variety of these compounds. The generation of these highly reactive electrophiles, allowed the reaction with the nucleophilic primary amine of 3-aminoquinuclidine **59**, affording low to moderate yields for ureas **72-74** (25 % - 68 %) (**Scheme 10**) and slightly better for thioureas **69-71** (32 % - 85 %) (**Scheme 9**).

The evaluation of the ability of compounds to induce Nrf2.EpRE pathway was conducted in AREc32 cell line. Unfortunately, the CD values obtained from concentration-response curves were above 60 μM. The lack of the electrophilic component, made ureas **72-74** and thioureas **69-71** less toxic in this cell line in comparison to **Family A** compounds. Thus, we cannot discard the potential action of them as Nrf2-EpRE inducers by non-electrophilic activation as PPI inhibitors.[212] The lack of activity might be related to the fact that none of the compounds shows a bifunctional aromatic moiety, as demonstrated for other known PPI inhibitors. Thus, considering the interesting pharmacological properties of our novel design, we can modify our derivatives to insert new substitution patterns to achieve this activity. Novel designs are already proposed and will be developed in further investigations.

Although **69-74** were not capable to induce Nrf2 and promote the expression of antioxidant molecules, **Family B** compounds showed a potent free radical scavenger capacity (**Table 12**), likewise melatonin and **Family A** compounds (**Table 4**). There was no difference between neither thioureas and ureas linkers, nor the substitution in the indole ring, indicating that the driving force of the radical chain reactions is the indole scaffold, as occurs in the "melatonin antioxidant cascade".[100]

Comparatively to **Family A**, **Family B** maintained the activity of α7-nAChRs modulation. When SH-SY5Y cells were stimulated by ACh in the presence of compounds **69-74**, a partial decrease of Ca^{2+} intracellular signal was observed, (**Table 13)**. Similarly to **Family A**, when PNU282989 was used in the presence of PAM PNU120596, a practically total reduction of fluorescence signal was achieved by all **Family B** compounds, in the same extent as MLA. Taking advantage of the knowledge acquired with **Family A**, we decided to perform response-concentration curves of each conpound

in the absence and presence of PNU120596 and MLA. The selectivity of **Family B** was confirmed by two facts, since we only could observe intracellular Ca^{2+} increase co-incubating cells previously with PAM PNU129605, as without it, that signal was not appreciated **(Figure B1, Appendix B)**, and by the use of a specific antagonist of α7-nAChRs, MLA, which decreasead the aforementioned signal, to zero **(Figure B1, Appendix B)**. Hence, they showed an agonistic behaviour with EC_{50} values in the low micromolar range (1.1 to 11.1 μM, **Table 14**). The lowest values (~1.0 μM) were indistinctly observed for the derivatives with a substituent at fifth position of the indole, both thioureas and ureas, as well as both enantiomers. Curiously, only three high EC_{50} values were obtained for urea (Cl) **(*S*)-72** (11.1 μM), urea (H) **(*R*)-74** (7.3 μM) and thiourea (H) **(*S*)-72** (5.2 μM).

Regarding the *in silico* studies, our docking analysis suggest that compound **(*S*)-69** interacts with α7-nAChR orthosteric site mainly via the quinuclidine ring containing the tertiary amine. This result was expected, since α7-nAChR known ligands, like PNU282989, contain the same moiety (**Figure 21**) or a similar one, such as nicotine and epibatidine (**Figure 20**) with a basic amine as the common pattern. Indeed, quinuclidine is located in the same region with a pose similar to that of **(+)-54**, being the utmost importance the cation - π interactions between the charged nitrogen and the aryl rings of W145 and Y188. However, with the disposition adopted by the thiourea and indole groups, no interactions between those groups and receptor were appreciated. Therefore, since only one intense interaction was presumably obtained with the quinuclidine moiety, it could explain the similar EC_{50} values determined, indicating same potency for all derivatives of **Family B**. The EC_{50} values were much higher than PNU282987, ABT-107 or TC-5619 (**Figure 21**), but in the same range as ABBF, which demonstrated to improve memory and cognitive processes with no addictive effects.[213] Thus, with these encouraging comparisons, the potency of our compounds could be enough to activate α7-nAChRs *in vivo*.

Finally, we were interested in assessing whether, despite losing Nrf2 induction activity, **Family B** compounds maintained the neuroprotective properties previously seen in **Family A** derivatives. Indeed, all compounds prevented cell death from oxidative stress and tauopathy. Comparing results from both models, **Family B** compounds displayed

higher neuroprotection values in the tau hyperphosphorylation pathology model, where differences between thioureas **69-71** and ureas **72-74** were hardly appreciated (**Table 15**). By contrast, slightly better percentages were obtained for thioureas **70** and **71** than for comparative ureas **73** and **74**, most probably because of they can act as direct ROS scavengers.[214]

The neuroprotectant activity of **Family B** derivatives is comparable to the **Family A** compounds, having even greater values in the tauophaty model. Thus, these outcomes might confirm that the agonism exerted by **69-74** over α7-nAChRs, would be enough to activate the pro-survival Jak2/PI3K/Akt signalling pathway. Moreover, it could indirectly induces Nrf2 nuclear translocation, leading to the expression of the endogen antioxidant machinery. In addition to this, and as could be seenI in **Family A** compounds, the indole moiety could bind to MT1 and/or MT2, eliciting the activaction of ERK/MAPK pathway, upregulating pro-survival proteins, preventing neuronal death. Nevertheless, this hypothesis should be further investigated.

In essence, changing the complex tricyclic structure of **Family A** compounds by the bycyclic quinucidine, we achieved a fast synthesis of new molecules with improved physicochemical properties. However, we lost one of the desired activities, the induction of Nrf2. Even so, **Family B** compounds presented a potent free radical scavenger effect and they behave as selective agonists of α7-nAChRs. Apparently, those activities seemed to be enough to display protective actions. In light of these outcomes, **Family B** compounds displayed a promising neuroprotective profile, which encourage us to further explore this strategy, after confirming their better neuro-PK qualities.

6 Conclusions/Conclusiones

The outcomes obtained throughout this Doctoral Thesis, as well as their subsequent analysis and discussion, allow us to establish the following conclusions:

1. The synthesis of **Family A** compounds rationally designed combining different pharmacophores was successfully achieved in a seven-linear step process with good overall yields and *ee*.
2. The complex tricyclic chiral dioxohexahydropyrroloquinoline of **Family A** is described for the first time as key structural motif to exert selective activity over α7-nAChRs.
3. The inclusion of two α,β-unsaturated systems made **Family A** compounds Nrf2 inducers.
4. The introduction of an indole scaffold with substituents present in melatonin provided an excellent free radical scavenger effect in both **Family A** and **Family B** compounds.
5. Compounds with voluminous and lypophilic substituents (Ph **54**, *m*.F-Ph **55** and CyHx **58**) apparently establish more stable interactions with targets, which could explain higher potency of Nrf2 induction, α7-nAChRs modulation, less AChE inhibition and scavenger activity than Pr **56** and CyPr **57.**
6. Dextrorotatory **Family A** enantiomers, displayed better results in almost all activities measured than levorotatory enantiomers. Moreover, there was a dextrorotatory preference in neuro-PK parameters such as $f_{u,plasma}$, $V_{u,brain}$ and $K_{p,uu,cell}$, which determine the differential plasma protein binding and brain disposition of the **Family A** compounds.
7. The neuroPK assessment of **(±)-56** and **(±)-57** showed that they have a very high plasma protein and non-specific brain binding and they are mainly distributed inside brain parenchyma. Nevertheless, $K_{p,uu,brain}$ indicated that **(±)-56** and **(±)-57** were effluxed from brain by unknown active transportation. Therefore, improvement of their physicochemical properties

would be necessary to have enough free compound inside brain able to exert its pharmacological response.

8. The replacement of the tricyclic chiral complex core by a bicyclic quinuclidine, simplified and accelerated the synthesis of **Family B** compounds, improved their physicochemical properties, and maintained the activity on α7-nAChRs, although was detrimental for Nrf2 induction.
9. The promising neuroprotective effect of **Family A** compounds was presumably obtained as a result of the combination of Nrf2/HO-1 induction, implication of PI3K/Akt and ERK1/2 pro-survival signalling pathways mediated by α7-nAChRs and MT1 and/or MT2 activation, respectively. A similar MOA is postulated to explain neuroprotective actions exerted by **Family B** derivatives.

The overall consideration of the outcomes of this Thesis suggests that multitarget combination of α7-nAChR activation, free radical scavenging and antioxidant effect, and Nrf2 induction in a single new molecular entity promotes neuroprotection and could represent a novel class of disease modifying therapies for multifactorial diseases such as AD. In light of results, this would be feasible developing (+)-56 as hit compound, improving its physicochemical properties.

Los resultados obtenidos a lo largo de esta Tesis Doctoral, así como su consiguiente análisis y discusión, nos ha llevado a establecer las siguientes conclusiones:

1. La síntesis de los compuestos de la **Familia A**, diseñada racionalmente combinando diferentes farmacóforos, se llevó a cabo exitosamente mediante un proceso lineal de siete etapas con buenos rendimientos totales y altos *ee*, haciendo factible la aproximación metodológica the hibridación.
2. La compleja estructura tricíclica quiral de dioxohexahidropirroloquinolina de la **Familia A** se describe, por primera vez, como un elemento estructural clave para ejercer actividad sobre los α7-nAChRs selectivamente.
3. La inclusión de dos sistemas α,β-insaturados, hace, a los compuestos de la **Familia A**, inductores de Nrf2.
4. La introducción de un esqueleto de indol con sustituyentes presentes en melatonina, proporciona un excelente efecto secuestrador de radicales libres en los compuestos de ambas **Familia A** y **Familia B**.
5. Los compuestos de la **Familia A** con sustituyentes más lipofílicos y voluminosos en la estructura tricíclica (Ph **54**, *m*.F-Ph **55** and CyHx **58**), establecen, aparentemente, interacciones más estables con las dianas, lo cual podría explicar la mayor potencia de inducción de Nrf2 y modulación de α7-nAChRs, menor inibición de AChE y capacidad secuestradora de radicales que Pr **56** y CyPr **57**.
6. Los enantiómeros dextrorotatorios de la **Familia A**, mostraron mejores resultados en casi todas las actividades medidas que los enantiómeros levorotatorios. Además, también se ha observado que los enantiómeros dextrorotatorios presentaron, preferentemente, mayores valores en los parámetros de neuro-PK como $f_{u,plasma}$, $V_{u,brain}$ y $K_{p,uu,cell}$, lo cual determina que los compuestos de la **Familia A** posean una unión a las proteínas del plasma y una disposición en el cerebro, diferencial.
7. Los compuestos cabeza de serie **(±)-56** y **(±)-57** mostraron una alta afinidad de unión por las proteínas del plasma y proteínas no específicas de cerebro, y se distribuyeron principalmente dentro del parénquima cerebral. Sin

embargo, los bajos valores estimados de $K_{p,uu,brain}$ de **(±)-56** y **(±)-57**, indican que los compuestos son expulsados del cerebro mediante procesos de transporte activo desconocidos, por lo que sería necesario mejorar sus propiedades físicoquímicas para aumentar la cantidad libre de compuesto en cerebro y pueda ejercer su respuesta farmacológica.

8. El reemplazo de la estructura tríciclica quiral por una quinuclidina bicíclica, simplificó la síntesis de los compuestos de la **Familia B**, en dos pasos, mejorando sus propiedades físicoquímicas, y manteniendo la actividad sobre los α7-nAChRs, aunque produjo la pérdida de la actividad de inducción de Nrf2.
9. Los prometedores efectos neuroprotectores de la **Familia A**, son obtenidos, presuntamente, como resultado de la combinación de la inducción de Nrf2/HO-1, y la implicación de las rutas de supervivencia Jak2/PI3K/Akt y ERK/MAPK mediadas por la activación de los receptores α7-nAChRs y MT1 y/o MT2, respectivamente. De forma análoga, se postula un mecanismo de acción similar para explicar las propiedades neuroprotectoras ejercidas por los compuestos de la **Familia B**.

La consideración general de los resultados de esta tesis sugiere que a combinación de la activación de los α7-nAChR, el efecto secuestrador de radicales libres y antioxidante y la inducción de Nrf2 en una única entidad molecular, promueve la neuroprotección y podría representar una nueva clase de terapias modificadora de la enfermedad para enfermedades multifactoriales como la Enfermedad de Alzheimer. A la luz de los resultados, esto sería factible desarrollando (+)-56 como compuesto cabeza de serie, mejorando sus propiedades fisicoquímicas.

7 References

(1) Organization, W. H.; 2015 ed.; WHO Library Cataloguing-in-Publication Data: 2015.

(2) Abellán García, A. A. G., A.; Pujol Rodríguez, R. . Un perfil de las personas mayores en España, 2017. Indicadores estadísticos básicos. *Informes Envejecimiento en red nº 15* [Online Early Access]. Published Online: 2017. (accessed 27/03/2017).

(3) Cipriani, G.; Dolciotti, C.; Picchi, L.; Bonuccelli, U. *Neurological Sciences* **2011**, *32*, 275.

(4) Association, A. s. *Alzheimer's & Dementia: The Journal of the Alzheimer's Association* **2018**, *14*, 367.

(5) Organization, W. H. 2018.

(6) Neurología, S. E. d. 2018; Vol. 05/05/2019.

(7) Cacace, R.; Sleegers, K.; Van Broeckhoven, C. *Alzheimer's & dementia : the journal of the Alzheimer's Association* **2016**, *12*, 733.

(8) Liu, C. C.; Liu, C. C.; Kanekiyo, T.; Xu, H.; Bu, G. *Nature reviews. Neurology* **2013**, *9*, 106.

(9) Association, A. s. 2019.

(10) Braak, H.; Braak, E. *Neurobiology of Aging* **1997**, *18*, 351.

(11) Watkins, P. B.; Zimmerman, H. J.; Knapp, M. J.; Gracon, S. I.; Lewis, K. W. *JAMA* **1994**, *271*, 992.

(12) Lao, K.; Ji, N.; Zhang, X.; Qiao, W.; Tang, Z.; Gou, X. *Journal of drug targeting* **2018**, 1.

(13) Cummings, J.; Lee, G.; Ritter, A.; Zhong, K. *Alzheimer's & dementia* **2018**, *4*, 195.

(14) de Lange, E. C. M.; van den Brink, W.; Yamamoto, Y.; de Witte, W. E. A.; Wong, Y. C. *Expert opinion on drug discovery* **2017**, *12*, 1207.

(15) Auld, D. S.; Kornecook, T. J.; Bastianetto, S.; Quirion, R. *Progress in neurobiology* **2002**, *68*, 209.

(16) Masters, C. L.; Bateman, R.; Blennow, K.; Rowe, C. C.; Sperling, R. A.; Cummings, J. L. *Nature Reviews Disease Primers* **2015**, *1*, 15056.

(17) Sanabria-Castro, A.; Alvarado-Echeverria, I.; Monge-Bonilla, C. *Ann Neurosci* **2017**, *24*, 46.

(18) Bartus, R. T.; Dean, R. L., 3rd; Beer, B.; Lippa, A. S. *Science* **1982**, *217*, 408.

(19) Drachman, D. A.; Noffsinger, D.; Sahakian, B. J.; Kurdziel, S.; Fleming, P. *Neurobiology of Aging* **1980**, *1*, 39.

(20) Mesulam, M. M. *The Journal of comparative neurology* **2013**, *521*, 4124.

(21) Schliebs, R.; Arendt, T. *Behavioural brain research* **2011**, *221*, 555.

(22) Tiveron, C.; Fasulo, L.; Capsoni, S.; Malerba, F.; Marinelli, S.; Paoletti, F.; Piccinin, S.; Scardigli, R.; Amato, G.; Brandi, R.; Capelli, P.; D'Aguanno, S.; Florenzano, F.; La Regina, F.; Lecci, A.; Manca, A.; Meli, G.; Pistillo, L.; Berretta, N.; Nistico, R.; Pavone, F.; Cattaneo, A. *Cell death and differentiation* **2013**, *20*, 1017.

(23) Isacson, O.; Seo, H.; Lin, L.; Albeck, D.; Granholm, A.-C. *Trends in Neurosciences* **2002**, *25*, 79.

(24) Coronel, R.; Bernabeu-Zornoza, A.; Palmer, C.; Muniz-Moreno, M.; Zambrano, A.; Cano, E.; Liste, I. *Molecular neurobiology* **2018**, *55*, 7107.

(25) Hardy, J. A.; Higgins, G. A. *Science* **1992**, *256*, 184.
(26) Panza, F.; Lozupone, M.; Logroscino, G.; Imbimbo, B. P. *Nature reviews. Neurology* **2019**, *15*, 73.
(27) Musiek, E. S.; Holtzman, D. M. *Nature neuroscience* **2015**, *18*, 800.
(28) Herrup, K. *Nature neuroscience* **2015**, *18*, 794.
(29) Iqbal, K.; Alonso Adel, C.; Chen, S.; Chohan, M. O.; El-Akkad, E.; Gong, C. X.; Khatoon, S.; Li, B.; Liu, F.; Rahman, A.; Tanimukai, H.; Grundke-Iqbal, I. *Biochimica et biophysica acta* **2005**, *1739*, 198.
(30) Rao, S. S.; Adlard, P. A. *Frontiers in molecular neuroscience* **2018**, *11*, 276.
(31) Iqbal, K.; Liu, F.; Gong, C. X. *Nature reviews. Neurology* **2016**, *12*, 15.
(32) Braak, H.; Braak, E. *Neurobiol Aging* **1997**, *18*, 351.
(33) Bejanin, A.; Schonhaut, D. R.; La Joie, R.; Kramer, J. H.; Baker, S. L.; Sosa, N.; Ayakta, N.; Cantwell, A.; Janabi, M.; Lauriola, M.; O'Neil, J. P.; Gorno-Tempini, M. L.; Miller, Z. A.; Rosen, H. J.; Miller, B. L.; Jagust, W. J.; Rabinovici, G. D. *Brain : a journal of neurology* **2017**, *140*, 3286.
(34) Kametani, F.; Hasegawa, M. *Frontiers in neuroscience* **2018**, *12*, 25.
(35) Halliwell, B. *eLS* **2015**.
(36) Di Carlo, M.; Giacomazza, D.; Picone, P.; Nuzzo, D.; San Biagio, P. L. *Free Radical Research* **2012**, *46*, 1327.
(37) Valko, M.; Leibfritz, D.; Moncol, J.; Cronin, M. T.; Mazur, M.; Telser, J. *Int J Biochem Cell Biol* **2007**, *39*, 44.
(38) Salim, S. *The Journal of pharmacology and experimental therapeutics* **2017**, *360*, 201.
(39) Prousek, J. In *Pure and Applied Chemistry* 2007; Vol. 79, p 2325.
(40) D, H. *Journal of Gerontology* **1956**, *11*, 298
(41) Bodnar, A. L.; Cortes-Burgos, L. A.; Cook, K. K.; Dinh, D. M.; Groppi, V. E.; Hajos, M.; Higdon, N. R.; Hoffmann, W. E.; Hurst, R. S.; Myers, J. K.; Rogers, B. N.; Wall, T. M.; Wolfe, M. L.; Wong, E. *J Med Chem* **2005**, *48*, 905.
(42) Zhang, J.; Lei, W.; Chen, X.; Wang, S.; Qian, W. *Molecular and clinical oncology* **2018**, *8*, 391.
(43) Nunomura, A.; Perry, G.; Aliev, G.; Hirai, K.; Takeda, A.; Balraj, E. K.; Jones, P. K.; Ghanbari, H.; Wataya, T.; Shimohama, S.; Chiba, S.; Atwood, C. S.; Petersen, R. B.; Smith, M. A. *Journal of Neuropathology & Experimental Neurology* **2001**, *60*, 759.
(44) Gong, C. X.; Liu, F.; Iqbal, K. *Journal of Alzheimer's disease : JAD* **2018**, *64*, S107.
(45) Van der Schyf, C. J. *Expert review of clinical pharmacology* **2011**, *4*, 293.
(46) Cavalli, A.; Bolognesi, M. L.; Minarini, A.; Rosini, M.; Tumiatti, V.; Recanatini, M.; Melchiorre, C. *J Med Chem* **2008**, *51*, 347.
(47) Kumar, A.; Tiwari, A.; Sharma, A. *Current neuropharmacology* **2018**, *16*, 726.
(48) Corradi, J.; Bouzat, C. *Molecular pharmacology* **2016**, *90*, 288.
(49) Sine, S. M.; Engel, A. G. *Nature* **2006**, *440*, 448.
(50) Hurst, R.; Rollema, H.; Bertrand, D. *Pharmacology & therapeutics* **2013**, *137*, 22.

(51) Spurny, R.; Debaveye, S.; Farinha, A.; Veys, K.; Vos, A. M.; Gossas, T.; Atack, J.; Bertrand, S.; Bertrand, D.; Danielson, U. H.; Tresadern, G.; Ulens, C. *Proc Natl Acad Sci U S A* **2015**, *112*, E2543.

(52) Rayes, D.; De Rosa, M. J.; Sine, S. M.; Bouzat, C. *The Journal of neuroscience : the official journal of the Society for Neuroscience* **2009**, *29*, 6022.

(53) Guerra-Alvarez, M.; Moreno-Ortega, A. J.; Navarro, E.; Fernandez-Morales, J. C.; Egea, J.; Lopez, M. G.; Cano-Abad, M. F. *J Neurochem* **2015**, *133*, 309.

(54) Dineley, K. T.; Pandya, A. A.; Yakel, J. L. *Trends Pharmacol Sci* **2015**, *36*, 96.

(55) Shytle, R. D.; Mori, T.; Townsend, K.; Vendrame, M.; Sun, N.; Zeng, J.; Ehrhart, J.; Silver, A. A.; Sanberg, P. R.; Tan, J. *Journal of Neurochemistry* **2004**, *89*, 337.

(56) Egea, J.; Buendia, I.; Parada, E.; Navarro, E.; Leon, R.; Lopez, M. G. *Biochemical pharmacology* **2015**, *97*, 463.

(57) Papke, R. L.; Stokes, C.; Damaj, M. I.; Thakur, G. A.; Manther, K.; Treinin, M.; Bagdas, D.; Kulkarni, A. R.; Horenstein, N. A. *Br J Pharmacol* **2018**, *175*, 1838.

(58) Salahudeen, M. S.; Nishtala, P. S. *Saudi pharmaceutical journal : SPJ : the official publication of the Saudi Pharmaceutical Society* **2017**, *25*, 165.

(59) Kabbani, N.; Nichols, R. A. *Trends in Pharmacological Sciences* **2018**, *39*, 354.

(60) Richardson, B. G.; Jain, A. D.; Speltz, T. E.; Moore, T. W. *Bioorganic & Medicinal Chemistry Letters* **2015**, *25*, 2261.

(61) Cock, J. M.; Sterck, L.; Rouze, P.; Scornet, D.; Allen, A. E.; Amoutzias, G.; Anthouard, V.; Artiguenave, F.; Aury, J. M.; Badger, J. H.; Beszteri, B.; Billiau, K.; Bonnet, E.; Bothwell, J. H.; Bowler, C.; Boyen, C.; Brownlee, C.; Carrano, C. J.; Charrier, B.; Cho, G. Y.; Coelho, S. M.; Collen, J.; Corre, E.; Da Silva, C.; Delage, L.; Delaroque, N.; Dittami, S. M.; Doulbeau, S.; Elias, M.; Farnham, G.; Gachon, C. M.; Gschloessl, B.; Heesch, S.; Jabbari, K.; Jubin, C.; Kawai, H.; Kimura, K.; Kloareg, B.; Kupper, F. C.; Lang, D.; Le Bail, A.; Leblanc, C.; Lerouge, P.; Lohr, M.; Lopez, P. J.; Martens, C.; Maumus, F.; Michel, G.; Miranda-Saavedra, D.; Morales, J.; Moreau, H.; Motomura, T.; Nagasato, C.; Napoli, C. A.; Nelson, D. R.; Nyvall-Collen, P.; Peters, A. F.; Pommier, C.; Potin, P.; Poulain, J.; Quesneville, H.; Read, B.; Rensing, S. A.; Ritter, A.; Rousvoal, S.; Samanta, M.; Samson, G.; Schroeder, D. C.; Segurens, B.; Strittmatter, M.; Tonon, T.; Tregear, J. W.; Valentin, K.; von Dassow, P.; Yamagishi, T.; Van de Peer, Y.; Wincker, P. *Nature* **2010**, *465*, 617.

(62) Shen, J. X.; Yakel, J. L. *Acta pharmacologica Sinica* **2009**, *30*, 673.

(63) Parada, E.; Egea, J.; Romero, A.; del Barrio, L.; Garcia, A. G.; Lopez, M. G. *Free radical biology & medicine* **2010**, *49*, 1815.

(64) Del Barrio, L.; Martin-de-Saavedra, M. D.; Romero, A.; Parada, E.; Egea, J.; Avila, J.; McIntosh, J. M.; Wonnacott, S.; Lopez, M. G. *Toxicological sciences : an official journal of the Society of Toxicology* **2011**, *123*, 193.

(65) Shaw, S.; Bencherif, M.; Marrero, M. B. *The Journal of biological chemistry* **2002**, *277*, 44920.

(66) Kihara, T.; Shimohama, S.; Sawada, H.; Honda, K.; Nakamizo, T.; Shibasaki, H.; Kume, T.; Akaike, A. *The Journal of biological chemistry* **2001**, *276*, 13541.

(67) Arias, E.; Alés, E.; Gabilan, N. H.; Cano-Abad, M. F.; Villarroya, M.; García, A. G.; López, M. G. *Neuropharmacology* **2004**, *46*, 103.

(68) Shen, J.; Wu, J. In *International Review of Neurobiology*; De Biasi, M., Ed.; Academic Press: 2015; Vol. 124, p 275.

(69) Guan, Z. Z.; Zhang, X.; Ravid, R.; Nordberg, A. *J Neurochem* **2000**, *74*, 237.

(70) Hellström-Lindahl, E.; Mousavi, M.; Zhang, X.; Ravid, R.; Nordberg, A. *Molecular Brain Research* **1999**, *66*, 94.

(71) Liu, Q.; Kawai, H.; Berg, D. K. *Proc Natl Acad Sci U S A* **2001**, *98*, 4734.

(72) Yu, W. F.; Guan, Z. Z.; Bogdanovic, N.; Nordberg, A. *Experimental neurology* **2005**, *192*, 215.

(73) Yang, W. N.; Ma, K. G.; Chen, X. L.; Shi, L. L.; Bu, G.; Hu, X. D.; Han, H.; Liu, Y.; Qian, Y. H. *Neuroscience* **2014**, *278*, 276.

(74) Ma, K. G.; Qian, Y. H. *Neuropeptides* **2019**, *73*, 96.

(75) Yang, T.; Xiao, T.; Sun, Q.; Wang, K. *Acta Pharmaceutica Sinica B* **2017**, *7*, 611.

(76) Navarro, E.; Buendia, I.; Parada, E.; Leon, R.; Jansen-Duerr, P.; Pircher, H.; Egea, J.; Lopez, M. G. *Biochemical pharmacology* **2015**, *97*, 473.

(77) Navarro, E.; Gonzalez-Lafuente, L.; Perez-Liebana, I.; Buendia, I.; Lopez-Bernardo, E.; Sanchez-Ramos, C.; Prieto, I.; Cuadrado, A.; Satrustegui, J.; Cadenas, S.; Monsalve, M.; Lopez, M. G. *Antioxid Redox Signal* **2017**, *27*, 93.

(78) Walker, D. P.; Wishka, D. G.; Piotrowski, D. W.; Jia, S.; Reitz, S. C.; Yates, K. M.; Myers, J. K.; Vetman, T. N.; Margolis, B. J.; Jacobsen, E. J.; Acker, B. A.; Groppi, V. E.; Wolfe, M. L.; Thornburgh, B. A.; Tinholt, P. M.; Cortes-Burgos, L. A.; Walters, R. R.; Hester, M. R.; Seest, E. P.; Dolak, L. A.; Han, F.; Olson, B. A.; Fitzgerald, L.; Staton, B. A.; Raub, T. J.; Hajos, M.; Hoffmann, W. E.; Li, K. S.; Higdon, N. R.; Wall, T. M.; Hurst, R. S.; Wong, E. H.; Rogers, B. N. *Bioorganic & medicinal chemistry* **2006**, *14*, 8219.

(79) Bagdas, D.; Wilkerson, J. L.; Kulkarni, A.; Toma, W.; AlSharari, S.; Gul, Z.; Lichtman, A. H.; Papke, R. L.; Thakur, G. A.; Damaj, M. I. *Br J Pharmacol* **2016**, *173*, 2506.

(80) Thomsen, M. S.; Mikkelsen, J. D. *Journal of neuroimmunology* **2012**, *251*, 65.

(81) Ramsey, C. P.; Glass, C. A.; Montgomery, M. B.; Lindl, K. A.; Ritson, G. P.; Chia, L. A.; Hamilton, R. L.; Chu, C. T.; Jordan-Sciutto, K. L. *Journal of Neuropathology & Experimental Neurology* **2007**, *66*, 75.

(82) Buendia, I.; Michalska, P.; Navarro, E.; Gameiro, I.; Egea, J.; Leon, R. *Pharmacology & therapeutics* **2016**, *157*, 84.

(83) Tonelli, C.; Chio, I. I. C.; Tuveson, D. A. *Antioxid Redox Signal* **2018**, *29*, 1727.

(84) Cuadrado, A.; Manda, G.; Hassan, A.; Alcaraz, M. J.; Barbas, C.; Daiber, A.; Ghezzi, P.; Leon, R.; Lopez, M. G.; Oliva, B.; Pajares, M.; Rojo, A. I.; Robledinos-Anton, N.; Valverde, A. M.; Guney, E.; Schmidt, H. *Pharmacological reviews* **2018**, *70*, 348.

(85) Schipper, H. M.; Song, W.; Tavitian, A.; Cressatti, M. *Progress in neurobiology* **2019**, *172*, 40.

(86) Schmidlin, C. J.; Dodson, M. B.; Madhavan, L.; Zhang, D. D. *Free radical biology & medicine* **2019**.

(87) Lastres-Becker, I.; Innamorato, N. G.; Jaworski, T.; Rabano, A.; Kugler, S.; Van Leuven, F.; Cuadrado, A. *Brain : a journal of neurology* **2014**, *137*, 78.

(88) Dinkova-Kostova, A. T.; Fahey, J. W.; Kostov, R. V.; Kensler, T. W. *Trends in food science & technology* **2017**, *69*, 257.

(89) Park, H. M.; Kim, J. A.; Kwak, M. K. *Archives of pharmacal research* **2009**, *32*, 109.

(90) Bergstrom, P.; Andersson, H. C.; Gao, Y.; Karlsson, J. O.; Nodin, C.; Anderson, M. F.; Nilsson, M.; Hammarsten, O. *Neuropharmacology* **2011**, *60*, 343.

(91) Zhang, R.; Miao, Q. W.; Zhu, C. X.; Zhao, Y.; Liu, L.; Yang, J.; An, L. *American journal of Alzheimer's disease and other dementias* **2015**, *30*, 183.

(92) Xu, Z.; Zhang, F.; Sun, F.; Gu, K.; Dong, S.; He, D. *Dimethyl fumarate for multiple sclerosis*, 2015; Vol. 4.

(93) Chaves, C.; Ganguly, R.; Ceresia, C.; Camac, A. *Multiple sclerosis journal - experimental, translational and clinical* **2017**, *3*, 2055217317702933.

(94) Satoh, T.; Kosaka, K.; Itoh, K.; Kobayashi, A.; Yamamoto, M.; Shimojo, Y.; Kitajima, C.; Cui, J.; Kamins, J.; Okamoto, S.; Izumi, M.; Shirasawa, T.; Lipton, S. A. *J Neurochem* **2008**, *104*, 1116.

(95) Marcotte, D.; Zeng, W.; Hus, J. C.; McKenzie, A.; Hession, C.; Jin, P.; Bergeron, C.; Lugovskoy, A.; Enyedy, I.; Cuervo, H.; Wang, D.; Atmanene, C.; Roecklin, D.; Vecchi, M.; Vivat, V.; Kraemer, J.; Winkler, D.; Hong, V.; Chao, J.; Lukashev, M.; Silvian, L. *Bioorganic & medicinal chemistry* **2013**, *21*, 4011.

(96) Pallesen, J. S.; Tran, K. T.; Bach, A. *J Med Chem* **2018**, *61*, 8088.

(97) Lerner, A. B.; Case, J. D.; Takahashi, Y.; Lee, T. H.; Mori, W. *Journal of the American Chemical Society* **1958**, *80*, 2587.

(98) Tan, D. X.; Zheng, X.; Kong, J.; Manchester, L. C.; Hardeland, R.; Kim, S. J.; Xu, X.; Reiter, R. J. *International journal of molecular sciences* **2014**, *15*, 15858.

(99) Balmik, A. A.; Chinnathambi, S. *Journal of Alzheimer's disease : JAD* **2018**, *62*, 1481.

(100) Tan, D. X.; Manchester, L. C.; Terron, M. P.; Flores, L. J.; Reiter, R. J. *Journal of pineal research* **2007**, *42*, 28.

(101) Ekmekcioglu, C. *Biomedicine & pharmacotherapy = Biomedecine & pharmacotherapie* **2006**, *60*, 97.

(102) Romero, A.; Egea, J.; Garcia, A. G.; Lopez, M. G. *Journal of pineal research* **2010**, *49*, 141.

(103) Shi, Y.; Fang, Y. Y.; Wei, Y. P.; Jiang, Q.; Zeng, P.; Tang, N.; Lu, Y.; Tian, Q. *Journal of Alzheimer's disease : JAD* **2018**, *63*, 911.

(104) Wu, Y. H.; Swaab, D. F. *Journal of pineal research* **2005**, *38*, 145.

(105) Wu, Y. H.; Feenstra, M. G.; Zhou, J. N.; Liu, R. Y.; Torano, J. S.; Van Kan, H. J.; Fischer, D. F.; Ravid, R.; Swaab, D. F. *The Journal of clinical endocrinology and metabolism* **2003**, *88*, 5898.

(106) Rosales-Corral, S. A.; Acuna-Castroviejo, D.; Coto-Montes, A.; Boga, J. A.; Manchester, L. C.; Fuentes-Broto, L.; Korkmaz, A.; Ma, S.; Tan, D. X.; Reiter, R. J. *Journal of pineal research* **2012**, *52*, 167.

(107) Zhou, J.; Zhang, S.; Zhao, X.; Wei, T. *Journal of pineal research* **2008**, *45*, 157.

(108) Olcese, J. M.; Cao, C.; Mori, T.; Mamcarz, M. B.; Maxwell, A.; Runfeldt, M. J.; Wang, L.; Zhang, C.; Lin, X.; Zhang, G.; Arendash, G. W. *Journal of pineal research* **2009**, *47*, 82.

(109) Rudnitskaya, E. A.; Muraleva, N. A.; Maksimova, K. Y.; Kiseleva, E.; Kolosova, N. G.; Stefanova, N. A. *Journal of Alzheimer's disease : JAD* **2015**, *47*, 103.

(110) Ali, T.; Kim, M. O. *Journal of pineal research* **2015**, *59*, 47.

(111) Hardeland, R.; Cardinali, D. P.; Brown, G. M.; Pandi-Perumal, S. R. *Progress in neurobiology* **2015**, *127-128*, 46.

(112) Wang, X. *CNS neuroscience & therapeutics* **2009**, *15*, 345.

(113) Giannoulia-Karantana, A.; Vlachou, A.; Polychronopoulou, S.; Papassotiriou, I.; Chrousos, G. P. *Neuroimmunomodulation* **2006**, *13*, 133.

(114) Leon, R.; Jawalekar, A.; Redert, T.; Gaunt, M. J. *Chemical Science* **2011**, *2*, 1487.

(115) Yu, D.; Zhang, Y. *Proc Natl Acad Sci U S A* **2010**, *107*, 20184.

(116) Alhamadsheh, M. M.; Palaniappan, N.; Daschouduri, S.; Reynolds, K. A. *J Am Chem Soc* **2007**, *129*, 1910.

(117) Wang, X. J.; Hayes, J. D.; Wolf, C. R. *Cancer research* **2006**, *66*, 10983.

(118) Cao, G.; Alessio, H. M.; Cutler, R. G. *Free radical biology & medicine* **1993**, *14*, 303.

(119) Ou, B.; Hampsch-Woodill, M.; Prior, R. L. *Journal of agricultural and food chemistry* **2001**, *49*, 4619.

(120) Biedler, J. L.; Helson, L.; Spengler, B. A. *Cancer research* **1973**, *33*, 2643.

(121) Lukas, R. J.; Norman, S. A.; Lucero, L. *Molecular and cellular neurosciences* **1993**, *4*, 1.

(122) McMillan, C. R.; Sharma, R.; Ottenhof, T.; Niles, L. P. *Neuroscience letters* **2007**, *419*, 202.

(123) Eaton, J. B.; Peng, J. H.; Schroeder, K. M.; George, A. A.; Fryer, J. D.; Krishnan, C.; Buhlman, L.; Kuo, Y. P.; Steinlein, O.; Lukas, R. J. *Molecular pharmacology* **2003**, *64*, 1283.

(124) Ellman, G. L.; Courtney, K. D.; Andres, V.; Featherstone, R. M. *Biochemical pharmacology* **1961**, *7*, 88.

(125) Mosmann, T. *Journal of immunological methods* **1983**, *65*, 55.

(126) Kamat, P. K.; Rai, S.; Nath, C. *Neurotoxicology* **2013**, *37*, 163.

(127)

(128) Webb, B.; Sali, A. *Current protocols in bioinformatics* **2016**, *54*, 5 6 1.

(129) Davis, I. W.; Leaver-Fay, A.; Chen, V. B.; Block, J. N.; Kapral, G. J.; Wang, X.; Murray, L. W.; Arendall, W. B., 3rd; Snoeyink, J.; Richardson, J. S.; Richardson, D. C. *Nucleic acids research* **2007**, *35*, W375.

(130) Hooft, R. W.; Vriend, G.; Sander, C.; Abola, E. E. *Nature* **1996**, *381*, 272.

(131) Schrödinger, LLC: New York, NY, 2018.

(132) Harder, E.; Damm, W.; Maple, J.; Wu, C.; Reboul, M.; Xiang, J. Y.; Wang, L.; Lupyan, D.; Dahlgren, M. K.; Knight, J. L.; Kaus, J. W.; Cerutti, D. S.;

Krilov, G.; Jorgensen, W. L.; Abel, R.; Friesner, R. A. *Journal of chemical theory and computation* **2016**, *12*, 281.

(133) Schrödinger, LLC: New York, NY, 2018.

(134) Greenwood, J. R.; Calkins, D.; Sullivan, A. P.; Shelley, J. C. *Journal of computer-aided molecular design* **2010**, *24*, 591.

(135) Friesner, R. A.; Banks, J. L.; Murphy, R. B.; Halgren, T. A.; Klicic, J. J.; Mainz, D. T.; Repasky, M. P.; Knoll, E. H.; Shelley, M.; Perry, J. K.; Shaw, D. E.; Francis, P.; Shenkin, P. S. *J Med Chem* **2004**, *47*, 1739.

(136) Halgren, T. A.; Murphy, R. B.; Friesner, R. A.; Beard, H. S.; Frye, L. L.; Pollard, W. T.; Banks, J. L. *J Med Chem* **2004**, *47*, 1750.

(137) Morris, G. M.; Huey, R.; Lindstrom, W.; Sanner, M. F.; Belew, R. K.; Goodsell, D. S.; Olson, A. J. *Journal of computational chemistry* **2009**, *30*, 2785.

(138) D.A. Case, I.Y. Ben-Shalom, S.R. Brozell, D.S. Cerutti, T.E. Cheatham, III, V.W.D. Cruzeiro, T.A. Darden, R.E. Duke, D. Ghoreishi, M.K. Gilson, H. Gohlke, A.W. Goetz, D. Greene, R Harris, N. Homeyer, S. Izadi, A. Kovalenko, T. Kurtzman, T.S. Lee, S. LeGrand, P. Li, C. Lin, J. Liu, T. Luchko, R. Luo, D.J. Mermelstein, K.M. Merz, Y. Miao, G. Monard, C. Nguyen, H. Nguyen, I. Omelyan, A. Onufriev, F. Pan, R. Qi, D.R. Roe, A. Roitberg, C. Sagui, S. Schott-Verdugo, J. Shen, C.L. Simmerling, J. Smith, R. Salomon-Ferrer, J. Swails, R.C. Walker, J. Wang, H. Wei, R.M. Wolf, X. Wu, L. Xiao, D.M. York and P.A. Kollman University of California, San Francisco., 2018.

(139) Wang, J.; Wolf, R. M.; Caldwell, J. W.; Kollman, P. A.; Case, D. A. *Journal of computational chemistry* **2004**, *25*, 1157.

(140) Maier, J. A.; Martinez, C.; Kasavajhala, K.; Wickstrom, L.; Hauser, K. E.; Simmerling, C. *Journal of chemical theory and computation* **2015**, *11*, 3696.

(141) Jakalian, A.; L. Bush, B.; Jack, D.; Bayly, C. *Journal of computational chemistry* **2000**, *21*, 132.

(142) Wang, J.; Wang, W.; Kollman, P. A.; Case, D. A. *Journal of molecular graphics & modelling* **2006**, *25*, 247.

(143) Roe, D. R.; Cheatham, T. E., 3rd *Journal of chemical theory and computation* **2013**, *9*, 3084.

(144) Humphrey, W.; Dalke, A.; Schulten, K. *Journal of Molecular Graphics* **1996**, *14*, 33.

(145) Tillement, J. P.; Urien, S.; Chaumet-Riffaud, P.; Riant, P.; Bree, F.; Morin, D.; Albengres, E.; Barre, J. *Fundamental & clinical pharmacology* **1988**, *2*, 223.

(146) Hammarlund-Udenaes, M.; Friden, M.; Syvanen, S.; Gupta, A. *Pharm Res* **2008**, *25*, 1737.

(147) Friden, M.; Gupta, A.; Antonsson, M.; Bredberg, U.; Hammarlund-Udenaes, M. *Drug metabolism and disposition: the biological fate of chemicals* **2007**, *35*, 1711.

(148) Loryan, I.; Sinha, V.; Mackie, C.; Van Peer, A.; Drinkenburg, W.; Vermeulen, A.; Morrison, D.; Monshouwer, M.; Heald, D.; Hammarlund-Udenaes, M. *Pharm Res* **2014**, *31*, 2203.

(149) Kalvass, J. C.; Maurer, T. S. *Biopharm Drug Dispos* **2002**, *23*, 327.

(150) Friden, M.; Ducrozet, F.; Middleton, B.; Antonsson, M.; Bredberg, U.; Hammarlund-Udenaes, M. *Drug metabolism and disposition: the biological fate of chemicals* **2009**, *37*, 1226.

(151) Loryan, I.; Friden, M.; Hammarlund-Udenaes, M. *Fluids Barriers CNS* **2013**, *10*, 6.

(152) Langlois, M.; Meyer, C.; Soulier, J. L. *Synthetic Communications* **1992**, *22*, 1895.

(153) Egea, J.; Buendia, I.; Parada, E.; Navarro, E.; Rada, P.; Cuadrado, A.; Lopez, M. G.; Garcia, A. G.; Leon, R. *Br J Pharmacol* **2015**, *172*, 1807.

(154) Carroll, F. I.; Ma, W.; Deng, L.; Navarro, H. A.; Damaj, M. I.; Martin, B. R. *J Nat Prod* **2010**, *73*, 306.

(155) Gallagher, R.; Chebib, M.; Balle, T.; McLeod, M. D. *Australian Journal of Chemistry* **2015**, *68*, 1834.

(156) Atkinson, A. P.; Baguet, E.; Galland, N.; Le Questel, J. Y.; Planchat, A.; Graton, J. *Chemistry* **2011**, *17*, 11637.

(157) Smirnova, N. A.; Haskew-Layton, R. E.; Basso, M.; Hushpulian, D. M.; Payappilly, J. B.; Speer, R. E.; Ahn, Y. H.; Rakhman, I.; Cole, P. A.; Pinto, J. T.; Ratan, R. R.; Gazaryan, I. G. *Chemistry & biology* **2011**, *18*, 752.

(158) Lipinski, C. A.; Lombardo, F.; Dominy, B. W.; Feeney, P. J. *Advanced drug delivery reviews* **1995**, *46*, 3.

(159) SwissADME 2016.

(160) ChemAxon 2018.

(161) Pajouhesh, H.; Lenz, G. R. *NeuroRx : the journal of the American Society for Experimental NeuroTherapeutics* **2005**, *2*, 541.

(162) Peterson, E. A.; Overman, L. E. *Proc Natl Acad Sci U S A* **2004**, *101*, 11943.

(163) Rouden, J.; Lasne, M. C.; Blanchet, J.; Baudoux, J. *Chem Rev* **2014**, *114*, 712.

(164) Pouységu, L.; Deffieux, D.; Quideau, S. *Tetrahedron* **2010**, *66*, 2235.

(165) Vo, N. T.; Pace, R. D.; O'Hara, F.; Gaunt, M. J. *J Am Chem Soc* **2008**, *130*, 404.

(166) Werber, J.; Wang, Y. J.; Milligan, M.; Li, X.; Ji, J. A. *Journal of pharmaceutical sciences* **2011**, *100*, 3307.

(167) Celie, P. H.; van Rossum-Fikkert, S. E.; van Dijk, W. J.; Brejc, K.; Smit, A. B.; Sixma, T. K. *Neuron* **2004**, *41*, 907.

(168) Li, S. X.; Huang, S.; Bren, N.; Noridomi, K.; Dellisanti, C. D.; Sine, S. M.; Chen, L. *Nature neuroscience* **2011**, *14*, 1253.

(169) Dvir, H.; Silman, I.; Harel, M.; Rosenberry, T. L.; Sussman, J. L. *Chemico-biological interactions* **2010**, *187*, 10.

(170) Darvesh, S.; Hopkins, D. A.; Geula, C. *Nature reviews. Neuroscience* **2003**, *4*, 131.

(171) Gazova, Z.; Soukup, O.; Sepsova, V.; Siposova, K.; Drtinova, L.; Jost, P.; Spilovska, K.; Korabecny, J.; Nepovimova, E.; Fedunova, D.; Horak, M.; Kaniakova, M.; Wang, Z. J.; Hamouda, A. K.; Kuca, K. *Biochimica et biophysica acta. Molecular basis of disease* **2017**, *1863*, 607.

(172) Brandt, R. B.; Laux, J. E.; Yates, S. W. *Biochemical medicine and metabolic biology* **1987**, *37*, 344.

(173) Leon, R.; de los Rios, C.; Marco-Contelles, J.; Huertas, O.; Barril, X.; Luque, F. J.; Lopez, M. G.; Garcia, A. G.; Villarroya, M. *Bioorganic & medicinal chemistry* **2008**, *16*, 7759.

(174) Tanaka, T.; Zhong, J.; Iqbal, K.; Trenkner, E.; Grundke-Iqbal, I. *FEBS letters* **1998**, *426*, 248.

(175) Zhang, Z.; Simpkins, J. W. *Brain research* **2010**, *1359*, 233.

(176) Boettler, U.; Sommerfeld, K.; Volz, N.; Pahlke, G.; Teller, N.; Somoza, V.; Lang, R.; Hofmann, T.; Marko, D. *The Journal of Nutritional Biochemistry* **2011**, *22*, 426.

(177) Browning, C.; Beresford, I.; Fraser, N.; Giles, H. *Br J Pharmacol* **2000**, *129*, 877.

(178) Vlahos, C. J.; Matter, W. F.; Hui, K. Y.; Brown, R. F. *The Journal of biological chemistry* **1994**, *269*, 5241.

(179) Alessi, D. R.; Cuenda, A.; Cohen, P.; Dudley, D. T.; Saltiel, A. R. *The Journal of biological chemistry* **1995**, *270*, 27489.

(180) Rowland, M. T., T. N. *Clinical pharmacokinetics. Concepts and applications.*; Third edition ed.; Lippincott Williams & Wilkins, 1995.

(181) Zhang, F.; Xue, J.; Shao, J.; Jia, L. *Drug Discovery Today* **2012**, *17*, 475.

(182) Abbott, N. J. *Journal of inherited metabolic disease* **2013**, *36*, 437.

(183) Yeleswaram, K.; McLaughlin, L. G.; Knipe, J. O.; Schabdach, D. *Journal of pineal research* **1997**, *22*, 45.

(184) Nakamura, A.; Osonoi, T.; Terauchi, Y. *Journal of diabetes investigation* **2010**, *1*, 208.

(185) Smith, D. A.; Beaumont, K.; Maurer, T. S.; Di, L. *J Med Chem* **2015**, *58*, 5691.

(186) Hasselström, J.; Svensson, J. O.; Säwe, J.; Wiesenfeld-Hallin, Z.; Yue, Q. Y.; Xu, X. J. *Pharmacology & Toxicology* **1996**, *79*, 40.

(187) Gandini, A.; Bartolini, M.; Tedesco, D.; Martinez-Gonzalez, L.; Roca, C.; Campillo, N. E.; Zaldivar-Diez, J.; Perez, C.; Zuccheri, G.; Miti, A.; Feoli, A.; Castellano, S.; Petralla, S.; Monti, B.; Rossi, M.; Moda, F.; Legname, G.; Martinez, A.; Bolognesi, M. L. *Journal of Medicinal Chemistry* **2018**, *61*, 7640.

(188) Affini, A.; Hagenow, S.; Zivkovic, A.; Marco-Contelles, J.; Stark, H. *Eur J Med Chem* **2018**, *148*, 487.

(189) Proschak, E.; Stark, H.; Merk, D. *Journal of Medicinal Chemistry* **2019**, *62*, 420.

(190) Gotoh, H.; Ishikawa, H.; Hayashi, Y. *Org Lett* **2007**, *9*, 5307.

(191) Franzen, J.; Marigo, M.; Fielenbach, D.; Wabnitz, T. C.; Kjaersgaard, A.; Jorgensen, K. A. *J Am Chem Soc* **2005**, *127*, 18296.

(192) Belowich, M. E.; Stoddart, J. F. *Chemical Society reviews* **2012**, *41*, 2003.

(193) Jackson, P. A.; Widen, J. C.; Harki, D. A.; Brummond, K. M. *J Med Chem* **2017**, *60*, 839.

(194) Dinkova-Kostova, A. T.; Massiah, M. A.; Bozak, R. E.; Hicks, R. J.; Talalay, P. *Proc Natl Acad Sci U S A* **2001**, *98*, 3404.

(195) Lo, S. C.; Li, X.; Henzl, M. T.; Beamer, L. J.; Hannink, M. *The EMBO journal* **2006**, *25*, 3605.

(196) Thompson, A. J.; Metzger, S.; Lochner, M.; Ruepp, M. D. *Neuropharmacology* **2017**, *116*, 421.

(197) Bouzat, C.; Sine, S. M. *Br J Pharmacol* **2018**, *175*, 1789.

(198) Alvarez, A.; Alarcón, R.; Opazo, C.; Campos, E. O.; Muñoz, F. J.; Calderón, F. H.; Dajas, F.; Gentry, M. K.; Doctor, B. P.; De Mello, F. G.; Inestrosa, N. C. *The Journal of Neuroscience* **1998**, *18*, 3213.

(199) Luchetti, F.; Betti, M.; Canonico, B.; Arcangeletti, M.; Ferri, P.; Galli, F.; Papa, S. *Free radical biology & medicine* **2009**, *46*, 339.

(200) Seelig, A. *European journal of biochemistry* **1998**, *251*, 252.

(201) Thais, B. F.; Mariana, C. F. S.; Michelle, C. P.; Roberto, P.-F. *Letters in Drug Design & Discovery* **2016**, *13*, 999.

(202) Hammarlund-Udenaes, M.; Bredberg, U.; Friden, M. *Current Topics in Medicinal Chemistry* **2009**, *9*, 148.

(203) Friden, M.; Winiwarter, S.; Jerndal, G.; Bengtsson, O.; Wan, H.; Bredberg, U.; Hammarlund-Udenaes, M.; Antonsson, M. *J Med Chem* **2009**, *52*, 6233.

(204) Loryan, I.; Sinha, V.; Mackie, C.; Van Peer, A.; Drinkenburg, W. H.; Vermeulen, A.; Heald, D.; Hammarlund-Udenaes, M.; Wassvik, C. M. *Molecular pharmaceutics* **2015**, *12*, 520.

(205) Rutkowska, E.; Pajak, K.; Jozwiak, K. *Acta poloniae pharmaceutica* **2013**, *70*, 3.

(206) Mazurov, A.; Hauser, T.; Miller, C. H. *Current medicinal chemistry* **2006**, *13*, 1567.

(207) Horenstein, N. A.; Leonik, F. M.; Papke, R. L. *Molecular pharmacology* **2008**, *74*, 1496.

(208) Li, X.; Wang, H.; Lu, Z.; Zheng, X.; Ni, W.; Zhu, J.; Fu, Y.; Lian, F.; Zhang, N.; Li, J.; Zhang, H.; Mao, F. *J Med Chem* **2016**, *59*, 8326.

(209) Kim, Y. J.; Ryu, J. H.; Cheon, Y. J.; Lim, H. J.; Jeon, R. *Bioorg Med Chem Lett* **2007**, *17*, 3317.

(210) Trippier, P. C. *Current medicinal chemistry* **2016**, *23*, 1392.

(211) Delbart, F.; Brams, M.; Gruss, F.; Noppen, S.; Peigneur, S.; Boland, S.; Chaltin, P.; Brandao-Neto, J.; von Delft, F.; Touw, W. G.; Joosten, R. P.; Liekens, S.; Tytgat, J.; Ulens, C. *The Journal of biological chemistry* **2018**, *293*, 2534.

(212) Richardson, B. G.; Jain, A. D.; Speltz, T. E.; Moore, T. W. *Bioorg Med Chem Lett* **2015**, *25*, 2261.

(213) Boess, F. G.; De Vry, J.; Erb, C.; Flessner, T.; Hendrix, M.; Luithle, J.; Methfessel, C.; Riedl, B.; Schnizler, K.; van der Staay, F. J.; van Kampen, M.; Wiese, W. B.; Koenig, G. *The Journal of pharmacology and experimental therapeutics* **2007**, *321*, 716.

(214) Kelner, M. J.; Bagnell, R.; Welch, K. J. *The Journal of biological chemistry* **1990**, *265*, 1306.

8 Annexes

Appendix A.

Table A1. Retention times, peak area, *ee*, optical rotation and purities of final compounds. In the first case, I performed the measurements by employing an Agilent Technologies 1220 Infinity LC VL G4288C UV-Vis wavelength detector with a ULTRON ES OVM chiral analytical reverse phase column, 5µm of diameter, 4.6 mm x 150 L, KH_2PO_4 buffer pH 4.3/ MeOH 70:30 as mobile phase with a flow rate of 1.0 mL/min and wavelength at 230 nm. In the second case, HPLC 1100 Agilent Technologies Diodo-Array detector system using a Zorbax Extend C18 15 cm x 4.6 mm reverse phase column, with a UV detector at 254 nm, coupled to a mass spectrometer was employed from the "Servicio Interdepartamental de Investigación (SIdI)" of Universidad Autónoma de Madrid.

Compound	T_{Rmajor} (min)	Area (%)	T_{Rminor} (min)	Area (%)	*ee* (%)	α_D (°) (c.mg/mL)	Purity (%)
(±)-54	2.983	65.67	3.813	34.33	31	-	100
(-)-54	3.787	94.30	3.167	5.70	89	- 90.5 (0.95)	100
(+)-54	2.977	93.62	3.607	6.38	87	+ 124.6 (0.65)	100
(±)-55	3.150	52.24	3.530	47.76	4	-	99
(-)-55	3.487	95.59	3.180	4.20	91	- 100.0 (1.30)	100
(+)-55	3.203	94.54	3.637	5.46	89	+ 50.0 (0.75)	93
(±)-56	4.113	54.93	2.823	44.67	10	-	99
(-)-56	4.300	92.26	3.040	7.74	85	- 113.8 (0.80)	100
(+)-56	2.960	94.08	4.613	5.92	88	+ 145.5 (0.55)	95
(±)-57	2.963	50.51	7.207	49.49	1	-	99
(-)-57	2.993	4.16	5.970	95.84	92	- 106.7 (0.75)	99
(+)-57	2.953	92.94	7.347	7.06	86	+ 107.1 (0.70)	99
(±)-58	4.423	73.15	6.030	26.85	46	-	100
(-)-58	5.313	91.80	4.300	8.20	84	- 103.3 (0.90)	97
(+)-58	4.147	90.46	5.693	9.54	81	+ 65.5 (1.10)	100

Table A2. *Per se* toxicity in AREc32 cell line incubated during 24 h.

Compound	1 µM	5 µM	10 µM	15 µM	LC_{50} (µM)
(±)-54	77.2 ± 5.0	71.4 ± 5.7	59.3 ± 4.6	57.6 ± 5.0	> 15
(-)-54	72.8 ± 5.9	74.5 ± 6.4	60.6 ± 5.2	47.6 ± 3.7	12.0 ± 3.6
(+)-54	72.0 ± 7.1	79.6 ± 5.0	64.8 ± 6.3	50.7 ± 5.9	> 15
(±)-55	92.4 ± 8.8	92.9 ± 7.4	59.2 ± 4.9	59.3 ± 2.2	>15
(-)-55	62.3 ± 3.5	72.4 ± 5.3	70.5 ± 8.2	53.6 ± 2.2	>15
(+)-55	93.4 ± 6.4	94.8 ± 3.3	62.2 ± 3.8	46.5 ± 1.9	13.1 ± 0.6
(±)-56	76.1 ± 10.2	94.5 ± 4.6	85.2 ± 3.2	69.0 ± 4.2	> 15
(-)-56	90.1 ± 9.1	86.9 ± 4.7	82.9 ± 3.6	71.5 ± 3.2	> 15
(+)-56	80.3 ± 7.4	87.1 ± 4.0	87.2 ± 3.2	83.9 ± 5.7	> 15
(±)-57	76.1 ± 2.6	87.1 ± 2.7	83.9 ± 3.0	80.9 ± 4.0	> 15
(-)-57	79.0 ± 12.0	86.4 ± 5.0	90.8 ± 5.2	95.1 ± 3.8	> 15
(+)-57	83.1 ± 3.7	93.0 ± 4.2	84.0 ± 3.5	75.5 ± 4.4	> 15
(±)-58	95.2 ± 2.1	57.3 ± 3.0	35.7 ± 4.8	35.5 ± 1.4	3.2 ± 1.5
(-)-58	83.0 ± 8.6	83.4 ± 5.9	36.3 ± 3.9	26.2 ± 2.1	9.1 ± 1.3
(+)-58	77.1 ± 5.6	72.8 ± 8.8	27.4 ± 1.9	24.4 ± 1.5	7.2 ± 1.9

Data are expressed as mean value ± SEM of at least two experiments by duplicate.

Table A3. *Per se* toxicity of compounds **54-58** in SH-SY5Y cell line incubated during 24h.

Compound	1 µM	10 µM	30 µM	LC_{50} (µM)
(±)-54	81.8 ± 2.4	67.6 ± 15.7	21.2 ± 3.2	14.6 ± 4.4
(-)-54	93.2 ± 3.4	90.0 ± 2.3	18.3 ± 2.7	19.8±0.9
(+)-54	92.6 ± 3.7	80.8 ± 5.0	20.8 ± 2.2	19.3±0.9
(±)-55	91.8 ± 3.0	82.5 ± 4.1	21.4 ± 2.7	19.6±0.6
(-)-55	94.3 ± 2.2	76.2 ± 7.5	20.7 ± 3.2	17.8±1.6
(+)-55	94.5 ± 2.3	91.1 ± 5.9	22.2 ± 2.7	20.9±1.2
(±)-56	99.5 ± 2.4	94.6 ± 2.9	65.1 ± 12.5	>30
(-)-56	97.6 ± 11.9	97.5 ± 0.4	61.5 ± 22.7	>30
(+)-56	96.4 ± 3.5	93.3 ± 2.7	75.8 ± 3.3	>30
(±)-57	95.8 ± 5.4	102.2 ± 2.5	91.9 ± 3.2	>30
(-)-57	99.0 ± 6.8	94.1 ± 3.2	87.0 ± 6.8	>30
(+)-57	96.8 ± 1.1	100.2 ± 9.1	80.5 ± 2.9	>30
(±)-58	99.4 ± 1.6	54.5 ± 13.5	18.3 ± 0.3	11.8±4.6
(-)-58	95.5 ± 5.3	19.9 ± 2.4	17.2 ± 1.2	2.1±0.2)
(+)-58	101.0 ± 3.0	22.9 ± 2.2	18.8 ± 0.4	2.4±0.1

Data are expressed as mean value ± SEM of at least three experiments by triplicate.

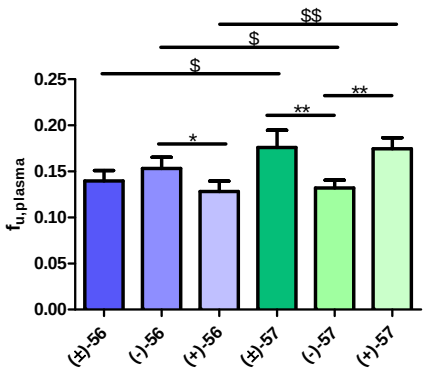

Figure A1. Unbound fraction in plasma for **56** (Pr) and **57** (CyPr) as mean value ± standard deviation of four replicates. One way ANOVA Newman-Keuls post-test was performed within same series. $^{*}p < 0.05$, $^{**}p < 0.01$. Unpaired *Student's t-test* was performed between derivatives $^{\$}p < 0.05$, $^{\$\$}p < 0.01$.

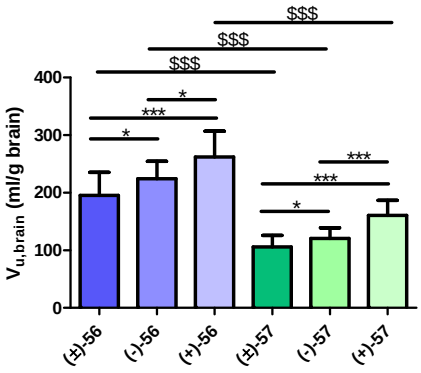

Figure A2. Volume of distribution in brain expressed in ml/g brain for propyl derivatives **56** (Pr) and **57** (CyPr) expressed in mean value ± standard deviation. One way ANOVA Newman-Keuls post-test was performed within derivative series, $^{*}p < 0.05$, $^{***}p < 0.001$. Unpaired *Student's t-test* performed between derivatives $^{\$}p < 0.05$, $^{\$\$\$}p < 0.001$.

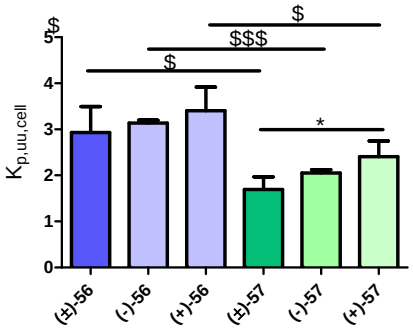

Figure A3. Cell partition coefficient $K_{p,uu,cell}$ for derivatives **56** (Pr) and **57** (CyPr) expressed in mean value ± standard deviation. One way ANOVA Newman-Keuls post-test was performed within derivative series, $^{*}p < 0.05$. Unpaired *Student's t-test* performed between derivatives $^{\$}p < 0.05$, $^{\$\$\$}p < 0.001$.

HPLC DATA

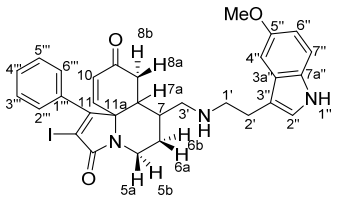

(±)-54

Page 1 of 1

Area % Report

Data File: D:\Enterprise\Projects\Default\Result\SArl1.17rac.rslt\SArl1.17rac.rslt.dat
Method: D:\Enterprise\Projects\Default\Method\sheila meoh 1.met
Acquired: 2/2/2016 6:32:34 PM (GMT +01:00)
Printed: 2/2/2016 7:19:29 PM (GMT +01:00)

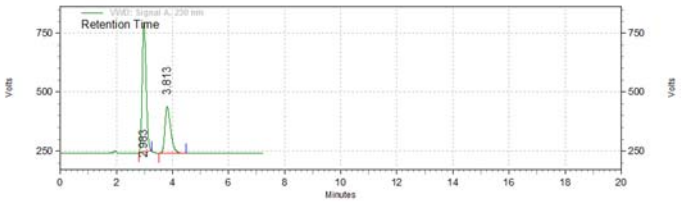

VWD: Signal A, 230 nm Results

Retention Time	Area	Area %	Height	Height %
2.983	89409466	65.67	9211396	73.80
3.813	46734196	34.33	3270641	26.20
Totals	136143662	100.00	12482037	100.00

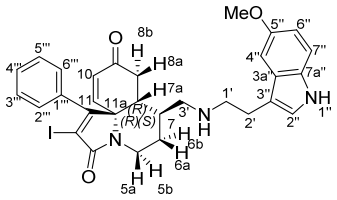

(-)-54

Page 1 of 1

Area % Report

Data File: D:\Enterprise\Projects\Default\Result\SA3.218R.rslt\SA3.218R.rslt.dat
Method: D:\Enterprise\Projects\Default\Method\sheila meoh 30 10'.met
Acquired: 5/26/2016 1:23:39 PM (GMT +02:00)
Printed: 5/26/2016 1:36:38 PM (GMT +02:00)

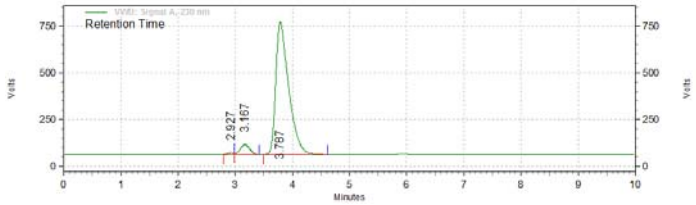

VWD: Signal A, 230 nm Results

Retention Time	Area	Area %	Height	Height %
2.927	1176214	0.60	146066	1.13
3.167	10061676	5.10	891534	6.90
3.787	186003861	94.30	11889744	91.97
Totals	197241751	100.00	12927344	100.00

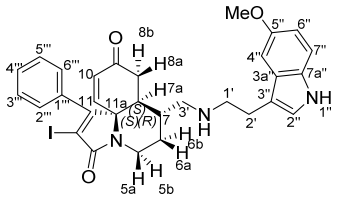

(+)-54

Page 1 of 1

Area % Report

Data File: D:\Enterprise\Projects\Default\Result\SA3.228S.rslt\SA3.228S.rslt.dat
Method: D:\Enterprise\Projects\Default\Method\sheila meoh 30 10'.met
Acquired: 6/8/2016 3:22:15 PM (GMT +02:00)
Printed: 6/8/2016 3:35:29 PM (GMT +02:00)

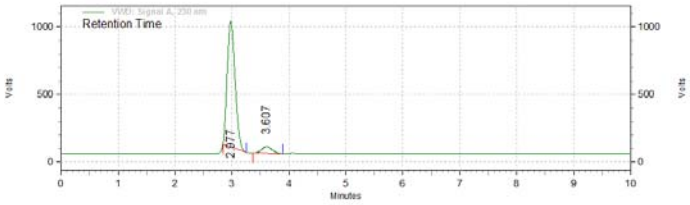

VWD: Signal A, 230 nm Results

Retention Time	Area	Area %	Height	Height %
2.977	149896779	93.62	15581461	94.88
3.607	10213984	6.38	840444	5.12
Totals	160110763	100.00	16421905	100.00

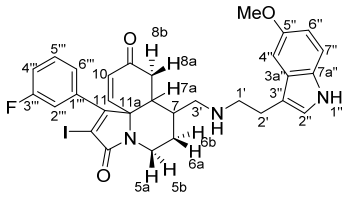

(±)-55

Page 1 of 1

Area % Report

Data File: D:\Enterprise\Projects\Default\Result\SA3.196RAC.rslt\SA3.196RAC.rslt.dat
Method: D:\Enterprise\Projects\Default\Method\sheila meoh 30 10'.met
Acquired: 5/26/2016 2:10:57 PM (GMT +02:00)
Printed: 5/26/2016 2:24:30 PM (GMT +02:00)

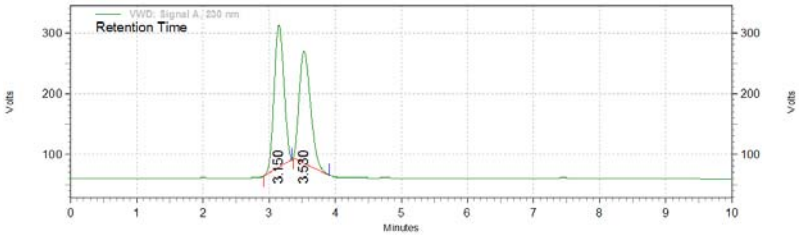

VWD: Signal A, 230 nm Results

Retention Time	Area	Area %	Height	Height %
3.150	40239341	52.24	3917959	55.87
3.530	36783151	47.76	3095021	44.13
Totals	77022492	100.00	7012980	100.00

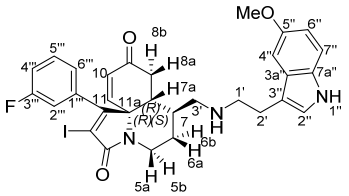

(-)-55

Area % Report

Data File: D:\Enterprise\Projects\Default\Result\SA3.176R.rslt\SA3.176R.rslt.dat
Method: D:\Enterprise\Projects\Default\Method\sheila meoh 30 10'.met
Acquired: 4/7/2016 6:55:19 PM (GMT +02:00)
Printed: 4/7/2016 7:21:28 PM (GMT +02:00)

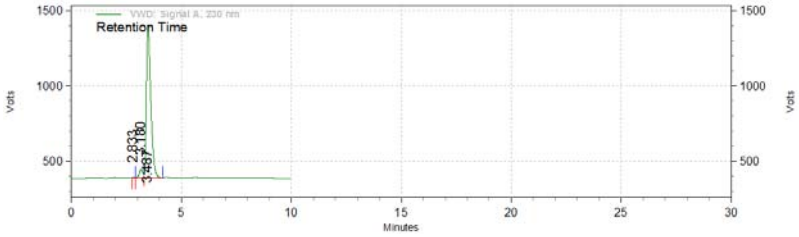

VWD: Signal A, 230 nm Results

Retention Time	Area	Area %	Height	Height %
2.833	505400	0.21	71756	0.40
3.180	10237207	4.20	950538	5.27
3.487	232989234	95.59	16999987	94.33
Totals	243731841	100.00	18022281	100.00

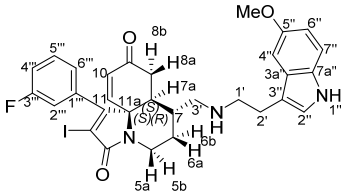

(+)-55

Area % Report

Data File: D:\Enterprise\Projects\Default\Result\SA3.204S.rslt\SA3.204S.rslt.dat
Method: D:\Enterprise\Projects\Default\Method\sheila meoh 30 10'.met
Acquired: 5/6/2016 4:27:41 PM (GMT +02:00)
Printed: 5/6/2016 4:51:42 PM (GMT +02:00)

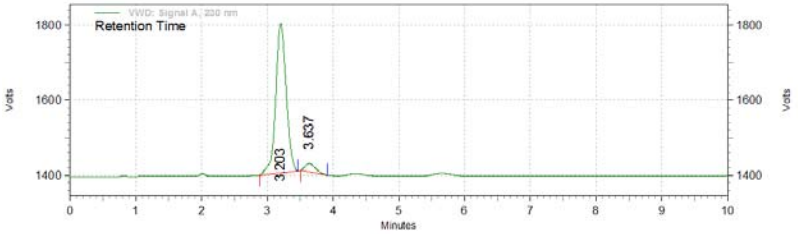

VWD: Signal A, 230 nm Results

Retention Time	Area	Area %	Height	Height %
3.203	73674795	94.54	6646916	94.56
3.637	4251122	5.46	382440	5.44
Totals	77925917	100.00	7029356	100.00

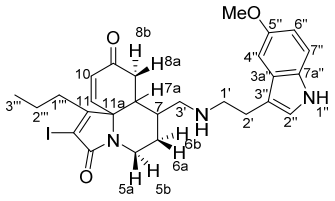

(±)-56

Page 1 of 1

Area % Report

Data File: D:\Enterprise\Projects\Default\Result\SA1.31RAC.rslt\SA1.31RAC.rslt.dat
Method: D:\Enterprise\Projects\Default\Method\sheila meoh 1.met
Acquired: 2/5/2016 4:44:27 PM (GMT +01:00)
Printed: 2/5/2016 5:26:33 PM (GMT +01:00)

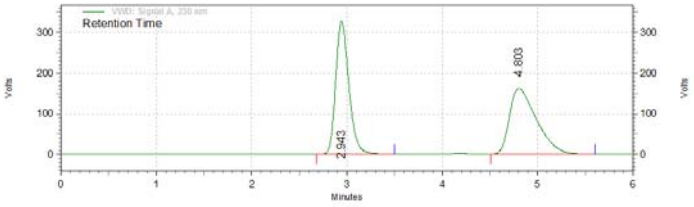

VWD: Signal A, 230 nm Results

Retention Time	Area	Area %	Height	Height %
2.943	53006771	49.74	5482055	66.80
4.803	53552513	50.26	2725110	33.20
Totals	106559284	100.00	8207165	100.00

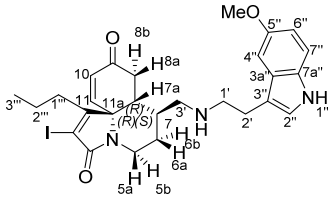

(-)-56

Page 1 of 1

Area % Report

Data File: D:\Enterprise\Projects\Default\Result\SA3.151R.rslt\SA3.151R.rslt.dat
Method: D:\Enterprise\Projects\Default\Method\sheila meoh 30 10'.met
Acquired: 3/3/2016 2:39:54 PM (GMT +01:00)
Printed: 3/3/2016 3:01:04 PM (GMT +01:00)

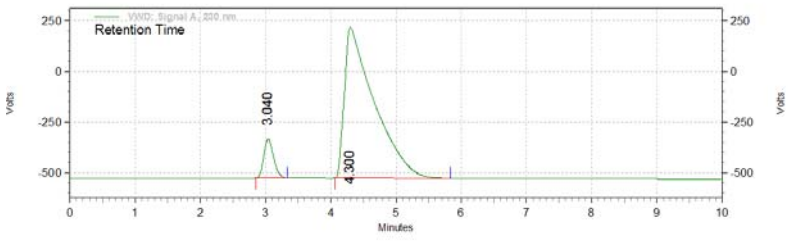

VWD: Signal A, 230 nm Results

Retention Time	Area	Area %	Height	Height %
3.040	33250804	7.74	3211016	20.46
4.300	396271807	92.26	12483742	79.54
Totals	429522611	100.00	15694758	100.00

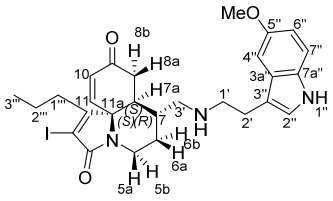

(+)-56

Area % Report

Data File: D:\Enterprise\Projects\Default\Result\SA3.210S.rslt\SA3.210S.rslt.dat
Method: D:\Enterprise\Projects\Default\Method\sheila meoh 30 10'.met
Acquired: 5/26/2016 1:12:21 PM (GMT +02:00)
Printed: 5/26/2016 1:24:47 PM (GMT +02:00)

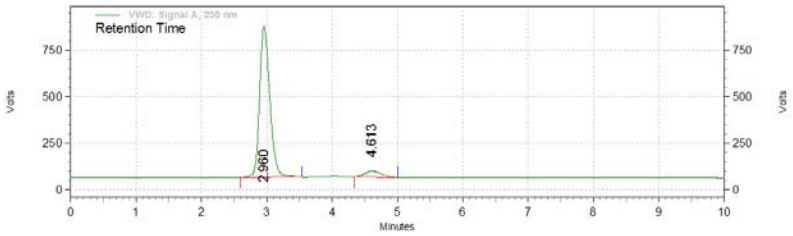

VWD: Signal A, 230 nm Results

Retention Time	Area	Area %	Height	Height %
2.960	148087343	94.08	13686892	96.16
4.613	9320992	5.92	545891	3.84
Totals	157408335	100.00	14232783	100.00

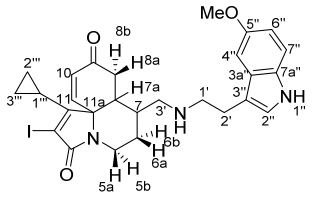

(±)-57

Area % Report

Data File: D:\Enterprise\Projects\Default\Result\SA3.177RAC.rslt\SA3.177RAC.rslt.dat
Method: D:\Enterprise\Projects\Default\Method\sheila meoh 30 10'.met
Acquired: 4/7/2016 6:40:34 PM (GMT +02:00)
Printed: 4/7/2016 6:57:57 PM (GMT +02:00)

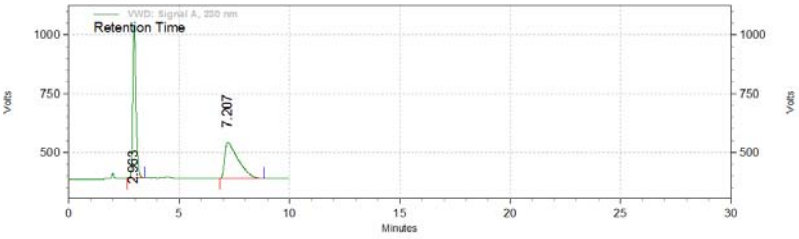

VWD: Signal A, 230 nm Results

Retention Time	Area	Area %	Height	Height %
2.963	111546250	50.51	10904408	80.70
7.207	109293608	49.49	2607821	19.30
Totals	220839858	100.00	13512229	100.00

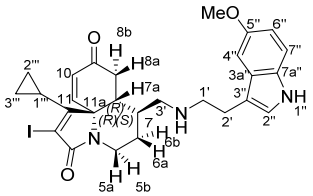

(-)-57

Area % Report

Data File: D:\Enterprise\Projects\Default\Result\SA3.220R.rslt\SA3.220R.rslt.dat
Method: D:\Enterprise\Projects\Default\Method\sheila meoh 30 10'.met
Acquired: 5/26/2016 1:34:47 PM (GMT +02:00)
Printed: 5/26/2016 1:48:38 PM (GMT +02:00)

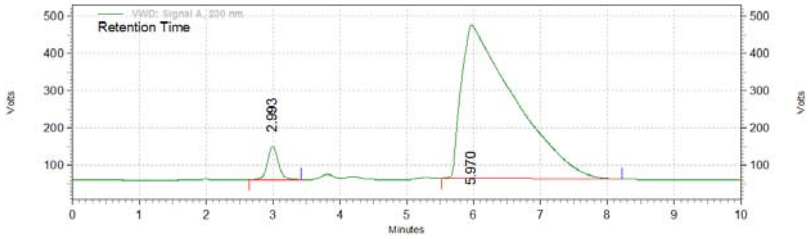

VWD: Signal A, 230 nm Results

Retention Time	Area	Area %	Height	Height %
2.993	16578733	4.16	1494532	17.79
5.970	381620057	95.84	6904920	82.21
Totals	398198790	100.00	8399452	100.00

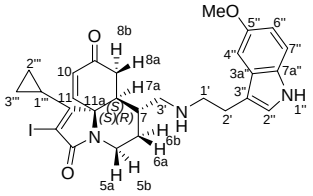

(-)-57

Area % Report

Data File: D:\Enterprise\Projects\Default\Result\SA3.219S.rslt\SA3.219S.rslt.dat
Method: D:\Enterprise\Projects\Default\Method\sheila meoh 30 10'.met
Acquired: 5/26/2016 1:47:41 PM (GMT +02:00)
Printed: 5/26/2016 1:59:17 PM (GMT +02:00)

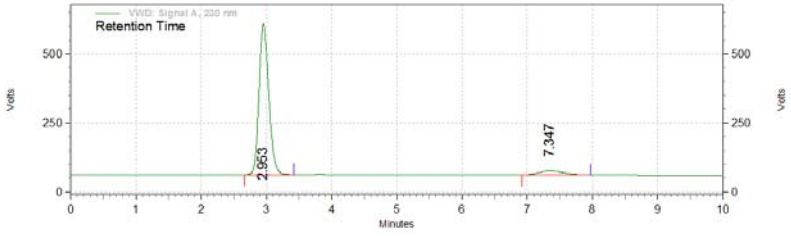

VWD: Signal A, 230 nm Results

Retention Time	Area	Area %	Height	Height %
2.953	95423308	92.94	9169898	97.17
7.347	7245107	7.06	266918	2.83
Totals	102668415	100.00	9436816	100.00

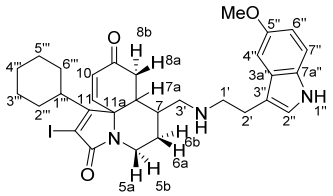

(±)-58

Area % Report

Data File: D:\Enterprise\Projects\Default\Result\SA3.165RAC.rslt\SA3.165RAC.rslt.dat
Method: D:\Enterprise\Projects\Default\Method\sheila meoh 30 10'.met
Acquired: 6/8/2016 3:34:49 PM (GMT +02:00)
Printed: 6/8/2016 3:47:00 PM (GMT +02:00)

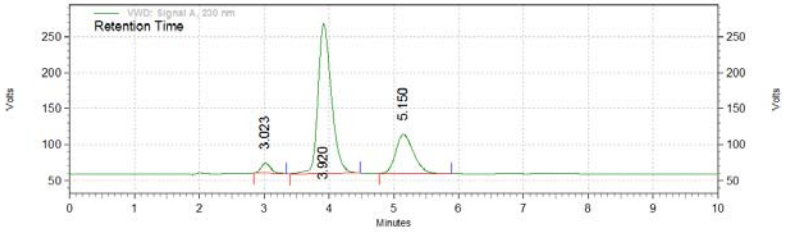

VWD: Signal A, 230 nm Results

Retention Time	Area	Area %	Height	Height %
3.023	2438772	3.49	234857	5.06
3.920	50137923	71.65	3491339	75.19
5.150	17401496	24.87	917166	19.75
Totals	69978191	100.00	4643362	100.00

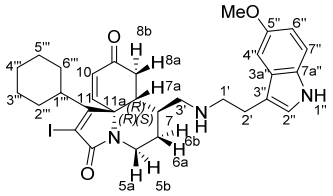

(-)-58

Area % Report

Data File: D:\Enterprise\Projects\Default\Result\SA3.203R.rslt\SA3.203R.rslt.dat
Method: D:\Enterprise\Projects\Default\Method\sheila meoh 30 10'.met
Acquired: 5/6/2016 4:14:38 PM (GMT +02:00)
Printed: 5/6/2016 4:45:18 PM (GMT +02:00)

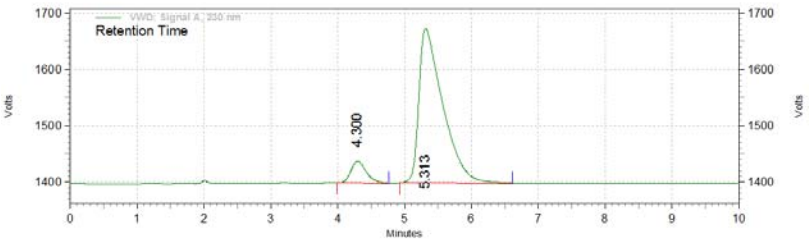

VWD: Signal A, 230 nm Results

Retention Time	Area	Area %	Height	Height %
4.300	10185939	8.20	645356	12.30
5.313	114004817	91.80	4599722	87.70
Totals	124190756	100.00	5245078	100.00

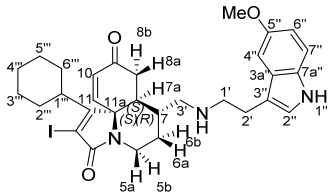

(+)-58

Area % Report

Data File: D:\Enterprise\Projects\Default\Result\SA3.202S.rslt\SA3.202S.rslt.dat
Method: D:\Enterprise\Projects\Default\Method\sheila meoh 30 10'.met
Acquired: 5/6/2016 2:12:53 PM (GMT +02:00)
Printed: 5/6/2016 4:16:22 PM (GMT +02:00)

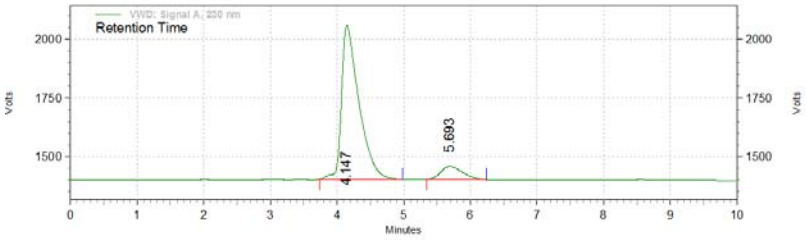

VWD: Signal A, 230 nm Results

Retention Time	Area	Area %	Height	Height %
4.147	199523721	90.46	11015728	92.19
5.693	21052857	9.54	932815	7.81
Totals	220576578	100.00	11948543	100.00

REPRESENTATIVE ^{1}H-NMR AND ^{13}C-NMR SPECTRA

2-iodo-7-(((2-(5-methoxy-1*H*-indol-3-yl)ethyl)amino)methyl)-1-phenyl-6,7,7a,8-tetrahydro-3*H*-pyrrolo[2,1-j]quinoline-3,9(5*H*)-dione 54

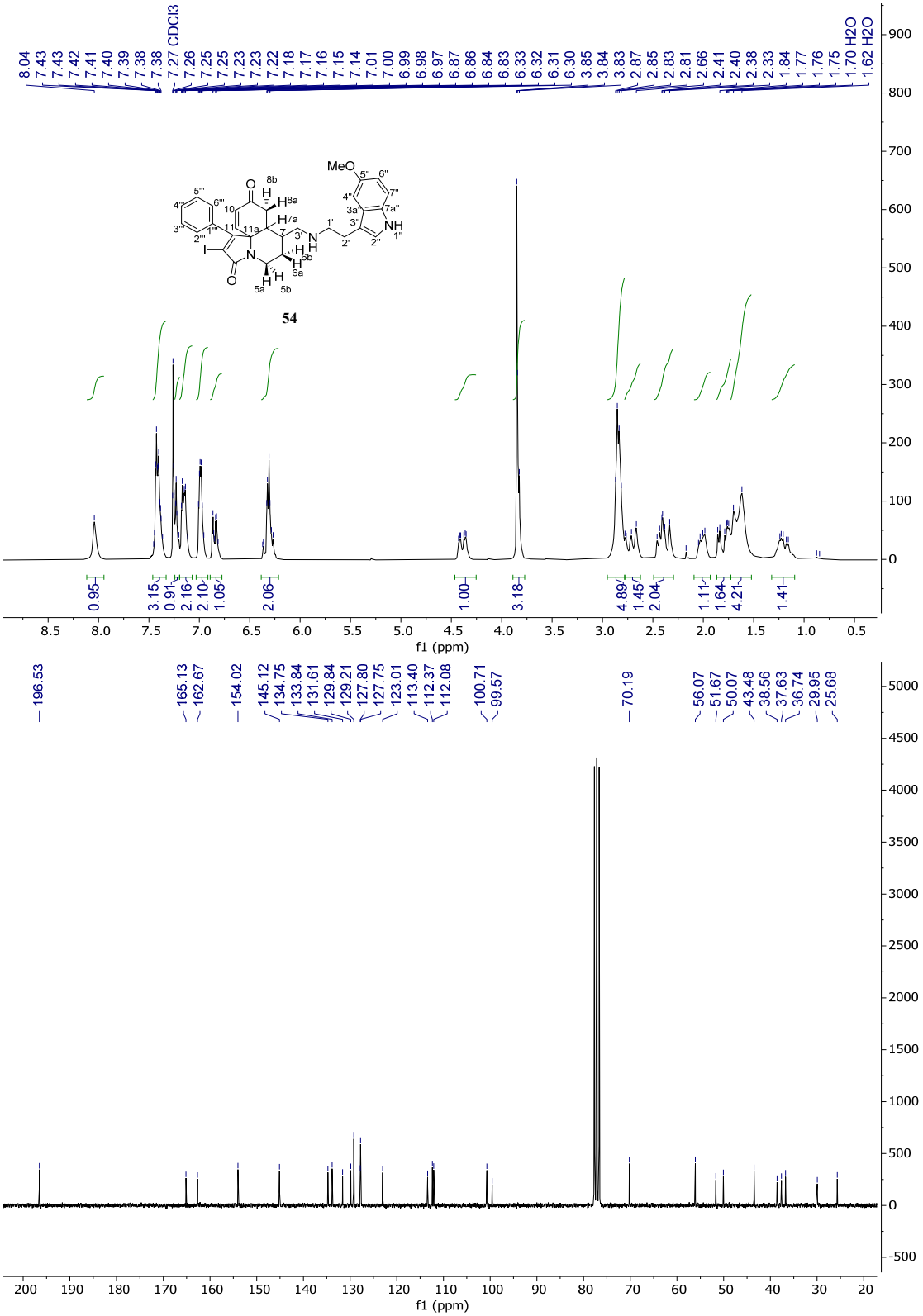

1-(3-fluorophenyl)-2-iodo-7-(((2-(5-methoxy-1*H*-indol-3-yl)ethyl)amino)methyl)-6,7,7a,8-tetrahydro-3*H*-pyrrolo[2,1-j]quinoline-3,9(5*H*)-dione **55**

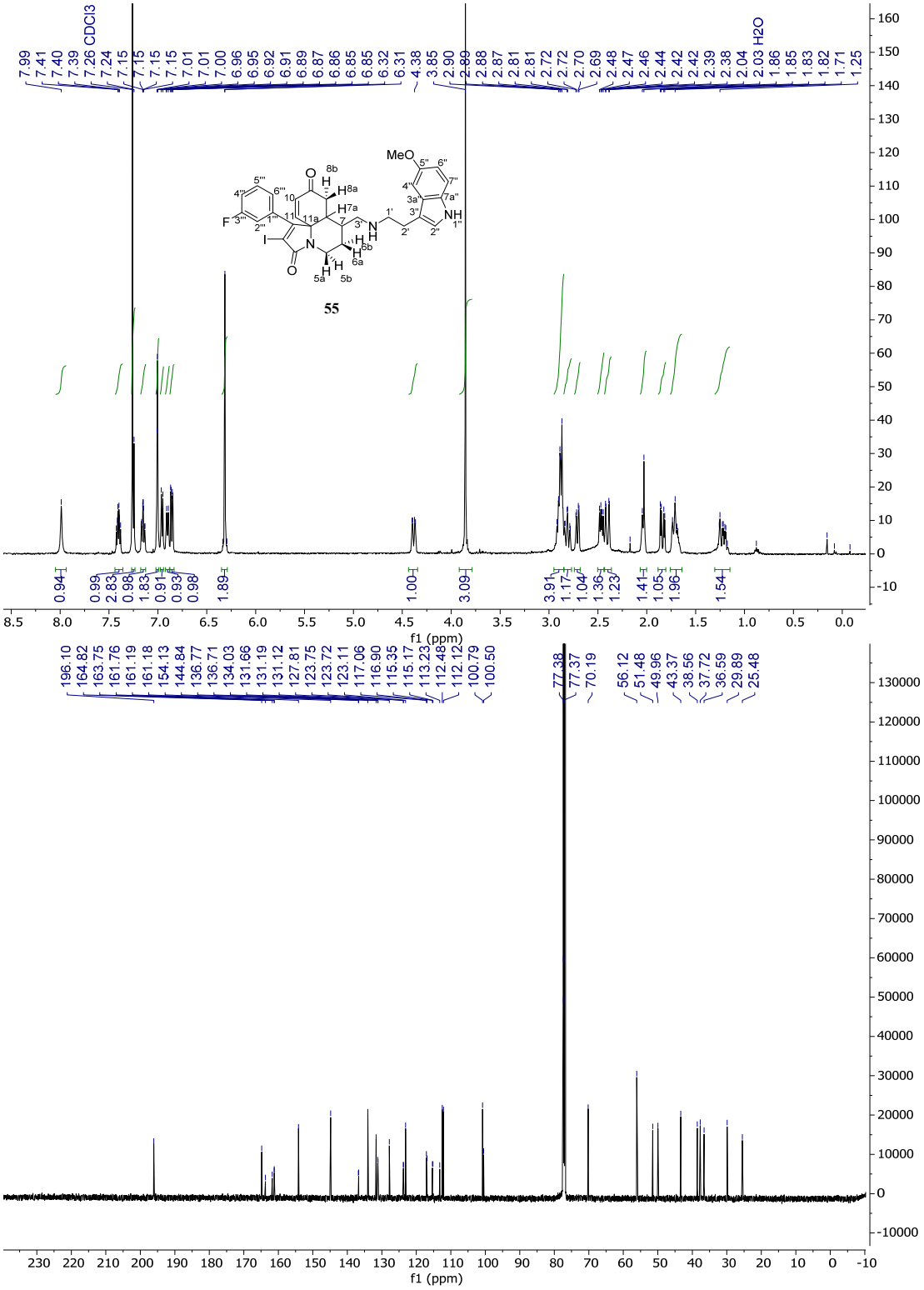

2-iodo-7-(((2-(5-methoxy-1*H*-indol-3-yl)ethyl)amino)methyl)-1-propyl-6,7,7a,8-tetrahydro-3*H*-pyrrolo[2,1-j]quinoline-3,9(5*H*)-dione **56**

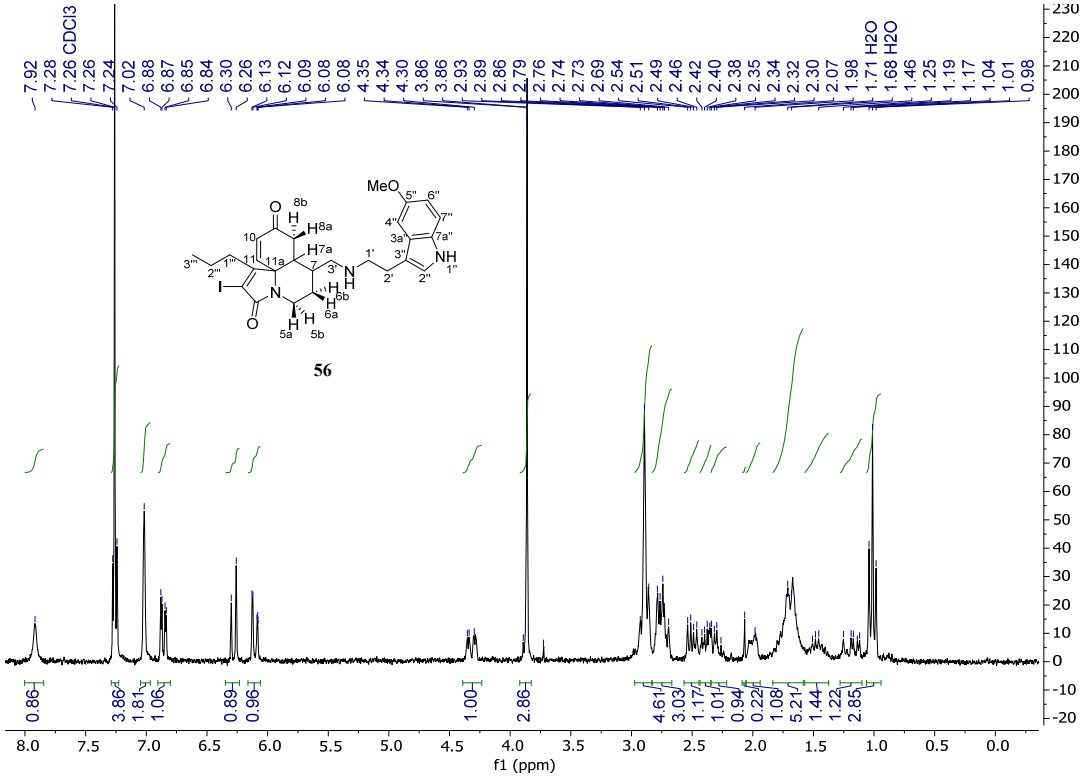

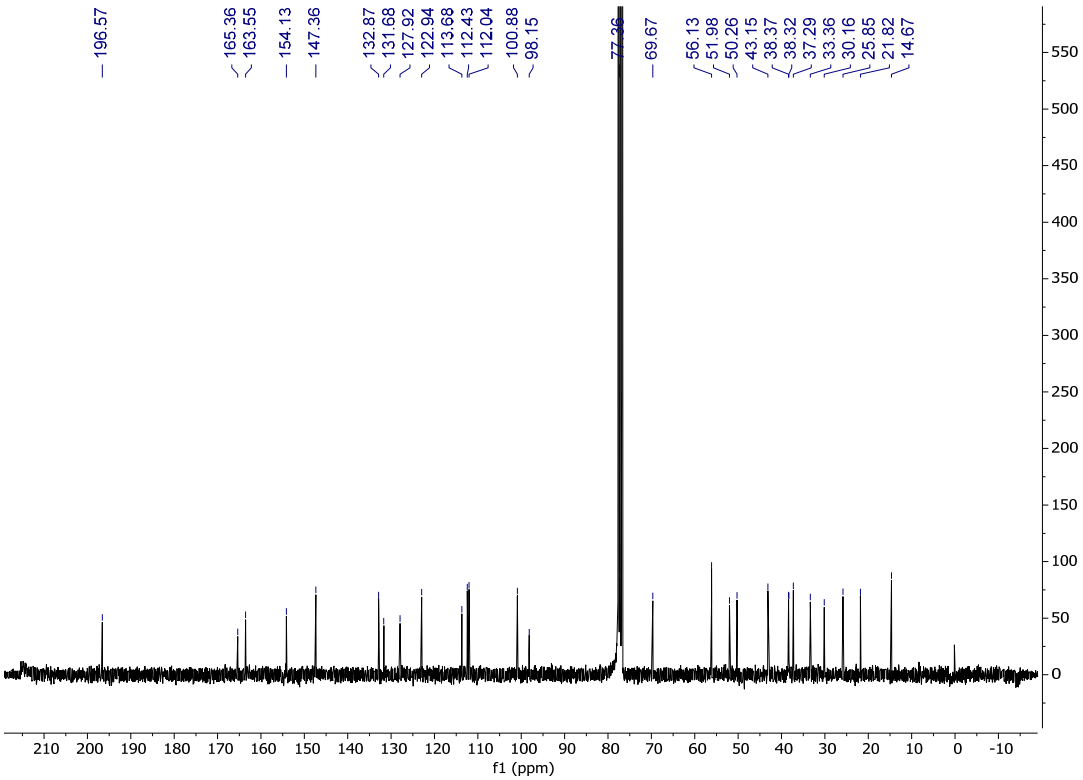

1-cyclopropyl-2-iodo-7-(((2-(5-methoxy-1*H*-indol-3-yl)ethyl)amino)methyl)-6,7,7a,8-tetrahydro-3*H*-pyrrolo[2,1-j]quinoline-3,9(5*H*)-dione 57

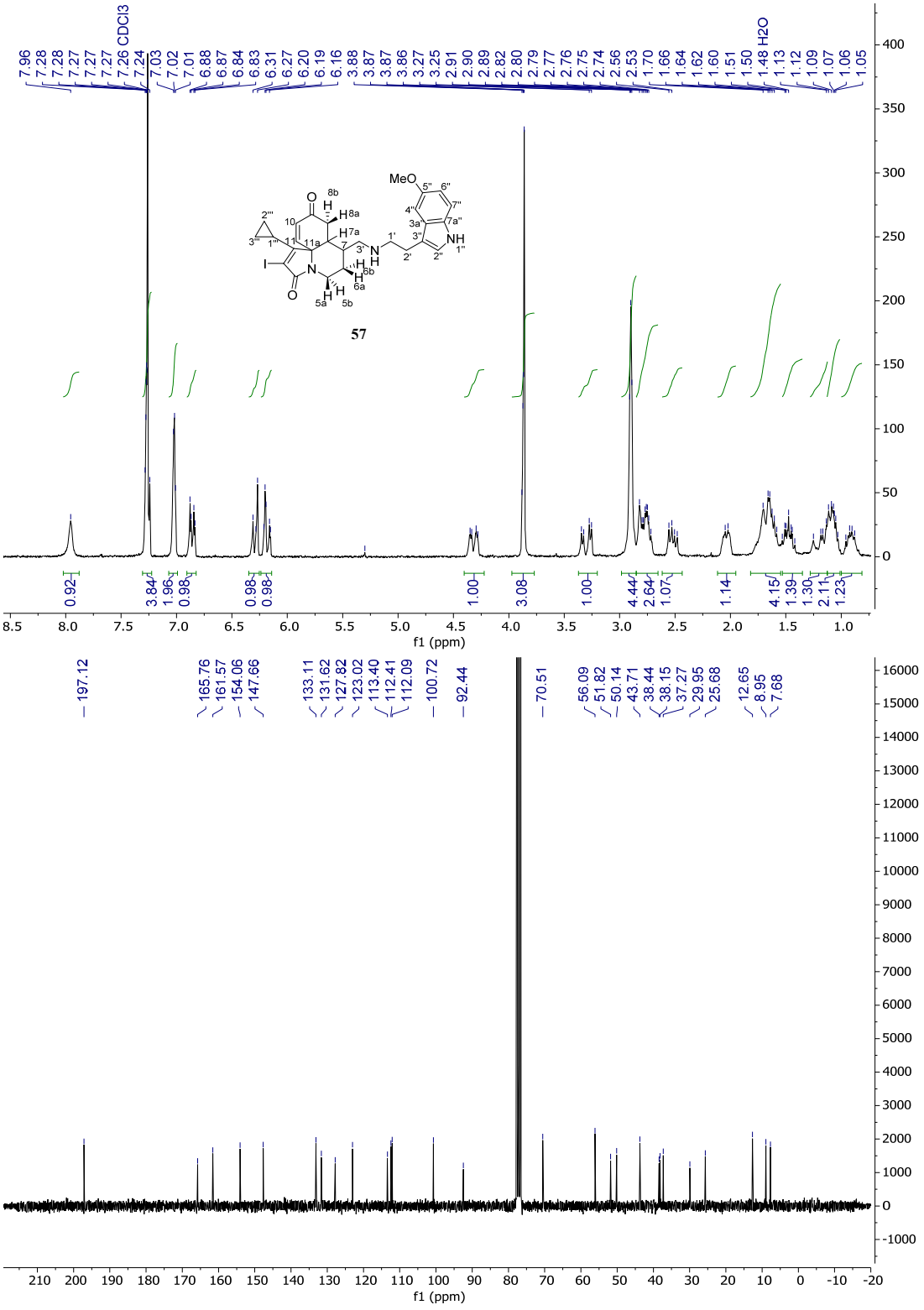

1-cyclohexyl-2-iodo-7-(((2-(5-methoxy-1*H*-indol-3-yl)ethyl)amino)methyl)-6,7,7a,8-tetrahydro-3*H*-pyrrolo[2,1-j]quinoline-3,9(5*H*)-dione 58

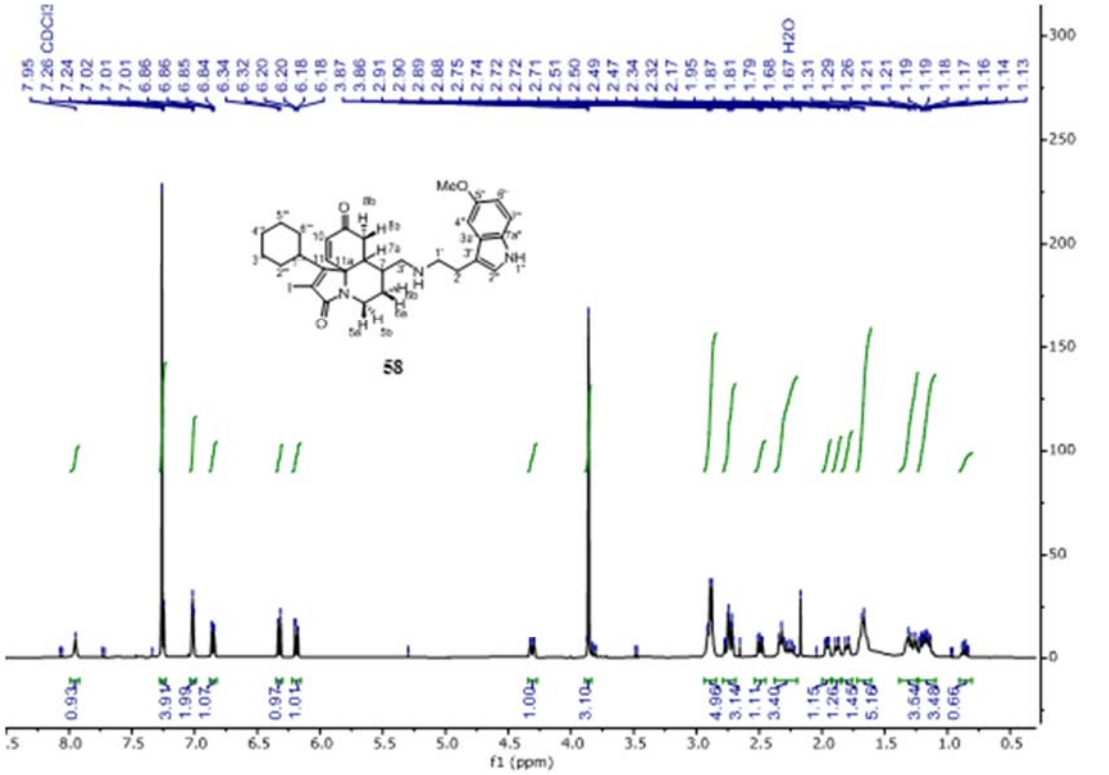

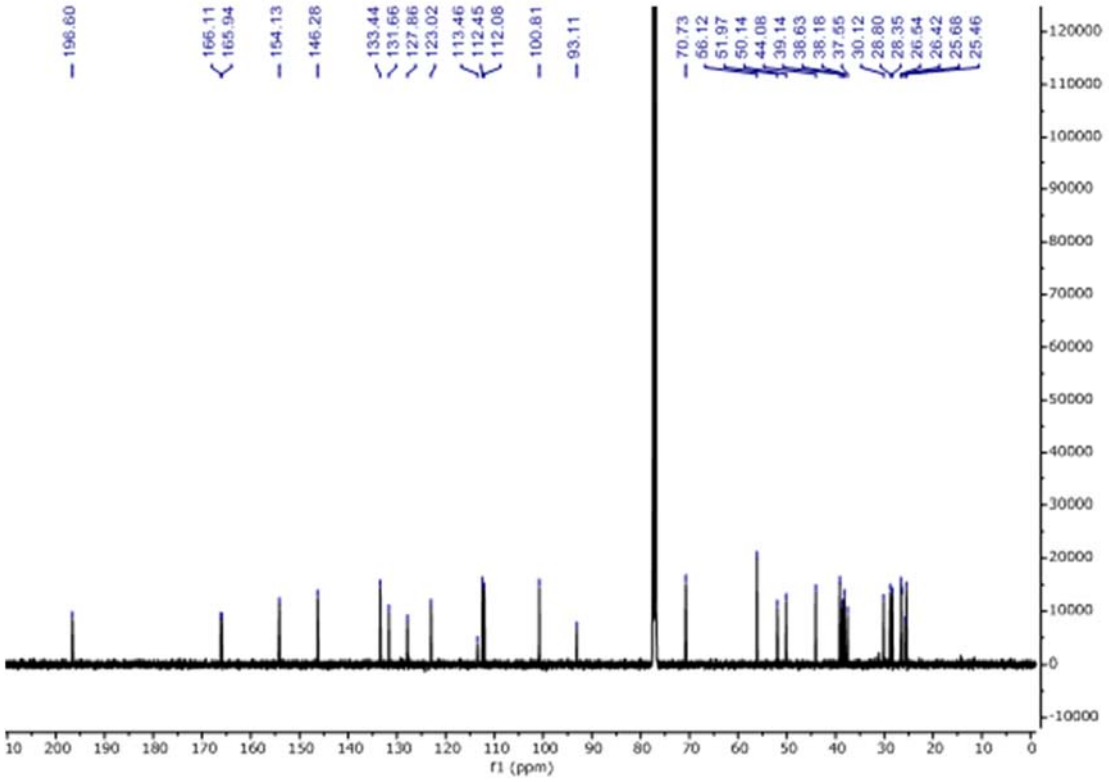

Appendix B

Table B1. *Per se* toxicity of compounds **68-73** in SH-SY5Y cell line incubated during 24h.

Compound	1 µM	10 µM	30 µM	LC_{50} (µM)
(*R*)-69	85.2 ± 5.1	90.7 ± 7.4	92.3 ± 11.4	>30
(*S*)-69	84.3 ± 6.6	90.4 ± 6.5	84.5 ± 7.4	>30
(*R*)-70	83.3 ± 4.1	75.3 ± 5.6	33.2 ± 5.2	22.0 ± 1.4
(*S*)-70	86.0 ± 5.0	74.4 ± 3.6	25.3 ± 4.7	19.0±1.0
(*R*)-71	76.7 ± 4.7	84.4 ± 2.3	88.6 ± 5.7	>30
(*S*)-71	91.2 ± 4.0	88.9 ± 6.5	85.1 ± 9.0	>30
(*R*)-72	85.2 ± 6.5	84.5 ± 3.8	95.0 ± 1.6	>30
(*S*)-72	92.7 ± 1.1	88.9 ± 2.9	92.5 ± 9.2	>30
(*R*)-73	75.0 ± 3.8	81.4 ± 5.4	83.7 ± 5.2	>30
(*S*)-73	87.1 ± 6.1	85.1 ± 7.3	85.7 ± 9.8	>30
(*R*)-74	76.1 ± 3.7	88.8 ± 8.2	93.9 ± 8.5	>30
(*S*)-74	88.4 ± 4.9	80.0 ± 6.2	81.2 ± 8.4	>30

Data are expressed as mean value ± SEM of four experiments by duplicate.

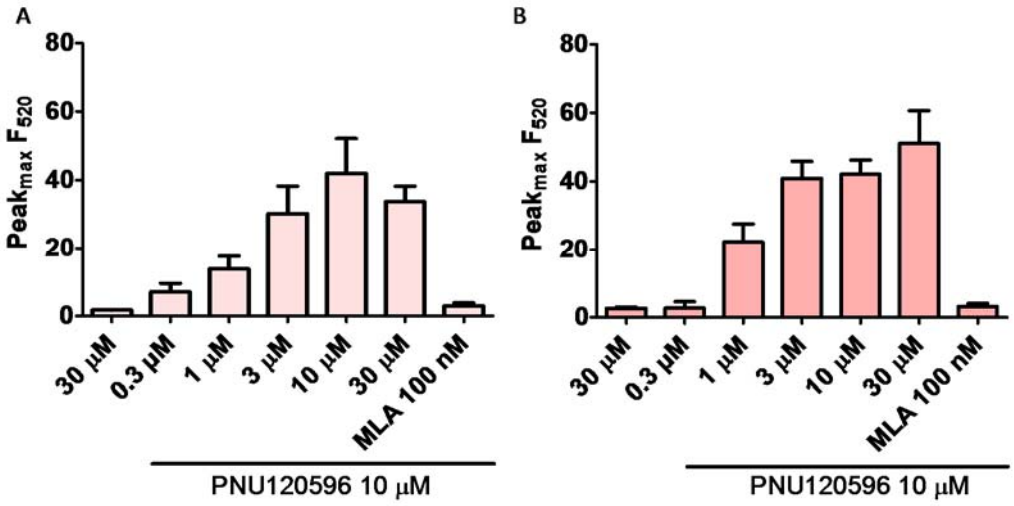

Figure B1. Intracellular Ca^{2+} increases mediated by **A) (*R*)-69** and **B) (*S*)-69**, at different concentrations in the absence or presence of the PAM PNU120596 (10 µM) and the selective α7-nAChR agonist MLA (100 nM).

HPLC DATA

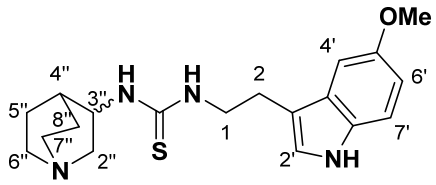

69

Area % Report

Data File: D:\Enterprise\Projects\Default\Result\SAQRAC12.rslt\SAQRAC12.rslt.dat
Method: D:\Enterprise\Projects\Default\Result\SAQRAC12.rslt\Sheila pH5.9-CH3CN5% 35'.met
Acquired: 4/18/2018 1:48:44 PM (GMT +02:00)
Printed: 4/18/2018 2:35:22 PM (GMT +02:00)

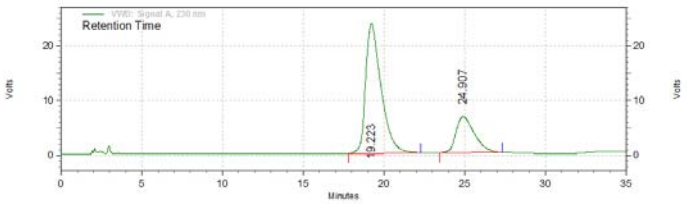

VWD: Signal A, 230 nm Results

Retention Time	Area	Area %	Height	Height %
19.223	26408630	75.34	397050	78.27
24.907	8645319	24.66	110228	21.73
Totals	35053949	100.00	507278	100.00

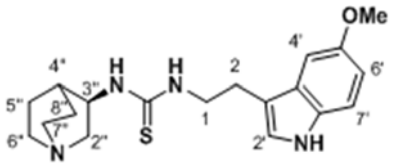

(*R*)-69

Area % Report

Data File: D:\Enterprise\Projects\Default\Result\SA4.259R.rslt\SA4.259R.rslt.dat
Method: D:\Enterprise\Projects\Default\Result\SA4.259R.rslt\Sheila pH5.9-CH3CN5% 35'.met
Acquired: 4/18/2018 2:30:43 PM (GMT +02:00)
Printed: 4/18/2018 5:22:23 PM (GMT +02:00)

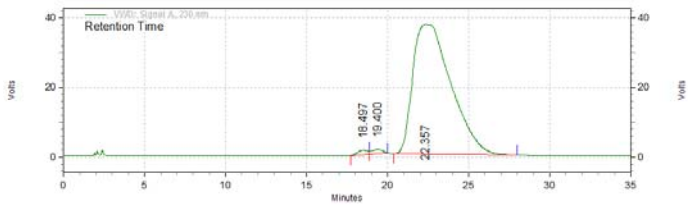

VWD: Signal A, 230 nm Results

Retention Time	Area	Area %	Height	Height %
18.497	919418	0.88	20763	3.12
19.400	905403	0.87	19398	2.92
22.357	102404620	98.25	625005	93.96
Totals	104229441	100.00	665166	100.00

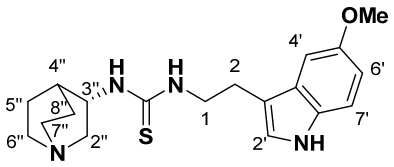

(*S*)-69

Area % Report

Data File: D:\Enterprise\Projects\Default\Result\SA4.260s.rslt\SA4.260s.rslt.dat
Method: D:\Enterprise\Projects\Default\Result\SA4.260s.rslt\Sheila pH5.9-CH3CN5% 35'.met
Acquired: 4/18/2018 3:14:46 PM (GMT +02:00)
Printed: 4/18/2018 4:09:35 PM (GMT +02:00)

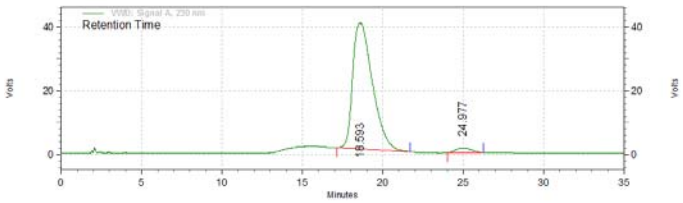

VWD: Signal A, 230 nm Results

Retention Time	Area	Area %	Height	Height %
18.593	56566360	97.21	663223	96.43
24.977	1625674	2.79	24538	3.57
Totals	58192034	100.00	687761	100.00

REPRESENTATIVE ^{1}H-NMR AND ^{13}C-NMR SPECTRA

1-(2-(5-methoxy-1*H*-indol-3-yl)ethyl)-3-(quinuclidin-3-yl)thiourea 69

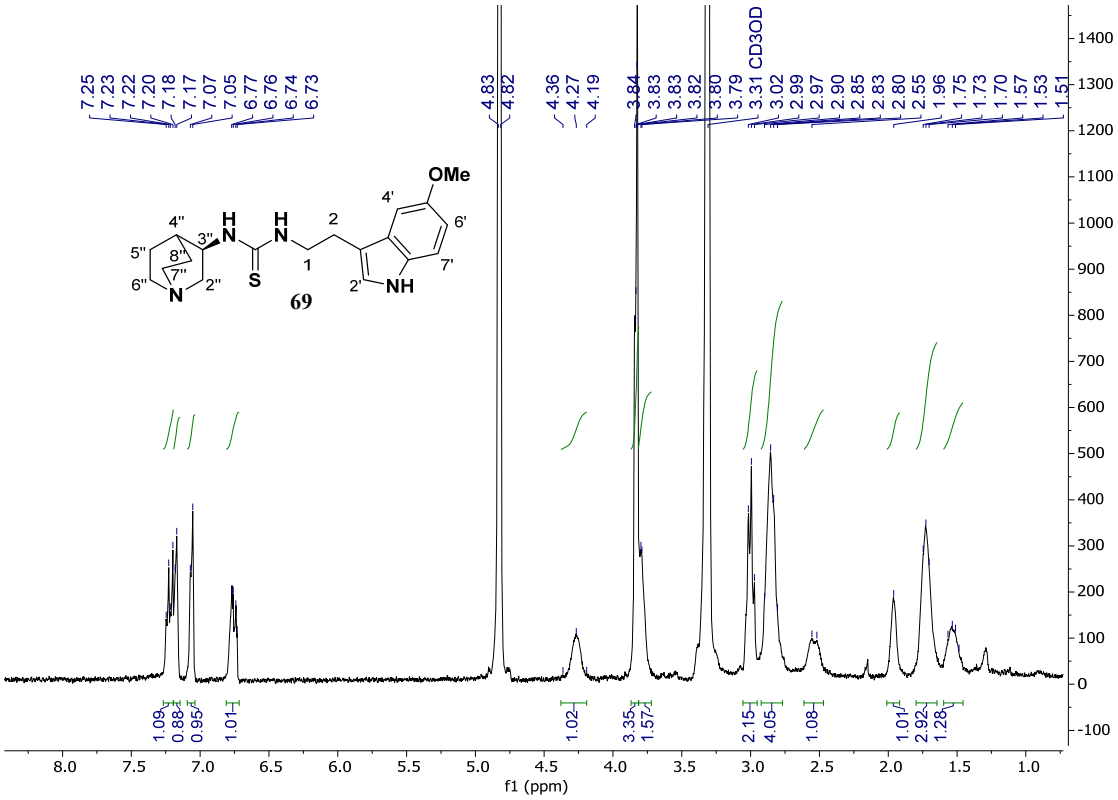

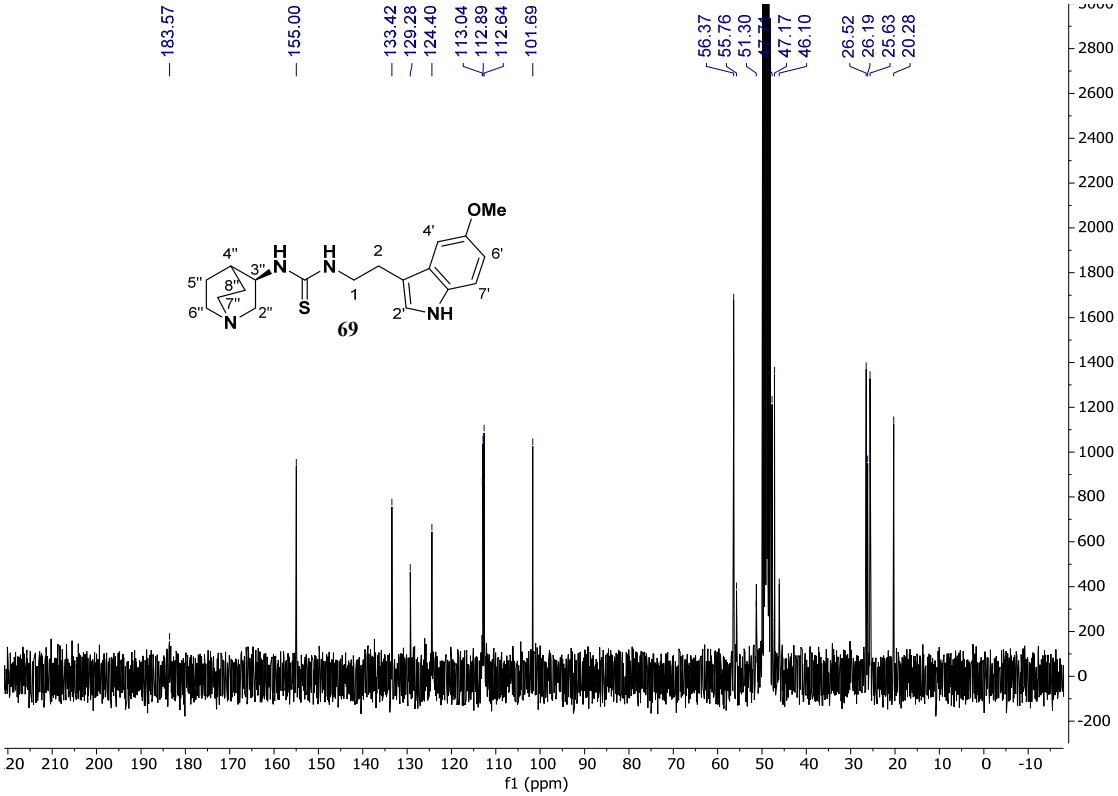

1-(2-(5-chloro-1*H*-indol-3-yl)ethyl)-3-(quinuclidin-3-yl)thiourea 70

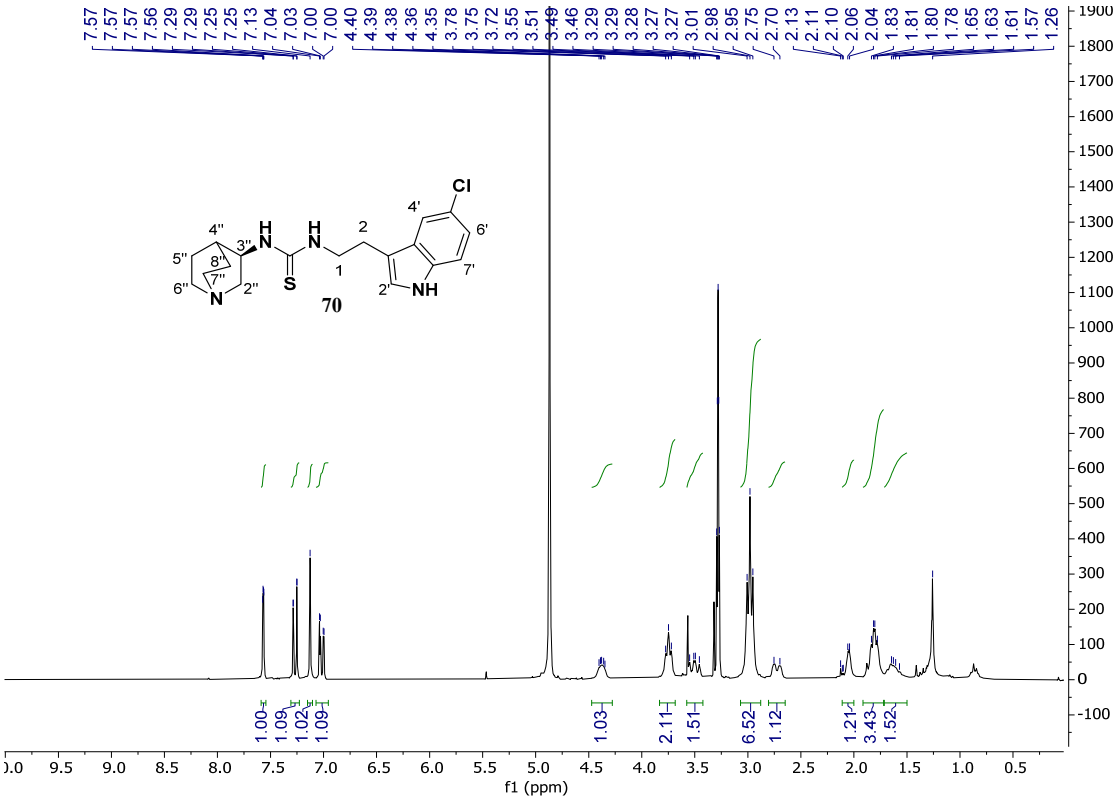

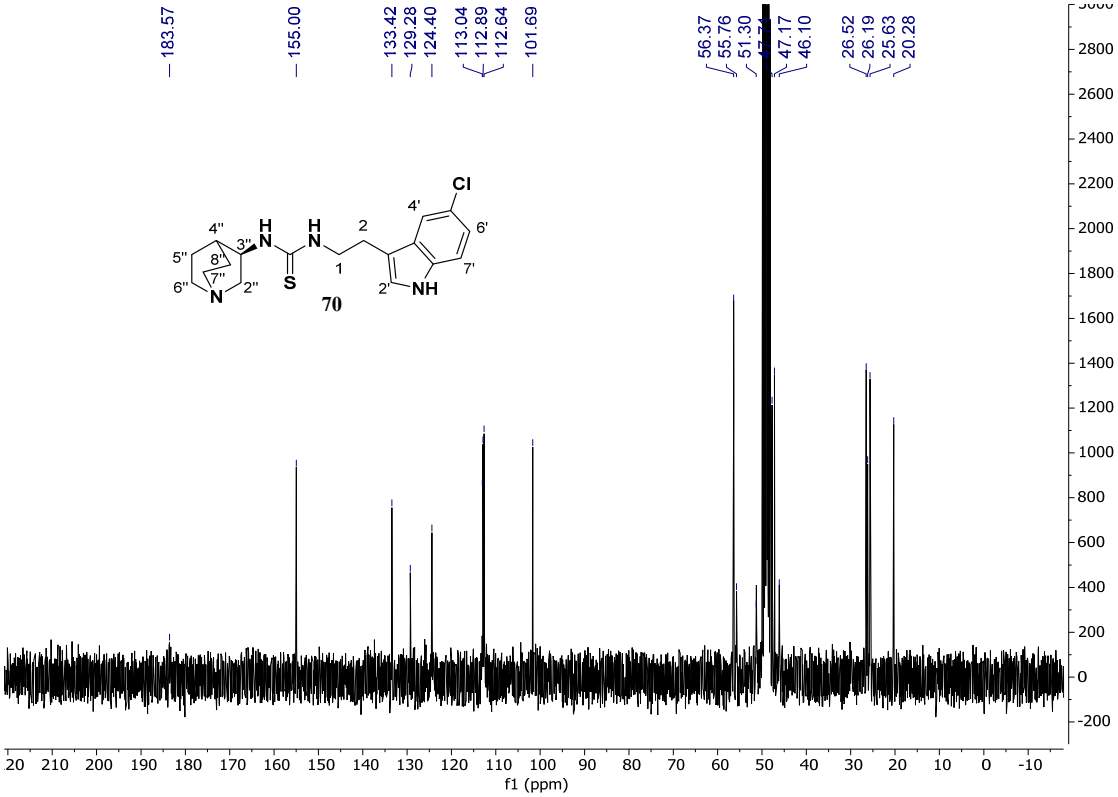

1-(2-(1*H*-indol-3-yl)ethyl)-3-(quinuclidin-3-yl)thiourea 71

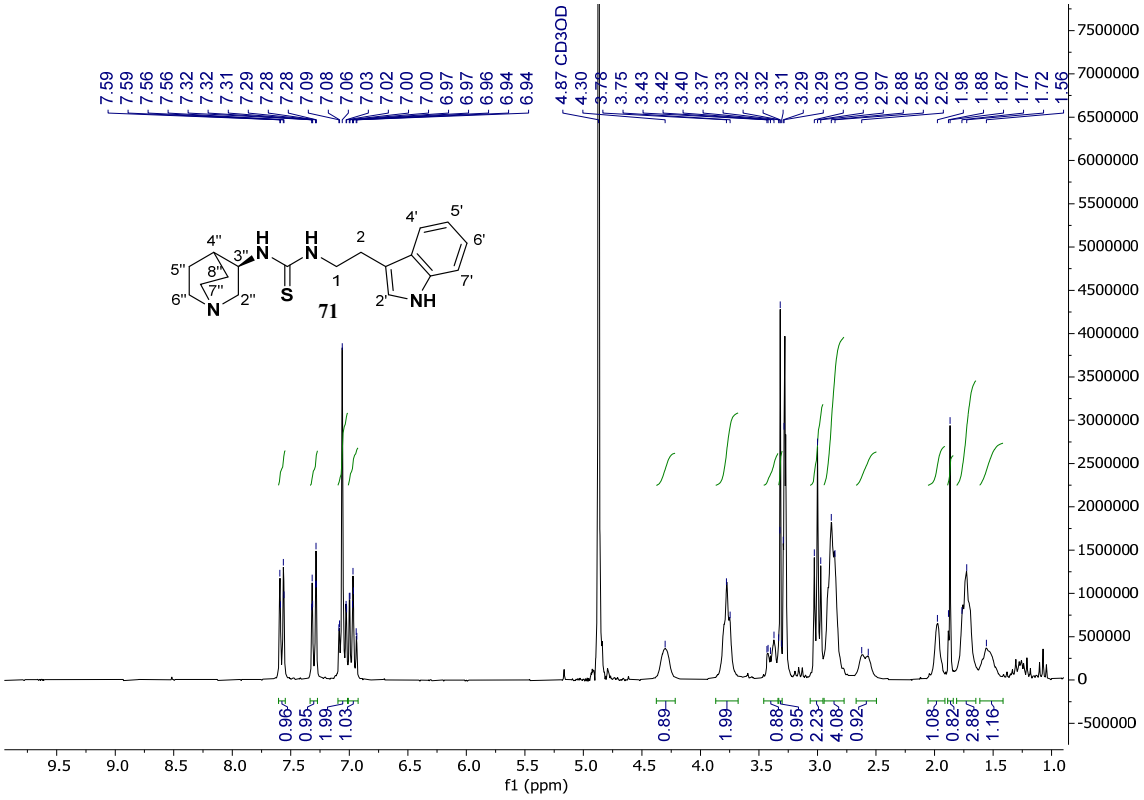

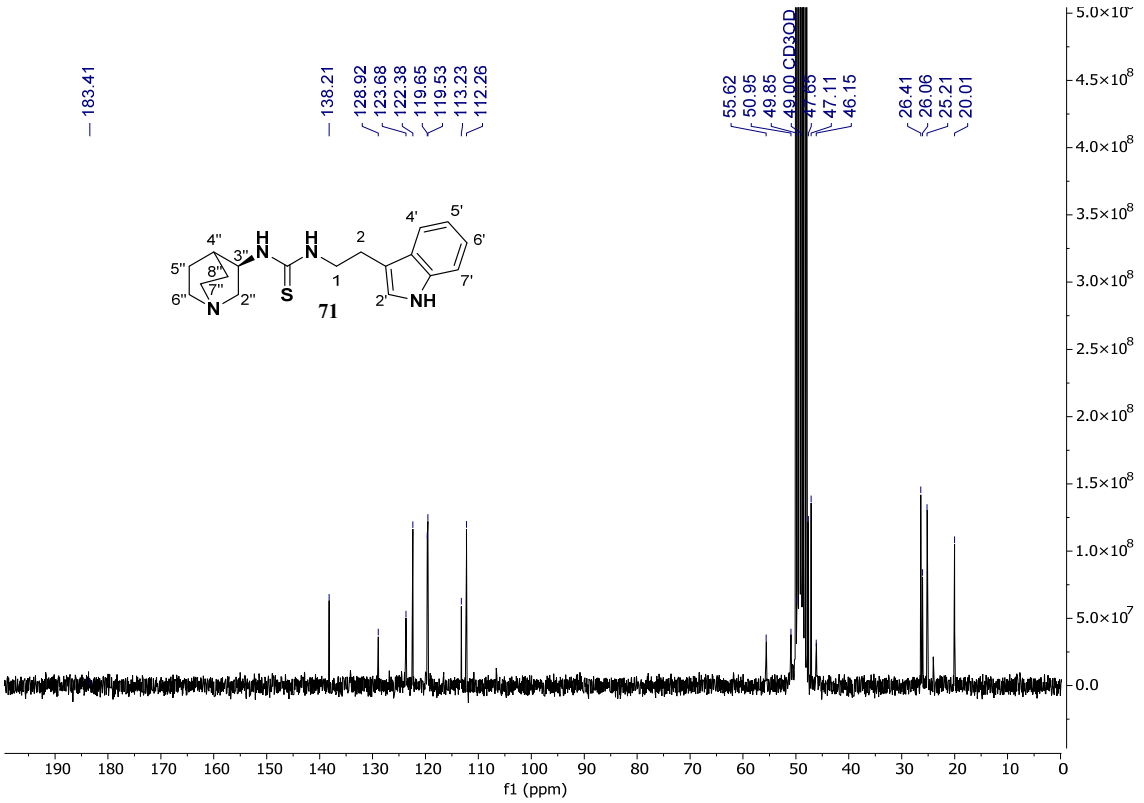

1-(2-(5-methoxy-1*H*-indol-3-yl)ethyl)-3-(quinuclidin-3-yl)urea 72

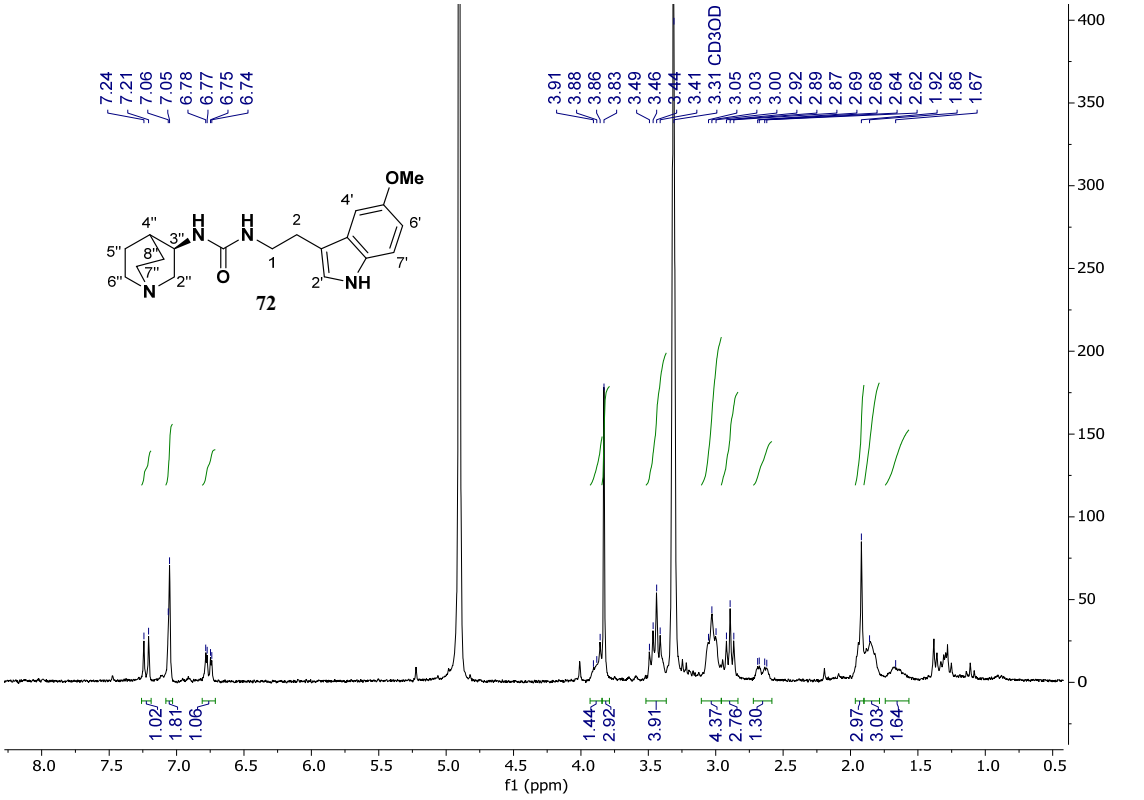

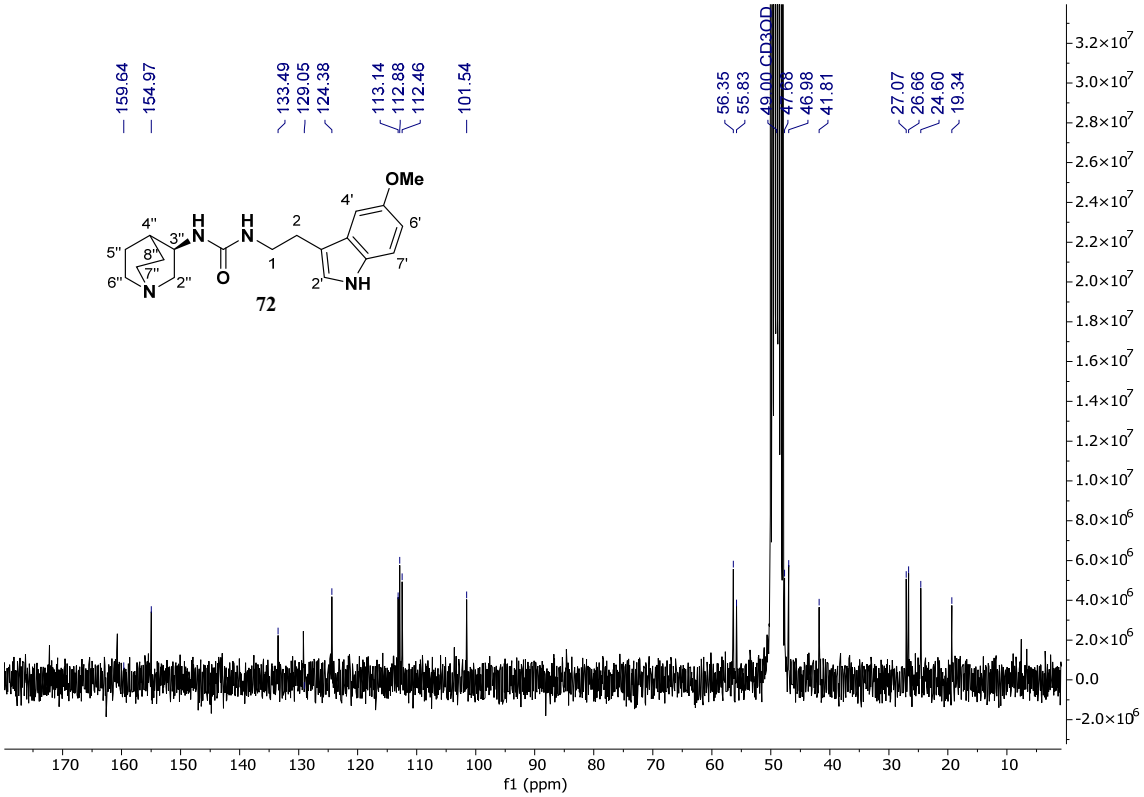

1-(2-(5-chloro-1*H*-indol-3-yl)ethyl)-3-(quinuclidin-3-yl)urea 73

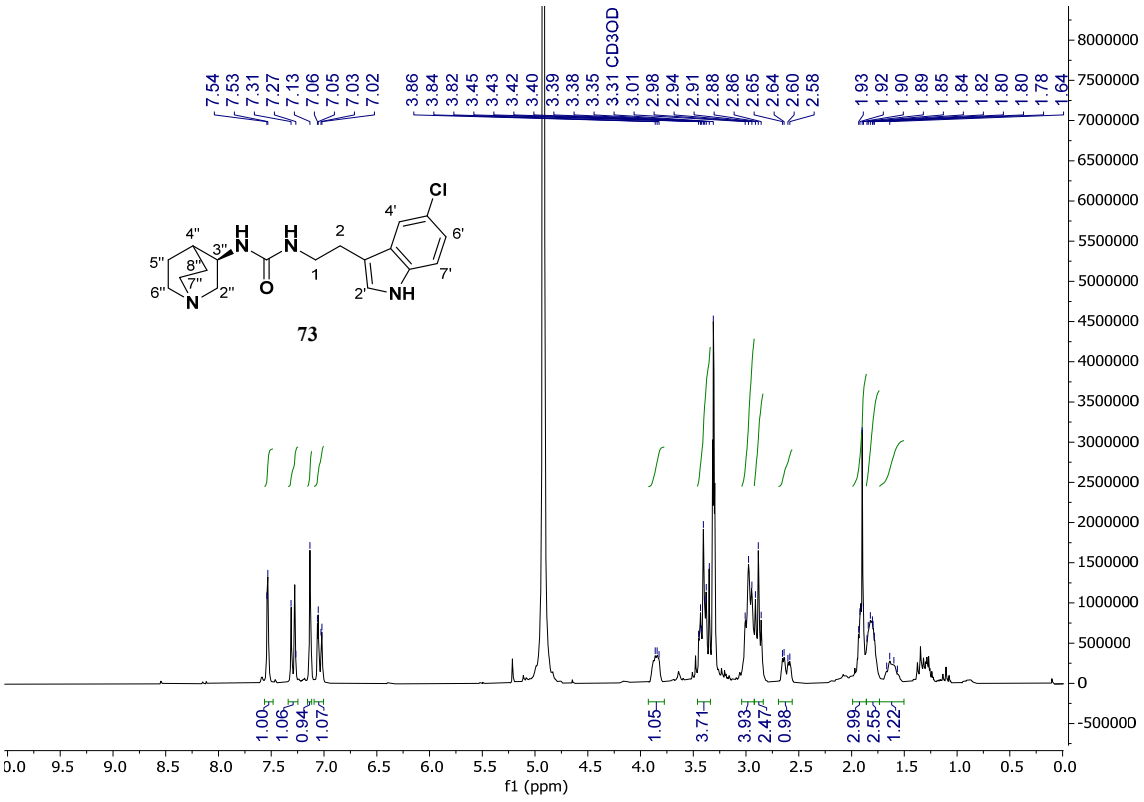

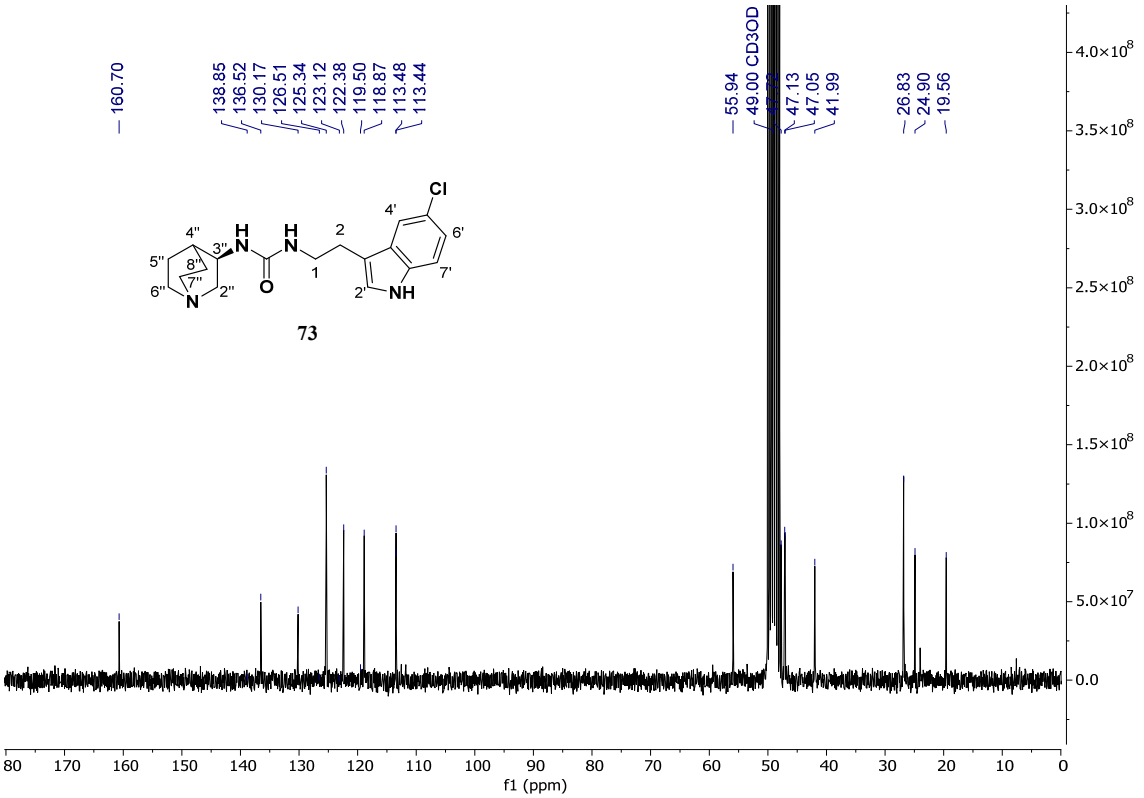

1-(2-(1*H*-indol-3-yl)ethyl)-3-(quinuclidin-3-yl)urea 74